Order Number 9108181

The mono-energetic positronium beam and the positronium scattering from surfaces

Tang, Shengzhang, Ph.D.

City University of New York, 1990

U·M·I
300 N. Zeeb Rd.
Ann Arbor, MI 48106

A

THE MONO-ENERGETIC POSITRONIUM BEAM AND THE POSITRONIUM SCATTERING FROM SURFACES

by

SHENGZHANG TANG

A dissertation submitted to the Graduate Faculty in Physics in partial fulfillment of the requirements for the degree of Doctor of Philosophy, The City University of New York.

1990

This manuscript has been read and accepted for the Graduate Faculty in Physics in satisfaction of the dissertation requirement for the degree of Doctor of Philosophy.

June 12, 1990
Date

Leonard O. Roellig Leonard O. Roellig
Chair of Examining Committee

June 12, 1990
Date

Joel I. Gersten
Executive officer

Marten L. den Boer

Karl F. Canter

Kelvin G. Lynn

Frederick W. Smith Frederick W. Smith
Supervisory Committee

The City University of New York

Abstract

THE MONO-ENERGETIC POSITRONIUM BEAM AND THE POSITRONIUM SCATTERING FROM SURFACES

by

Shengzhang Tang

Advisor: Professor L. O. Roellig

Using the mono-energetic high intensity positron beam at Brookhaven National Laboratory as a variable energy positron source, a mono-energetic positronium (Ps) beam of variable (0—80 eV) energy and an angular width of 5° has been successfully constructed and used to conduct the Ps surface reflection and scattering measurements. The Ps atoms were produced by the positrons' charge-exchange collisions with Ar atoms, when a high intensity positron beam was magnetically guided into a differentially pumped gas cell of 10^{-3} torr Ar. The Ps surface reflection and scattering measurements were performed on a cleaved LiF(100) surface and a cleaned Cu(100) surface. The Ps emission from both surfaces bombarded by low energy ($\leq$150 eV) positrons was also measured to help us understand the Ps surface interaction and explore new applications of Ps emission in surface studies. Strong Ps specular reflection of 30% at energy below 7 eV and 1$\sim$3% up to 50 eV was observed from the LiF(100) surface with an angular width about the same as that of the Ps beam. The Ps scattering of a few percent was observed from the Cu(100) surface. Our measurements also showed Ps surface scattering was very sensitive to the surface condition. A theoretical model considering the surface potential reflection and the ion core scattering was used to understand our measurements. Our data analysis showed that there was relatively high intensity of Ps scattering by the ion cores on both surfaces, strongly suggesting the positronium surface diffraction can be observed in the future with a proper experimental set up.

Acknowledgements

This thesis project would be impossible without extensive support and invaluable help from many people with whom I have been privileged to work. Especially, I wish to express my deep gratitude to Prof. L. O. Roellig, Dr. K. G. Lynn, and Prof. K. F. Canter for their continuous support, patient teaching, insightful guidance, careful reading of this thesis, and very helpful comments; and for their personal interests for my general welfare and future career. My thesis advisor, Prof. Roellig, not only has offered me constant encouragement and sound advice, and helped me to overcome the difficulties in every step of this research project, but also has been giving me some valuable lessons on how to be a good scientist. The entire research project has been conducted at the Brookhaven National Laboratory (BNL) in collaboration with the Particle Solid Interaction (P.S.I) group. The group leader, Dr. Lynn, has provided all the necessary support for this project, and for my working at BNL. His teaching and encouragement helped me to gain the confidence in the experimental research. His enthusiasm and hard work has been an inspiration to me during this project. Both Prof. Roellig and Dr Lynn have made a great effort to secure the success of this project against the unexpected external constraint. My knowledge on the diffraction physics and the positronium interaction with surfaces has been enriched through numerous discussion with Prof. Canter. I have also been benefited from his rigorous approach in research. The important contribution to this project by Dr. A. P. Mills, Jr. and Prof. S. Berko is grateful acknowledged. Dr. M. Weinert who has taken time to discuss some of the theoretical treatments in this thesis has my gratitude for giving me some incisive suggestions. I have also been benefited through the discussions with Drs. R. J. Drachman, P. M. Platzman, A. Ishii, S. J. Ward, and J. W. Davenport. To Dr. A. Viescas not only for his large contribution in constructing the positronium beam and its data acquisition system, but also for his critical role in the later part of the Ps scattering measurements, I am especially grateful. I am

indebted to Dr. M. H. Weber, for his large contribution in constructing the HFBR positronium beam and for the major responsibility he took in a large part of the measurements on LiF. Dr. B. L. Brown's important contribution in constructing the Ps beam is gratefully acknowledged. I am very grateful to J. J. Hurst for his effort to oversee the operating of HFBR beam, for his technical assistance, and for his helpful advice on various matters. Special thanks are extended to M. Carroll, J. Rutherford, M. Taylor, and J. Zahradka for their efforts at different stages of this project to keep the positron beam operating, and also for their helpful suggestions and technical assistance; to Dr. A. Moodenbaugh for the fabrication of Cu^{63} pellets; and to the Dr. D. C. Rorer, T. Holmquist, and N. Houvener of HFBR for their help in the routine preparation of Cu^{64}. R. Khatri is thanked for his valuable assistance in some of the experimental measurements. Dr. D. M. Chen's encouragement and valuable suggestions are greatly appreciated. Mrs. M. McKeown is thanked for her help on various computer related problems. Mrs. E. Morello is thanked for her effort to make all the routine arrangements for my working and staying here. I would also like to thank all the members, visitors, and follow students of P.S.I group for their help, support, friendship, tolerance, and senses of humor, which has made my time in this group a very memorable one. I am very grateful to Mrs. S. Schneider for helping me to gain confidence in writing in English. I would like to acknowledge with my gratitude Prof. S. Lee's teaching and encouragement in my earlier part of the graduate study course.

No words can express my gratitude to my family, especially my parents, who have always had faith in their son through their life time of encouragement, support, and guidance. Without their support and help in every step of the course of my education, I would have never been able to undertake this project and finish it.

Table of Contents

List of Tables

List of Figures

Chapter 1
INTRODUCTION

Great progress has been made in surface science in the last two decades. The progress is reflected not only by the tremendous information gained by scientists during this exciting time, but also by the wide range of the various techniques invented or developed in the process by those scientists striving to achieve deeper and more accurate understanding of surfaces and surface interactions. Some of the techniques, surface x-ray scattering and diffraction, neutron scattering, and luminescence studies for example, were developed from those used in bulk studies. Some of the techniques were developed to study surfaces or near surfaces, like Auger, photoemission, and ion scatterings. Some of the techniques were developed to study the top-most layer on the surfaces, such as scanning tunneling microscopy (STM), low energy electron diffraction (LEED), and atom scatterings. Each of these techniques provides some information about the interested surfaces in its unique way. The information that one gets from these different techniques give one views of a surface from different aspects; they, in some cases, are complimentary to each other, and verify each other in some other cases. Because new techniques may bring a significant improvement of our understanding of surface science, which happened quite often in the past such as the case of the application of STM, scientists are still very actively looking for new techniques to study surfaces. Our current effort of utilizing the positron beam and the positronium beam to study surfaces is such an attempt.

Six decades ago, Dirac (1930), as part of his theory of electron energy, postulated the existence of positrons, antiparticles of electrons with the same mass and spin,

but opposite charge and magnetic moment. A few years later, Anderson (1932,1933) experimentally proved the existence of positrons in the cosmic ray. After Anderson's discovery, Mohorovičić (1934) postulated the possible existence of positronium (Ps) atoms, electron-positron bound state pairs similar to hydrogen atoms with positrons replacing protons. A number of discussions and calculations on the energy levels and decay rates at different states of Ps had been carried out by various researchers* at the time when Deutsch (1951) proved the existence of Ps with the first production of Ps (in gases), and the first experimental measurement of the decay rate of triplet Ps. The discoveries of positrons and positronium generated excitement among atomic and nuclear physicists, because positrons and positronium, both light and simple particles, provided scientists great objects with which they could verify their developed theories and propose new theories for more complicated particle and systems. The scientists at the time also foresaw the great potential of using positrons and positronium as probes to study the solid state physics and quickly got into action.

About two decades after positrons was first postulated, the experiment conducted by DeBenedetti and others (1949) "to measure the anticolinearity of the two annihilation [γ-rays] quanta much more carefully than had been previously done" revealed "that the gamma-rays of annihilation are not exactly anticolinear and that their angle is determined by the motion of the electrons in the solid matter where the annihilation took place" (DeBenedetti 1967). DuMond and his associates (1949) had also "proved with very accurate measurements of energy that the width of the annihilation radiation is also affected by the electron motion." (DeBenedetti 1967) These discoveries mark the start of a new era of positron physics, an era of the research on interactions of positron and positronium in condensed-matter.

Early studies of positron solid state interaction were carried out mainly by two different approaches. The first approach was to measure the lifetimes of the positrons

* See, for example, Pierenne 1946, Wheeler 1946, Ore and Powell 1949, and Yang 1950.

in different materials. The second one was to study the annihilation γ-rays including the angular correlations and energy spectroscopic information of γ-rays. A small variation to the second approach was the measurement of triple coincidence of annihilation γ-rays which would indicate the possibilities of positronium formation in different materials. These studies provide vast information on a wide range of materials, especially information about defects in the materials and the electronic structures of the materials*.

Even though the positrons from β-decay of radioactive nuclei was proved to be a very useful probe for solid state physics research, its continuous energy distribution spectra restricted the scope of its application. Madansky and Rasetti (1950) realized this at the very early stage of positron research on solid state physics and tried to form a beam of low energy positrons by moderating fast positrons from a radioactive source Cu^{64}. They failed to observe the expected slow positrons, probably because of contaminated surfaces and the short positron diffusion length in not highly crystaline samples and the low sensitivity due to a high background of fast positrons (there was no energy filter in their apparatus, so they had to take the difference between the measurement of both fast and slow positrons and the measurement of only fast positrons). The effort of moderating fast positrons from a radioactive source, however, was proved to be a crucial and necessary step for later positron solid state research. Solid state surface studies by positrons and positronium would be impossible without moderated positrons. The ideas of the positron surface trapped state and positronium emission, which Madansky and Rasetti proposed as possible causes for their failure to observe slow positrons, were ingenious predictions verified by experimental observations decades later and have been utilized as important techniques to study solid state surfaces, even melting surfaces. Some years later after the initial attempt, Cherry (1958) succeeded in observing the slow positrons moderated by a

* For review see, for example, Stewart and Roellig 1967.

chromium-plated mica surface using his apparatus equipped with a velocity selector (which eliminated the background from fast positrons and increased the sensitivity). The moderating efficiency, which is the ratio of slow positrons yield to the total number of fast positrons emitted by the radioactive source, was about 3×10^{-8} for his low energy positron beam. About a decade later, another group (Groce and others 1968, Costello and others 1972) had produced a beam with the intensity of a few slow positrons per second (an efficiency of $10^{-7} \sim 10^{-6}$) to conduct the measurement of the total scattering cross section of positron in helium. These two studies started research applications of slow positron beams. After the first success of moderating fast positron, a search was made, in the following two decades, for better positron moderators that would give a high moderating efficiency with a low energy and angular spread. A large variety of materials and surfaces were tested. In the early seventies, Canter and others (1972) made a very important discovery. By using a moderator of MgO-coated gold vanes in a venetian-blind geometry, they succeeded in converting high energy β^+ into slow positrons with an efficiency of 3×10^{-5}, which was one to two orders of magnitude higher in efficiency than any other moderators at the time. As the efficiency of the moderators was improved, systematic studies of the interactions of positrons with solid state surfaces became feasible. In return, the study of the interaction of positrons with solid state surfaces helped physicists realize that the positron interaction with surfaces was one of the most crucial factors in the moderation process and great care had to be given to surface preparation. Starting in the late seventies, the search for better moderators was conducted with well prepared and atomically cleaned surfaces in ultra-high vacuum environments. This improvement in the experimental technique for searching new moderators was proved to be very fruitful*. A number of single crystal metal surfaces, Cu(111)+S (Mills 1979) and W(110) (Vehanen and others 1983) for example, were found to be very efficient moderators

* See Mills 1983 and references cited for a complete review.

with an efficiency of 10^{-3} expected by Madansky and Rasetti at the very beginning of their effort. As the result of these improved moderators, a few mono-energetic positron beams were constructed and employed to carry out systematic studies of solid state physics, especially the surface physics. Availability of the relatively high positron beams not only pushed the study of solid state surface into a new era, it also made testing for better moderators much easier. Some single crystal or polycrystal metal foils were systematically tested as possible transmission moderators with these beams. The efficiency of these transmission moderators, though not as high as those single crystal reflection moderators, is quite reasonable in the range of $1 \sim 7 \times 10^{-4}$ (Lynn and others 1985a, Gramsch and others 1987). While the reflection moderators are still widely used with Co^{58} sources which are usually fabricated into a pin shape, the transmission moderators which do not have the difficulty of source shadowing are now widely used with Na^{22} sources. A variation of the reflection moderator is the tungsten mesh or vanes. Even though its actual efficiency, $10^{-6} \sim 5 \times 10^{-5}$ (Dale and others 1980), is much lower than the theoretically predicted value of 7×10^{-4} (Brusa 1985), it is used in a few beams as a moderator.

In the research project which will be described in detail in the following chapters, Cu(111) evaporated on a W(110) substrate was used both as a source and as a self-moderator whenever a reasonable epitaxial growth of Cu was achieved. In the events that the self-moderator failed, likely due to bad epitaxial growth, impurities, or surface contamination, a W(100) single crystal foil was used as a transmission moderator.

In their recent study of positron interaction with rare gas solids, Gullikson and Mills (1986) found that there was a high yield of "hot" positrons re-emitted from rare gas solids because positron can not be completely thermalized in the rare gas solids with its large band gap. Thus, a new moderator with a high efficiency of 7×10^{-3} was discovered (Mills and Gullikson 1986). Currently, the high intensity low energy

positron beam employed for the research project described in the following chapters is being relocated to Building 480 of Brookhaven National Laboratory and being renovated to take full advantage of this newly discovered high efficiency moderator of solid Neon. It is expected that this beam would provide $\sim 10^9$ mono-energetic positrons per second.

The pursuit of better moderators with even higher efficiency or with less cost but relatively high efficiency, continues. Lynn and others (1989) recently developed a new cone-shaped positron moderator with efficiency about 0.14%. The field enhanced moderator, in which electric field is applied to increase the mobility of positrons to the emitting surface, was suggested more than a decades ago (Lynn and Mckee 1979, and later discussed by Beling and others 1987), but the experimental attempts have not been very successful. Though no success has been reported, the experimental tests are still being conducted at BNL. There are also several efforts to improve the efficiency of the W foil transmission moderators. Recently, a cone-shaped reflector was used in the tests of foil transmission moderators at BNL. The reflector was positioned immediately after the foil and the source with bigger opening facing the foil and the source and smaller end towards the beam. It was reported that the efficiency was doubled with the application of this reflector (Wu and others 1990). The effort to improve the efficiency of single crystal metal foils was also reported (Zafar and others 1988).

Even though the study on solid state physics with positrons had been productive before the relatively high intensity mono-energetic beams were available, the application of these beams started a new era of the research on the solid state surface physics with positrons. With mono-energetic positron beams, researchers can control the positron penetration depth and the locations where the majority of incident positrons annihilates with electrons. Researchers can label the information which

they achieve from positrons' annihilating at different depths*. This development also made surface study with positrons possible. Researchers can make positrons only interacting with the electrons, ion cores, and atoms near the surfaces or on the surfaces by controlling the incident positron energy. Thus, a whole new field of surface study with low energy positron beam was opened.

The field of surface study with low energy positrons has been very active and fruitful*. Research efforts in this field have been centered on the measurements of the events taking place after low energy positrons' striking on solid state surfaces. Fig.1.1 illustrates a few events may take place after the impact of positrons. A few examples of these efforts are the angular correlation of annihilation radiation (ACAR), time of flight measurements (TOF), low energy positron diffraction (LEPD), positronium emission measurements and positron Auger experiments. While some of the techniques developed like ACAR can be used to observe several events, some of the others such as the time of flight measurement were designed to measure one event only. All of them, however, would provide researchers some informations about the surfaces studied. The techniques described in later part of this chapter are just a few examples of the application of the mono-energetic positron beam in the surface research, which are also related, in different degree, to the research project described in this thesis. For a complete review, readers are suggested to read Schultz and Lynn 1988 and the proceedings for various recent workshops or conferences on application of positron annihilation.

While some of techniques use channel plates to detect low energy positrons and positronium directly, a great number of techniques detects low energy positron and positronium by detecting the annihilation photons. When a positron overlaps with an electron resulting an annihilation, two or more photons would be emitted to carry away the energy of the mass of a positron and a electron. Every photon has its energy

* See, for example, Schultz and Lynn 1988 for a complete review.

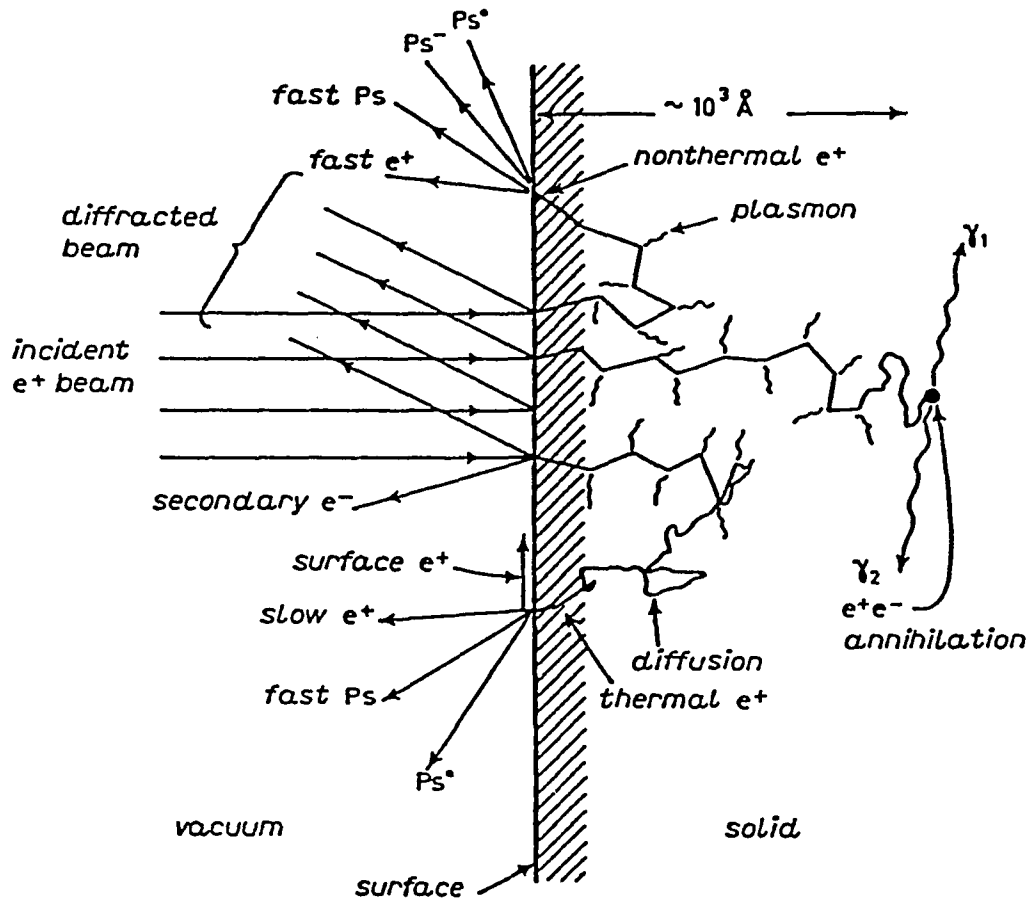

Figure 1.1 Positron interaction with a surface

(from Mills 1983)

of $h\nu$, momentum $h\nu/c$, and spin of 1, where ν is frequency of the photon, h and c are Plank's constant and speed of light in vacuum. At least two photons have to be emitted during the annihilation in a vacuum to conserve the momentum and energy (because emission of a single photon would result a non-vanishing momentum in the frame of center of mass of the annihilating electron and positron). For the pair of a positron and an electron whose spins are antiparallel to each other (^{1}S total spin = 0), two photons would be emitted to conserve the total spin and parity; for the pair whose spins are parallel to each other (^{3}S total spin = 1), three photons would be emitted to conserve the total spin and parity. A single photon emission is possible if a third particle is involved to conserve the total momentum. The possibility for that process, however, is extreme low (even in comparison with three photons process). Some efforts were made to detect that precess in the past (Lynn and others 1980). The three photons annihilation is less probable than the two photons annihilation because it is a higher order process. Dirac (1930) calculated the spin-averaged cross section for two γ-photon annihilation process and its result in the low-velocity limit is

$$\sigma_{2\gamma} = \pi r_0^2 (c/v), \tag{1.1}$$

where r_0 is the classical electron radius. Ore and Powell (1950) calculated the cross section for three γ-photons process in the low-velocity limit and gave the ratio of the spin-averaged cross section for two γ-photons and three γ-photons annihilation as

$$\sigma_{2\gamma}/\sigma_{3\gamma} = 372. \tag{1.2}$$

This result also applies to the case that the electron-positron pair forms a positronium atom in the ground (S) state, as the Coulomb binding in the positronium atom has a negligible effect upon the decay probability (Ore and Powell 1949). In its ground state, a positronium atom can be either in singlet ^{1}S (S = 0) state, which is called para-positronium, or triplet ^{3}S (S = 1) state, which is called ortho-positronium. Because

of conservation of charge conjugation,* a para-positronium can decay only through a even number, predominantly two, photon annihilation process, a ortho-positronium can decay only through a odd number, predominantly three, photon annihilation process (Ore and Powell 1949, and Yang 1950). Because the two photons annihilation has a larger cross section than that of the three photons annihilation, the life time of para-positronium is much shorter than that of ortho-positronium. From the result of Dirac one can get the life time of para-positronium is (Wheeler 1946 and Wallace 1960)

$$\tau_1 = 2(\hbar c/e^2)^4(\hbar^2/me^2c) = 1.25 \times 10^{-10} sec. \tag{1.3}$$

Ore and Powell(1949) also gave the life time of ortho-positronium as

$$\tau_3 = 1.42 \times 10^{-7} sec. \tag{1.4}$$

In the two photons annihilation process for both an unbound electron-positron pair or a bound pair (para-positronium), the two photons emitted are always anti-parallel to each other and have the same energy in the electron-positron pair's center of mass frame. The two photons would have different energies in the laboratory frame if the electron-positron pair's center of mass frame has appreciable velocity in laboratory frame, and the two photons would not travel exactly anti-parallel in the laboratory frame under this condition. In the three photons annihilation process, however, the three photons emitted have their energy spectrum and angular distribution both in its center of mass frame and in the laboratory frame. Efforts have been made to measure those angular correlation of annihilation photons under different conditions and to study the energy shift of annihilation photons in the laboratory frame.

The two dimensional angular correlation of annihilation radiation (ACAR) has been widely used in the study of condensed matters**. Now with newly developed

* See Chapter 2 for more details.

** See Berko 1983 and references cited for a review.

two dimensional position sensitive high efficiency γ-ray detectors and computer assisted data aquisition and image reconstruction facilities, ACAR has become a powerful and unique tool to study the bulk electronic structures and defects of condensed matters. As described above, if the annihilating electron-positron pair has an appreciable momentum in the laboratory frame before its annihilation, there would be a deviation from the anticolinearity of the two γ photons in the laboratory frame. By measuring this deviation, ACAR technique can give the detailed information of momentum distribution of electron-positron pairs in solid before its annihilation. After the positrons enter the bulk of condensed matters, they are slowed down by various collision and scattering process (depending on their energy) and thermalized in very short time (on the order of $\sim 10^{-12}$ second). An overwhelming majority of annihilation processes are involved with free or semi-free positrons with only thermal energy overlapping with electrons in the solid. As most of electrons in solid have much higher kinetic energy than thermal energy, the total momentum of an annihilating electron-positron pair is contributed mainly from that of the electron. Therefore, the electron momentum density in solid can be deducted from the measured momentum distribution of electron-positron pairs by ACAR. A two dimensional electronic structure in solid can be measured with 2-D ACAR. And three dimensional electronic structure can, in principle, be reconstructed with sufficient two dimensional measurements and sophisticated computer facility. The 2-D ACAR technique has been used to determine the electron momentum density and Fermi surface for different materials. The ACAR measurements are also sensitive to the presence of positronium in the bulk. It is known that positronium can not survive in the perfect or near perfect crystals of metal or semiconductor because of its high electron density, but the presence of positronium in insulator crystals, amorphous compounds, and crystals with high density of defect or vacancy have been reported. Those positronium atoms have very little kinetic energy, because majority of them are formed by thermalized positrons

and therefore have very low energy, and a few that had appreciable energy initially would lose the energy quickly through various collision and scattering processes. If the electron spin distribution in bulk is isotropic, one quarter of positronium would be para-positronium and three quarters of positronium would be ortho-positronium. Because of the low kinetic energy of positronium, the two γ photons emitted from para-positronium have little deviation from anticolinearity resulting a very sharp peak in the center of ACAR spectrum. The γ photons from decay of ortho-positronium would give rise to a very broad spectrum due to its angular distribution of three photon process. Therefore, the presence of positronium would be easily detected by ACAR, though quantitative analysis of positronium in the bulk with ACAR is rather complicated and, some times, extremely difficult. The triple coincidence measurement of three photon process (decay of ortho-positronium), on the other hand, has been very effective for quantitative measurement of positronium in bulk. The lifetime measurements are also employed to analyse the presence of positronium. Used with other techniques, ACAR has been a effective probe to study the electronic structures of a wide range of the materials. With the sucess of ACAR in the bulk applications, it's highly desirable to extend this technique to the surface study. But to do so, a high intensity mono-energetic low energy positron beam is required. The progress on the slow positron beams made it feasible to extend ACAR technique to the surface study. With the construction of several high intensity positron beams, the ACAR measurements have carried out at several institutions. The first ACAR measurement on a Cu(121) surface (Howell and others 1985) and an Al(100) surface (Lynn and others 1985b) not only proved the feasibility of this extended technique and its importance, but also provided some new important information about the positron interaction with surfaces studied and raised some new questions. Later, this technique was systematically applied to study the interactions of positrons with three low index surfaces of aluminum, Si(111)-(7 $\times$ 7), and Si(100)-(2 $\times$ 1) surfaces (Chen 1987, Chen

and others 1987, 1989). In this study, the effects of the adsorption of oxygen on Al surfaces and hydrogen on a Si(111)-(7 × 7) surface were also explored. The measurements of this study confirmed three important process taking place after the incidence of low energy positrons: spontaneous positronium formation and emission, positrons bound in a surface state, and thermally desorbed positronium atoms. Using the time reversal symmetry, Chen and others (Chen 1987, Chen and others 1987) showed that the momentum density functions of the positron surface state annihilation and bulk annihilation possess inversion symmetry with respect to the momentum **p**, i.e.:

$$\rho_{s.s}(\mathbf{p}) = \rho_{s.s}(-\mathbf{p}), \tag{1.5}$$

$$\rho_{bulk}(\mathbf{p}) = \rho_{bulk}(-\mathbf{p}). \tag{1.6}$$

But for the momentum density function of annihilating positronium,

$$\rho_{Ps}(\mathbf{p}) = 0 \quad for\ p_{\perp} > 0, \tag{1.7}$$

because the positronium formed on surfaces of metal and semiconductors are emitted into vacuum ($p_{\perp} > 0$ represents the Ps move into the bulk). Based on this theory, they developed a method to separate accurately components of surface state annihilation, bulk annihilation, and positronium formed at surface from experimental spectra of ACAR (Chen 1987, Chen and others 1987). With this new method they extrapolated detailed information of emitted Ps and surface state positrons. This information not only gave a better understanding of positron surface states, but also established that the momentum distributions of positronium emitted from surfaces are sensitive to the surface conditions and reflect the electron density of states near the surface, therefore a new surface spectroscopy, angle-resolved positronium emission spectroscopy, can be developed to study the surface electronic structure*. This is a further advance from the positronium velocity spectroscopy of the electronic density of states which

* See Chen 1987, Chen and others 1987, Chen and others 1989 for more detail.

was originally suggested by Mills and others (1983). This new approach was also used later on to study positronium emission from from a graphite surface being bombarded by slow positrons and to obtain what researchers believe to be an evidence for a new positronium emission mechanism, the phonon-assisted positronium formation (Sferlazzo and others 1988).

The time of flight (TOF) is another approach researchers have been taken to measure the momentum density of the positronium emitted from surfaces. The pioneer work was carried out by Mills and others (1983). Using a pulsed positron beam, they measured the velocity distribution of the positronium emitted from an Al(111) surface within 18° forward direction after 1-2 keV positrons are implanted into the surface. From their measurement, they concluded that the "fast" (not thermal) positronium formation process at a metal surface is not a adiabatic process but a sudden one in which the metal is left in an excited state and positronium energy spectrum shows a step extending from $-\phi_{P_s}$ (where ϕ_{P_s} is the positronium work function of the surface) toward lower energies. Furthermore, they pointed out this finding implies that positronium velocity spectroscopy can be an unique probe of the electronic density of states near the surface of a solid. This lay the foundation for both the later positronium velocity spectroscopy measurements on different surfaces and the angle-resolved positronium emission spectroscopy with ACAR described above.

The positronium velocity spectroscopy has been employed by various researchers to study a wide range of surfaces. Howell and others (1986, 1987) used this technique to study the positron interaction with surfaces of different metals. Using the pulsed intense positron beam generated by 100-Mev electron linac at the Lawrence Livermore National Laboratory, Howell and others (1987b) measured the velocity distribution of positronium emitted within a 30° half angle cone from clean, well-annealed, single-crystal surfaces of Al(111), Cu(100), Ni(100), and Au(100) after 2000 keV positrons

were implanted into those surfaces. They found that the energy spectra of emitted positronium from different surfaces have similar shape and the model proposed by Mills and others (1983) could explained the spectra reasonably well. But they also found some discrepancies between experimental measurement and theoretical prediction at low positronium energies spectra for Au and Ni. The detailed velocity spectroscopy of emitted positronium was also carried out for a Pb(100) surface which has positive work function for positron and smaller negative positronium work function (ϕ_{e+} = 2.06 eV and ϕp_s = -0.73 eV as compared to the negative positron work function and ~ -2 to -3 eV positronium work function for other metals surface described above) (Howell 1987a).

Using the same technique and experimental set up, Howell and others (1986) also measured the kinetic energy distributions of positronium emitted within 30° half angle cone from both the well annealed surfaces and the ion sputtered surfaces of Al(111), Cu(100), Ni(100), and Au(100) for different incident positron energies. From those measurement, they observed the positronium produced not only by the thermalized positrons picking electrons from the surface of metals, but also by backscattered positrons picking up electrons at the surface of metals especially in the cases where the incident positron energies are less than 100 eV. They thus confirmed the existence of the third mechanism for producing positronium at metal surface besides the two known mechanisms: positronium emission as the result of negative positronium work functions, and the thermal desorption of positronium from those positrons in the surface states, both of which are the results of thermalized positrons' diffusing back to the surface of metal. This new observation suggested that the correction should be made correspondingly when positronium fraction measurement technique is used to establish the positron diffusion profile and to measure the defect in the solid especially in the low incident positron energy cases. More importantly, it also suggested another possible approach to produce the energetic positronium atoms

(higher than positronium work functions). Gidley and others (1987) have pursue the idea even further. To enhance the effect of elastic back-scattering and reduce the effect of inelastic scattering especially for higher incident positron energies, they proposed and carried out the observation of positronium production "by scattering a well-collimated small-diameter beam of 30-400 eV positrons off surfaces of Al(110) and clean and oxygen-coated Cu(100) at glancing angles of 6°-42° with respect to the surface." They measured the angular distribution of the emitted positronium atoms and its FWHM of 20°. They also measured relative Ps formation efficiency as function of incident energy and incident angle and found it to be at order of 3% - 5% (Gidley and others 1987). Their finding indicated that it may be feasible to construct an energetic positronium beam using glancing angle scattering of positrons mechanism.

The positronium velocity(or "time of flight") spectroscopy has also been used to study the single crystal insulator compounds such as SiO_2, MgO, and alkali halides crystals (Sferlazzo and others 1987, Tuomisaari and others 1989). It is known that positronium can be formed in the bulk of many wide-band-gap insulators in contrast to the cases of metals and semiconductors in which positronium can only be formed at the surface due to the high density of conduction electron in the bulks. Sferlazzo and others (1987) measured the kinetic energy distribution of positronium emitted from SiO_2 and MgO single crystal surfaces bombarded by 500-900 eV positrons. While a delocalized, excitonic-like positronium Bloch state has been observed in SiO_2, no Bloch state positronium has been reported for MgO. The researchers found the kinetic energy distribution of the emitted Ps have different characteristics as well. A nearly mono-energetic component at 3.27 ± 0.4 eV along with a broader component of $\sim$1.5 eV FWHM were observed in the spectrum for SiO_2, while a much broader energy distribution was observed for MgO. For SiO_2, the researchers attribute the large portion (40-60%) of the Ps yield to the emission of bulk positronium diffusing to

the surface and being ejected with the energy of negative work function and smaller portion (15%) of the Ps yield to the thermal activation of physisorbed positronium. For MgO, however, the positronium emission could be only speculated to be largely due to the electron captures of epithermal positrons escaping from MgO. It was expected by the researchers that the further verification would be carried out by the future ACAR measurement. Using same apparatus at Lawrence Livermore National Laboratory and same technique employed for the study of velocity spectroscopy of the positronium emitted from metal surfaces after positron bombardment, the researcher (Tuomisaari and others 1989) measured the energy and angular distribution of the positronium emitted from the surfaces of the single-crystal alkali halides LiF, NaF, KCl, KBr, and KI which were bombarded by the 0.1-4 KeV positrons. They found that positronium was emitted from these surfaces primarily normal to the surface with a very narrow angular spread and a narrow energy distribution around a single peak in most of cases, with exception of LiF surface. The angular distribution of positronium emitted from LiF surface was found to be nearly isotropic limited by $\cos\theta$ and the energy distribution of positronium emitted from LiF surface was found to be much broader with two distinct energy components instead of a narrow single peak as in the cases for other alkali halides surfaces. From their finding they concluded that most of the positronium emitted from the alkali halides single crystal surfaces following positron implanted into these surface was formed in the bulk by capture of a valence electron, subsequently diffused to the surface, lost the energy in the process, and eventually was ejected from the surface with added energy of negative work function; the additional higher energy group of positronium atoms emitted from a LiF(100) surface was probably formed by the conduction electron captured by the positrons leaving the surface (spur process).

Using the phenomenon of positronium emission from metal surfaces bombarded by positrons, Gidley and others (1982) demonstrated the feasibility of using polarized

low energy positron beam as a new probe to study the surface magnetism. By measuring the asymmetry in formation of the triplet spin state of positronium, orthopositronium, on Ni(110) surface when either the Ni magnetization or the positron beam polarization was reversed, they deduced the polarization P_{e^-}, of electrons captured at the surface. The temperature dependence of P_{e^-} that they measured was in qualitative agreement with calculations of the critical exponent for the surface-layer magnetization. They also found that their measurements were very sensitive to an adsorbed mono-layer of oxygen on the sample surface. Their observation strongly suggested that a polarized low energy positron beam could be developed into a potentially very surface sensitive probe for the surface magnetism.

Another example of the positron's applications in solid state surface study is the low energy positron diffraction (LEPD), a technique similar to the well established low energy electron diffraction. The technique of low energy electron diffraction (LEED) has been widely accepted as a very useful tool to study surface structures of single crystals and to characterize surface conditions of a given sample (Pendry 1974). By analyzing the LEED data and comparing it with the simulation results of various theoretical model, one can, in principle, obtain the detailed information such as atomic positions near or at the surface of the sample including the possible surface or near surface reconstruction or relaxation, the long range ordering and symmetry of the sample surface, and the surface binding with or without adsorbates. The complexity of the model simulation caused by the multi-scattering from the sub-surface layers, and the lack of the accurate and effective treatment of the many indistinguishable body system that one has to face in the practical data analysis and data fitting with various theoretical model, however, make it almost impossible to use the LEED technique to its full potential and to identify all the surface structures unambiguously with the LEED alone, in spite of the enormous success of LEED in providing valuable information for various surface studies. It is, therefore, desirable to develop other

techniques which would give the information about the surface complementary to that from the LEED. It would be more beneficial if the other technique developed would share some similarity with the LEED so that certain comparison could be made and some insight into the interaction of the probes with the samples could be gained. The positron low energy diffraction (LEPD) seems to fall into this category. With its absence of exchange interaction with the electron in the solid, its different correlation effects in the solid, and strong repulsive core potential they encountered instead of strong attractive core potential for electrons, LEPD seems to be an ideal complement for LEED.

The efforts to develop this new probe have been reported after the mono-energetic positron beams became more widely available. In their measurements of specular reflection intensity of positrons versus incident beam energy, Mills and Platzman (1980) observed a single large maximum ~3.5 eV wide peaked near the expected first Bragg peak energy in the specular (0,0) beam spectrum from Cu and Al (111) surfaces. They also qualitatively analyzed this and their other observation including the smaller Bragg peaks for Al(110) and Al(100) and the absence of higher order peaks in their spectra. Around the same time, Rosenberg and others (1980) measured the scattered intensity of positron from a Cu(111) surface versus scattered angle and incident energy of positrons. They detected peaks at the predicted $(0,\bar{1})$ and $(0,\bar{2})$ diffraction angles and observed the maxima corresponding to the primary Bragg peaks in their experimental profiles of diffracted beam intensities versus energy. Weiss and others (1983) continue their research effort and reported more detail measurements including additional data on Cu(100) surface. They also compared their measurement with a theoretical model and further discuss the potential of LEPD as a surface-structure probe. Cook and others (1984) applied this technique to a clean single crystal LiF(100) surface. They measured the intensity profile for the elastic specular reflection of 5-100 eV positrons from a LiF(100) surface (with incident an-

gle and reflection angle at 45°) with their time of flight set ups and found several maxima in their profile. Mills and Crane (1985) systematically measured the specular reflection intensity as a function of the incident energy of positrons on different alkali halides surfaces and observed strong first-order Bragg peaks and several higher-order peaks. All these observations clearly indicated the feasibility of LEPD as a practical surface study tool complementary to LEED. It is also clear through these efforts that a high quality (electrostatically guided) low energy positron beam with its characteristics comparable to the typical low energy electron beam used in conventional LEED is needed for actual application in surface studies and for a comparison with LEED measurements. New efforts have been made to construct such a beam and to use it for LEPD measurements. Two beams capable of generating both positron and electron beams with 1 mm deg. phase space in low energy range (~20-200 eV) were reported (Frieze and others 1985, Canter and others 1987). With such a beam at Brookhaven National Laboratory, Mayer and others (1987) made a detailed comparison measurement of LEPD and LEED for a Cu(100) surface. The information of the surface structure which they obtained through their data analysis was consistent with the information obtained using other techniques. Their experimental results also confirmed the earlier observation of Weiss and others (1983) that inelastic scattering for positrons is much stronger than that for electrons. Horsky and others (1989a) applied LEPD in conjunction with LEED to determine the relaxed atomic geometries of the semi-conductor CdSe cleavage surfaces. They found that their LEPD analyses gave the relaxation structure parameters for two cleavage faces by optimal fit at values different from those given by analyses of LEED measurements which they carried out on the same surface under the same condition. Furthermore, their LEPD measurements yielded significantly better agreement between theoretical and experimental intensity profiles (I-V curves) than their LEED measurements did. Horsky and others (1989b) also reported the first evidence for threshold effects, or surface state resonance (as it

is sometime called), in their LEPD measurements on the (100) surfaces of NaF and LiF. These late developments clearly indicated that the LEPD technique is gradually maturing and yet, its potential in surface study is still waiting to be fully realized by future efforts. The results from those experiment confirmed the early expectation of the researchers that LEPD would reduce the complexity of the data analysis encountered by LEED due to its lack of exchange interaction with electrons in the solid and its stronger inelastic scattering effect, and thus could enable researcher to obtain the surface structure information complementary to the that from LEED. They also provide researchers some insight and deeper understanding of both LEED and LEPD techniques.

The research efforts and observations described above are just a fraction of the progress taking place in the growing field of the surface research with mono-energetic positron beams. There is a number of novel techniques and experiments such as positron microscope recently developed independently by Brandes, Canter, and Mills (1988) at Brandeis University and House and Rich(1988) at University of Michigan, positron Auger experiment(Weiss and others 1988), and positron internal total reflection at solid vacuum interface(Britton and others 1989), which is not described in this thesis. A few examples given above, however, clearly demonstrated the wide range of application of mono-energetic positron beams in the surface research. And more importantly, these examples also showed the importance of the efforts involving developing new techniques of the surface research with positrons.

The surface research is not the only field benefited from the availability of the mono-energetic positron beam. With a variable mono-energetic positron beam, valuable information about different interfaces and multilayer films can be obtained (Schultz and Lynn 1988). The development of low energy positron beams also made some novel experiments such as positron trapping (which could lead to production of

positron plasma and anti-hydrogen,)(Surko and others 1989) and positron channeling possible(Andersen and others 1971, Schultz and others 1988). Another field benefited greatly from the development of positrons is atomic physics. For example, the mono-energetic positron beam has made the systematic studies of the positron-gas scattering, the positronium formation in gases, and the positronium-gas scattering possible*; it also has provided a tool for fundamental study of positronium. (The positronium formation will be discuss in more detail in Chapter 2.) The progress made in understanding of positronium formation from solid surfaces, in thin films, and in gases with the use of mono-energetic positron beams raised the possibility of using positronium, a light atom with the mass of only twice of that of an electron, for surface research.

Various kinds of particles, such as photons of different energies, atoms, ions, neutrons, electrons and positrons, have been employed for the surface studies. A few common approaches including the study of the scattering, absorption, luminescence and re-emission or emission of other particles from the surfaces following the incidence of one or more types of particles. Among them, the surface scattering studies have been proved to be very effective and fruitful in gaining the understanding of various surface characteristics such as the surface ordering (including the surface reconstruction and relaxation), surface binding, and interactions between surface adsorbates and their substrates. A few examples of the probes used in the surface research are low energy atoms and ions scattering, low energy electron diffraction, low energy positron diffraction, neutron scattering, and X-ray scattering. The scattering study of each kind of particles, however, has its limitation due to the characteristics of the particle employed. It is very common that several probes have to be utilized to obtain sufficient information about the surfaces in question. It is almost always desirable to

* See Stein and Kauppila 1982, Charlton 1985, Dupasquier and Zecca 1985, and the proceedings for various recent workshops or conferences on interactions of positrons with gas.

have additional probes available for the further understanding of the surface studied. It is motivated by this very reason, the positronium surface scattering and low energy positronium diffraction was proposed (Canter 1984) and the research project of this possible new probe was initiated by the researchers of the consortium: Berko, Canter, Lynn, Mills, and Roellig.

Ideally, a surface probe should interact with atoms or ion cores on the top layers with strong enough cross section so that this scattering can be effectively detected, yet not too strong so the theoretical calculation would not have to deal with the difficulties and complications of the multi-scattering process. It also should have no or little interaction with the atoms or ion cores in the bulk so the signals detected is the one reflecting the surface structure not that for the bulk. It also should have the characteristic wave length in the same range as the typical interatomic spacing length in the solid so researchers would be able to deduct the surface structure information from the experimental data. An ideal probe with this wave length should also have the energy to penetrate the surface potential to interact with the individual atoms or ion core on the top layer of a sample. At present, there is no such an ideal surface probe available. But efforts have been made to develop some probes which possess most of the characteristics described above and to develop techniques which would compensate some probes' lack of certain desirable characteristics.

In the case of LEED (Pendry 1974), the low energy electrons are scattered by electrons and ion cores in the top few layers of a sample with reasonable high cross sections. They also have a reasonably short inelastic mean free path (IMFP) so the electrons back-scattered to the surface are those scattered mainly by the ion cores near the surface, yet the IMFP is long enough so the coherence diffractions from the different layers are possible. The structures and atomic binding information, in principle, can be deducted from the LEED patterns and I-V curves from different

diffracted beams. The difficulties one would face in application of LEED would be the task of dealing with a many body system, the exchange interactions, and the multi-scattering process. Various theoretical models have been established to simulate the LEED spectra from different crystal faces of single crystals samples with the surface structure as the variable parameters so they can be compared with experimental spectra and thus the actual surface structure can be determined. This approach enable researchers to obtain a lot of valuable information about the surface structure of various single crystals and adsorbates on these surfaces despite the complexity of the probe. Because of the multi-scattering effect due to the Coulomb interaction of incident electrons with ion cores and atoms in samples, computing difficulties in dealing with the exchange interaction of electrons, a many body system, and multiple parameters of the surface structures, it is quite often difficult to obtain the accurate information of the surface structures or adsorbate structure unambiguously through the interpretation of the experimental data of LEED. The complication is reduced in the analysis of low energy positron diffraction data because of lack of the exchange interaction of incident positrons and shorter IMFP. LEPD computations have found to fit experimental data on surfaces of CdSe better than that for LEED (Horsky and others 1989a). While LEPD can provide some valuable information of surface structure complementary to LEED, it is still limited by the complication in the spectra computation due to the multi-scattering effect and the multi-parameters of the surface structure.

Another type of the commonly used probes is the atom scattering and diffraction from surfaces, such as the helium diffraction and scattering from surfaces, which has been a very powerful tool to determine the surface structures, surface ordering, and surface phase transition of samples (Hoinkes 1980 and Dunning 1989). To be sensitive to surface structures, the de Broglie wavelength of the incident atoms has to be in the order of interatomic spacing which is on the order of $\sim$1 Å or longer and

corresponding to energy on the order of ~0.02 eV for helium. In this energy range, the incident atoms are incapable of penetrating the surfaces, and, therefore, are sensitive to the surface conditions. The atoms with such low energy can not approach the ion cores very closely, instead, they are scattered mainly by the corrugated averaged surface potential and form a diffraction pattern which reflects the corrugation on the surface. Since the corrugation reflects the surface geometrical arrangement with or without adsorbates, and also reflects the ordering or ordering change on the surface, the information about the surface structure, surface adsorbates, and surface ordering can, in principe, be deducted. The corrugation of the surface potentials for metals are much weaker than those for semiconductors or insulators because the repulsive potential which scatters and diffracts the incident atoms are mainly due to the overlapping of the electron wave functions of the incident atoms and those of electrons on the surface, and the electrons are not strongly localized in the metals as those in the semiconductors or insulators. The application of this technique, in some case, has been hampered by the difficulties in obtaining an accurate treatment of the atom-surface interaction potential. The surface states of the incident atoms at such low energy also complicate the theoretical treatment, though some interesting information about surface can sometime be obtained through analysis of the atom-surface scattering pattern under the surface resonance condition. This probe is also not sensitive to the dynamics properties of crystal structures because the incident atoms are incapable of getting sufficient close to the ion cores.

The another example of neutral probes is the neutron scattering (McTague and others 1979). Since the scattering cross sections of neutrons with atoms, electrons, or ion cores are very small, the difficulty in dealing with multiple scattering would be avoid in the computation for neutron scattering case and the probe can penetrate the ion cores or atoms, therefore, it is sensitive to the dynamic properties of the nuclear motion. For the surface studies, the diffraction signals from the bulk can

often be filtered out by selecting the detecting region of k space. This advantage made the neutron scattering a very good candidate to be a probe for study of adsorbed monolayers on different surfaces. The low level of signal that is caused by extremely small value of the scattering cross section can be partially compensated by employing finely divided substrate samples with a large total surface area (typically $\sim 10^3$ m^2) and a high flux neutron beam. This technique has been employed to study the structure, dynamics, and phase transition of ideal physisorbed and chemisorbed films on a large uniform substrate. But its application to broader range of study is limited by the lack of the substrates with large uniform surface areas which are necessary for the determination of structure and collective dynamics of monolayer adsorbates with this probe.

The X-ray surface scattering and diffraction, one of the newly developed surface probes, has been used successfully in studies of surface structure, surface adsorbates, and surface ordering (such as surface roughing and surface melting). It fulfills many of the requirements of an ideal surface probe (Feidenhans'l 1989 and Robinson 1990). Similar to the case of neutron scattering, the difficulty involving the multiple scattering process is eliminated because of small scattering cross section of X-rays with electrons, ion cores, and atoms; the signals from the bulk can be filtered out by selecting the detecting region in the k space; the probe is sensitive to the dynamics of the atoms or ion cores on the surface. Yet, the higher cross section of X-rays (higher than that of neutrons), the reasonably high reflectivity at the near glancing angle (which is due to the fact that the refraction indexes of most material for X-rays are slight lower than that of vacuum), and, most importantly, the growing access to a synchrotron X-ray facility which offers high flux (a few order higher than conventional rotating anode sources) and high resolution X-ray beam have made this probe much more feasible for a wide range of surface studies than neutron. The range of the researches with this probe is still expanding rapidly. The success of the X-ray surface

scattering is a proof that surface probes which possess most of the characteristics of an ideal surface probe can be developed.

The positronium atom had been proposed as a potential surface probe (Canter 1984). As a neutral weakly bound light particle, it has a few appealing characteristics which may be very helpful in surface studies. It is much lighter than common atoms (about three order of magnitude less in mass), which would make it much more energetic than common atoms like helium and argon for same de Broglie wave length. For example, the energy of positronium having de Broglie wave length of 1 Å (which is the same order as that of interatomic spacing on the surface) is ~75 eV comparing to 0.02 eV (2 meV) for helium (argon) having same de Broglie wave length. Thus the positronium with required wave length is capable of approaching the ion cores very closely and therefore is sensitive to the detailed and localized structure or ordering of the studied surface. It is a neutral particle so its long range interaction with electrons or ion cores is expected to be weaker than the coulomb interaction as is the case for electrons, positrons, or ions. It is also weakly bound with 6.8 eV binding energy in vacuum. It can be easily ionized (break up) during the collision with electrons, ion cores, and atoms when their relative kinetic energy is greater than positronium's binding energy. Positronium can also easily lose its kinetic energy to electrons through elastic collision process because its mass is only twice of that of a electron and large momentum transfer is possible. These effects ensure that the positronium atoms elastically scattered (without losing their kinetic energy) back from a surface are those that are only elastically scattered by the surface potential or/and ion cores or atoms at top layer of the surface, as those which penetrate deeper into the surface would either break up or lose their energy and therefore attenuate away. This makes positronium surface scattering and diffraction a potentially promising surface probe. Furthermore, it is also believed that positronium can not exist in the single crystal of metals or semiconductors except in those with the high density of local inhomogeneity such

as defects, grain boundaries, or interfaces, because of the relative high density of electrons in those single crystals. Thus the positronium scattered back from the surface of single crystals of metals or semiconductors would only reflect the surface conditions of these crystals.

To fully estimate the potential of the low energy (1–100 eV) positronium as a surface probe, information about the scattering process of positronium with electrons, ion cores, and atoms is needed. The information about the surface positronium interaction potentials of samples is also needed. Unfortunately, there are only a few works carried out in this area. Several calculations have been carried out to estimate the scattering cross section of positronium with free electrons for energy range below the positronium binding energy (Ward and others 1987, Melezhik and Vukajlović 1988). There is also an estimate of the ionization cross section of positronium in the collision process with free electrons (Peach 1989). A model of weakly physisorbed positronium at metal surfaces was proposed (Platzman and Tzoar 1985, 1986) to explain the thermally desorbed positronium from metal surfaces, an effective positronium surface interaction potential was also proposed in the model. A possible approach was also proposed to calculated the positronium break up probability in the solid state samples (Ishii 1988). The positronium-hydrogen (Fraser 1961a, Hara and Fraser 1975, Drachman and Houston 1976) and positronium-helium (Fraser 1961b, Fraser and Kraidy 1966) elastic scattering cross sections in low energy range were also calculated. However, much more detailed information than those few available is needed to appraise this probe theoretically. The experimental approach, however, had been becoming more and more feasible as a high intensity mono-energetic positron beam was developed and became available at the Brookhaven National Laboratory and various energetic positronium formation processes were studied.

A positronium beam was constructed at Brookhaven National Laboratory (Roellig

and others 1987) to explore the potential of this new probe, the positronium surface scattering and low energy positronium diffraction. An experimental effort has been made to measure the positronium reflections and scattering from the single crystal (100) surfaces of LiF (some of the measurements on the LiF(100) surface were reported by Weber and others 1988) and Cu at different conditions. The measurements of energetic positronium emission from the surfaces following the positrons' impact were also taken. My thesis research project is an integral part of this experimental effort. I have participated in and contributed to the construction and operation of the mono-energetic positronium beam, and all the measurements taken with this beam.

In next part of the thesis, our effort to develop this new probe will be described. Chapter 2 of this thesis will describe the high intensity mono-energetic positron beam in the High Flux Beam Reactor (HFBR) at BNL, with which the project was conducted. It will also discuss the production of energetic positronium atoms. The mono-energetic positronium beam we constructed at HFBR with the HFBR positron beam will be described in detail. Some of the underlying principles for the production of mono-energetic positrons and positronium atoms will also be discussed. The experimental apparatus for our positronium surface interaction studies will also be described in this chapter. The experimental measurements would be presented in Chapter 3, which will include the positronium reflection measurement from a LiF(100) surface, the preliminary positronium scattering measurement from a Cu(100) surfaces, and some positronium emission measurements from these two surfaces following the low energy positron bombardment. The data represented in chapter 3 will be analyzed and discussed in Chapter 4. Some simple theoretical models for the experiment will also be offered and discussed in this chapter. The last chapter will summarize our effort, and describe the ongoing work in the continuous effort to study the interaction of positronium with surfaces. Some suggestions for future research will be offered at the end of this chapter.

Chapter 2
THE EXPERIMENTAL APPARATUS AND TECHNIQUES

Since the first production of the moderated mono-energetic positrons (Cherry 1959), the research activity with slow positrons has been steadily growing. The full scale application of the low energy mono-energetic positron beam, however, was not realized until the later part of the seventies when the positron moderators with efficiency as high as 0.1% was developed and implemented into actual positron beams. As more and more positron beams with reasonable high intensity were constructed, more and more positron research projects are becoming feasible, some of these projects have been carried out. It is the development of the high intensity mono-energetic positron beam, in particular the construction of the high intensity mono-energetic positron beam with the flux of $1 \times 10^6 \sim 1 \times 10^8$ e^+ /sec at the High Flux Beam Reactor (HFBR) at BNL, and the results of the recent research activities on positronium production that made our positronium surface reflection and scattering experiments feasible. In this chapter, the high intensity positron beam at HFBR and the first positronium beam constructed at HFBR utilizing the HFBR high intensity positron beam, with which this research project was carried out, will be described. The experimental set ups, samples used and its preparations will also be reported and discussed.

§2.1 The HFBR High Intensity Positron Beam

A high intensity positron beam was constructed at High Flux Beam (Neutron) Reactor (HFBR) of BNL to take advantage of the high flux thermal neutron available

at HFBR. Through the neutron capture process, a portion of Cu^{63} irradiated in the HFBR would be converted to radioactive Cu^{64} which emits positrons through β decay process. Using the radioactive copper itself as self-moderator, or a thin single crystal tungsten foil as a transmission moderator, a large amount of mono-energetic low energy positrons can be produced. With a proper set of positron extraction lens, a positron energy filter, and a low loss positron guiding set up, the HFBR beam can deliver mono-energetic positrons at flux of $10^6 \sim 10^8\, e^+$/sec.. The HFBR high intensity positron beam has been described in details with a quantitative analysis in some publications and writings before (Lynn and other 1987, Weber 1988). In the following description of the beam, more emphasis will be put on qualitative discussion of its characteristics and the underlying principles involved. Some modifications made after those publication will also be reported here.

2.1.1 The positron sources — Two types of positron emission processes are commonly utilized to generate the positrons for the research need. One of them is the β^+ decay process, the other one is the pair production process. The utilization of the β^+ decay process usually involves the use of radioactive nuclei like Na^{22}, Co^{58}, and Cu^{64}; the utilization of pair production is usually achieved with the bremsstrahlung of a high energy ($\gg 2\, m_e c^2$) electron beam, generated by a LINAC, hitting a target.

The most widely used positron sources are the radioactive nuclei such as Co^{58} and Na^{22} which have reasonable long life time (half life time is 71days and 2.6years for Co^{58} and Na^{22} respectively) and are commercially available in small and medium activity. Cu^{64} is not widely used due to its fairly short life time (the half life time for Cu^{64} is 12.8 hours), though it have been used occasionally in some experiments. The positron beams which use these radioactive isotopes as their sources do not require to be located close to the big facility and can be constructed almost anywhere. But their intensities are limited by availability of commercial isotopes and are restricted

due to the safety hazard in the source installation for high activity sources. A LINAC based positron beam, on the other hand, can deliver high intensity pulsed positrons. Several LINAC based high intensity pulse positron beams have been constructed and have been used for various positron research (Howell and others 1982, Graff and others 1984). The effort to further improve the efficiency of positron production by LINAC (Dorikens and others 1987) and to increase the time resolution of the pulsed positron beam (Mills 1989) were reported. The accessibility to a LINAC can sometimes be difficult to obtain and the space limitation in a typical LINAC also can limit the range of the experiments that can be carried out with this type of positron beams.

Another approach to increase the positron beam intensity is to produce high activity β^+ isotopes with a cyclotron or a neutron reactor. Some efforts to produce high purity Na^{22} with a 18 MeV cyclotron were reported recently (Saam and others 1989). At Brookhaven National Laboratory (BNL), high activity Cu^{64} was successfully produced by irradiating Cu^{63} in the HFBR at BNL and was used as the positron source for the high intensity beam. The thermal neutron capture process Cu^{63} (n_o, γ) Cu^{64} (where n_o represents thermal neutrons) was utilized in this production.

The decay scheme of Cu^{64} is shown in Fig. 2.1.1. Even though the short life time of Cu^{64} limits the maximum amount of Cu^{64} per gram of the irradiated copper and makes it necessary to change the source about every other day, the high flux of thermal neutron available in the irradiation ports at HFBR makes it possible to produce the sufficient high activity for our beam, and our remote controlled source transportation and preparation set up was designed to protect researchers from any radiation hazard and to be used frequently. The short life time also allows the researchers to carry out the necessary maintenance activity in the source area safely without having to wait for a long period of time. Table 2.1.1 lists some of properties of copper isotopes which are important for our source preparation.

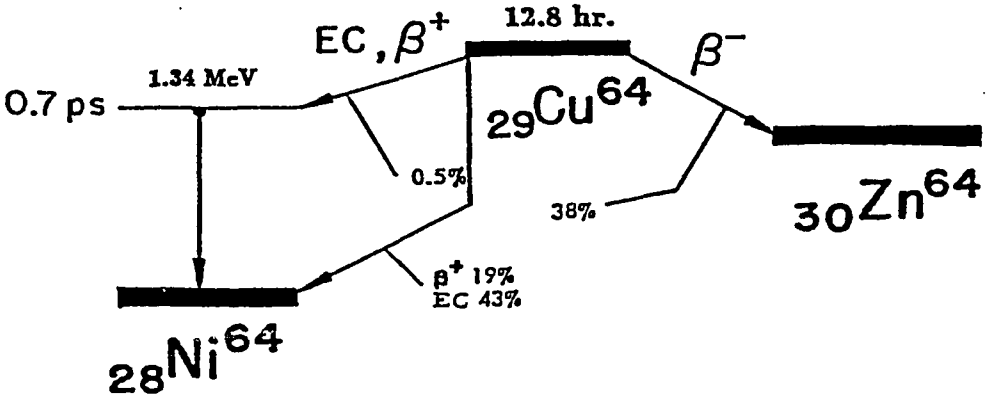

Figure 2.1.1 The decay scheme of Cu^{64}.

(from Lederer and others 1967.)

Table 2.1.1 some properties of copper.

melting point	1083°C
boiling point	2595°C
abundance of Cu^{63}	
in natural copper	69.1%
atomic weight of natural Cu	63.546 grams/mol
atomic weight of Cu^{63}	62.92959 grams/mol
production of Cu^{64}	Cu^{63} (n_o, γ) Cu^{64}
thermal neutron capture	
cross section of Cu^{63} σ	$4.5 \times 10^{-24} cm^2$
half life time of Cu^{64} $T_{1/2}$	12.8 hours
β^+ fraction	19% of decay

The flux of thermal neutrons in the port of HFBR where our copper pellets were irradiated is:

$$f = 8.3 \times 10^{14} n_o \, / \, cm^2 sec. \qquad (2.1.1)$$

So the production rate λ_p for Cu^{64} per Cu^{63} atom is:

$$\lambda_p = f \cdot \sigma = 8.3 \times 10^{14} \times 4.5 \times 10^{-24}/sec = 3.735 \times 10^{-9} \; / \, sec. \tag{2.1.2}$$

And the decay rate λ_d for Cu^{64} is:

$$\lambda_d = \frac{\ln 2}{T_{1/2}} = 1.504 \times 10^{-5} \; / \, sec. \tag{2.1.3}$$

If we let N_{63} and N_{64} represent the number of Cu^{63} and Cu^{64} respectively, then the changes of copper in the reactor port can be described as:

$$dN_{63} = -\lambda_p N_{63} \, dt \, ; \tag{2.1.4}$$

$$dN_{64} = (\lambda_p N_{63} - \lambda_d N_{64}) \, dt \, . \tag{2.1.5}$$

The solution for above equations are given by:

$$N_{63}(t) = N_{o63} \, e^{-\lambda_p t}, \tag{2.1.6}$$

$$N_{64}(t) = N_{o63} \, \frac{\lambda_p}{\lambda_d - \lambda_p} \, e^{-\lambda_p t} \left[1 - e^{-(\lambda_d - \lambda_p)t} \right] , \tag{2.1.7}$$

where N_{o63} is the initial number of Cu^{63}. So the activity $R(t)$ after time t is:

$$R(t) = N_{o63} \, \frac{\lambda_p \lambda_d}{\lambda_d - \lambda_p} \, e^{-\lambda_p t} \left[1 - e^{-(\lambda_d - \lambda_p)t} \right] . \tag{2.1.8}$$

If n is the number of Cu^{63} atoms per gram, then the activity per gram $r(t)$ after time t is:

$$r(t) = n \, \frac{\lambda_p \lambda_d}{\lambda_d - \lambda_p} \, e^{-\lambda_p t} \left[1 - e^{-(\lambda_d - \lambda_p)t} \right] . \tag{2.1.9}$$

The time needed for the maximum value of the activity is:

$$t_{max} = \frac{1}{\lambda_d - \lambda_p} \ln\left(\frac{\lambda_d}{\lambda_p}\right) = 6.39 \text{ days}. \tag{2.1.10}$$

For natural copper, only 69.1% of it is Cu^{63}. Fortunately, there is isotopically enriched Cu^{63} with abundance of $Cu^{63} > 99.7\%$ commercially available from the Oak Ridge National Laboratory. While most of our experiments were carried out with the source produced from isotopically enriched Cu^{63}, the natural copper was also used to cut the cost whenever the increase by enriched Cu^{63} was not absolutely necessary. With Cu^{64}, only 19% of the activity result in the emission of positrons. The remainder of the decay is through β^- decay and electron capture process. Taking the β^+ fraction into the consideration, one can get that the maximum positron activity per gram of isotopically enriched Cu after the neutron irradiation is

$$r^+_{max} = 182.96 \text{ Curie } e^+ \text{/gram.} \tag{2.1.11}$$

The Fig.2.1.2 shows the positron activity of the source produced from isotopically enriched Cu^{63} irradiated in the irradiation port at the HFBR as a function of the irradiation time. The activity increases very fast at the beginning of the irradiation. A high percentage of the maximum activity can be reached in the first two days, as:

$$r^+(2days) = 169.64 \text{ Curie } e^+ \text{/gram} = 92.7\% \text{ of } r^+_{max}. \tag{2.1.12}$$

In our experiments, a pellet of 100 $\sim$ 120 mg isotopically enriched Cu^{63} was irradiated for two days in the irradiation port at HFBR before being transported into our source chamber. This pellet would be prepared following a standard process that will be describe later to make our positron source which would last for two to three days. The activity of this type of the source would be about 17 to 19 Curie e^+. But only estimated 30% to 50% of this activity can be utilized for the reasons will be give in the later part of this section.

2.1.2 The moderation of fast positrons— The positrons generated by a β^+ process or a pair production process are emitted over a very broad spectrum of energy. A wide range of positron research projects relies on the use of mono-energetic positrons. As

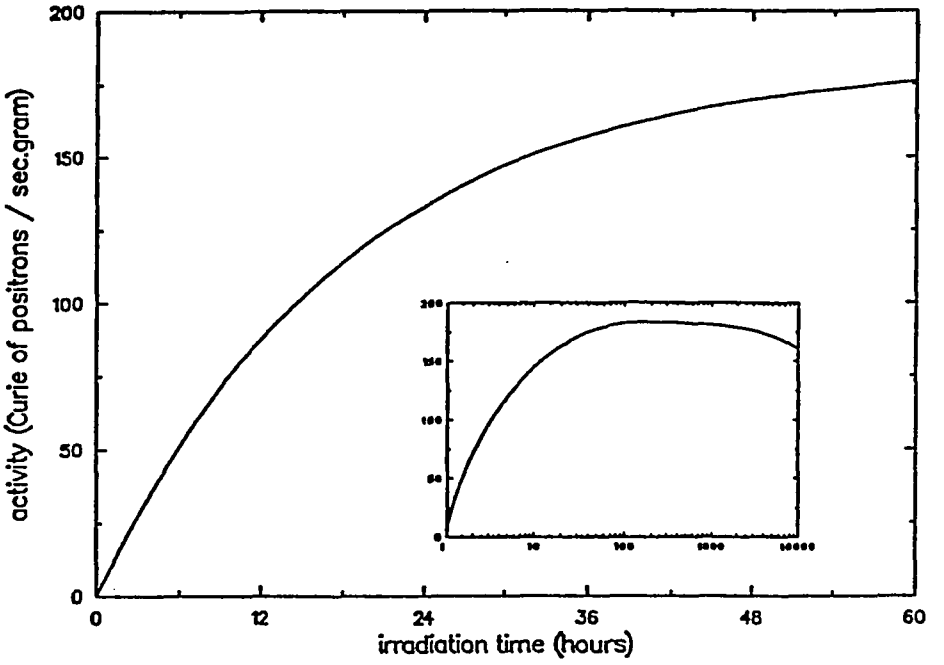

Figure 2.1.2 The positron activity per gram of the copper source produced by irradiating the isotopically enriched Cu^{63} as function of irradiation time. The main figure shows the increase of the activity during the first 3 days of irradiation. The insert illustrates its over all time dependence: a fast increase at the beginning, a long plateau after the maximum, and slow falling as Cu^{63} being exhausted by the process.

being described in Chapter 1., there have been continuous efforts to develop efficient methods to moderate those fast positrons*.

The most commonly used approach of moderating positrons is to slow down these fast positrons in a crystal via various excitation and inelastic scattering process. Most

* See chapter 1 for description of some of the research efforts and progress in developing positron moderators.

of these fast positrons are thermalized within first 10^{-12} second (with the exception of the solid Ne moderator). Some of these thermal positrons will diffuse to the surface of the solid if diffusion length of the solid is sufficient long and implantation of positrons into the solid is not too deep. For some of crystals surfaces, the work function of positron are negative. Therefore, some of the thermal positrons diffused to these surfaces would be emitted from these surfaces with a maximum energy equal to negative value of work function. A illustration of this process can be seen in Fig. 1.1.

To estimate the efficiency of a moderator, which is usually defined as the ratio of detectable positrons re-emitted from the moderator to the number of positrons generated by the radioactive nucleus source, and characteristics of the moderated positrons, some quantitative information on positron implantation in the moderators, positron diffusion length in the moderators, positron work function of the moderators' surfaces, and positron re-emission coefficient (the ratio of the number of the re-emitted positrons to the total number of the positrons diffusing back to the surface) of the moderators' surfaces is needed.

When a positron enters a surface, it will be quickly slowed down by losing its energy through various processes such as core excitations, inelastic scattering with electrons in solid, and plasmon excitations. Implantation probability can be loosely defined as the probability per unit distance of a positron being thermalized at distance z from the surface it entered. To a good approximation the implantation probability for a β^+ can be expressed as (Brandt and Paulin 1977, Mills 1979, Beling and Charlton 1987):

$$P_{imp}(z,\theta) = \alpha \sec\theta \, e^{-\alpha z \sec\theta}, \qquad (2.1.13)$$

where θ is the angle of the incident positron momentum with respect to the surface normal and α is the attenuation coefficient of the moderator materials for the β^+

spectrum, which can be empirically expressed as function of density of the moderator, ρ, and endpoint energy, E_{max}, of β^+ spectrum with emperical constant A as:

$$\alpha = A\rho \Big/ E_{max}^{1.14}. \tag{2.1.14}$$

After these fast positrons are thermalized, they will diffuse in the solid within their free diffusing lifetime τ (typically about 100 – 200 psec.) before they annihilate with electrons in the solid, some of them may diffuse to a surface of the solid if the surface is not too distant away(within the diffusion length l_d). The probability of the positrons diffusing to the surface, P_d, can be express as a function of l_d and z', the distance between where positrons being thermalized and the surface concerned (it may not be the same surface where positrons enter the solid), as:

$$P_d(z') = e^{-z'/l_d}, \tag{2.1.15}$$

where $l_d = (D\tau)^{1/2}$ is the positron diffusion length and D is the diffusion coefficient of the positron in the material.

For those thermal positrons which diffuse to the surface, their fate are determined by several factors including the surface electronic structure, the positron work function of the surface, and the surface condition (like the density of surface defects and impurity). The electron work function ϕ_- was defined, when concerning the photo-electric effect in the twenties, as the minimum energy required for an electron to escape from a surface. It includes the contributions both from the bulk, namely electron's chemical potential μ_-, and the surface, namely the surface dipole barrier D. The positron work function ϕ_+ is defined in exactly the same way as that for an electron, where μ_- is replaced by μ_+, which includes the the repulsion part from the ion cores and the attraction part from the electrons in the crystal, and the effect of the surface dipole barrier D is negative instead of the positive effect that electrons

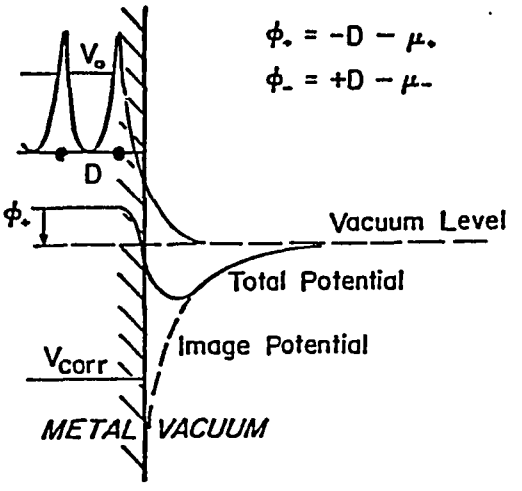

Figure 2.1.3 The single-particle potential for a thermalized positron at the surface region with a negative positron work function. The positron chemical potential includes the attractive correlation potential V_{corr} (from the conduction electrons in the crystal) and the repulsive zero-point potential V_o (from ion cores)(Schultz and Lynn 1988).

experience. The work functions for positrons and electrons can be express as:

$$\begin{aligned} \phi_+ &= -D - \mu_+; \\ \phi_- &= +D - \mu_- . \end{aligned} \tag{2.1.16}$$

While the electron work function is about a few eV for most of the crystal faces, the reversal of the surface barrier's effect makes the positron work function to be very small, and even negative for some crystal faces. For surfaces with a positive positron work function, (even when it is small,) there is no significant amount of thermal energy positrons that will be emitted from the surface except in the case of the solidified crystals of rare gases. For surfaces with a negative positron work function, however, some of the thermal positrons diffusing to the surfaces can be emitted to the vacuum with a energy of the negative value of ϕ_+. Fig. 2.1.3 adopted

from Schultz and Lynn (1988) illustrates the potential experienced by a single positron near a surface with a negative positron work function.

Not all the positrons that escape from the bulk will be re-emitted into vacuum. As shown in Fig.2.1.3, there is a small potential well just outside the surface for positrons due to the image potential. Some of the escaped positrons will be trapped at the surface because of this small potential well. Also, a fraction of those positrons will pick electrons near or at surface and form positronium, which is emitted into vacuum. The probability of those thermal positron being emitted once they reach the surface, P_e, depends on the material, the orientation of the crystal surface, and the surface condition.

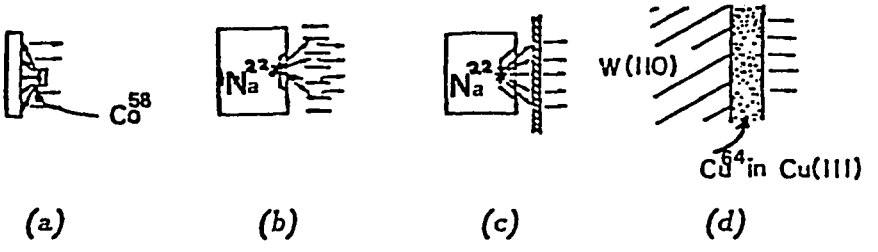

Figure 2.1.4 Some of the commonly employed positron moderator geometries. (a)A reflection moderator: a Co^{58} source is positioned in front a single crystal (W, Cu, or Ni are commonly used); (b)A W vane moderator: Na^{22} source is right behind a annealed W vanes; (c)A transmission moderator: a single crystal or polycrystal foil is placed in front a Na^{22} source; (d)A self-moderator: Cu(111) with small percentage of Cu^{64} is epitaxially grew on a W(110) single crystal surface.

The longitudinal energy width of positrons re-emitted from the clean single crystal

moderator surfaces is usually about 75 meV at room temperature, which is believed due the thermal broadening (K_BT is $\sim$ 26 meV). And the angular spread of the re-emitted positrons is on the order of $\sqrt{K_BT/\phi_+}$. Various positron source/moderator geometries are developed. Fig.2.1.4 shows a few that are commonly employed. Even though it is almost impossible to calculate exactly the efficiency of various type of moderators because there are, in addition to the factors described above, other factors such as the self absorption of the source, the variations in geometry employed in the practical case, the variations in surface condition (i.e. the roughness and impurities), and the differences in extraction fields, it is possible and beneficial to carry out some simplified estimate of the efficiency of the moderators. For a reflection moderator, the thermal positrons are emitted from the surface that the fast positrons entered. The efficiency can be estimate as:

$$\epsilon = \int_0^\infty \int_0^{\pi/2} P_{imp}(z,\theta) \cdot P_d(z) \cdot P_e \, dz \sin\theta d\theta. \tag{2.1.17}$$

Using the expression for P_{imp} and P_d in Eq.(2.1.13) and Eq.(2.1.15), one can get:

$$\begin{aligned} \epsilon &= P_e \alpha \int_0^\infty \int_0^{\pi/2} \sec\theta \, e^{-\alpha z \sec\theta} \, e^{-z/l_d} \, dz \, sin\theta d\theta \\ &= \alpha l_d P_e \ln[1 + 1/(\alpha l_d)]. \end{aligned} \tag{2.1.18}$$

If it is assumed that only one half of the fast positrons from radioactive source enter the moderator, then a factor of 1/2 has to be added. Also using the Eq.(2.1.14), we have:

$$\epsilon = \frac{0.5 A \rho (D\tau)^{1/2}}{E_{max}^{1.14}} P_e \ln\left[1 + \frac{E_{max}^{1.14}}{A\rho (D\tau)^{1/2}}\right]. \tag{2.1.19}$$

Eq.(2.1.19) indicates the following qualities are desirable for a good moderator: (1) a low endpoint energy of the β^+ decay nucleus; (2) a long positron free diffusing lifetime in the moderator; (3) a large positron diffusion coefficient in the moderator (i.e. the

moderator has a large diffusion length), (a) a high density, ρ, of the moderator; and (5) a high emitting probability P_e at the surface. Among these quantities, the positron diffusing life time in the material does not vary so much to have a significant effect on the efficiency of the moderators. The limited availability of the usable β^+ emitter usually does not allow the positron researchers to have much choice of the radioactive sources they can use so the endpoint energy is rarely a factor the researcher can optimize. But its role in the efficiency does put radioactive sources into a position superior to that of electron accelerator sources as the energy of later source is usually much higher than that of radioactive source. The efforts have been made to optimize other factors. Majority of the positron moderators used nowadays (with exception of solidified rare gas) are high density single crystals or polycrystals such as tungsten or copper. These crystals usually have extremely low impurity and are annealed to ensure the crystals have large degree crystal ordering and very low density of defects, thus positrons will not be trapped at the impurity sites or the defect sites, resulting in a larger diffusion coefficient. Various crystal surfaces have been tested to optimize the positron emission probability P_e and some adsorbate have been employed to increase the P_e such as the case of Cu(111)+S, in which a fraction of monolayer of S was coated on a cleaned and well annealed single crystal Cu(111) surface and a factor of 2 increase in P_e over that for clean Cu(111) surface was reported (Mills 1979). We, however, only observed ~20% increase in our experiments.

For transmission moderators, the estimate is a little more involved. Similar to Eq.(2.1.17) and Eq.(2.1.8), the efficiency for transmission moderator can be expressed as:

$$\begin{aligned}\epsilon &= \int_0^d \int_0^{\pi/2} P_{imp}(z,\theta)\cdot P_d(d-z)\cdot P_e\, dz \sin\theta d\theta \\ &= P_e\,\alpha \int_0^d \int_0^{\pi/2} \sec\theta\, e^{-\alpha z \sec\theta}\, e^{-(d-z)/l_d}\, dz\, sin\theta d\theta,\end{aligned} \tag{2.1.20}$$

where d is the thickness of the transmission moderator foil. Again, we have add a factor of 1/2 to Eq.(2.1.20) assuming only one half of the fast positrons generated by the radioactive source will enter the moderator. And using Eq.(2.1.14), we have:

$$\epsilon = \frac{0.5\,A\rho(\mathrm{D}\tau)^{1/2}}{E_{max}^{1.14}}\mathrm{P}_e \int_0^1 \frac{e^{-\left[A\rho d\Big/(E_{max}^{1.14}x)\right]} - e^{-d/(\mathrm{D}\tau)^{1/2}}}{x - A\rho(\mathrm{D}\tau)^{1/2}\Big/E_{max}^{1.14}}dx. \qquad (2.1.21)$$

Even though the expression for ϵ is more complicated, it can be seen that the factors that we discussed above in the case of the reflection moderator play the similar roles here. Therefore, it is still desireable to have a high density, low defect, low impurity, highly ordered, and well annealed single crystals or polycrystals with surfaces that have high P_e. In addition, the thickness of the foil should be on the order of the positron diffusion length $l_d = (\mathrm{D}\tau)^{1/2}$ of the crystal because only those positrons that thermalized in the bulk within the distance of a few diffusion lengths l_d can make it to the surface. In practice, W or Ni foils of a few thousand to ten thousand Å are used. The thinner foils seem to have higher efficiency which is consistent with above conclusion as l_d is on the order of a thousand Å or less for most of moderators used.

The self moderator that was employed in the research project described in this thesis can be treated with similar approach that we used to discuss the properties of reflection moderators and transmission moderators above. Though the quantitative estimate of the efficiency of a self moderator is much more involved and complicated than those for reflection and transmission moderators, the moderation process itself can be understood qualitatively as a combination of a reflection moderator and a transmission moderator*. Mills(1979, 1980b) has reported that the well annealed, high purity Cu(111) with a fraction of monolayer of S coating(exposing the clean Cu(111) surface to H_2S) can be a reflection moderator with relatively high efficiency.

* The quantitative analysis of the self moderator can be found in Lynn and others 1987, and Weber 1988.

Lynn (Canter and Mills 1982) further proposed and tested that epitaxial growth of an $\approx$ 1000 Å thick Cu(111) film on a cleaned single crystal W(110) substrate possibly also coated with a fraction of monolayer of S could make a high efficiency ($\epsilon \sim 1\%$) reflection moderator with a narrow energy spread. Mills (1980) also proposed that it might be possible to generate the high activity Cu^{64} β^+ source and to make it into a Cu(111) single crystal film by epitaxial growth on a single crystal substrate, thus resulting in a self moderated positron emitter. This idea, however, was not realized until the construction of the high intensity positron beam at HFBR where Cu^{64} has been made by irradiating Cu^{63} with thermal neutron (as discuss in 2.1.1 above).

The moderation process of this self moderated source can be understood qualitatively in following discussion. A large fraction of the fast positrons generated by the Cu^{64} isotopes are slowed down in the copper crystal itself, but, similar to the case of reflection and transmission moderators, only those positrons that are thermalized within the diffusion length l_d away from the emitting surface can diffuse to the surface and be emitted from the surface to vacuum with energy of negative ϕ_+. So for those fast positrons generated by those Cu^{64} isotopes at surface or very close to the surface (the distance to the surface is $\ll l_d$), moderation process is dominantly reflection moderation because only the fast positrons traveling towards bulk would be slowed down and the fast positrons traveling toward the vacuum would escape to the vacuum without losing much of their initial energy (notice that $l_d \ll \alpha^{-1}$). For those fast positrons generated by those Cu^{64} isotopes away from the surface but within the distance of diffusion length, the moderation process is combination of reflection moderation and transmission moderation, i.e. the fast positron traveling towards the bulk would be slowed down and the ones that are thermalized within the distance of l_d have a chance to diffuse to the surface and be re-emitted, and some of those fast positrons traveling towards vacuum would also be thermalized before they make to

the surface then diffuse to the surface and be re-emitted. For those fast positrons generated by Cu^{64} isotopes deeper in the bulk (the distance to the surface is $>$ or $\gg l_d$ but $< \alpha^{-1} + l_d$, where α^{-1} is the implantation depth), the moderation process then is dominantly transmission moderation, i.e. the fast positrons traveling deeper into the bulk would not be thermalized within l_d distance away from the surface therefore can not diffuse back to the surface, the fast positrons traveling towards vacuum would have a good chance to be thermalized at somewhere a distance of l_d or less away from the surface in the bulk then diffuse to the surface. For those positrons generated from the Cu^{64} isotopes too far away from the surface (the distance to the surface is $>$ or $\gg l_d + \alpha$), they almost do not contribute to the re-emission of low energy positron at all as they would be thermalized too far away from the surface to diffuse back to the surface. The discussion above is based on single crystal radioactive copper film without any effects from the substrate. The single crystal W(110) substrate would have some positive effects on the moderation process if the copper film is thin enough. Again, the two qualities, l_d and α^{-1} (diffusion length and implantation length respectively), are the criteria used here. If the thickness of copper film is less than l_d, while some fast positrons will be thermalized in the copper film and diffuse to the surface, majority of those positrons traveling towards substrate will enter the substrate (because the implantation length is much longer than the diffusion length in this case,) and be thermalized in the substrate and some of those thermalized not far from the copper vacuum interface comparing to the diffusion length will diffuse to the surface of copper. The substrate behaves similarly to a reflection moderator. If the thickness of the copper film is bigger than the diffusion length but less than the sum of implantation length and diffusion length, the slow positrons moderated in the substrate can not contribute to the re-emission of the thermal positrons, but the reflection of some fast positrons from the high density tungsten substrate will contribute to the re-emission of thermal positrons as those reflected fast positrons

may be thermalized in the copper and diffuse to the surface. The substrate is like a partial reflector for fast positrons. This effect also takes place in the first case (when thickness of the copper film is $< l_d$), but the reflection moderation effect in that case is much bigger than this effect. If copper film is thicker than that described in the second case, the substrate hardly contributes to the re-emission of thermal positrons.

The efficiency of the self moderation process can be seen qualitatively from the above discussion. The moderation efficiency of copper single crystal film is expected to peak at thickness slightly bigger than the diffusion length and then to decreases gradually. The contribution from the tungsten as reflection moderator to re-emission of slow positrons is predominant component when copper film is very very thin, then gradually decreases and vanishes quickly after the thickness of copper film exceeds the diffusion length; the contribution of tungsten as reflector of fast positrons is very small and only peaks with the thickness of copper film at about diffusion length. The total moderation efficiency is relative high when the copper film is very thin (mainly from tungsten), increases slowly, peaks at the thickness about the diffusion length, and decreases sharply first (due to the drop of the tungsten's contribution) then changes to slow decrease (due to the decrease of the copper's efficiency). The diffusion length of positron in copper is on the order of 1000 Å (100 nm) and implantation length (α^{-1}) is on the order of 3×10^5 Å (3×10^4 nm). Fig.2.1.5 (from Weber 1988) shows the result from the quantitative estimate of the efficiency, which is consistent with the qualitative discussion above.

As the self moderator is also the source, the efficiency and source activity per area, which is proportional to the thickness of the copper film, are related to each other. The number of thermal positrons emitted per unit area is the quantity more important for actual beam construction consideration. While the moderation efficiency decreases as thickness of copper film continues to increase after reaching the diffusion length,

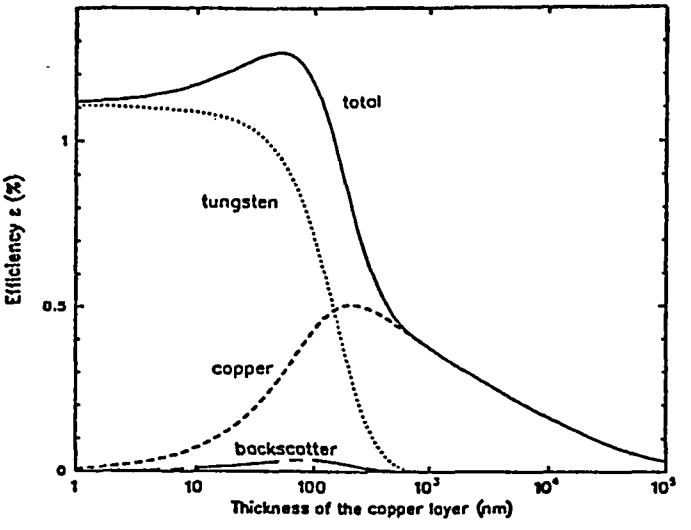

Figure 2.1.5 The quantitative estimate of the total efficiency (—) of a self moderated radioactive copper film that is epitaxially grown on a W(110) single crystal substrate as function of the thickness of copper film (from Weber 1988). Also shown in the figures are various contributions to the total efficiency: from the copper film (- - -), contributed by the fast positron backscattering from W substrate (- — -), and the part that moderated in W substrate (···).

the activity per area continues to increase proportional to the thickness of the copper film. Therefore the total number of emitted thermal positrons per unit area, which is the product of the activity per unit area and the moderation efficiency, continues to increase as the thickness of copper film increases even after the efficiency reach its maximum, because the increase in activity more than compensates the decrease of the efficiency. It reaches the plateau when the thickness of copper film is bigger than the implantation length. Fig. 2.1.6 shows the behaviour of product of the total efficiency and thickness of copper film (that is linear proportional to the activity) from the quantitative analysis (Weber 1988), which is consistent with the discussion above.

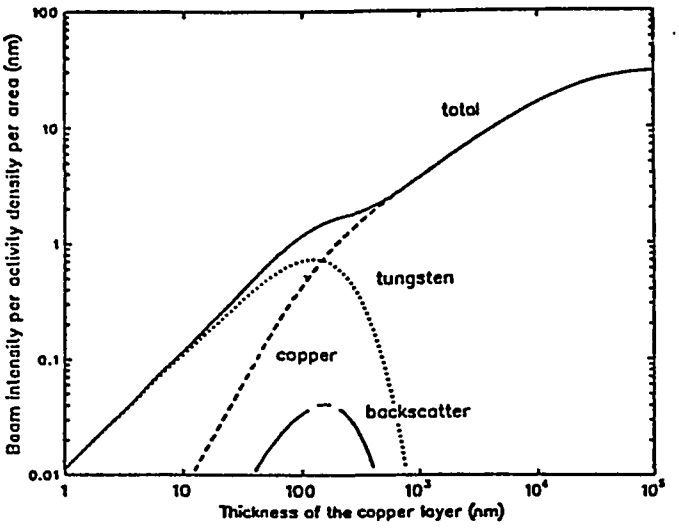

Figure 2.1.6 The product of the efficiency and thickness of copper film as function of thickness of copper film from the same quantitative estimate(Weber 1988) in Fig. 2.1.5. The symbols are also the same as in fig. 2.1.5.

At the Brookhaven National laboratory, a high intensity mono-energetic positron beam has been constructed and has been operating utilizing the self moderation process. The full potential of self moderated positron emitter, however, has not been completely realized. The self absorption of the positron source due to its own thickness is one of the factor that limit the beam intensity. This problem can be greatly reduced if the radioactive copper can be made close to pure Cu^{64} isotopes. At the present, the Cu^{64} is only less than 1/4000 of the total copper. If a process can be developed so that only Cu^{64} will be deposit, then the maximum number of emitted thermal positrons per unit area will be increased by factor of 4000 as the activity of copper film at the same maximum thickness would be increase by a factor 4000, or use same amount of Cu^{64}, i.e. same activity, the thickness of copper film will be reduced from a few hundreds μm to a few nm where efficiency will be much higher ($\approx$ a factor of ten). Some feasibility study has been carried out at BNL and a

laser isotope separator was proposed (Roellig 1988). Some preliminary research has been conducted on different laser excitation process of Cu^{63} and Cu^{64} (Engleman and others 1987).

For the research project described in this thesis, the self moderation process and, occasionally, the transmission moderation process were employed. But the new efforts have been made recently at BNL to renovate the source chamber of our high intensity beam and to relocate it at Building 480 of BNL. The major change in the new source chamber is the installation of the cryogenic cold head in the chamber so the new solidified rare gas Neon moderator can be employed in the slow positron production process. The solid Ne moderator by far is most efficient positron moderator available with efficiency as high as 0.7% (Mills and Gullikson 1986). The preliminary test at BNL resulted in a efficiency of $\sim$ 0.6% with a 350 μCi Na^{22} source(Khatri and others 1990). The similar efficiency was confirmed on the new positron beam constructed at Building 480 of BNL with a 100 mCi Na^{22} source very recently. It is expected that this new facility will eventually deliver a high flux $\sim$ 10^9 e^+ /sec. positron beam.

The high efficiency of solid Ne can be understood as following. The fast positron will lose most of their initial energies through various scattering and excitation process after they enter the solid Ne, just as in the other moderation process. But because of large band gap of Ne, a threshold energy E_{th} of inelastic scattering exists (E_{th} is also the positronium formation threshold energy in Ne), below which the positrons can only lose their energy through phonon scattering. Thus, a very large portion of the fast positrons entering the solid Ne would quickly be slowed down to the energy $E_{th} \approx 16$ eV, then moving in the solid Ne for relatively long time before significantly losing much more energy. Those positrons are, sometime, called epithermal or "hot" positrons. Some of the epithermal or positrons will be able to diffuse to the surface, to overcome the surface barrier, and to escape to the vacuum. Because of the residual

kinetic energy of those positrons and inefficiency of positrons' phonon emission energy loss process in the solid Ne at T = 5K, these positrons also have very long effective diffusion length. Therefore, a relative large portion of positrons implanted in the solid Ne will diffuse to the surface and be re-emitted to the vacuum again, resulting in a high moderation efficiency. The energy spread of re-emitted low energy positrons is broader than other moderation process likely for the same reason responsible for the high moderation efficiency. But this disadvantage of solid Ne moderator is almost always outweighed by its high moderation efficiency, and can be compensated by re-moderation process in a lot of cases.

2.1.3 The HFBR high intensity mono-energetic positron beam facility and its operation — The HFBR positron beam facility has been constructed, so the researchers can safely utilize the high activity positron source generated at the HFBR on the routine basis. Because of the short life time of Cu^{64}, the new sources have to be introduced into the facility almost every other day to keep the high positron intensity of the beam. To ensure that every source transfer is carried out safely, smoothly, and successfully, a detailed operation procedures was developed and the researchers were required to follow it to the letter. During the last few years, some modifications have been implemented both to the beam and to the operation procedure to increase the positron beam intensity and to further reduce the safety risk. In the remain part of this section, the positron beam facility and its operation procedure will be described.

The radioactive Cu^{64} have been produced by inserting a copper pellet contained in a standard capsule assembly into the HFBR irradiation port. The preparation of the source capsule assembly is an integral part of the positron production. Fig.2.1.7 is the cross section diagram of the source capsule assembly. Its main body was made of aluminum to reduce the unnecessary radiation in the production process as the radiation activity from the neutron irradiated aluminum decays much faster than

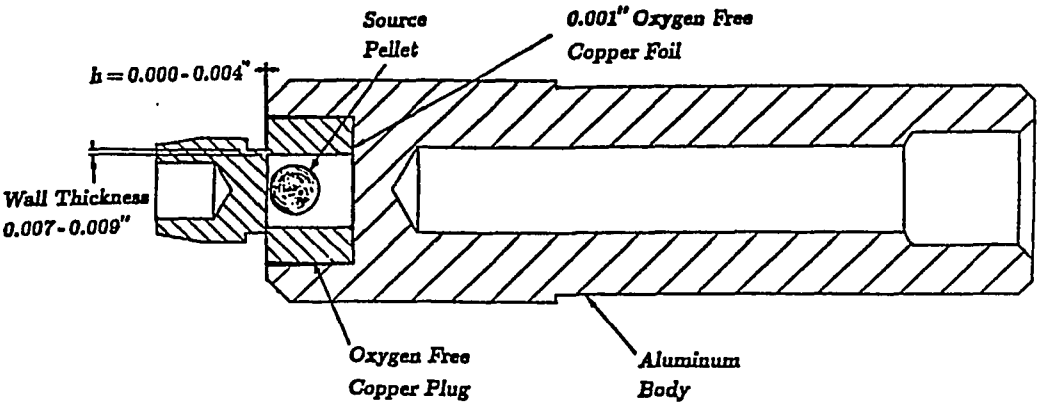

Figure 2.1.7 The source capsule assembly.

that from most of neutron irradiated metals. The source pellets, as discussed at the beginning of this section, are made of either (chemically) purified (> 0.999999) natural copper or isotopically enriched Cu^{63} (Cu^{63} $\sim$ 99.7%) with additional chemical purification. They are made into ball-shaped pellets by an arc-melting furnace. The impurity in the source pellets may create at least two difficulties for the positron production: one possible problem is the production of some long life time radioactive elements after the neutron irradiation, and the other is the reduction of the moderation efficiency of the copper self moderator because the impurities reduce the effective diffusion length of the thermal positrons in the crystal and also prevent a perfect epitaxial crystal growth. Great cares have been taken in every steps of the operation to prevent such contamination to the source pellets. The oxygen free copper plug is used in the source capsule assembly to contain the source pellet instead of the plug made of aluminum* The oxygen free copper foils are used in the source assemblies

* The two dimensions given in the Fig. 2.1.7 are very critical because they affect the strength of the copper plug and the shearing mechanism. A too thick wall (or negative h value which would increase the wall thickness effectively) would make the shearing process likely to fail, resulting in a safety hazard, and too thin wall of the plug may result in a premature break off of the tip part of the plug and lose the source pellet in the process, which would be a major safety accident. The numbers show in the Fig. 2.1.7 are the ones used after long period operation test and a few modifications. All the copper plugs are inspected professionally for their dimensions.

to separate the source pellets from the aluminum bodies. Together with the copper plug, it creates an entire copper environment for the source pellet in the assembly. Before the source capsules are assembled, the source pellets are etched in aqua regia until no surface contamination is visible and polycrystal grain clearly visible under the microscope. This step would eliminate the surface contamination and copper oxides. The copper plugs and copper foils are also etched before the assembling. All the source capsule assembly parts are cleaned with acetone and alcohol before the final assembling, in which the capsules are assembled as shown in Fig.2.1.7 in a clean environment. Then the capsules are put into a e-beam welding facility where the copper plugs are e-beam welded to the aluminum bodies "vacuum tight" in a low vacuum ($10^{-4} \sim 10^{-5}$ torr) environment. Thus the source pellets are kept in a low vacuum surrounding after the e-beam welding and before being transferred into the source chamber. The manual assembling process have always been scheduled to take place shortly before the e-beam welding operation so that the copper pellets do not accumulate any copper oxides on the surface. After the e-beam welding process, the capsule are put into a container with high pressure helium (about 350 P.S.I.) for about twelve hours and then immediately transferred into a vacuum environment to check helium trace. If the test is negative, the e-beam welding is vacuum tight, otherwise the e-beam welding procedure has to be repeated. After the completion of e-beam welding, a 25 ft. long, 1/4 in. dia. aluminum tube has to be welded to the end of the capsule (the right side in fig.2.1.7) to facilitate the insertion of the capsule into the HFBR port.

Before a source capsule assembly is inserted into the irradiation port, both the experimenters and the reactor operator have to check the integrity of the capsule. The exterior of the source capsule and the tube attached are cleaned again with acetone and alcohol before the insertion. Table 2.1.2 shows the list the available irradiation ports at HFBR. The port usually used for this project was the Port 14, though the

Table 2.1.2 HFBR Irradiation facilities (*"HFBR Handbook"*).

Facility	Flux, neutrons/cm^2-sec		Heating Rate, W/g (in aluminum)	Useable Dimensions	
	Thermal	Fast (>1 MeV)		Diam (cm)	Length (cm)
V10	2.7×10^{14}	7.5×10^{11}	0.38	2.4	7.6
V11	1.5×10^{14}	9.0×10^{10}	0.23	2.0	7.6
V12	3.8×10^{14}	8.3×10^{11}	1.20	2.4	7.6
V13*	8.3×10^{14}	9.0×10^{13}	6.0	1.5	7.6
V14	8.3×10^{14}	9.0×10^{13}	6.0	1.9	7.6
V15	2.0×10^{14}	3.0×10^{14}	12.0	1.9	7.6
V16*	2.0×10^{14}	3.0×10^{14}	12.0	1.5	7.6

*Accessible for placement and removal of samples only during reactor shutdown. V13 and V16 can accommodate two samples each of the size given.

Port 12 was occasionally used when the Port 14 was occupied for other research projects. The source capsule assembly is usually irradiated for two to three days in the port.

Since the capsule and tube inserted in the port are highly radioactive, heavy shielding have to be employed to ensure a safe operation. The Reactor Division has a facility which can safely cut the Al tube off of the capsule and transfer the capsule assembly to the top of our positron beam facility. To eliminate the high level radiation from the capsule, a concrete block house was constructed to contain the positron beam facility. This house has 2 ft. thick concrete wall with one layer of lead bricks in the middle. Fig. 2.1.8 shows most of parts of the positron beam facility at the source end.

During the source transfer process, the capsule is first dropped into the dryer from the top of the block house to clean off any residual heavy cooling water from the reactor port. The capsule is dropped into the shear mechanism after being dried. The shear mechanism is designed to shear off the tip part of the copper plug at the

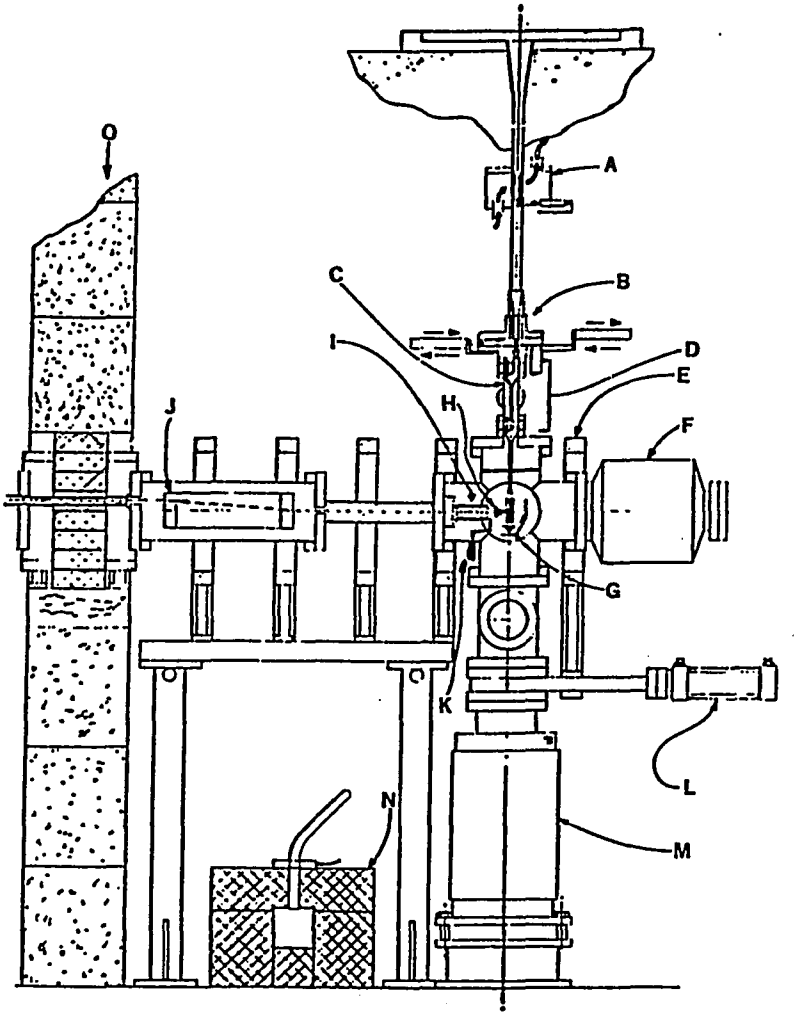

Figure 2.1.8 The HFBR high intensity mono-energetic positron beam facility. Shown in this diagram are the various components of the facility: A. the dryer; B. the shear mechanism; C. the radiation monitor; D. the vacuum air lock; E. the guiding magnet coil; F. the Ti pump; G. the evaporation crucible; H. the W(110) substrate and pellet guiding tube assembly; I. the extracting lenses; J. the E×B energy filter; K. the movable transmission moderator; L. the pneumatic valve; M. the ion pump; N. the spent capsule pig; O. the shielding wall of the "Block House."

head of the capsule so the source pellet can fall into the guiding tube leading to the vacuum air lock. This set up can also dump the tip sheared off from the capsule and sheared empty capsule into the spent capsule pig which is heavily shield by lead bricks. The pellet is guided into the vacuum air lock set up which is pumped by a pumping system consisted of a turbo molecular pump and cryo-pump. It usually take twenty to thirty minutes to pump the air lock section below 10^{-5} torr, after which the source pellet is then dropped into the evaporation crucible in the source chamber through the guiding tube by opening the bottom butterfly valve in the air lock for five seconds. During the whole process, the reading from the two radiation detectors, one right under the shear mechanism at the top of the air lock and the other at the bottom of air lock, were monitored, recorded, and compared with the readings from previous drop process in the every step of the process to confirm the position of the pellet, to ensure the shutter, shear mechanism, and air lock functioning according to the design, and to help determine the cause of any malfunction should it take place. Two video cameras were also installed inside the block house, one is aimed at the view port at the top of the source chamber and provides a top view of the inside the source chamber via a mirror and the other one couples to the side-viewport of the source chamber. These two cameras can help monitor the activity in the source chamber, especially the process of epitaxial single crystal film growth. But it is also used to confirm the arrival of the pellet in the evaporation crucible.

The source evaporation usually takes place immediately after the source pellet is transferred to the evaporation crucible. An epitaxially grown single crystal radioactive Cu(111) film is used as a self moderated slow positron source and the quality of this epitaxially grown single crystal film is the key factor in obtaining a high efficiency of the moderation. Because of the block house is inaccessible during the operation due to the high radiation level, the crystal growth process can not be monitored effectively. The operation is carried out with some emperical set ups and parameters.

At the beginning of this project, the epitaxial growth of Cu(111) film on a single crystal W(110) substrate with our set up was tested with high purity natural copper. The quality of the crystal film grown was checked by the X-ray diffraction. From this test, the emperical set ups and parameters were obtained. Later, in attempt to improve the efficiency of the moderation, another experiment was conducted with the duplicated the source chamber, a Varian LEED and retarded Auger system, and high purity natural copper pellets. It was believed that the additional LEED and Auger system would give the information not only about the quality of the epitaxially grown single crystal film as the X-ray diffraction did but also about the surface condition of the film which is important for the positron moderator (as being discussed earlier). Another advantage of this set up was that the process could be monitored in situ between the steps of the process. From these two experiments and the accumulated the operation records, the emperical set ups and parameters and the procedure of the operation that have been used in the source preparation operation in this project were obtained. The brief description of this procedure will be given below

The single crystal W(110) substrate is fully annealed before the operation. The substrate is usually checked with X-ray diffraction before the installation to ensure that only the high crystal quality substrate is used. The substrate is heated to above 2000°C for two to there minutes in UHV environment then lower the temperature gradually. It is also desirable to oxygen-treat the substrate to eliminate any possible carbon diffusing out from the bulk of the tungsten. The oxygen treatment is carried out in a vacuum chamber with base pressure in the 10^{-10} torr range. The substrate is heated to barely red hot, about 900°C, then the 5×10^{-7} torr of oxygen is introduced by leaking in the high purity oxygen gas. After the substrate has been kept in such condition for about thirty minutes or so, the oxygen leak is stopped and the chamber is pumped down again to the base pressure of 10^{-10} torr range. Then, the substrate is flushed to above 2000°C for a short time(30 *sec.* – 1 min) to clean out any

carbon monoxide or/and dioxide created on the surface during the treatment. This procedure is repeated for a few times. The first annealing and oxygen treatment of the substrate is usually carried out in a separated chamber which the heating and pumping are much more easily achieved than in the source chamber on the beam. It was indicated in our test that it is not necessary to repeat the oxygen treatment frequently. It is only important to treat it before the first use. But the annealing of the substrate is carried out every time before the evaporation starts. Both the substrate and the crucible are fully degassed before the pellet is introduced. The annealing and degassed of the substrate and empty crucible are usually carried out before the drop process or during the drop process to minimized the source decay loss caused by the source preparation time. (It usually follows the operation in which both the used the copper film and the residual copper in the crucible are evaporated onto a Ta sheet.) After the pellet is introduced into the crucible, the pellet and crucible are degassed to eliminate any impurity, then the substrate is degassed again to eliminate any surface contamination caused by the opening of the air lock.

The evaporation operation usually takes about fifteen to twenty minutes during which a copper film of about 1 cm diameter and a few hundreds μm thick is evaporated onto the substrate. The mass of evaporated copper film is usually only about one third to one half of that of the pellet. The remainder of the copper are being evaporated onto the surface of the various components in the chamber. It is found through the test with natural copper that the pre-heating of the substrate gives better epitaxial growth. The substrate usually is heated with half the power needed for annealing at the beginning of the evaporation then reduced the power to zero gradually in the first six to eight minutes, after which the substrate is believe to be being kept hot by the heat generated by crucible. The annealing of the film follows the evaporation process. The crystal is turned to facing the top viewport so the annealing can be monitored though the video camera. The annealing usually is carried out by heating

the substrate slowly to barely glowing and reducing the power slowly to ensure a slow cooling. After the annealing, a fraction of monolayer of S is coated onto the film by introduce H_2S into chamber at 1×10^{-6} torr for 100 seconds. The S coating usually increase the efficiency by 20% or more (see the earlier discussion on the positron moderation).

In some occasion, the procedure described above failed to produce a sufficient amount of slow positrons; then a single crystal W(100) transmission moderator would be employed. This transmission moderator is oxygen treated, annealed, and degassed similarly to the tungsten substrate. The detailed annealing procedure was reported by Gramsch and others (1987). It is normally first cleaned and tested in another set up before the installation. Its efficiency of moderation in other set up is about 4×10^{-4}. It is mounted on a linear feedthrough controlled by a stepping motor that can be operated from the outside the block house so it can be inserted into the beam (when it is employed) or withdraw from the beam (when the self moderator works).

When sufficient amount of slow positrons is produced either by the self moderator or the transmission moderator, slow positrons are accelerated to the desired beam energy (usually from 60 to 200 eV) by the extraction lenses and guided into a E×B filter. The E×B filter is used to separated the moderated slow positrons from those fast positrons. When passing through the E×B filter, the positrons would drift in the direction perpendicular to both electric field and magnetic field (which is the guiding field for the beam with its direction parallel to the beam direction) for a distance depending on their velocity, electric field, and magnetic field. With proper electric and magnetic field, only the moderated positrons can be drifted for the "right" distance to be able to exit the filter without hitting the chamber wall. The moderated slow positrons emerging from the filter will be magnetically guided out of the block house to the gas cell. The Fig. 2.1.9 shows both the energy distribution of the positron

beam and its integrated spectrum measured by a calibrated NaI detector (see section 2.3. for the detection set up).

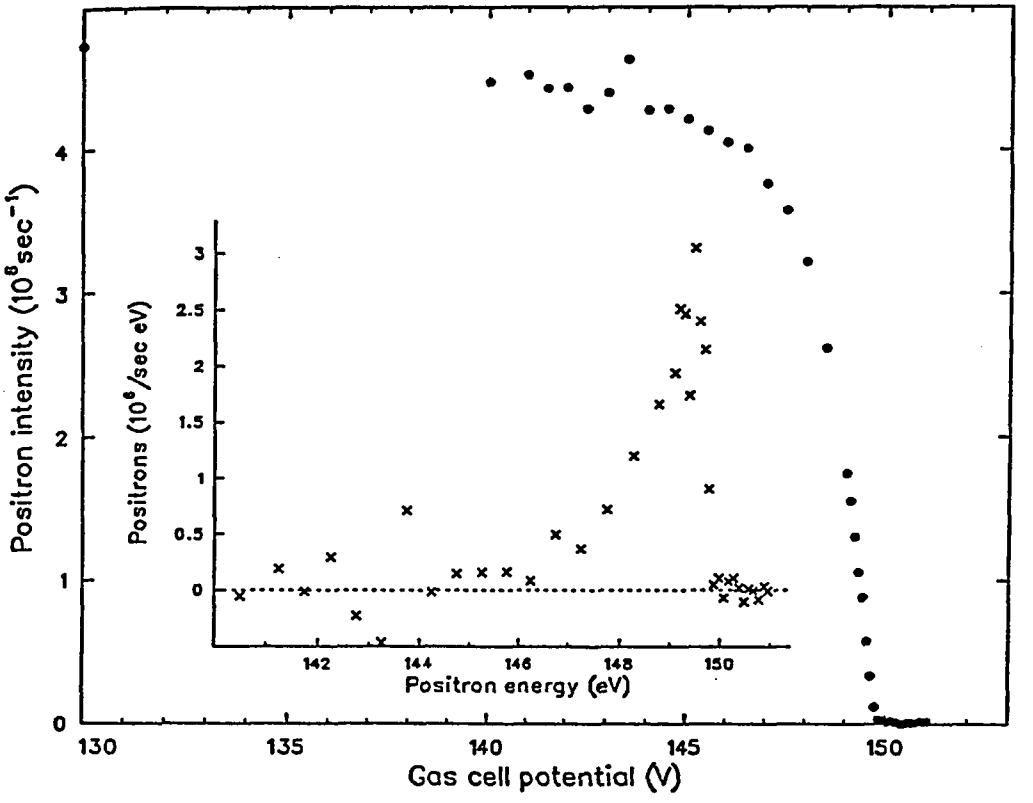

Figure 2.1.9 The integral spectrum of the longitudinal energy distribution of the HFBR positron beam. The • shows the positron beam intensity as function of the gas cell potential. In the insert, the × shows the positron longitudinal energy distribution of the positron beam obtained by taking the negative value of the first derivative of the integral spectrum.

§2.2 The HFBR Mono-Energetic Positronium Beam

Using the HFBR high intensity mono-energetic positron beam as our low energy positron source, we had constructed a mono-energetic positronium beam to conduct our experiments of the positronium scattering and reflection from surfaces. With the high flux of positrons delivered by the high intensity positron beam at HFBR, this positronium beam can provide a flux of up to 2000 mono-energetic positronium atoms per second. In this section, some properties of positronium which are related to this project will be discussed, and various approaches of positronium production, which are the background knowledge used for the designing, the constructing, and modifying of our positronium beam, will also be discussed. The positronium beam that we constructed in HFBR and its experimental facility will be described in detail.

*2.2.1 Positronium** — Positronium is a bound state of an electron-positron pair. The positronium atoms are very similar to hydrogen atoms with positrons replacing the protons. There are, however, also some significant differences between positronium atoms and hydrogen atoms. These differences are of the consequence of positronium's being a particle and antiparticle system in which two particles have the same mass, the same magnitude of the magnetic moments, and a finite probability of annihilating with each other. By comparing some properties of positronium and hydrogen, one can achieve a better understanding of positronium because the properties of the hydrogen atoms are well understood. The Schrödinger energy levels (or Bohr spectroscopic structure) of positronium are similar to that of hydrogen, but different in both values and the fine structures. For a hydrogen atom, the reduced mass† of the

* For a detailed description of the properties of positronium and a complete review of the recent theoretical and experimental research efforts on positronium, see, for example, works by Stroscio (1975), Berko and Pendleton (1980), and Rich (1981).

† the μ is used here as the reduced mass for a two body system and it should not be confused with the one used in last section as the chemical potential or the one used later as the magnetic moment.

two body system μ_H is:

$$\mu_H = \frac{m_p m_e}{m_p + m_e} \approx m_e, \quad \text{as} \quad m_p \gg m_e, \tag{2.2.1}$$

where m_p and m_e are the mass of a proton and a electron respectively. For positronium, however, the reduced mass of the system μ_{Ps} is given by:

$$\mu_{Ps} = \frac{m_e m_{e+}}{m_e + m_{e+}} = \frac{1}{2} m_e, \quad \text{as} \quad m_e = m_{e+}, \tag{2.2.2}$$

where m_{e+} is the mass of a positron. The Schrödinger energy levels(or Bohr spectroscopic structure) of positronium are thus rescaled by a factor of 1/2 and are given as:

$$E_n(\mathrm{Ps}) \approx \frac{1}{2} E_n(\mathrm{H}) = \frac{m_e c^2 \alpha^2}{4n^2}, \tag{2.2.3}$$

where $\alpha = e^2/\hbar c \approx 1/137$ is the fine structure constant. This results in the binding energy of positronium to be about 6.8 eV. Similarly, the first excited state of positronium has binding energy $\sim$ 1.7 eV. Similarly to the case of hydrogen, each energy level E_n of positronium is further split into several sub-levels. The energy level splitting (removal of degeneracy) of positronium, however, is quite different from that of hydrogen, because the principal factors causing the removal of the degeneracy are different from those in hydrogen. For hydrogen, the main contributing factor to the degeneracy removal is the spin-orbit (l – s) coupling, and the interaction of the electron spin with nuclear spin (s – I coupling) can be treated as a small perturbation resulting in a hyperfine structure because the magnetic moment of the nuclear spin is much smaller than those of electron spin and orbital angular momentum. For positronium, the equality of the mass and magnitude of the magnetic moment for positrons and electrons makes the spin-spin (s – s) interaction between the electron and positron the main factor to the removal of the Coulomb degeneracy. The virtual electron-positron annihilation also contributes significantly to the removal of degeneracy (its

contribution to the energy splitting is on the same order as that from the spin-spin coupling) (Berko and Pendleton 1980). Fig. 2.2.1 (reproduced from above ref.) shows the energy diagram for positronium and hydrogen, where the notation is defined similarly to the one used in the atomic physics as $n^{2s+1}l_j$ where $\mathbf{j} = \mathbf{l} + \mathbf{s}$.

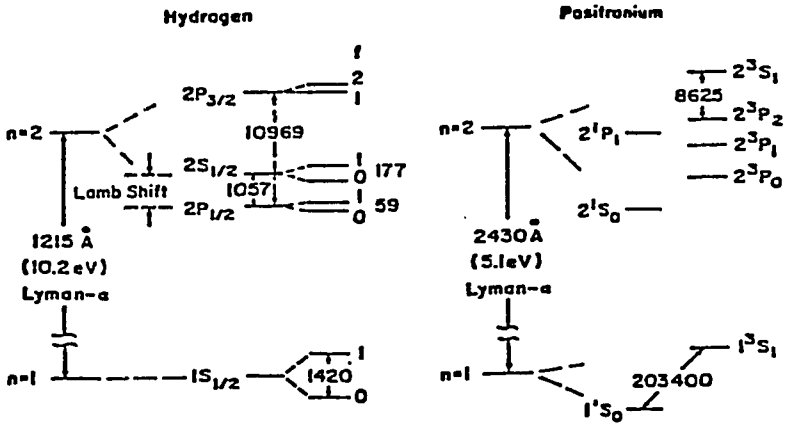

Figure 2.2.1 The schematic comparison of the n=1 and n=2 energy levels of hydrogen and positronium. The energy level differences are given in MHz to the nearest MHz (from Berko and Pendleton 1980). The exact values of the energy level differences are given in the text and table 2.2.1.

The fine structure splitting of energy between the triplet state and singlet state for the ground state in the lowest order are given as (Berko and Pendleton 1980):

$$\begin{aligned} &\mathrm{E}(1^3S_1) - \mathrm{E}(1^3S_0) = \Delta\mathrm{E}_1 \\ &\text{with} \qquad \Delta\mathrm{E}_1 = \frac{7}{3}\alpha^2\mathrm{E}_1(\mathrm{Ps}), \end{aligned} \tag{2.2.4}$$

where a factor of 4/3 comes from the spin-spin coupling and a factor of 3/3 comes from the virtual annihilation mechanism for this splitting. Higher order correction also has been calculated, the energy splitting calculated to the α^6 term can be expressed as:

$$\Delta\mathrm{E}_1 = \frac{\alpha^4 m_e c^2}{4}\left[\frac{7}{3} - \frac{\alpha}{\pi}\left(\frac{32}{9} + 2\ln 2\right) - \frac{5\alpha^2}{6}\ln\alpha\right]. \tag{2.2.4'}$$

Similarly, the corresponding lowest order energy splitting between the triplet and singlet ΔE_2 for n=2 is $\Delta E_2 = \Delta E_1/8$. The corrections to the n = 2 nonrelativistic energy levels to the order α^4 and α^5 in MHz are given in Table 2.2.1 (reproduced from Stroscio 1975).

Table 2.2.1

Correction to the n=2 nonrelativistic energy level in MHz (Stroscio 1975)

state	α^4 shift	α^5 shift
$2\,^1S_0$	-18135	357
$2\,^3S_1$	7413	232
$2\,^1P_1$	-3536	-3
$2\,^3P_2$	-981	1
$2\,^3P_1$	-5360	-5
$2\,^3P_0$	-10835	-16

The optical transitions between those energy levels follow the same selection rules as hydrogen atoms do, which require that:

$$\Delta s = 0, \quad \Delta l = \pm 1, \quad \textit{and} \quad \Delta j = 0, \pm 1. \tag{2.2.5}$$

Only 2P positronium can optically decay into the ground state of 1S, the probability of 2S→1S decay is extremely low because of the selection rules. Fig. 2.2.2 (reproduced from Schrader and Jean 1988) shows schematically the decays of the positronium states. The decay rates for both annihilation decay and optical decay are also given. The only significant optical decay from the n=2 states to the ground state is the 2P→1S Lyman-α decay. The life time of 2P states against Lyman-α decay is about 3.19×10^{-9} seconds, which is much shorter than the life time of 2P states against the annihilation decay (see Fig. 2.2.2) and makes the optical decay the dominant decay process for the 2P states.

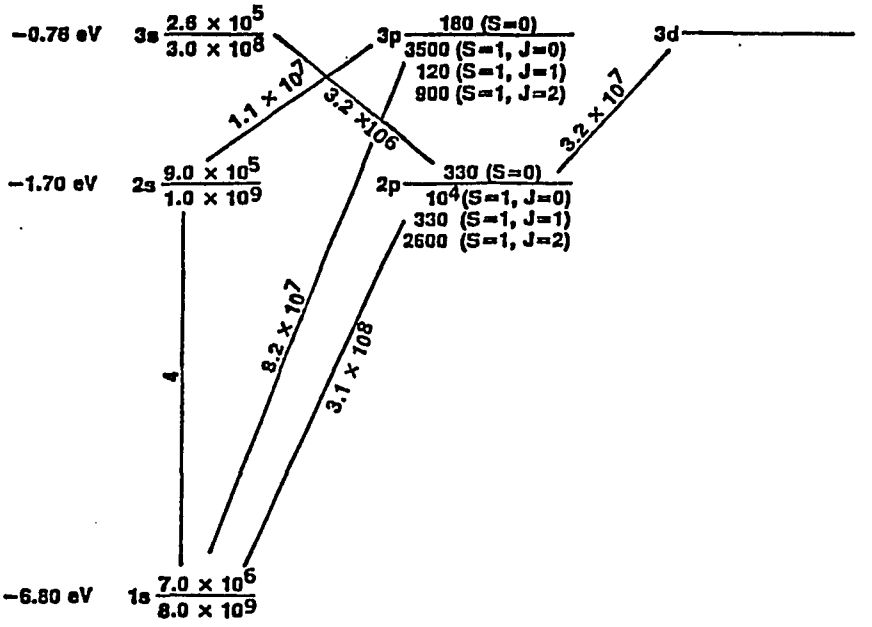

Figure 2.2.2 The decay diagram of Ps states for two- and three-photon annihilation decay and optical decay. The annihilation decay rates are given below and above each energy level for two- and three photon processes respectively. The optical rates are also given. The units are in s^{-1} (from Schrader and Jean 1988).

For the positronium ground state (n=1), the zero order Zeeman energy splitting is zero, because the magnetic moments of electrons and positrons have the exactly same value but opposite sign. The higher order effect, though is small, does exist. The positronium Hamiltonian in a static magnetic field H_o is given as (Stroscio 1975):

$$\mathcal{H} = \mathcal{H}_o + \mu_o g_1 s_1 \cdot H_o + \mu_o g_2 s_2 \cdot H_o = \mathcal{H}_o + V, \tag{2.2.6}$$

where $\mathcal{H}_o$ is the unperturbed Hamiltonian, μ_o is the Bohr magneton ($= e\hbar/2m_e c$), g_i is the gyromagnetic ratios for electrons and positrons with $-g_2 = g_1 = g_e$, and s_i are the spin operators for the electron and the positron. If H_o is taken in the z-direction, V can be written as:

$$V = \frac{g_e \mu_o H_o}{2}(\sigma_z^1 - \sigma_z^2), \tag{2.2.7}$$

where σ_x is the Pauli spin matrix. This leads to the only non-vanishing off-diagonal elements for the ground state level:

$$\begin{aligned} \langle {}^1S_0, m=0 \,|\, V \,|\, {}^3S_1, m=0 \rangle &= \mu_o g_e \mathrm{H_o}; \\ \langle {}^3S_1, m=0 \,|\, V \,|\, {}^1S_0, m=0 \rangle &= \mu_o g_e \mathrm{H_o}. \end{aligned} \tag{2.2.8}$$

The diagonalization results in the following energy levels under the magnetic field:

$$\begin{aligned} &\mathrm{E}(1\,{}^3S_1,\, m=\pm 1) = \mathrm{E}(1\,{}^3S_1), \\ &\mathrm{E}(1\,{}^3S_1,\, m=0) = 0.5\,[\mathrm{E}(1\,{}^3S_1) + \mathrm{E}(1\,{}^3S_1)] + 0.5\,\Delta\mathrm{E}_1\sqrt{1+x^2}, \\ &\mathrm{E}(1\,{}^1S_0,\, m=0) = 0.5\,[\mathrm{E}(1\,{}^3S_1) + \mathrm{E}(1\,{}^3S_1)] - 0.5\,\Delta\mathrm{E}_1\sqrt{1+x^2}, \end{aligned} \tag{2.2.9}$$

where $x = 2g_e\mu_o\mathrm{H}/\Delta\mathrm{E}_1$, and $\Delta\mathrm{E}_1$, $\mathrm{E}(1\,{}^3S_1)$, and $\mathrm{E}(1\,{}^1S_0)$ are the same ones given before. The magnetic field does not have an effect on the $m = \pm 1$ states, but generates the mixing of the $m = 0$ states of the triplet and the singlet. The energy splitting between the $m = \pm 1$ and $m = 0$ for the ortho-positronium is:

$$\Delta\mathrm{E}_{1,0}(1\,{}^3S_1) = 0.5\,\Delta\mathrm{E}_1(\sqrt{1+x^2} - 1). \tag{2.2.10}$$

Being a higher order effect, it is relatively small. For example, the energy splitting is only about 0.7% of $\Delta\mathrm{E}_1$, or 5.75 μeV for the magnetic field of 1000 G; therefore, the ortho-positronium is oblivious to the magnetic field involved in this project (which is far below 1000 G). The quenching effect and the the mixing of the state with para-positronium are completely negligible in this project. The Stark effect of external electric field E would not affect the ground state because the S state is the only orbital state in the ground state. It does, however, generate a state mixing between 2S and 2P states. The coupling matrix elements $\mathrm{V}_{2s,2p}$ are on the order of $6a_o e|\mathrm{E}|$ where a_o is the Bohr radius for hydrogen. The state mixing is proportional to the $\mathrm{V}_{2s,2p}/\Delta\mathrm{E}_{2s,2p}$ for the case where $\mathrm{V}_{2s,2p}$ is small in comparison with $\Delta\mathrm{E}_{2s,2p}$ where the $\Delta\mathrm{E}_{2s,2p}$ is the energy difference between the 2S and 2P states (see Table 2.2.1 for

the calculated value of 2S and 2P states). Because the triplet $2\,^3S_1$ state has much longer life time than $2\,^3P_j$ states (which has a life time of $3.19nsec$ against optical decay to $1\,^3S_1$ states), the state mixing by the Stark effect would cause the reduction of $2\,^3S_1$ state (quenching of 2S). For positronium atoms which travel in the magnetic field, there is motional Stark effect with effective electric field $\mathbf{E}_{eff} = \gamma\beta \times \mathbf{H}$ where $\beta = \mathbf{v}/c$, $\gamma = 1/\sqrt{1-\beta^2}$, $\mathbf{v}$ is the velocity of Ps, and $\mathbf{H}$ is the magnetic field. This effect affects those Ps atoms traveling perpendicular to the magnetic filed most, but does not affect those traveling along the magnetic field (Lewis and Hughes 1982).

Historically, Deutsch and Dulit (1951) experimentally measured the fine structure splitting of energy ΔE_1 for 1S states by measuring the small amount of mixing of the triplet and singlet states under the uniform static magnetic field. There have been active experimental efforts to measure the energy structure of positronium. Some of good examples of such efforts are the first observation of Lyman-α radiation (2P$\rightarrow$1S) from the positronium by Canter, Mills, and Berko (1975), the first observation and measurement of $2\,^3S_1 \rightarrow 2\,^3P_2$ energy splitting of positronium by Mills, Berko, and Canter (1975), the observation of $1\,^3S_1 \rightarrow 2\,^3S_1$ transition in positronium with two photon excitation (Chu and Mills 1982), and accurate measurement of the corresponding energy interval (Chu and others 1984).

Another major difference between hydrogen atoms and positronium atoms is that positronium is a transient state instead of a stable state like hydrogen because of the electron-positron annihilation. The annihilation takes place when the wave function of a positron overlaps that of an electron. Positronium is an electron-positron bound state with a finite probability of the wave function overlapping of the positron and the electron. The momentum and the energy of the annihilating electron-positron pair are carried away by the photons emitted during the annihilation. The momentum

and energy of a photon can be express as:

$$\mathrm{E} = h\nu \quad and \quad \mathrm{P} = h\nu/c, \tag{2.2.11}$$

where h is the Planck's constant, ν is the frequency of the photon, and c is the speed of light in vacuum. The number of the annihilation photons is determined by the conservation of momentum, energy, total spin, and charge conjugation. A free positronium atom can not decay through a annihilation process that emits a single photon, because the energy and momentum can not be simultaneously conserved in this process (a photon can not have non-vanishing energy without having the non-vanishing momentum in the center of mass frame of the positronium). The charge conjugation is the operation replacing all particles by their antiparticle without changing any other physical property, such as momentum or spin. It is believed that the charge conjugation property is invariant during the annihilation of the electron-positron pair. The charge conjugation, the interchanging of the electron and positron in Ps, results in a factor of $(-1)^{l+s}$ to the wave function of Ps (a factor $(-1)^{l}$ comes from the orbital wave function; a factor $(-1)^{s+1}$ comes from the spin wave function, a factor (-1) comes from the fact that the electron and positron have opposite intrinsic parity), while a factor of $(-1)^{n}$ would be produced to the wave function of the n photon system under the charge conjugation (Wolfenstein and Ravenhall 1952, Berko and Pendleton 1980). The following general selection rule, therefore, applies to the annihilation decay of positronium:

$$(-1)^{l+s} = (-1)^{n}. \tag{2.2.12}$$

From this selection rule, it is clear that para-positronium can only decay into even number of photons and ortho-positronium can only decay into three or larger odd number of photons.

The annihilation decay rates or the life time of positronium against such decays can be calculated with the knowledge of the free electron-positron annihilation

cross sections and the wave function of positronium, as "the Coulomb binding in the positronium atom has a negligible effect upon the decay probability" (Ore and Powell 1949). The cross section for the two photon annihilation in the low velocity limit (i.e. $v \ll c$ is given as (Dirac 1930):

$$\sigma_{2\gamma} = \pi r_0^2 c/v, \tag{2.2.13}$$

where r_0 is the classical radius of the electron, c is the velocity of light in vacuum, and v is the relative velocity of the electron-positron pair. The cross section for three photon annihilation process is much smaller as it is a higher order effect comparing to the two photon annihilation process. The ratio of the cross sections between the three photon event and two photons events in the low velocity limit is given by (Ore and Powell 1949):

$$\sigma_{3\gamma}/\sigma_{2\gamma} = \frac{4(\pi^2 - 9)}{3\pi}\alpha \approx 1/371.6, \tag{2.2.14}$$

where α is the fine structure constant given before. The cross section is more than a factor of α less for three photon process. The correction of higher order of α has been added to the Eqs. (2.2.13) and (2.2.14) (see Stroscio 1975 for a review). The cross section for four photon annihilation is calculated to be a factor of 9×10^{-5} (on the order of α^2) less than that for two photon process (McCoyd 1965). The cross section for even higher number photon annihilation is expected to be negligible small comparing to two or three photon process (with factors of higher order of α); therefore, the para-positronium decay predominantly through the two photon annihilation and the ortho-positronium decay predominantly through three photon annihilation. From the cross section of the annihilation given above and the wave function of positronium (particularly $\psi(0)$, its value at r=0), the life time of the singlet para-positronium ($1\,^1S_0$) can be deduced as (Pirenne 1946 and Wheeler 1946):

$$\tau_1 = 2\frac{1}{\alpha^5}\frac{\hbar}{m_e c^2} \approx 0.125\, nsec. \tag{2.2.15}$$

Similarly, the life time of the triplet ortho-positronium (1^3S_1) is given as (Ore and Powell 1949):

$$\tau_3 = \frac{9\pi}{2(\pi^2-9)}\frac{1}{\alpha^6}\frac{\hbar}{m_e c^2} \approx 141.8\, nsec.. \qquad (2.2.16)$$

Similar to the annihilation cross section, the correction term of higher order of α has been added to the life time given above. There have also been a number experimental efforts to measure the life time of ground state positronium with high precision*.

The annihilation decay rates and the life time against such decay for excited states of positronium have also been calculated. For n=2 states, a slower rate or longer life time is expected as the overlap of the electron and positron decrease with increase of the n ($\rho(0) = |\psi(0)|^2 \propto 1/n^3$ for S states). For 2P states of positronium, its optical decay (to 1S state) rates are much larger than the annihilation decay rates (see Fig. 2.2.2 for the decay rates of annihilation decay and optical decay) so the overwhelming majority of 2P positronium atoms optically decay (Lyman-α) into 1S states (then decay through annihilation of 1S states) before they can annihilate in 2P states. For positronium in 2S states, however, its life time is still determined by the annihilation decay rates, because the optical decay to the 1S ground state is prohibited by the selection rules discussed earlier. The life time for 2S triplet and singlet states are 1.14 μsec and 1.0 $nsec$ respectively, which are much longer (factor of 8 as expected from n^3) than those for the 1S states.

As discussed in Chapter 1, the characteristic of the photons emitted during the annihilation process depends on the process. For the two photon annihilation process, the conservation of the momentum and energy requires that the two photons be emitted in opposite direction with the same energy of $m_e c^2 = 511$ keV in the center of mass (CM) frame of the electron-positron pair. For the three photon annihilation

* See the review papers that motioned at the beginning of this section for the historical effort and see, for example, Westbrook and others 1987 for the recent work.

process, the conservation of the total momentum and energy allows the photons be emitted over a continuous energy spectrum with maximum energy of $m_e c^2$ because one more photon is emitted. The calculations have been carried out to estimate the energy distribution of those photons emitted. Fig. 2.2.3 shows the spectra at CM frame from various calculations and the very latest experimental measurements. In the laboratory frame, the velocity of the CM frame of annihilating electron-positron pair would result in a deviation from the anticolinearity of the emitted photons and the equality of the photons for the two photon annihilation. The velocity of para-positronium, in principle, can be deducted from either the angular correlation of the emitted photons or the Doppler shift of the photons' energies. The velocity of the CM frame would also result in a variation in the spectra of emitted photons from the three photon annihilation process. The broad spectra of emitted photons from the decay of ortho-positronium have been utilized to identify the existence of positronium atoms in the studies of positron-gas scattering, positron-solid state interaction, and emission of positronium from the solid state surfaces.

The short life time of para-positronium make it impossible at the present time to utilize para-positronium atoms as a probe to study other systems except the ones in which the para-positronium is formed. The ortho-positronium atoms, on the other hand, have a longer life time, which enables the ortho-positronium atoms to travel some distance before their decay if the ortho-positronium atoms are energetic. For example, an ortho-positronium atom of 1 eV can travel about 6 cm within its life time of 141.8 *nsec*, and the one with energy of 20 eV can travel about 27 cm within its life time. The ortho-positronium therefore can be used to study the other system such as solid state surfaces, if a sufficient high flux of positronium can be produces and directed to the system to be studied.

Besides its own decaying process, several other processes can take place dur-

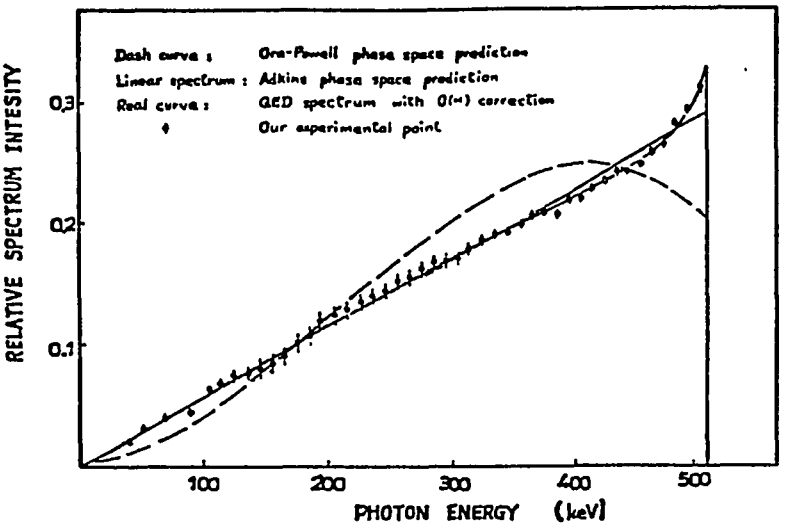

Figure 2.2.3 The experimental and theoretical energy spectra of the γ photons emitted in the three photon annihilation decay of ortho-positronium. The Dash curve is from the Ore-Powell phase space prediction; the linear spectrum represents the Adkins phase space prediction; the solid line curve is the QED spectrum with $O(\alpha)$ correction; the o with error bars are the experimental observation by Chang and others (from Chang and others 1985).

ing the ortho-positronium interaction with other systems. For examples, the ortho-positronium atoms can be elastically scattered or inelastically scattered by ion cores, electrons, and atoms. They can be excited to their excited states during the interaction; they can be ionized (break up) into unbound electrons and positrons; they can also be converted to para-positronium atoms (spin flip) and then decay quickly through the two photon annihilation; or the positrons in the positronium atoms may annihilate with the electrons in the surrounding (the "pick up" annihilation) through the two photon annihilation when positronium atoms are in an environment of a relatively high electron density. For the application of positronium in solid surface studies, these processes are the key factors determining the feasibility of the application, the scope of the applications, and the type of the measurements in the applications. The

knowledge of these processes are very important for both the understanding fundamental physics and the applications of positronium in solid state surface studies. Yet little is known in this area despite very active theoretical and experimental research efforts in the fundamental aspects of positronium such as the energy fine structure and decay rate. This research project will provide some information on the positronium interaction with solid state surface and various matters, and more importantly, to prompt a much larger scope of both experimental and theoretical research efforts in understanding the positronium interaction with matter and developing positronium into a useful probe for the solid state surface physics research.

Some results of the limited research efforts in positronium interactions are mentioned in the Chapter 1 and will be discussed in the following sections or later chapters. One of such results that has been utilized in the design of the experimental detection system for this project is the ortho-positronium spin flip and breaking up in the high electron density environment. In an environment where the electron density is relatively high, the positrons in the positronium atoms can not distinguish between the those electrons originally bound to the positrons or the electrons in the environment. This results in a high probability of electron exchanges between the electrons originally bound to the positrons and those in the environment. If the spins of the electrons in the environment are oriented randomly, the conversion of ortho-positronium to para-positronium would have a very high probability of occurring. This would lead some of ortho-positronium decay through para-positronium decay process, a two photon annihilation with much shorter life time. There is also a high "pick up" probability, i.e. the positrons can easily annihilate with other electrons that are not bound to them in the environment, and this process would also result in the decay of the positronium atoms through two photon annihilation. If the electron density is similar to the one in the positronium atoms, the positronium would be dissolved in this environment because the positrons can not be bound to any individual

electrons any more. The positrons from the dissolved positronium atoms would likely be annihilated by electrons surrounding them due to the high electron density. All these effects reduce the life time of ortho-positronium and also result in the decay of ortho-positronium atoms through a two photon annihilation. The first experimental observation of such events were reported by Deutsch (1951) in the very report that he reported the first observation of positronium. In his experiment, he observed the sharp decrease of the three photon annihilation decay events after he replaced the pure N_2 gas (with which a delayed three photon annihilation decay component was first observed) by a mixture of N_2 and only 3% of NO. This, pointed out by Deutsch, is due to the fact that NO molecules contain an odd number of electrons, so the triplet states of positronium in the environment of NO are expected to be converted into the singlet state very rapidly by an electrons exchange and then decay through the much faster two photon annihilation process. The processes described above are utilized in our detection of positronium. A metallic annihilation plate or a channel plate and a two γ photon coincidence measurement set up are used in our system to detect the positronium. It is believe that majority of ortho-positronium atoms that hit the plate will be either dissolved in the high electron density environment and subsequently annihilate with electrons in the plate, or will annihilate through the "pick up" annihilation process, or will be quickly converted into short life time para-positronium atoms and then decay rapidly. In any of these cases, the annihilation process is the fast two photon annihilation process instead of slow three photon annihilation process. The detection set up will be discussed in detail in the later section.

2.2.2 The production of positronium atoms and a positronium beam — Since the Deutsch's discovery of positronium in gas almost forty years ago, various types of positronium production have been observed and utilized to study the related interactions. Among those reported, the positronium production in the gas via the positron-

gas interaction and the positronium emission from solid state surfaces following the positron bombardment on the surface are the most common approaches. Those two type of production will be discussed in this section.

As shown in Fig. 1.1 in chapter 1, a number of events can take place after positrons strike a surface. Among them, the most well known event is the re-emission of slow positrons, for it makes the production of mono-energetic positrons possible. Another event taking place after positrons' impact is the emission of (thermal or energetic) positronium from the surface. Several processes can result in the emission of positronium from the surface and the characteristic of emitted positronium varies with each emission process. When positrons enter the surface with relative high energies, the majority of them will be able to penetrate into the bulk. They then will lose their energy through various excitation and inelastic scattering processes and be thermalized very quickly. Some of these thermalized positrons may diffuse back to the surface if they are thermalized within a distance of diffusion length away from the surface (see §2.1.2 for the detail of the thermalization process of incident positrons). Some of the thermal positrons diffusing back to the surface may form positronium with the electrons on the surface and leave the surface with energy $-\varepsilon_{P_s}$ if the potential for such form positronium at just outside the surface,

$$\varepsilon_{P_s} = \phi_+ + \phi_- - E_B^\infty, \tag{2.2.17}$$

is negative, where ϕ_- and ϕ_+ are the work for electrons and positrons respectively (see §2.1.2 for more the definition of work function for electrons and positrons), and $E_B^\infty = 6.8$ eV is positronium binding energy in the vacuum. The relative large value of E_B^∞ makes ε_{P_s} to be negative for many surfaces. The thermal positrons diffusing back to the surface may also be trapped at the surface due to a surface potential well, at elevated temperatures, these trapped positrons may be thermally desorbed as Ps atoms and be emitted to the vacuum. In some crystals of insulators, positronium may

be formed in the bulk when some bound electrons are liberated during the energy loss process of positrons. These positronium atoms may diffuse to the surface and be emitted to the vacuum if the work function for positronium defined as (Sferlazzo and others 1987, Schultz and Lynn 1988):

$$\phi_{Ps} = E_B - E_B^{\infty} - \mu_{Ps}, \tag{2.2.18}$$

is negative, where E_B is the Ps binding energy in the crystal. Because E_B usually is smaller than E_B^{∞}, ϕ_{Ps} is negative for number of crystals such as LiF and NaF. All three processes discussed above involve only those positrons that are thermalized in the bulk. The positronium atoms emitted through these process typically have energy ranging from thermal energy KT to a few eV. Another process that produce the positronium emission from the surface involves the non-thermal positrons. While a large portion of positrons are thermalized in the bulk, a very small percentage of incident positrons can, in effect, be scattered back to the surface with relatively high energy up to the incident energy, those positrons can also pick up electrons at the surface, form positronium atoms, and be emitted to the vacuum with relatively high energy. The positronium produced in this process are usually emitted over a broad spectrum of energies. The energy spread came mainly from the energy spread of the energetic positrons. Because these positrons include all the positrons which have not completely thermalized, their energies can range from the original incident energy for those scattered without energy loss to a few eV for those which already undergo various inelastic scattering and excitation. This positronium production process can be further enhanced with at least two different ways. One of them is to use a thin film or foil as the target of positron bombardment. If the foil is sufficiently thin, some of the incident positrons would be still very energetic when they approach the surface on the other side of the foil and some of these energetic positrons would pick up electrons at the surface to form positronium and leave the surface as energetic positronium atoms. The other way is to make positrons strike the surface at a near

glancing angle, so the large portion of positrons can be scattered back toward the surface without positrons' penetrating deeply into the bulk and without too much energy loss because they have much fewer chance to lose their energy in the bulk comparing to those penetrate deeply into the bulk. Those (near glancing angle) back scattered energetic positrons would also have very good chance to pick electrons and form energetic positronium which would be emitted to the vacuum. Another process which is related to the positronium emission from the surface is the Ps^- emission from the surface. In this process, a positron pick up two electrons instead one at the surface, forms a positronium minus ion, Ps^-, and is emitted to the vacuum. The calculated binding energy of Ps^- against break up into Ps and a free electron is 0.3266 eV and its expected 2γ annihilation decay rate is $\Gamma \approx 2 nsec^{-1}$ (Mills 1983).

All the production processes have been experimentally observed and reported*. It is, however, the energetic positronium production process that involves the non-thermal positrons and Ps^- production that are most important to this project, because it may provide a practical way to produce the energetic positronium atoms. Some of the experimental results will be discussed briefly.

The positronium negative ions were observed after directing a 400 eV positron beam at a 40 Å carbon foil (Mills 1985). The efficiency is estimated to be $(2.28 \pm 0.3) \times 10^{-4}$. Theoretically the Ps^- produced can be accelerated and filtered to the desired energy and then be neutralized (photodetachment) by a laser (Bhatia and Drachman 1985). The energetic positronium of 10–500 eV emitted from a 50 Å carbon foil with a continuous energy spectrum approximately proportional to $E^{-3/2}$, when the foil

* A review of the observation and applications of the first production process can be found in Schultz and Lynn 1980; Chen (1987) would provide an example of studies on surface positrons thermal desorbed as positronium atoms while Tuomissari and others (1989) would provide an example of observations on the positronium that is formed in bulk, diffuses to the surface, and is emitted to the vacuum with maximum energy of positronium work function. The observations on energetic positronium production with non-thermal positrons and production of Ps^- will be discussed in this section.

was bombarded by a positron beam of a few keV, was later reported (Mills and Crane 1985a). The efficiency was measured to be about 10^{-4} positronium per positron per eV per sec. per steradian at 50 eV.

The energetic (10–100 eV) positronium production with about 20° FWHM by scattering a well-collimated small diameter positron beam of 30–400 eV off the single crystal Al(100) and Cu(100) surfaces with the glancing-angle geometry was reported (Gidley and others 1987). The total efficiency of a few percent was reported. The information of the energy distribution of positronium emitted is not available due to the lack of the sufficient instrumentation to analyse the Ps energy on the experiment set up at the time, though the assumption of a nearly elastic one-electron capture process made by the authors seemed to be consistent with their experimental observation of angular distribution of the emitted positronium which can be explained in term of the captured electrons' momentum parallel to the surface.

The availability of the mono-energetic positron beams had made systematic studies of positronium formation in gases possible. With the mono-energetic positron beam, the Ps formation measurements can be carried out in the region separated and well shielded from the fast positron source (β^+ decay source) so the signal to noise ratio is greatly improved from the earlier experiments in which the positrons were thermalized in the gas then formed positronium atoms by charge exchange in the gas. The mono-energetic positron beam also enabled the researchers to obtain the positronium formation cross sections in gases as the function of positron energies. The positronium formation in the gases have been studied by various groups. The total positronium formation for different gases have been reported. (see, for example, Griffith 1984 for a review.) There also have been active theoretical efforts on the positronium formation in gases. Various calculations of both total and differential cross sections for n=1,2 positronium in H_2 and He were reported (Mandal and others

1979, Khan and Ghosh 1983, Khan and others 1985). Those calculated positronium formation differential cross sections are peaked at the forward direction (the direction of positrons' incidence). From the results of those experimental and theoretical efforts, a mono-energetic positronium beam by positronium formation in the gas with a gas cell set up was proposed (Brown 1985, 1986). This proposed beam would have a production efficiency about 0.1% mono-energetic positronium per mono-energetic positron. The energy of the positronium produced can be varied by varying the incident positron energy.

Fig. 2.2.4 shows some of the possible positronium production set ups. Based on this information, a differentially pumped gas cell for the positronium production was designed and constructed for this research project. The decision to utilize the gas cell approach is based on our desire to construct a positronium beam with reasonably high efficiency which is mono-energetic, and can be built within reasonable amount of time. The Ps^- production approach, with its possibility to be accelerated to any desirable energies and filtered because of its charge, may be a useful way to make high energy mono-energetic positronium for the future. The short life time of Ps^- and the lack of the experience in photodetachment of Ps^-, however, make it not feasible for the immediate application. The Ps production with a thin carbon foil is very practical approach to make the positronium with various energies. The Ps is produced in a UHV environment with this approach, which is a very important factor for surface studies, yet the broad energy spectrum of produced Ps required a proper energy analysis set up, such as a time of flight apparatus, which can be built but required much more efforts and time. The approach of the metal surfaces with the glancing angle geometry positron incidence is a very promising one. The lack of the information on its energy spectrum at the time, however, made its application in this project impossible. The gas cell approach was very appealing at the time for several reasons. Its efficiency of positronium formation was estimated to be reasonable high

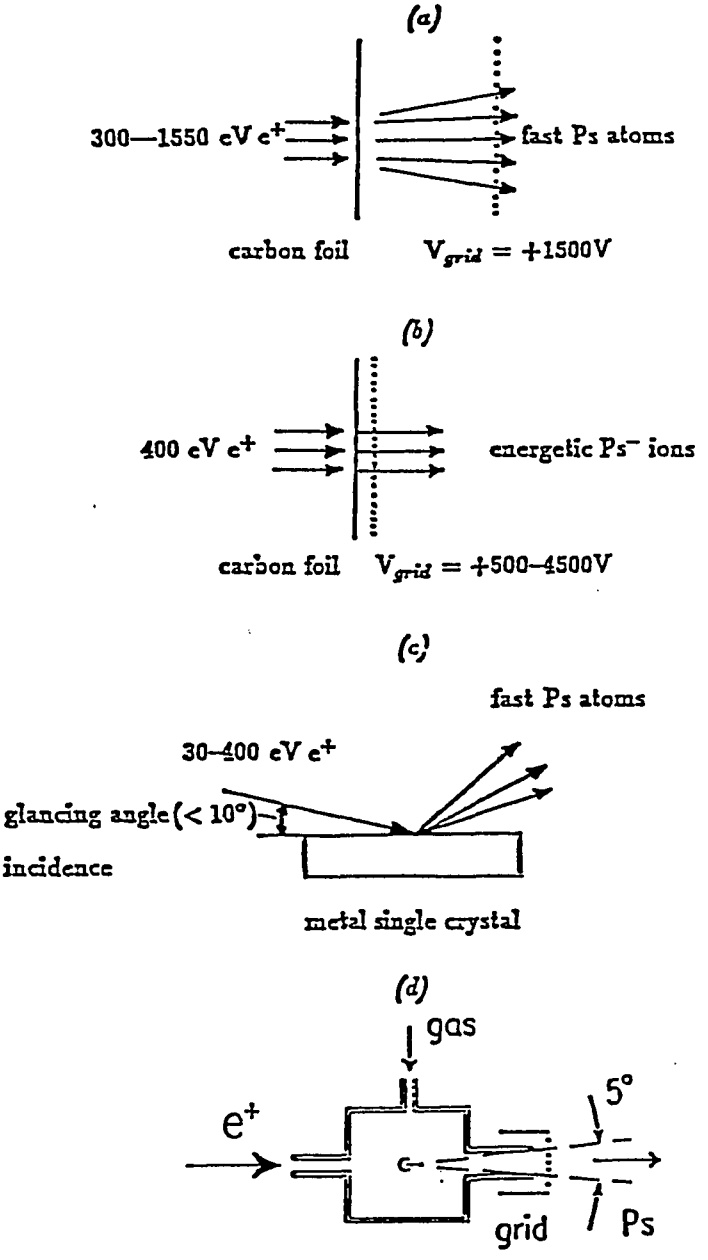

Figure 2.2.4 Some of the possible positronium beam production set ups. *(a)* The fast positronium production with a carbon foil; *(b)* the production of energetic Ps^- ions; *(c)* the emission of fast positronium by glancing angle incidence of low energy positrons on a metal single crystal surface; *(d)* the variable energy positronium production with a gas cell.

from the positronium cross section measurements, and the differential cross section calculation indicated that formation is peaked at forward direction, which make a usable positronium beam with finite diameter possible. The positronium produced in this approach is highly mono-energetic especially in low energy range and the very small portion of contamination to the main mono-energetic positronium are of discrete energies in contrast to the other production approach where the energies are over a broad spectrum of energy. These characteristics are very important for the surface scattering and diffraction experiments where the mono-energetic positronium beam is required. The disadvantage of the gas cell is its relative high gas pressure, but it can be partially remedied by using differential pumping, in which the experimental chamber's pressure would be a few orders lower than the gas cell, and the condition can be further improved in the future by employing a gas jet instead of a uniform high gas density gas cell. Another positive factor is that the gases used in the positronium production such as He or Ar are inert and do not react to surfaces in the room temperature. The mono-energetic positronium production with a gas cell will be discuss in the following text.

Table 2.2.2 The positron interaction with gas.

Interaction	Threshold energy (eV)	
	He	Ar
$e^+ + A \rightarrow e^+ + A$	0.0	0.0
$e^+ + A \rightarrow Ps + A^+$	17.7	8.9
$e^+ + A \rightarrow e^+ + A^*$	21.2	11.8
$e^+ + A \rightarrow Ps^* + A^+$	22.8	14.0
$e^+ + A \rightarrow e^+ + e^- + A^+$	24.5	15.7
$e^+ + 2A \rightarrow Ps + A^+ + A^*$	38.9	20.7

Ps^* and A^* represent the excited states $n \geq 2$ for the positronium atom and gas atom respectively.

When positrons enter the gas cell, a number of interactions with the gas atoms are possible. Table 2.2.2 list some of the interactions that may take place in the order of their threshold energies. The channel for each interaction will be open as soon as the positron's energy reaches the threshold energy for that interaction. Because the threshold energy for elastic scattering is zero (the channel is always open), it is the dominant process in the very low energy range. As our main concern is the positronium formation, the positron elastic scattering process in the gas will not be discussed here except those aspects that affect the positronium formation process. In view of positronium formation, the positron elastic scattering by gas atoms is mainly considered as an attenuation factor for the positrons available to form the positronium atoms. Only those being elastically scattered in the forward direction contribute to the positronium formation. The energy they lost during those scattering and the transverse velocity they gained in the process, however, affect the energy characteristic of the positronium beam. The energy loss involved in the elastic scattering is the recoil energy of the gas atom. As the mass of the gas atom is far more greater than that of the electrons, the recoil energy is expected to be low. It is important to know its value also for the case of positronium formation process. Fortunately, it is can be estimate relatively easily for the cases of elastic scatterings, positronium formation, and even inelastic scatterings if all the energy losses can be accounted for, though the exact solution may be a little complicated. As the kinetic energy of gas atoms is the thermal energy about (3/2)KT, the velocity of gas atom in room temperature ($\sim 1.4 \times 10^5$ cm/sec for helium and $\sim 4.3 \times 10^4$cm/sec for argon atom) is much lower than those for electrons ($\sim 5.9 \times 10^7$cm/sec, for example, at only 1 eV). It is a reasonable good approximation to assume, for the simplicity, that the gas atom is at the rest before the interaction. With this assumption, the process can be illustrated by Fig. 2.2.5. A positron comes in with the energy with the velocity v_o and $E_o = v_o^2/2m_e$ (m_e is the mass of a positron or an electron), loses energy Q (Q is zero for

elastic scattering), and then leaves with mass m' ($m' = m_e$ for positron elastic or inelastic scattering), velocity $\mathbf{v}'$, and energy $E' = v'^2/2m'$ at the scattering angle θ, resulting in an energy $E_A = v_A^2/2M_A$ (where $\mathbf{v}_A$ and M_A is the velocity and mass for the gas atom respectively) gained by the gas atom. The conservation of energy and momentum requires that:

$$E_0 = Q + E' + E_A; \tag{2.2.19}$$

and:

$$m_e\mathbf{v}_0 = m'\mathbf{v}' + M_A\mathbf{v}_A. \tag{2.2.20}$$

From Eq. (2.2.20), one can get:

$$M_A^2v_A^2 = m_e^2v_0^2 + m'^2v'^2 - 2m_em'\mathbf{v}_0 \cdot \mathbf{v}' \tag{2.2.21}$$

or

$$M_A^2v_A^2 = m_e^2v_0^2 + m'^2v'^2 - 2\cos\theta m_em'v_0v'. \tag{2.2.22}$$

Considering Eq. (2.2.19) and the relations between the velocities and energies, one can reduce Eq. (2.2.22) to:

$$(M_A + m')E_A = (m_e + m')E_0 - m'Q - 2\cos\theta\sqrt{m_em'}\sqrt{E_0(E_0 - Q - E_A)}. \tag{2.2.23}$$

Because $M_A \gg m_e$ or m', and $E_A \ll E_0$ or Q, Eq. (2.2.23) can be approximated as:

$$E_A = \frac{1}{M_A}\left[(m_e + m')E_0 - m'Q - 2\cos\theta\sqrt{m_em'}\sqrt{E_0(E_0 - Q)}\right]. \tag{2.2.24}$$

For the positron elastic scattering, $m' = m_e$ and Eq. (2.2.24) becomes:

$$^{el}E_A = \frac{2m_eE_0}{M_A}(1 - \cos\theta). \tag{2.2.25}$$

For the positron inelastic scattering, it becomes:

$$^{inel}E_A = \frac{m_e}{M_A}\left[2E_0 - Q - 2\cos\theta\sqrt{E_0(E_0 - Q)}\right]. \tag{2.2.26}$$

For the positronium formation process, $m' = 2m_e$ and Eq. (2.2.24) is reduced to:

$$^{Ps}E_A = \frac{m_e}{M_A}\left[3E_o - 2E_{th} - 2\sqrt{2}\cos\theta\sqrt{E_o(E_o - E_{th})}\right], \qquad (2.2.27)$$

where E_{th} is the threshold energy for positronium formation.

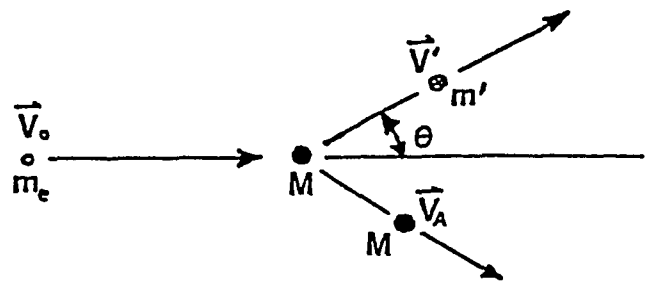

Figure 2.2.5 A diagram of the positron interaction with the gas atom (including the scattering and positronium formation). o is incident positron with a mass m_e; • is the gas atom with a mass M; ⊗ is the scattered positron or the positronium formed with a mass m' (which is m_e for a positron and $2m_e$ for a positronium atom).

For the case of elastic scattering, the recoil energy of the gas atom is about $4m_e/M_A$ of E_o at the maximum (corresponding to the case of 180° scattering), which is about 0.054% for helium and 0.0054% for argon. The effect would even be lower for those elastically scattered in the forward direction. From above estimate, one can conclude that the recoil energy of the gas atom, or the loss of the positron energy during the elastic scattering process is negligible. For the positronium formation case, the recoil energy is also very small. Table 2.2.3 lists a few values of the ratio between the recoil energy of the gas atom and the positron incidence energy for various positron incidence energies and positronium emission angles. Eq. (2.2.27) also shows that for those positronium atoms emitted in the forward direction, which form the positronium beam, the energy loss through the recoil of the gas atoms is lower than

for those emitted backward. The energy loss from the recoil energy of the gas atom is much much smaller than the energy spread (fraction of eV) of the incoming positrons, so it has little effect on the energy of the positronium produced.

Table 2.2.3 The ratio between the recoil energy of the gas atom ${}^{Ps}E_A$ and the positron incidence energy E_o in the positronium formation process is given by $m(n)$ where ${}^{Ps}E_A/E_o = m \times 10^n$.

E_o(eV)	He			Ar		
	0°	45°	90°	0°	45°	90°
20	3.7(-5)	7.5(-5)	1.7(-4)	3.9(-8)	8.4(-6)	2.9(-5)
50	2.5(-6)	9.3(-5)	3.1(-4)	1.1(-6)	1.1(-5)	3.6(-5)
75	7.6(-6)	1.1(-4)	3.4(-4)	1.5(-6)	1.2(-5)	3.8(-5)
100	1.1(-5)	1.1(-4)	3.6(-4)	1.7(-6)	1.2(-5)	3.8(-5)

When the positron incidence energy exceeds the threshold energy for positronium formation E_{th}, positronium formation will start to take place. The threshold energy is determined by the first ionization energy E_i of the gas atoms and the positronium binding energy E_B. As the binding energy is about the same in the low density inert gases as in the vacuum, it is just E_B^∞ defined before, which has a value of 6.8 eV. The first ionization energies for helium and argon are 24.5 eV and 15.7 eV respectively, so the positronium formation threshold energies are 17.7 eV and 8.9 eV respectively. The energy of positronium is the positron incidence energy minus the positronium formation threshold energy (as discussed above, the recoil energy of the gas atom is negligible). It is expected that the formation cross section should increase rapidly immediately following the threshold energy, reaches its maximum, then decrease as the positron incidence energy continues to increase. Experimental efforts to measure the total cross sections of positronium in different gases have been reported (see, for examples, Fornari and others 1983, Griffith 1984, Fromme and others 1986, Diana

and others 1986). Theoretical calculations of the total cross section for positronium formation have also been reported (Khan and Ghosh 1983, Mandal and others 1979). The Fig. 2.2.6 shows the measurements of the total cross sections in both helium and argon by the Texas' group. Table 2.2.4 shows some theoretical calculations of the positronium formation total cross section for helium by two approximations (Khan and Ghosh 1983, Mandal and others 1979). The distorted-wave polarized orbital method (Khan and Ghosh) is the most recent approximation method and is considered more accurate than the other method. No result has been reported yet on the calculation of the positronium formation total cross section in argon.

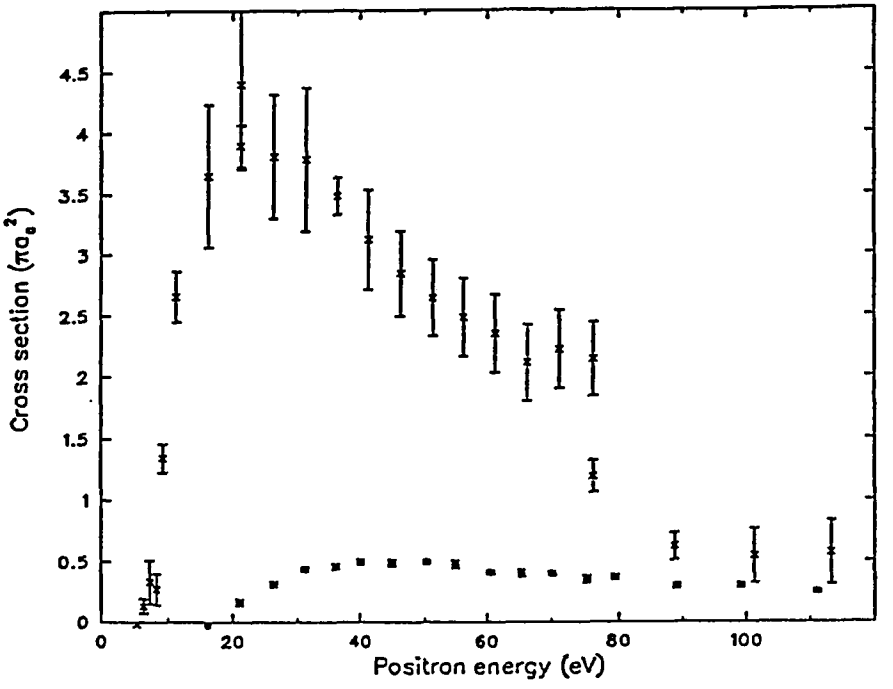

Figure 2.2.6 The total positronium formation cross sections for helium (•) and for argon (×) measured by Fornari and others (1983) and Diana and others (1986).

Table 2.2.4 The total positronium formation cross sections calculated for helium by two different approximation methods.

Positron Energy(eV)	A(πa_o)	B(πa_o)
19.0	0.17160	
20.0	0.2094	0.0921
24.5	0.32546	0.3303
28.0	0.39056	0.4581
40.0	0.4156	0.5449
60.0	0.2644	0.3474
100.0	0.0955	0.129

A: The result from the distorted-wave polarized orbital method (Khan and Ghosh 1983).

B: The result from the distorted-wave approximation (Mandal and others 1979).

For a positronium beam produced in a gas cell, the information on the positronium differential cross sections is even more crucial than the total cross sections, because only those positronium atoms formed within a cone in the forward direction will contribute to the total intensity of the positronium beam. The size of the cone will depends on the individual design of the gas cell and the beam apparatus. Unfortunately, few experimental efforts have been reported on the measurements of the positronium formation differential cross section. The theoretical calculation does provide some information on the positronium formation differential cross sections for helium, but no result yet has been reported for argon. Fig. 2.2.7 shows the the theoretical value of the positronium formation differential cross sections in helium gas for different energies with different approximations. These results, though different from each other, clearly indicate the positronium formation cross section is peaked in the forward direction when the positron energy exceeds the positronium formation

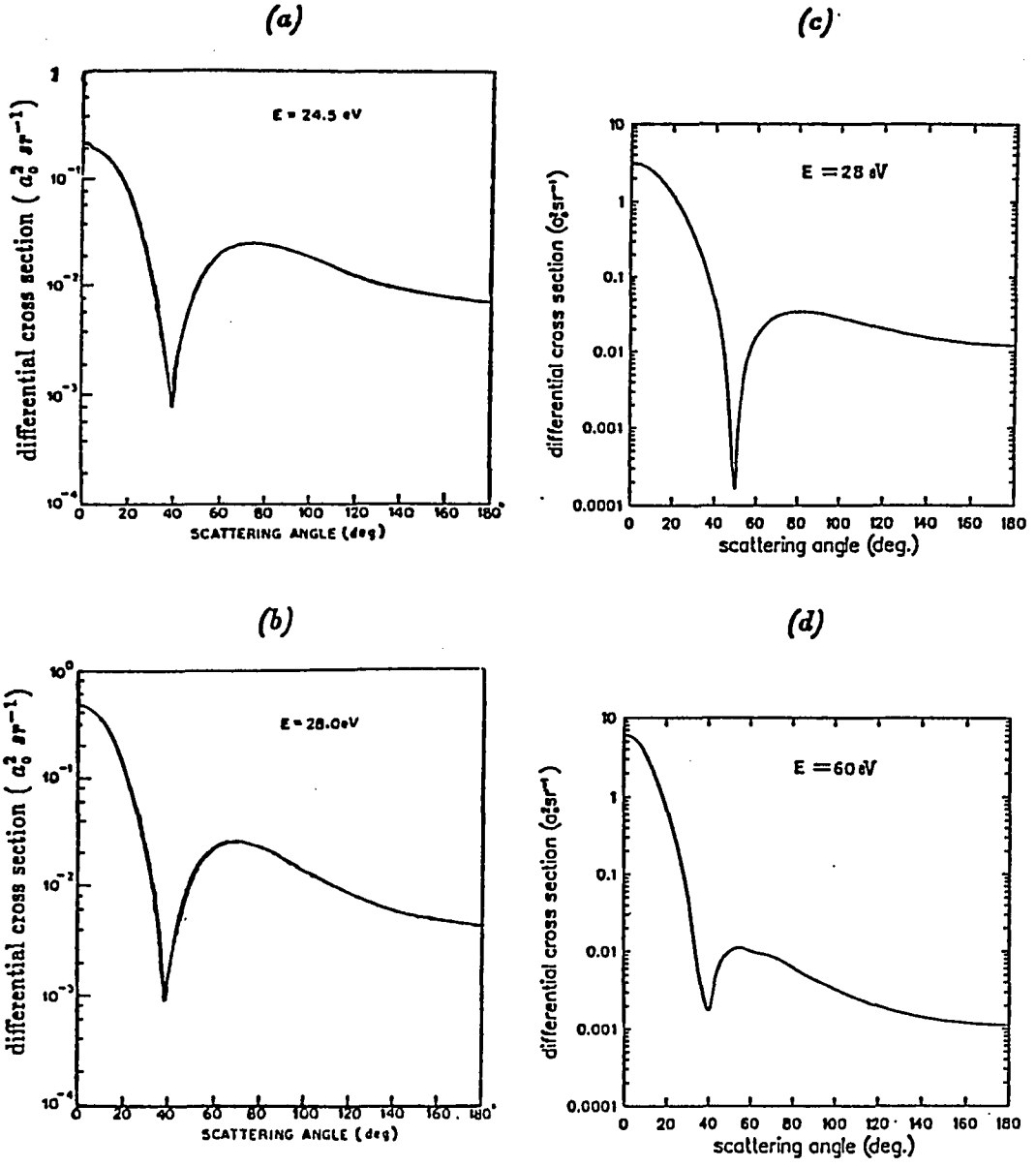

Figure 2.2.7 The calculated positronium formation differential cross sections for helium for different positron energy by different approximation methods: *(a)–(b)* are by distorted-wave polarized orbital method (Khan and Ghosh 1983); *(c)–(d)* are by distorted-wave method (Mandal and others 1979). The positron incidence energies are indicated in the plots.

threshold energy by a few eV. This can also be seen from the value of the following ratio:

$$\left(\frac{d\sigma}{d\Omega}\right)\Big/\left(\frac{\sigma_{total}}{4\pi}\right) \equiv \left(\frac{d\sigma}{d\Omega}\right)\Big/\left(\frac{d\sigma}{d\Omega}\right)_{isotropic}, \qquad (2.2.28)$$

which is the ratio between the actual differential cross sections at the given direction and the "isotropic differential cross section" defined as the total cross section divided by the total solid angle 4π. (If the process is isotropic, this ratio will be one and the differential cross section will be equal to "isotropic differential cross section.") Table 2.2.5 gives the value of this ratio for three different energies in the forward direction (θ=0) by two approximation approaches. Although the values by different approaches are different from each other, they both are greater than one at energy 10ev or more above the positronium formation threshold energy and indicate a very large proportion of positronium atoms are formed in the forward direction at those energies. This value also increases with the increase of the positron energy. This behavior seems to be consistent with the belief that the transverse momentum of the formed positronium is due to the the electron momentum associated with the orbital energy of the electron therefore more positronium atoms should be formed in the forward direction as the ratio between the positron energy and the orbital energy of the electron increases. Since there is no theoretical calculation available for argon, it can only be speculated that the positronium atoms formed in the argon gas may be more strongly peaked in the forward direction, because the orbital energy of the outermost electron in argon is less than that in helium.

There is an energy region for positrons in which the only possible inelastic event is the positronium formation. This region is sometime called the "Ore" gap region. It is very small because other inelastic channels open only a few eV higher. For helium or argon, the next channel is the positron inelastic scattering resulting in excited states of the gas atoms. This interaction contributes only to the attenuation of the incoming

Table 2.2.5 The values of the ratio define by Eq. (2.2.28) for helium by two different approximation method.

Positron Energy(eV)	A	B
20.0	0.18147	
24.5	2.7653	
28.0	5.121	27.64
40.0		46.8
60.0		71.7

A: The result from the distorted-wave polarized orbital method (Khan and Ghosh 1983).

B: The result from the distorted-wave approximation (Mandal and others 1979).

positron beam but not to the quality of the formed positronium beam, therefore can be treated just like other attenuation factors such as elastic scattering. We can also treat the positron ionization of the gas atoms similarly. Another interaction of positrons with gas, the formation of positronium atoms in excited states, is, however, the factor that affects not only the measured intensity of the positronium beam but also the quality of the positronium beam. Because the binding energy of positronium atoms in $n = 2$ states is about 5.1 eV less than that of the ground state positronium, the formation threshold energy is about 5.1 eV higher than that of ground state positronium atoms. Their kinetic energy is then about 5.1 eV lower than that of ground state positronium. There are one (spin) singlet 2S state ($2\,^1S_0$), three singlet 2P states ($2\,^1P_1$), three (spin) triplet 2S states ($2\,^3S_1$), and nine triplet 2P states ($2\,^3P_i$, $i = 0, 1, 2$). Among them, all twelve 2P states can decay to ground state 1S quickly by Lyman-α optical decay. As discussed in 2.2.1, the decay rate of 2P states by annihilation is much longer than that by the optical decay, so the life time of 2P states is the life time of 2P states against optical decay, which is calculated to be

about $3.19nsec$. The four 2S states can only decay through the annihilation because of the selection rules for optical decay (as discussed in 2.2.1). Their life time against annihilation are $1nsec$ and $1.14\mu sec$ for the singlet and triplet states respectively, eight times of that for 1S states. There are no quantitative measurements reported on the formation of positronium atoms in excited states in the gas. There is an theoretical effort to estimate the formation cross sections of positronium atoms in the $n = 2$ states for positron scattering from hydrogen and helium atoms (Khan and others 1985). Fig. 2.2.8 shows the calculated cross sections for 2S and 2P states as function of the positron energy by Khan and others. Fig. 2.2.9 shows the ratio of the calculated cross sections of 2S and 2P (Khan and others 1985) to that of 1S calculated by the same approximation method (Khan and Ghosh 1983). It is clear that there is an appreciable portion of positronium atoms in the excited states, especially at positron energy near 50 eV, in the positronium formation process in helium. There are no theoretical or experimental results on the formation of positronium in excited states in the positron argon atom scattering process. Even though an appreciable portion of $n = 2$ states is expected for positronium formation in argon, it is difficult to speculate quantitatively.

The effect of formation of positronium atoms in excited states is two fold. For positronium atoms in the spin singlet 2S state, they decay quickly by annihilation with a life time of $1nsec$. For positronium atoms in singlet 2P states, they optically decay into singlet 1S state with a life time of $3.19nsec$ (before they decay by annihilation in 2P states) then quickly decay by annihilation with life time of $0.125nsec$. Both of the singlet states 2S and 2P do not contribute to the positronium beam intensity we measure at the end of the beam, as they decay through different channels long before reach the detectors at the end of the beam unless the detector is purposely placed very close to the gas cell. Thus the formation of positronium atoms in spin singlet excited state has little effect on the making of mono-energetic positronium

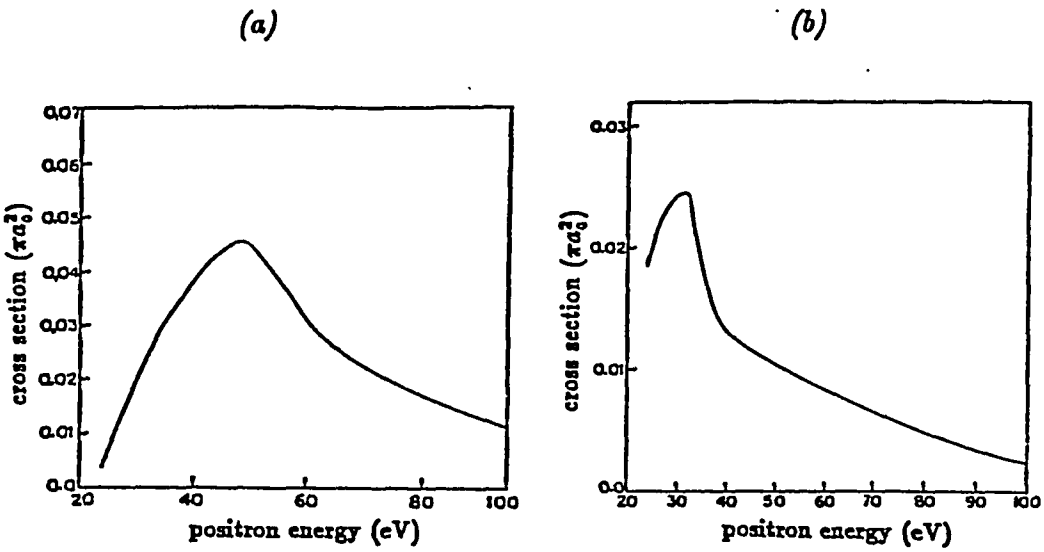

Figure 2.2.8 The cross sections for Ps formation in the 2S *(a)* and 2P *(b)* states in e^+-He scatterings (Khan and others 1985).

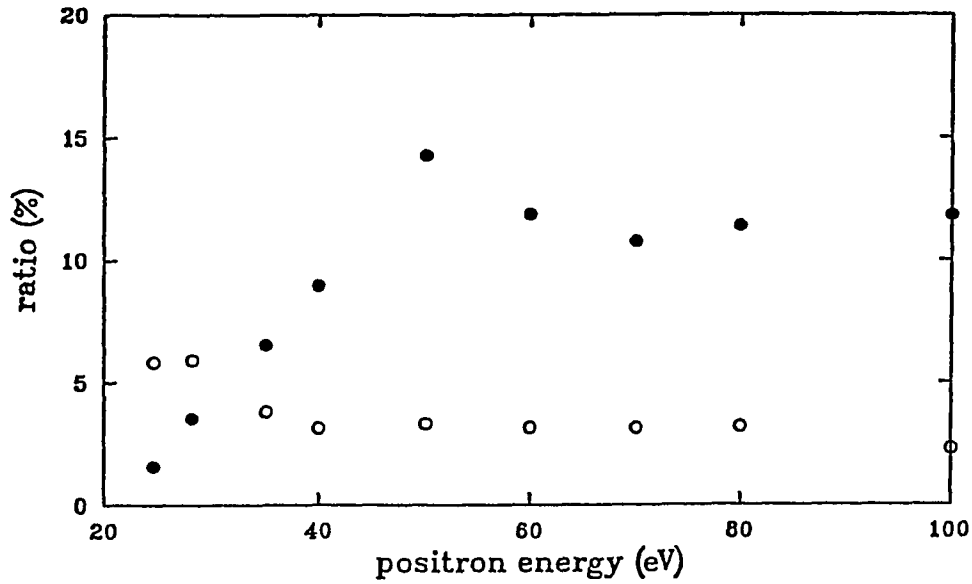

Figure 2.2.9 The ratios of the Ps formation cross sections of 2S (•) and 2P (o) states to that for the ground state (Khan and others 1985).

beam. For the positronium atoms in the spin triplet 2P states, they optically decay to ortho-positronium atoms quickly with a life time of $3.19nsec$. They contribute to the positronium beam intensity we measured, but they are also (5.1 eV) less energetic than those originally formed ortho-positronium so they suffer more loss on the flight path than those originally formed at the ground state. It also represents a small amount of contamination to the mono-energetic positronium beam. For positronium atoms in spin triplet 2S state, they can only decay through the annihilation with a life time of $1.14\mu sec$. Since their life time is relatively long, they suffer much less loss on their flight path than those in the ground state. They contribute to the total positronium beam intensity. They are also (5.1 eV) less energetic than those in the ground state. For those experiment in which delivering maximum number of positronium to a certain distance is the goal, the formation of positronium atoms in $2\,^3S_1$ states represents a advantage that can be utilized. For those experiments in which a single type of mono-energetic positronium atoms are needed to study their interaction with surface or matters, the formation of positronium atoms in $2\,^3S_1$ states represents another complication, for they not only create a small contamination to the mono-energetic positronium beam (as 2P positronium atom do), but they also do not interact with the studied target exactly same way as ortho-positronium atoms do. Thus the formation of positronium atoms in spin triplet excited states has a negative effect on the making mono-energetic positronium beam and possibly produces some difficulties in the application of the positronium beam.

The extent of this effect depends on the percentage of the positronium atoms in the excited states in the positronium beam and survival rates of both ground state ortho-positronium atoms and positronium atoms in the excited state. It has been argued that the much less value of the binding energy of $n = 2$ positronium atoms make them vulnerable against breaking up during their collision with gas atoms in the gas cell. At same time, larger scattering cross sections with gas atoms for those

excited positronium atoms are also expected because of their larger physical size (two time in size, four times in physical cross section, and eight times in volume of that of ground state positronium atoms). These two factors, if verified to be the case, would greatly increase the loss of those positronium in the excited states and, therefore, reduce the their effect considerably.

Another two process that should be considered are the elastic and inelastic scattering of positronium by the gas atoms in the gas cell. The elastic scattering by the gas atoms reduces the flux of the formed positronium beam because it changes the travel direction of some of the scattered positronium atoms and effectively removes them from the beam, but those positronium being scattered forward by the gas atoms suffer little loss of the energy due to the much heavier mass of the gas atoms (similar to the case we discuss earlier for the positron scattering by the gas atoms) and do not worsen the quality of the mono-energetic positronium beam. The inelastic scattering of positronium atoms not only effectively removes some of positronium atoms out of the positronium beam, it also contributes to the energy spread of the positronium beam because those positronium atoms inelastically scattered in forward direction will suffer an energy loss for amount of excitation energy of the gas atoms. The effect of these two process to the positronium production are not significant in the low density gas cell set up. When the density the gas in the gas cell is increased, the effect of those two process becomes more appreciable. The scattering of positronium in gas by gas atoms is also believed to be responsible for the plateau of the positronium beam flux after its initial increase with the increase of the gas density (pressure). In our positronium beam, this effect is believed to be insignificant.

Another factor which may reduce the flux of the positronium beam is the transverse energy of the incident positrons. For a positron of energy E with a small amount of transverse energy E_t in the magnetic field, it travels in a spiral motion along the

magnetic field lines (beam direction). Even though it propagates along the beam direction, its momentum is not parallel to the beam direction at any given instance and has an angle $\theta (\sim \sqrt{E_t/E})$ with the beam direction. Since more positronium atoms are formed in the initial direction of incident positrons, the positrons with some transverse energies contribute less to the production of positronium atoms in the forward direction than the positrons without transverse energy do, representing a reduction of efficiency. The actual loss depends on the distribution of transverse energy of the incident positrons, the values of the differential positronium formation cross sections at the given energy, and the geometry of the actual beam.

Armed with the knowledge discussed above, we began the construction of the variable energy mono-energetic positronium at the HFBR.

2.2.3 The HFBR positronium beam and its experimental apparatus — Using the HFBR high intensity positron beam as the mono-energetic positron source and employing a differentially pumped gas cell, we constructed a mono-energetic positronium beam. The Fig. 2.2.10 shows the overview of the entire positron and positronium beam. The mono-energetic positrons filtered by a **E**×**B** filter are guided out of the block house by the magnetic field and into a magnetic beam switcher (splitter). The switcher can either deliver the positron beam into a straight through port or bend the beam to a port about 30 degree from the original beam direction. The positronium beam constructed at HFBR is connected to the straight port on the switcher while another experiment ("search for the single photon annihilation" experiment) is connected to the port on the side through a bending solenoid. The two diffusion pumps and a turbo-molecular pump are used to facilitate the differential pumping of the gas cell. Of the positronium atoms produced in the gas cell, those traveling in the forward direction are guided into the experimental chamber by the baffle tube at the end of the gas cell. The detector at the experimental chamber can measure

both the positronium beam intensity and the positronium atoms scattered from the sample surface.

As being discussed in section 2.2.2, the gas cell production mechanism has reasonable high efficiency and is capable to produce highly mono-energetic positronium, but also requires a relative high gas pressure, typically on the order of 10^{-3} torr. Since the positronium surface scattering experiments are the main experiments being performed for this project, a good vacuum environment is required in the experimental chamber as in any other surface experiments. To maintain the maximum positron yield from the self-moderated positron source (described in section 2.1.2), the source chamber also has to be kept in a good vacuum condition. The differential pumping set up in this system is designed to maintain a relative low pressure for both experimental chamber and the source chamber while the positronium production is taking place in the gas cell.

Two diffusion pumps are used in the system because of their high pumping speed especially for the inert gas (some commonly used pumps like ion pumps, even though they can pump most of cases efficiently, can not pump the inert gas very efficiently), their tolerance for the high gas pressure, and their low cost. The two diffusion pumps used in this set up are the Varian VHS–6 pumps which have pumping speed of $2400l$/sec. for air. To prevent any possible backstream to the beam from the pumps, the cryotraps are used together with those diffusion pumps. The air-operated gate valves are also installed between the diffusion pumps with cryotraps and the beam. The combination of the diffusion pump, cryotrap, and gate valve has lower pumping speed of about $940l$/sec.. Comparing to the diffusion pump alone, it provides much cleaner and safer pumping unit with reasonable pumping speed. A Balzers turbo-molecular pump with the pumping speed of $1500l$/sec (for N_2 and $1550l$/sec. for He) is used in the experimental chamber, because it not only has a very high

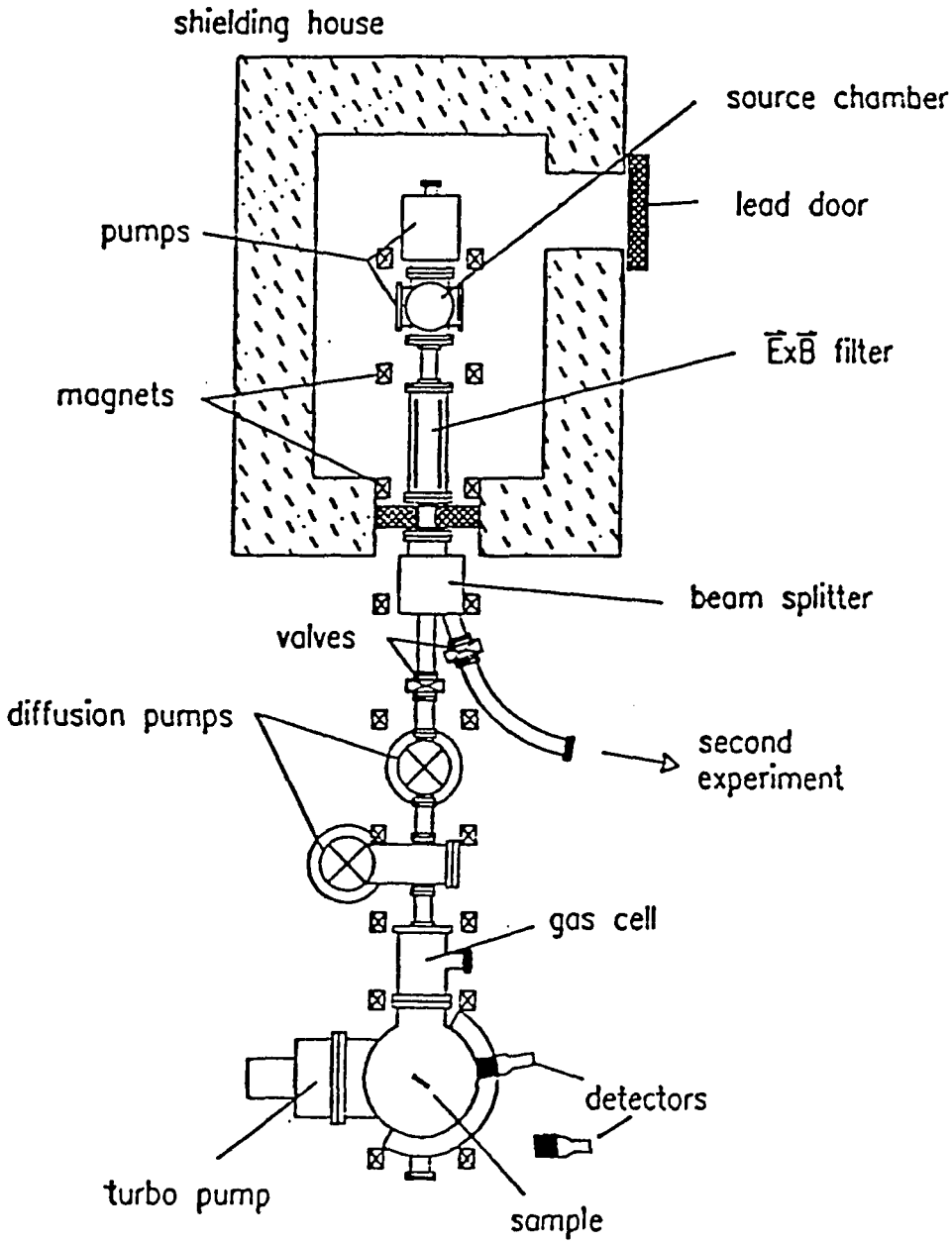

Figure 2.2.10 The overview of the positron and positronium beam and positronium-surface scattering experiment facility.

pumping speed and is tolerant to the high gas load but also can provide an ultimate pressure of UHV, which is extremely important to the experimental chamber. The gas baffle tubes of 5/8" dia. are installed at the conjunctions between the gas cell and experimental chamber, between the gas cell and the diffusion pump, between the two diffusion pumps, and between the first diffusion pump and the positron beam switcher to facilitate the differential pumping.

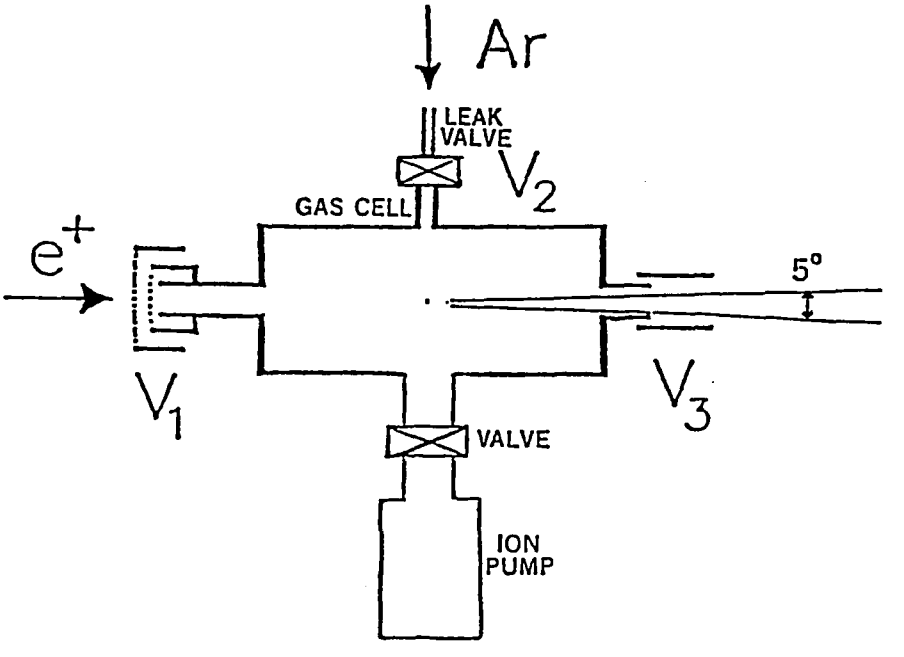

Figure 2.2.11 The diagram of the gas cell.

The functioning structure of the gas cell is illustrated in Fig. 2.2.11. The length of the gas cell is 22 cm. As shown in the Fig. 2.2.11, there is grid in front of the gas cell floated at a variable voltage V_1. It is mainly used as a positron beam switch. When it is biased with a positive voltage, typically 200 $\sim$ 300 V, higher than positron beam energy, it rejects the positron and prevents the positron entering the gas cell, therefore effectively turns the beam "off;" when it is grounded, the incoming positrons can then pass the grid and enter the gas cell thus effectively turn the beam "on." The gas cell

is also can be floated electrically at voltage V_2, so the energy (E_{e+}) of positrons in the gas can be varied by setting different voltages V_2 at the gas cell ($E_{e+} = E_{beam} - eV_2$) for the positron beam of the constant energy (E_{beam}). Since the positronium atoms formed in the gas cell are highly mono-energetic, the energy of the formed positronium atoms are determined by the energy of positrons at the gas cell. Thus the energy of formed positronium atoms can be controlled by the voltage on the gas cell, and this is the method we used in this project to change the energy of positronium atoms formed in the gas cell. The grid connected to the gas cell is installed to ensure the parallel (to the beam axis) electrical field when V_1 and V_2 have different values so the positrons can be accelerated or decelerated without increasing their transverse velocity.

The gas cell has small diameter necks at the both ends as part of the gas baffle to restrict the gas flow at both end. A leak valve is used to introduced the gas atoms needed for positronium production. It is a piezoelectric leak valve controlled by a Perkin-Elmer Ion Gauge controller with a pressure control optional board which provides 0–100 V to the valve according the pressure reading from the gauge to maintain a constant gas pressure in the gas cell. There is also a electrically floated tube at the exit of the gas cell. This tube has dual functions, one of which is to be a gas baffle tube to restrict the gas flow to the experimental chamber, and another is to be a positron rejector to prevent any residual positron in gas cell from coming into the experimental chamber if a high positive voltage (typically 200 $\sim$ 300 V) is applied to the tube during the experiments in which only positronium atoms are needed. A 60l/sec. ion pump with a vacuum gate valve is used to help pump out any non-desirable residual impurity gas (any non-Ar gases) and to achieve a better ultimate pressure for gas cell before the high purity Ar gas is introduced into it, compensating the insufficient pumping due to the differential pumping set up. The ion pump is valved off from the gas cell when the Ar gas is introduced into the gas cell.

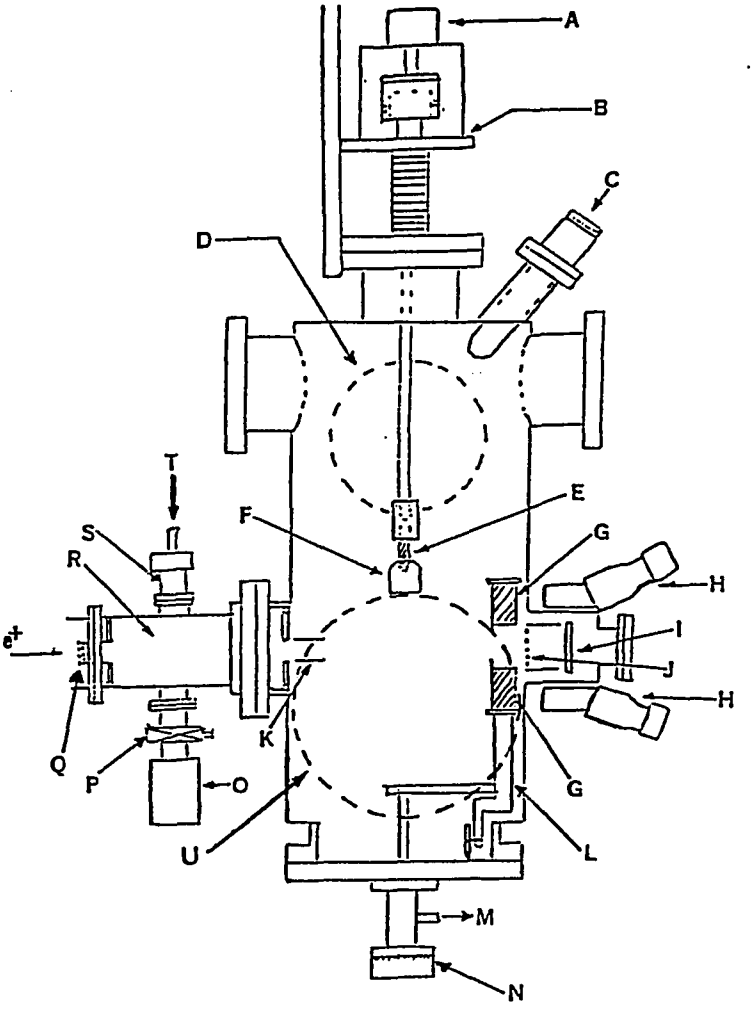

Figure 2.2.12 The diagram of the gas cell and the experimental chamber(not to scale). The various facilities shown in the figure are noted as: A. the computer controlled stepping motor; B. sample manipulator; C. ion sputtering gun; D. LEED and Auger facility; E. insulator rod; F. the sample holder and heater; G. internal heavy metal shielding; H. BGO detectors; I. channel plate used as an annihilation plate; J. the positron rejection grid; K. gas baffle and charge rejection tube; L. the cart for the annihilation plate and shielding; M. differential pumping outlet to roughing pump; N. the differentially pumped rotary port as the cart manipulator; O. a small ion pump; P. vacuum valve; Q. beam "on" or "off" grid; R. gas cell; S. piezoelectric leak valve for gas inlet; T. high purity Ar inlet; U. turbo-molecular pump port.

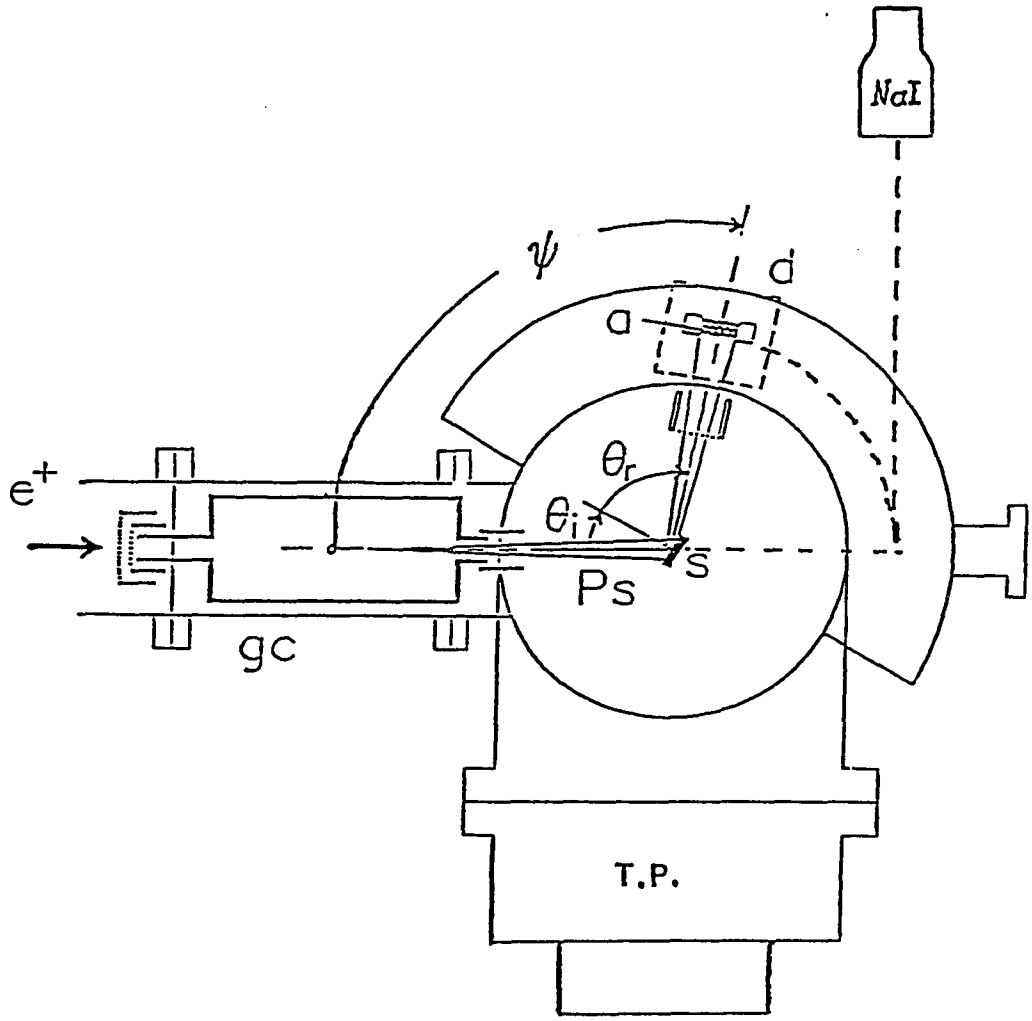

Figure 2.2.13 The top view of the gas cell and the experimental chamber(not to scale). The notations are: *gc* for the gas cell; *s* for the sample; a for the annihilation plate; *d* for the detector set up including the annihilation plate and two BGO scintillator detectors (see Fig. 2.2.12 for the geometry of the detector set up); *NaI* for the NaI scintillator detector; and *T.P.* for the turbo-molecular pump.

The Figs. 2.2.12&2.2.13 provide views of the gas cell and experimental chamber at different angles. The Fig. 2.2.14 gives an enlarged view of the detector set up. Not being shown in the figures is the external heavy lead shield for the detectors.

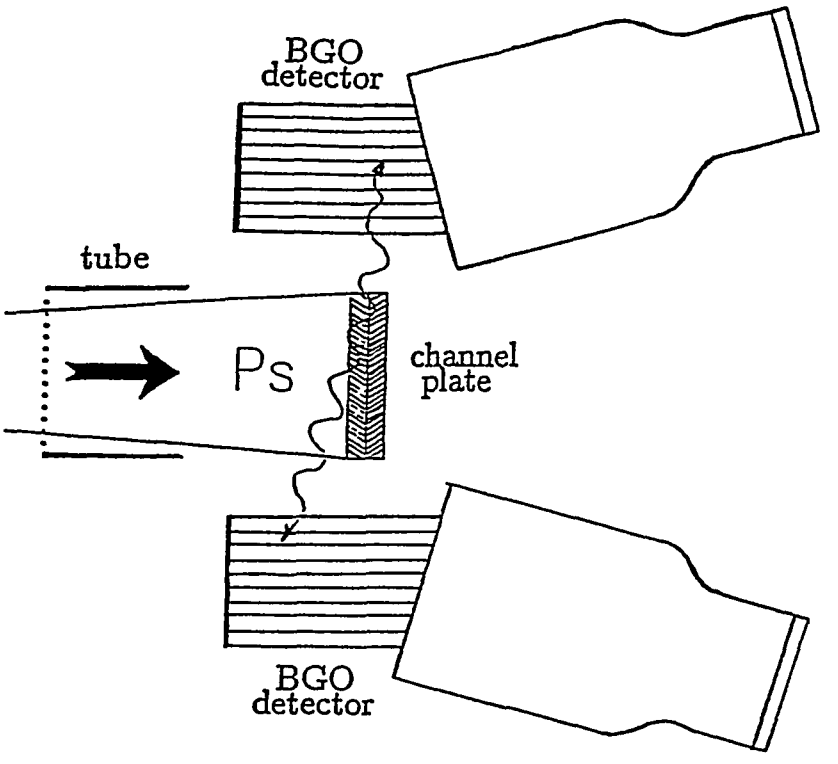

Figure 2.2.14 The enlarged diagram of the detector set up

The components of the experimental chamber are for one of the two main functions: positron or positronium detection and preparation or controls of the samples. While most of the components for the preparation or controls of the samples are concentrated in the top of part of the chamber, those for the detection are mainly located at the beam level or below.

The sample manipulator is framed on a six inches O.D. flange and is mounted on the center top port of the experimental chamber. This manipulator has about 12 inches linear (z direction) motion capability, about one inch in plane (x-y direction) motion capability, and 360° rotation capability. Its rotation is driven by a stepping motor which is normally controlled by the same computer that controls the data taking and also can be operated manually. The other motions are controlled manually.

The sample holder and heater assembly is mounted on the manipulator rod through a piece of Al_2O_3 insulator rod and a coupler so the sample assembly can be electrically floated. The assembly contains the mounting frame for the sample and a heater. Different heater have been used for different samples. A conduction heating was used to heat the LiF sample while an e-beam heating was used for heating the Cu sample. There is LEED and Auger facility and an ion sputtering gun mounted on the top portion of the chamber for the sample surface preparation. The sample can be positioned at the beam level for the surface scattering experiments, or at the level of LEED and Auger facility(which is about nine inches higher than the beam level) to monitor the sample surface condition, or at the position for ion sputtering by the ion gun mounted at the top side port, or any positions between those positions described.

The detection set up includes the channel plate as an annihilation plate, an electrically floated tube with a grid in front the plate, internal heavy metal shielding, two bismuth germanate (BGO: $Bi_4Ge_3O_{12}$) scintillator detectors arranged above and below the annihilation plate (geometry shown in Figs. 2.2.12&2.2.14), one NaI scintillator position 12.5 to 14 inches away on the side of annihilation plate when it is in the straight through beam position, and external lead shielding. The annihilation plate, the tube with the grid, and internal shielding are all supported by a rotatable cart which can be rotated along the side of experimental chamber as shown by the dash line in Fig 2.2.13. The cart is rotated by a slack-free rotary made of a differential rotary port at the bottom of the experimental chamber. The lead shielding of thickness up to four inches is used externally to shield the both BGO and NaI detector from the background radiation in the HFBR. The detection efficiency of the system will be discussed briefly in the next section. The important dimensions of the experimental chamber include the distance of 15 cm between the exit of the gas cell and the center of the chamber where sample is positioned and the distance of 16 cm between the center of the chamber and the position of the annihilation plate.

The ultimate pressure of the experimental chamber after baking is about 5×10^{-10} to 1×10^{-9} torr. The pressure for the experimental chamber during the production of positronium atoms when the gas cell is filled with Ar gas at 10^{-3} torr (corrected for Ar) is about 8.5×10^{-6} to 1×10^{-5} torr (uncorrected for Ar). It is certainly not the most desirable vacuum pressure for the surface scattering experiments, but the tests carried out in the experimental chamber with a residual gas analyzer clearly indicated no significant increase of the levels of the impurity gas atoms or molecules but the Ar gas. The partial pressures of various gas atoms and molecules such as H_2, H_2O, CO, CO_2, N_2, and O_2 after the Ar gas is introduced into the gas cell and the pressure of experimental chamber goes up four orders (in the range of high 10^{-6} to low 10^{-5} torr) only change to the values between half to two times of the values measured when experimental chamber at ultimate pressure (before the introduction of Ar gas into the gas cell). As far as the active impurity gases such as H_2, H_2O, CO, and O_2 concerned, vacuum condition for experiments is similar to the case where no Ar gas is introduced and the pressure is in the 1×10^{-9} range. Even though there is still a room for improvement, the condition in the experimental chamber is much better than that indicated by the vacuum gauge. At the very later stage of the experiment, an effort was made to improve the condition by increase the length of the baffle tube between the gas cell and the experimental chamber. Also being considered as a possible improvement in this direction for the future is an additional differentially pumped gas baffle, which has an external pump connected to the middle of the gas baffle tube through a special feedthrough so that most of the gas enter the gas baffle tube from the gas cell would be pumped away by the external pump and never reach the experimental chamber. Another consideration is a gas jet in the gas cell where a jet of gas would be ejected into the gas cell perpendicularly to the beam direction from one side of the gas cell and be pumped away by a pump at the other side of the gas cell, creating an environment of a relatively high density Ar gas without

generating a significant Ar gas flow towards the experimental chamber direction.

§2.3 The Efficiency Of The Ps Beam And Its Detection Set Up

The performance of the positronium beam and its detection set up is the most important factor affecting the positronium surface scattering measurements. The evaluation of the performance of the positronium beam also relies on the performance of the detection set up. In this section the detection set up used for this project will be described and discussed, then the measured efficiency of the positronium beam will be reported and discussed.

2.3.1 The detection set up — The detectors used in this project are mainly the scintillator detectors. The working principle of scintillator detectors is well understood and well known and will only be mentioned briefly. Though there is a great variety of scintillator detectors, they all consist of a scintillation phosphor and a photomultiplier tube. A scintillation phosphor is a material capable of converting radiation energy such as γ-ray photons, X-ray photons, α, and β particles into a pulse of light through the ionization of the atoms in the material by the radiation energy. A photomultiplier is used to detect the light pulses and to convert them into electronic pulses. The pulse height of the electronic pulses will depend on the radiation energy, and in some energy range it will be proportional to the radiation energy. Thus the scintillator detectors can be used not only for radiation intensity (counts or timing) measurements, but also for spectroscopic (energy) studies of the radiation in some cases. In this project, the scintillator detectors are mainly used to measure the count rates of either positrons or positronium atoms by measuring the counts of γ-ray photons. The relation of the pulse height with the energy of γ photon is also used to set our electronics to eliminate some background and undesirable scattered photons.

In the early stage of this project, a channeltron (CEM: Channel Electron Multiplier) or a channel plate (CEMA: Channel Electron Multiplier Array) was also used

to detect positrons and positronium atoms. It was expected to increase the signal to noise ratio significantly by the triple coincidence of its signal with the signals of the two scintillators. While it was very efficient to detect any positrons or the positronium with energy higher than its binding energy of 6.8 eV, it seemed to be not sensitive to positronium atoms with energy below their binding energy. Similar observation has been made elsewhere(Charlton and Laricchia 1990). It has been speculated that a Channeltron(CEM) or a channel plate(CEMA) can only detect the positronium atoms efficiently when they have energy high enough to break up into separate positrons and electrons(both charged). The life time of a channel plate (CEMA) would be greatly reduced if it is operated in a relatively high gas pressure similar to that in our experimental chamber when the gas cell is operating. Another phenomenon observed in early use of the channeltron(CEM) was that it seemed to be also sensitive to neutral gas drafting into the experimental chamber from the gas cell, thus creating an additional background. To avoid these complications, the channel plate(CEMA) has been used only as an annihilation plate as described in the last section and below.

The main detection set up we used in this project, as described briefly in the last section, is a combination of an internal annihilation plate and two BGO scintillators. Fig. 2.2.14 is an enlarged diagram of the detector set up. Also shown is the combination of a tube and a grid which can be electrically floated to any voltage and has been used as positron rejector by biasing it with high positive voltage when measuring positronium atoms. An annihilation plate is used so that positrons in the ortho-positronium atoms would likely annihilate with electrons of the plate rather than the electrons of positronium atoms and result in two photon annihilation events of the majority ortho-positronium atoms. (Without the annihilation plate, only photons from three photon annihilation, the decay process of ortho-positronium at a much slower rate, of a fraction of the positronium atoms would be emitted locally and be

detected.) The two BGO detectors are arranged above and below the annihilation plate outside the vacuum chamber. Two detectors are used for the coincidence measurements. This greatly reduces the background noise in the single count rate caused by annihilation photons from elsewhere in the experimental chamber and the gas cell measured by a single scintillator detector, because, in principle, only the annihilation taking place in the vicinity of the annihilation plate can generated those (almost) anti-parallel photon pair that can trigger the coincidence counts of both BGO detector simultaneously.

A channel plate (CEMA) is used as the annihilation plate because it is believed that its array of small channels would reduce the chances for incident positronium atoms to bounce off the surface of the annihilation plate, therefore would increase the detection efficiency. The high density bismuth germanate (BGO: $Bi_4Ge_3O_{12}$) single crystal was chosen as the scintillation phosphors for its high absorption coefficient for γ-ray, which is about 2.5 times of that of NaI, a more widely used scintillation phosphor. Because of the high absorption coefficient, the size of the crystal can be significantly (about 2.5 linearly) reduced to accommodate our experimental set up. The photomultiplier tubes used with the BGO scintillators are RS2238 photomultipliers made by Hamamatsu because these tubes are designed to be much less sensitive to magnetic fields than conventional ones which are much less tolerant to the magnetic field and its change. With these photomultiplier tubes, the detector can be used in the experimental region directly without the use of those "light-pipe" commonly employed for scintillator detectors operating near or in a magnetic field.

The detection set up was designed so that it can be moved horizontally to circle the center of the chamber (see Figs. 2.2.12&2.2.13). When the detection set up is positioned to face the incoming beam ($\psi = 180°$ where ψ is defined in Fig. 2.2.13), the intensity of the positron beam or the positronium beam can be measured with

the sample out of the way. The positronium scattering can also be measured, if the sample be lowered into the beam level and the detector is positioned at the desired angle (ψ). It is highly desirable for the surface scattering experiment that the detector can be move to cover the half circle ($\psi = 0 - 180°$), but other factors and restrictions have to be considered in designing the chamber. The original design of the experimental chamber gave a detector moving range of about 100° (ψ ranges from 80°, perpendicular to the beam, to 180° facing the beam), but the actual range has been reduced to about 85° (ψ ranges from 95° to 180°) because additional internal shielding had to be installed in the chamber, further restricting the angular range of the detector's movement.

In principle, this detector set up is the only detector we need to carry out the entire experiment including the measurements of the positron intensity, positronium intensity, and the fraction of the scattered positronium atoms for concerned geometry, but several factors such as the high intensity of the positron beam, the change of the source intensity made it more desirable to have another detector capable of monitoring the positron beam intensity. At the beginning of the experimental cycle, the intensity of the positron beam is on the order of a few million positron per second. Since the detector set up described above is designed to measure the low counts of scattered positronium atoms with maximum efficiency, the solid angle of the annihilation detection for the BGO detectors is relatively large. As a result, the BGO detector would be saturated when used to measure the positron beam intensity at the beginning of the experimental cycle and produce a serious "pile up" effect on the electronics, precluding the accurate measurements of the positron beam intensity. While it is conceivable that the BGO detector could be taken out from the set up and be positioned a distance away from the plate to carry out this task, the beam time loss due to the re-adjustment of electronics for the new position and the construction of an external shield for detector in each position make it much more

desirable to have another detector for this job. An independent detector located in a fixed position also provides more consistent beam intensity measurements as a good reference for the normalization within one experimental cycle and between the experimental cycles. For this purpose, a $3'' \times 3''$ NaI scintillator has been used. As shown in Figs. 2.2.12& 2.2.13, this detector is positioned $12.5''$ to $14''$ away from the annihilation in the direction perpendicular to the beam on the side of experimental chamber.

2.3.2 The operation of the detector — To obtain the accurate measurements with the detector set up in our system, every effort must be made to ensure that detectors are properly calibrated and all background signals have been correctly accounted for, reduced to the possible minimum, and subtracted from the total counts. A detailed discussion on the calibration and background reduction of our detector has been offered elsewhere(Weber 1988), so the similar discussion will not be repeated here, instead, only the essential points for the proper operation of the detector set up will be discussed.

In our experiment, it has been assumed that almost all the positrons and positronium atoms hitting the annihilation plate will be annihilated on the plate, therefore the detector in our system has the same detection efficiency for both positrons and positronium atoms and also can be calibrated by a small calibrated encapsulated positron source(from which none of the emitted positrons can escape but annihilate inside). For our project, the absolute counting rate is only necessary for the positron beam intensity. For the positronium beam efficiency measurements and the surface scattering measurements, only the relative counts are essential, i.e. only the count ratio of the positronium beam intensity to the positron beam intensity is essential to the measurement of the positronium beam efficiency and the count ratio of scattered positronium to the positronium beam intensity is needed for surface scattering

experiment. Reduction and proper subtraction of the background signal are crucial to all the measurements. For the BGO-annihilation plate set up, several steps have been taken to reduce the background signal and to ensure its proper subtraction. As mentioned in the last section, a pair of heavy metal shield is installed to reduce the γ-ray photons generated in gas cell and chamber reaching the BGO detectors. An external shield of up to $4''$ thick lead has been used to shield the BGO detectors. Both the internal and external shield reduces the background signal rate for each individual detector and and accidental coincidence rate ($R_c^{acc.}$), which is on the order of:

$$R_c^{acc.} = 2R_1R_2\Delta t, \tag{2.3.1}$$

where R_1 and R_2 are the single rates for detector one and two, and Δt is the time window set on the coincidence electronics. It is possible for a single photon to deposit some energy in each of two detectors due to the scattering process, but the energy of the photons would be lower in the second detector entered than the first one. Furthermore, the energy deposited in either of the two detector is less than the total photon energy. To reduce false coincidence counting from this process, the energy window in the detector electronics has been set fairly narrow so that only those pulses within FWHM pulse height range of 511 keV γ-ray (the width of the corresponding energy range is on the order of 120 keV for our BGO detectors) will be accepted for the trigging of the coincidence. Caution must be taken with the setting of the energy window, because the pulse height varies when the detectors are moved in the magnetic field and a small change of the pulse height over a long period of time is also observed. To ensure the consistency of the detection efficiency, the energy window of the electronics was re-adjusted whenever the detector was moved and at the beginning of every experimental cycle. High energy photons in the background can not be eliminated through this approach as their energy is large enough to deposit sufficient energy in both detectors to produce the pulses within the energy window

if the photon goes through both detectors. The external shield would reduce this effect partially. Fortunately, the intensity of the background high energy photons are fairly constant so it can be subtracted from our measurement through careful background measurements. Similarly, the NaI detector is shielded with lead bricks so that only the photons emitted within vicinity of the annihilation plate will reach the NaI detector without attenuation by the lead shield. The energy window in the electronics of NaI detector is also set so that only those pulses within FWHM pulse height range of 511 keV of γ-ray (FWHM is on the order of 60 eV for NaI detector used in our experiment) would be accepted. The same caution and procedure to set energy window for BGO detectors also has been practiced on NaI detectors. The energy window setting for detector electronics is usually accomplished with the help of a Multi-Channel Analyzer (MCA) in the pulse height analysis (PHI) mode. The energy output from the amplifier is used as the output for MCA input, while the timing output (pulse with standard pulse height) gated by the energy window is used as the gate input for MCA. The energy window thus can be visualized by MCA display and the proper adjustment then can be easily made.

The efficiency $\mathcal{E}_{e+}$ of a detector to detect the positron annihilation γ-ray (for two photon process only) can be approximately expressed as:

$$\mathcal{E}_{e+} = 2 f_{\Omega}\, f_{att.}\, \epsilon, \tag{2.3.2}$$

where f_{Ω} is the ratio of the detecting solid angle of the detector to the total solid angle 4π, f_{att} is the attenuation factor due to the loss of γ photons in the path to the detector, and ϵ is the detector's intrinsic efficiency for the photons at the given energy. The single rate (R) of the detector then can be written as:

$$R = \mathcal{E}_{e+} I_o = 2 f_{\Omega}\, f_{att.}\, \epsilon\, I_o, \tag{2.3.3}$$

where I_o is the positron (two photon) annihilation rate. If two detectors are positioned so that they have a space inverse symmetry about the annihilation plate or a small

encapsulated positron source, the coincidence efficiency ($\mathcal{E}^c_{e+}$) and the coincidence rate (R_c) for the positron (two photon) annihilation process with an annihilation rate of I_o can be approximately written as:

$$\begin{aligned} \mathcal{E}^c_{e+} &= 2 f_t \, f_\Omega \, f_{att.1} \, f_{att.2} \, \epsilon_1 \, \epsilon_2, \\ R_c &= 2 f_t \, f_\Omega \, f_{att.1} \, f_{att.2} \, \epsilon_1 \, \epsilon_2 \, I_o, \end{aligned} \tag{2.3.4}$$

where the detecting solid angle is assumed to be the same or the smallest f_t value has to be used, f_t is the reduction coefficient due to the imperfection of the coincidence electronics which is often assumed to be unity or close to one (it can be quite smaller than one in practice depending on the time window setting of the coincidence electronics). From Eqs. (2.3.3)&(2.3.4) we have

$$R_1 R_2 / R_c = (2 f_\Omega / f_t) I_o, \tag{2.3.5}$$

and

$$\begin{aligned} R_c / R_1 &= f_t \, f_{att.2} \, \epsilon_2 = (f_t / f_\Omega) \mathcal{E}^2_{e+}; \\ R_c / R_2 &= f_t \, f_{att.1} \, \epsilon_2 = (f_t / f_\Omega) \mathcal{E}^1_{e+}. \end{aligned} \tag{2.3.6}$$

If the both f_t and f_Ω are known or can be easily estimated, then we can deduce the detector efficiency and the positron annihilation rate from the two single rates and the coincidence rate of the two detectors ranged in the coincidence geometry. In our experiment, however, it is much easier to get the efficiency by using a small calibration source instead of estimating f_t and f_Ω*. Calibration has been carried out periodically in our experimental operation.

The Fig. 2.3.1 shows the block diagram of our data taking set ups use for the positron beam intensity measurements, positronium beam intensity measurements, and positronium surface scattering measurements. Most of our data taking processes

* The calibration source we used is a small encapsulated Na^{22} source with the activity of 1.046 μCi calibrated at October 1, 1987.

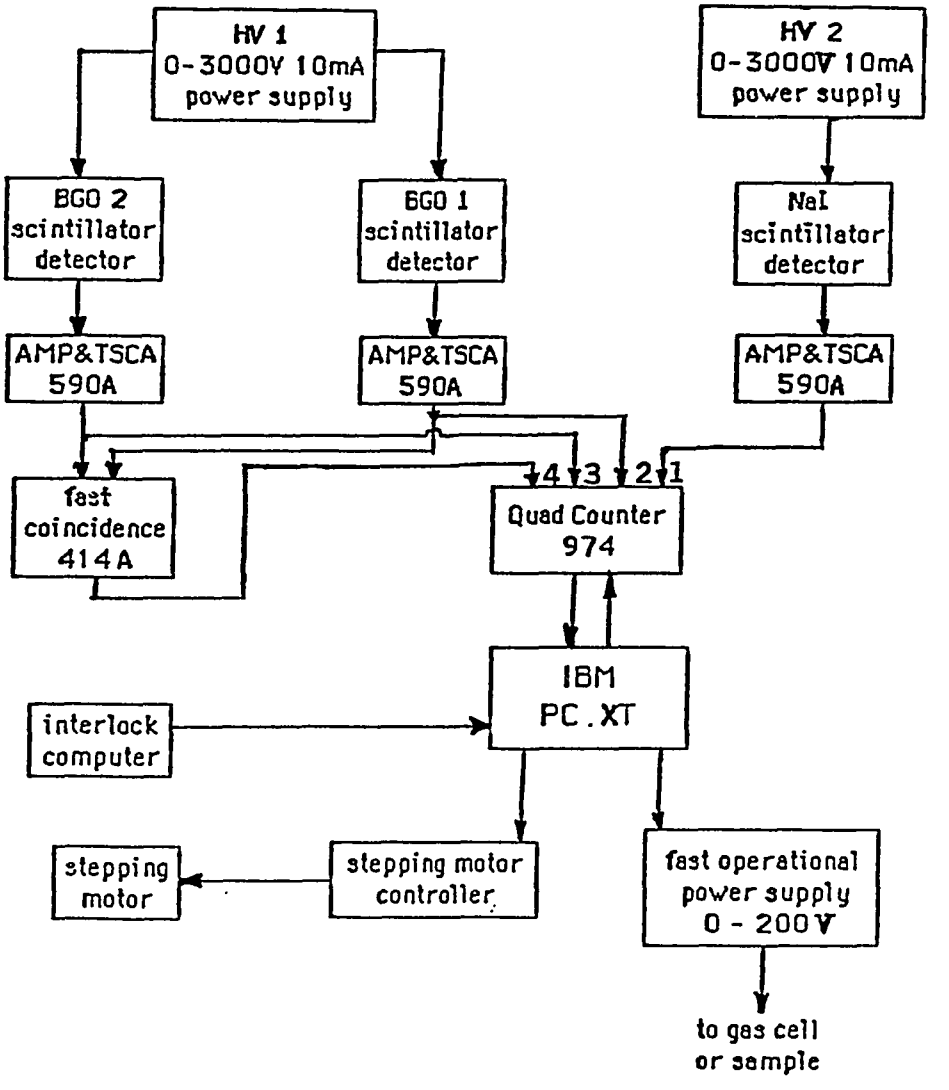

Figure 2.3.1 The block diagram of our data acquisition system. The model numbers are those for EG&G Ortec electronics.

are operated by a IBM PC/XT computer. The single count rates of all detectors and the coincidence rate of the two BGO detectors are all collected by an EG&G Ortec fast Quad Counter. The computer interfaces with the Quad Counter through a RS232 line. The computer is responsible to start and stop the Quad Counter's collecting data and also sets the time parameters for collecting cycle. The computer also operates a fast operational power supply through its D/A port. This operation power supply provides the voltage bias for the gas cell (, which determines the positronium energy,) for positronium runs or the voltage bias for samples in the positronium emission experiments (to control the energy of the incident positrons). For positronium scattering measurements the computer controls the rotation of the sample though the stepping motor on the sample manipulator whose controller is operated by the TTL output from the computer. The computer also receive the input from the other computer that operates the interlock and stops the experiment if the interlock indicating the malfunction of certain vacuum equipment or failure of certain part of the vacuum system.

2.3.3 The positronium beam efficiency — The efficiency of the positronium beam can be measured once the detection set up is correctly established. The Fig. 2.3.2 illustrates geometry of the positronium beam intensity measurements. From the diameter of the annihilation plate and the baffle tubes, the positronium atoms that we measured are estimated to be those emitted within a cone (with its apex at the center of the gas cell) that has full opening angle of 5°.

In measuring the positronium beam intensity, several factors have to be taken into the consideration. One of these factors is the decay of positronium atoms on their flight path. For para-positronium, its 1.25×10^{-10} second life time make it impossible for it to go anywhere beyond the gas cell. For ortho-positronium on the other hand, the survival rate is relatively high. Fig. 2.3.3 shows the ortho-positronium survival fraction as functions of energy for two different distance 31 cm and 42 cm,

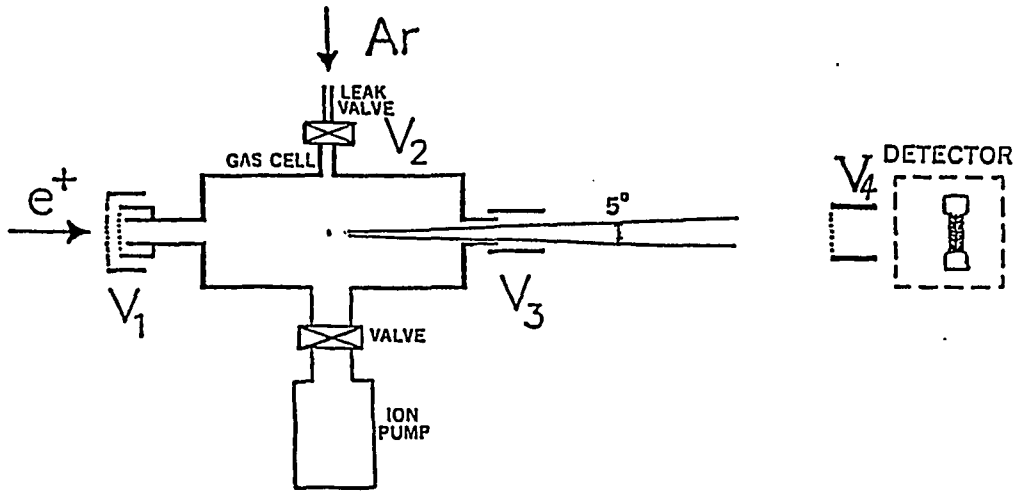

Figure 2.3.2 The geometry of the positronium beam intensity measurement (not to scale).

which are the distances from the detector to the exit of the gas cell and the center of the gas cell respectively. With the knowledge of the survival fraction, the formation efficiency of positronium in the gas cell can be estimated from the positronium beam efficiency measured by the detector at the end of the beam. For the positronium surface scattering measurements, the scattered fraction, defined as the ratio of the count rate of the detected positronium atoms scattered by the surface to the total count rate of the positronium beam detected when the detector set up is facing the beam, does not depend on the value of the survival fraction because the detector set up and experimental chamber, as discussed early, are designed in such way so that the flight path of positronium atoms exiting the gas cell and directly entering the detector set up facing the beam is exactly the same as that of positronium atoms exiting the gas cell and striking the sample surface then being scattered into the detector rotated at the scattering position.

The other factor should be considered is the decay of the positron source. Since we used Cu^{64} whose half life time is 12.8 hours as our positron source, the effect of the

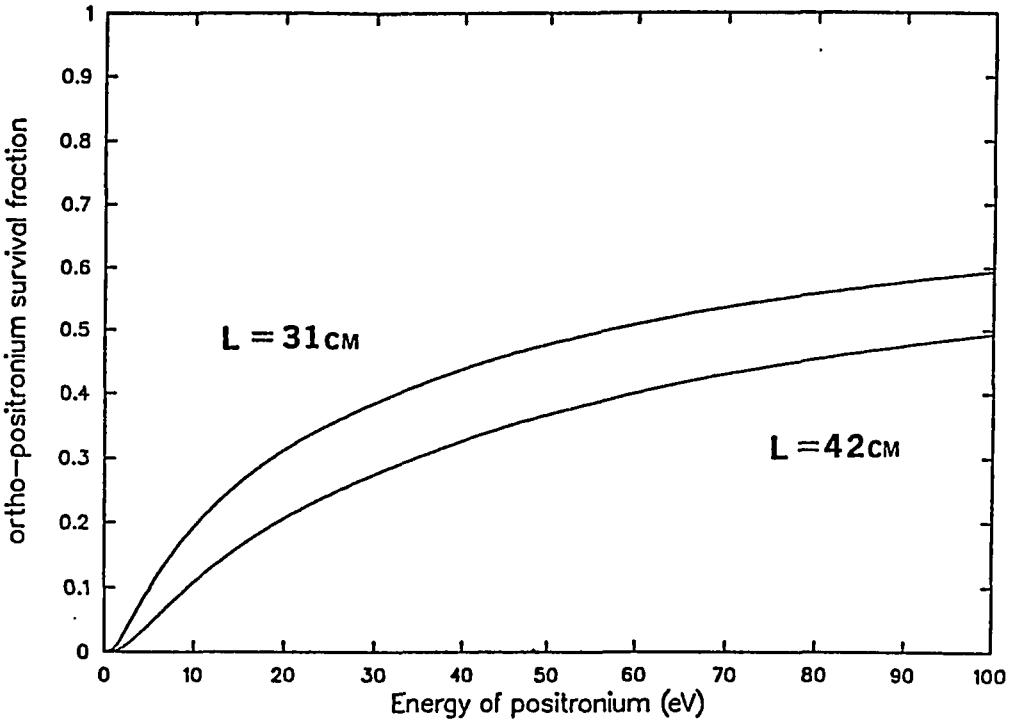

Figure 2.3.3 The survival fraction of ortho-positronium as function of the positronium energy for two different flight path: 42 cm for the lower curve and 31 cm for the top curve.

source decay is significant in our measurements for both positronium beam efficiency and positronium surface scattering. Fortunately, this effect can be easily corrected in the data analysis. Some brief discussion will be given here which also applies to the data analysis of the positronium surface scattering measurements.

For most of our experiments, we usually measure the counts as function of one parameter. The actual data taking is carried out by our computer data acquisition set up. The computer would interface with the electronics to change the parameter and interface with the detector electronics to start collecting counts after the parameter set. To make the beam condition for each data point similar, the collecting time for each data point usually is fairly short for each "sweep" but the same sweep is being repeated many times to accumulate required amount of counts. To make correction

for the source decay and to relate the measurements carried out in different experimental cycles with different positron beam intensities, we usually "normalize" our data to a reference time in the experimental cycle when the positron beam intensity is measured, and calculate what the corresponding count rate would be if under the beam condition at the reference time by taking into account of the decay factor. This procedure will be show here. If we assume that our measurement started at time T_s from the reference time, where $T_s > 0$ if it started after the reference time and $T_s < 0$ if its started before the reference time, and the counts rate we would measure at the reference time is R_0, then the count rate r_s at the actual start time is:

$$r_s = R_0 e^{-T_s/\tau}, \tag{2.3.7}$$

where $\tau = T_{1/2}/\ln 2$ and $T_{1/2} = 12.8$ hours. If there are P data points for the sweep of duration t_{sw} and the counting time for each point is t_p (notice that t_{sw} is usually greater than $n\,t_p$ because there is time gap between point to change the parameter and, in some measurements, to count for the background), then the count rate for jth point at first sweep r_{1j} is:

$$r_{1j} = R_{0j}\, e^{-(T_s + j\, t_{sw}/P)/\tau}, \tag{2.3.8}$$

and counts n_{1j} collected for jth point in the first sweep is

$$\begin{aligned} n_{1j} &= r_{1j} \int_0^{t_p} e^{-t/\tau} dt \\ &= \frac{r_{1j}}{\tau}\left(1 - e^{-t_p/\tau}\right) \\ &\approx r_{1j}\, t_p = R_{0j}\, t_p\, e^{-(T_s + j\, t_{sw}/P)/\tau}, \end{aligned} \tag{2.3.9}$$

because $t_p \ll \tau$ (t_p is usually on the order of 10 sec. to 100 sec., while τ is about 4.6×10^4 sec.). Since there is a decay factor $e^{-t_{sw}/\tau}$ relating $r_{i+1\,j}$ to $r_{i\,j}$, the same

factor would relate the counts $n_{i+1\,j}$ to $n_{i\,j}$. The total counts N_j for jth point for total S sweeps would be:

$$\begin{aligned} N_j &= \sum_{i=1}^{S} n_{i\,j} \\ &= n_{1\,j} \sum_{i=0}^{S-1} e^{-i\,t_s w/\tau} \\ &= n_{1\,j}\,\frac{1-e^{-S\,t_{sw}/\tau}}{1-e^{-t_{sw}/\tau}} \\ &= R_{oj}\,t_p\,\frac{1-e^{-S\,t_{sw}/\tau}}{1-e^{-t_{sw}/\tau}}\,e^{-(T_s+j\,t_{sw}/P)/\tau}. \end{aligned} \tag{2.3.10}$$

Then R_{oj} can be expressed as:

$$R_{oj} = \left(\frac{N_j}{t_p}\right)\frac{1-e^{-t_{sw}/\tau}}{1-e^{-S\,t_{sw}/\tau}}\,e^{(T_s+j\,t_{sw}/P)/\tau}. \tag{2.3.11}$$

To simplify the analysis even further, we usually set the time for each sweep fairly short so $t_{sw} \ll \tau$ and then the Eq. (2.3.11) reduces to:

$$R_{oj} = \left(\frac{N_j}{t_p}\right)\frac{1-e^{-t_{sw}/\tau}}{1-e^{-S\,t_{sw}/\tau}}\,e^{T_s/\tau}. \tag{2.3.12}$$

The relation between the count rate at the reference and the total counts is thus same for all points. From Eq. (2.3.11) or Eq.(2.3.12) we can deduct R_{oj} from the total counts we collect for jth point, thus we can normalized all our data to the count rate at the reference time. This applies to the each single rate as well as to the coincidence rate.

For positronium beam efficiency measurements, different points represent the different voltages biased on the gas cell, thus different positron energies ($E_{e+} = E_{beam}$

$-$ eV$_2$ where E_{e+} is the positron energy in the gas cell, E_{beam} is the positron beam energy, and V$_2$ is the gas cell voltage). And the positronium energy E_{Ps} then is:

$$\begin{aligned} E_{ps} &= E_{e+} - E_{th} \\ &= E_{beam} - eV_2 - E_{th}, \end{aligned} \tag{2.3.13}$$

where E_{th} is the positronium formation threshold energy defined in section 2.2.2. Fig. 2.3.4 shows the total coincidence counts of one of our experimental measurement of positronium beam efficiency where the Ar pressure at the gas cell is 10^{-3} torr corrected. The "beam off" data were taken with the grid in front the gas biased to 200 V so no moderated positrons could enter the gas cell. Following the procedure we discussed above, we subtract the beam off counts from the beam on counts to get rid of the background and normalized the subtracted total coincidence counts to a reference time, then took the ratio of the normalized coincidence rate of detected positronium to that of the positron which is taken at the reference time or normalized to the reference time in the same way to get positronium beam efficiency in terms of the coincidence counts of Ps per positron. Fig. 2.3.5 illustrate this ratio. From the calibration of the detector system, we can also calculate the relative intensity of positronium beam at the annihilation plate per positrons. Fig. 2.3.6 shows the result. The values are calculated from the combination of several measurements to reduce the statistics error. The solid line in the Fig. 2.3.6 is a smoothed fitting curve which we can used for the normalization of the positronium scattering measurements. The insert in the Fig. 2.3.6 shows the same value in the lower energy range in a larger scale.

The measured coincidence counts of positronium (when the detector is facing the beam) per incident positron such as those shown by Fig. 2.3.5 are dependent on the efficiency of the detection set up, yet they can be used to normalized the same counts obtained from the scattering measurements for this very reason because those from

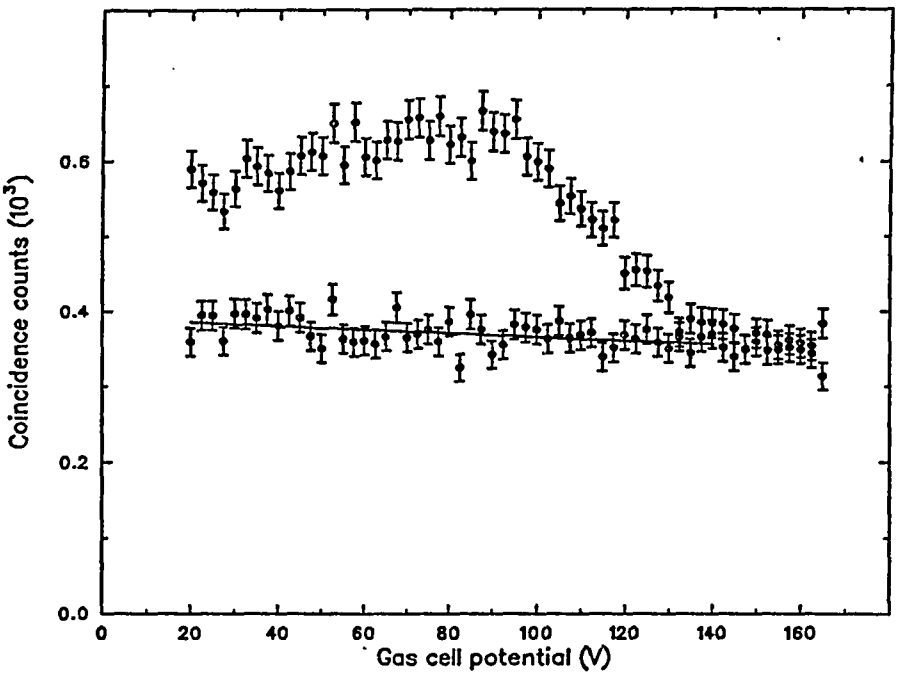

Figure 2.3.4 The total coincidence counts measured as function of the gas cell potential with detector set up facing the Ps beam, where the positron beam energy is 150 eV and the Ar pressure at the gas cell is 10^{-3} torr corrected. The • are the counts collected with the grid in front the gas cell grounded so the positron could enter the gas cell ("beam on") while o are the counts taken when the grid was at 200 eV and rejected the positron beam ("beam off").

the scattering are dependent on the efficiency of detection set up exactly the same way and the ratio of these two counts would eliminate the factor from the efficiency of the detection set up, resulting in the absolute scattering fraction.

The relative intensity of positronium at the annihilation plate per positron shown in Fig. 2.3.6 are independent to the efficiency of the detector set up. Using the results of Fig. 2.3.6, the decay of time flight can be compensated to obtain the intensity of ortho-positronium formed in the defined cone per incident positron and can, in

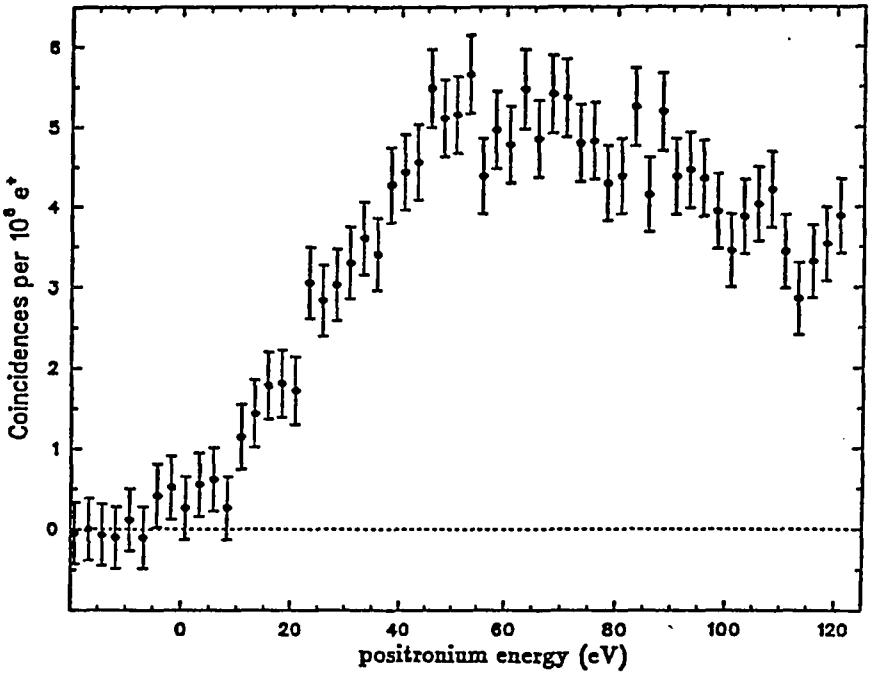

Figure 2.3.5 The coincident count intensity of Ps atoms reaching the annihilation plate per incident positron as function of the energy of the positronium atom formed.

principle, compare with other experiments involving the positronium formation in the gas cell, especially the measurement of the differential cross sections for positronium formation in Ar. But there is no report on any theoretical calculation or experimental measurement on the differential cross sections for the positronium formation in Ar so no accurate comparison can be made. There was the experimental measurement on the positronium formation total cross section in Ar (see Fig. 2.2.6) by the group in the Center for Positron Studies at Texas (Fornari and others 1983). If we assume the ratios of the differential cross sections to the total cross section for positronium formation in Ar are similar to those in He. Then we can quantitatively compare our result with the total cross section measurements for positronium formation in Ar with the help of theoretical ratios of the differential cross sections to the total cross section for positronium formation in He as a bridge.

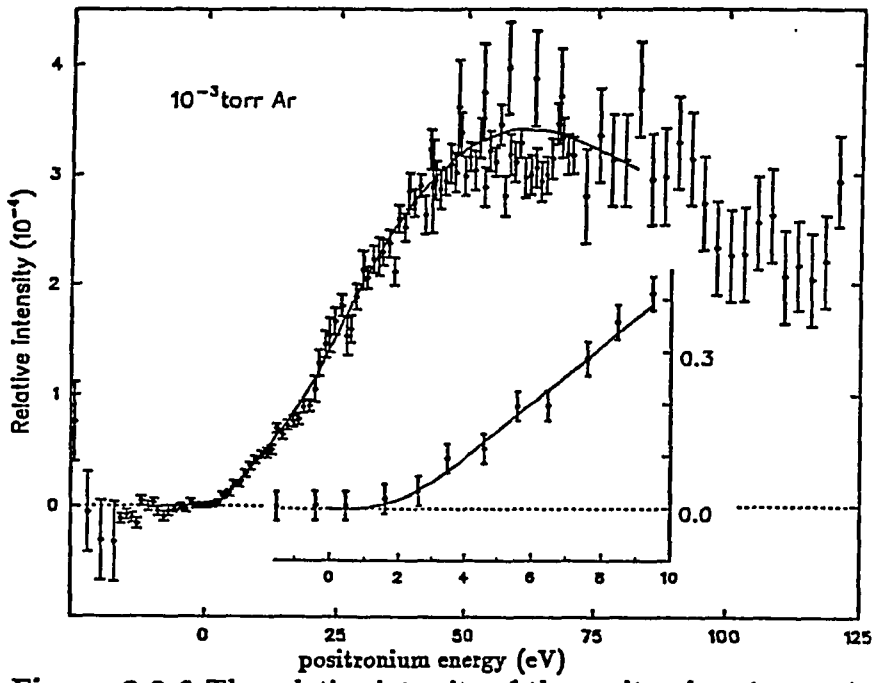

Figure 2.3.6 The relative intensity of the positronium beam at the annihilation plate per incident positron as the function of the formed positronium energy.

To estimate the efficiency, following steps can be taken. If we assume the total cross section of all possible scatterings which scatter the positrons off the beam both elastically and inelastically as σ and we can approximately assume σ is a constant in the gas cell (or we can take σ as a average value in the gas cell), then we know the positron beam intensity $I(x)$ at any point x with the center of the gas cell as $x = 0$ is

$$I(x) = I_o e^{-n\,\sigma(x + l_d/2)}, \tag{2.3.14}$$

where I_o is the positron beam intensity before entering the gas cell, n is the density of gas atoms in the gas cell, and l_d is the total length of the gas cell. For each atom, its contribution to formed positronium beam can be written as:

$$\Delta I_{P_s}(x) = I(x) \int \left(\frac{d\sigma}{d\Omega}\right)_{P_s} d\Omega. \tag{2.3.15}$$

where the range of the integral is determined by the collimation of the beam (for our beam, the 5° cone as discussed earlier) and the position of the atom. For the estimate, we use a constant $\Delta\sigma_{P_s}$ to approximate the integral and we have total intensity of formed positronium atoms which contribute to the beam is

$$\begin{aligned} I^f_{P_s} &= \int_{-l_d/2}^{+l_d/2} n\Delta\sigma_{P_s} I(x)dx \\ &= \left(\frac{\Delta\sigma_{P_s}}{\sigma}\right) I_0 \left(1 - e^{-n\sigma l_d}\right). \end{aligned} \tag{2.3.16}$$

For most of cases, the σ is rather small, so we can expand the exponential to only the first two terms and have:

$$I^f_{P_s} \approx n\,\Delta\sigma_{P_s}\, l_d\, I_0. \tag{2.3.17}$$

The intensity of positronium beam we measured suffers a loss due to the decay on the flight path as we discussed earlier. The para-positronium would not make it to the annihilation plate, contributing a loss factor of 3/4. The survival fraction of ortho-positronium atoms f_{or} is given in Fig. 2.3.3. Since the positronium atoms are formed at the different position in the gas cell, the survival fraction is different for Ps atoms formed at the different position. We, again, taking an approximate approach and assume an average fight path which is the distance from the center of the gas cell to the annihilation plate and write the actual positronium beam intensity we measure as:

$$I_{P_s} = (3/4) f_{or} I^f_{P_s}, \tag{2.3.18}$$

where f_{or} is evaluated for the flight path between the center of the gas cell to the annihilation plate of 42 cm. To compare the measured total cross section for the positronium formation in Ar with our I_{P_s}, we have to link the measured total cross section to the value $\Delta\sigma$ we defined earlier. Since there is no information on the relation between the total and differential cross section for the positronium formation

in Ar, we, for the approximate estimate, use the calculated the total and differential cross sections for that in He to obtain the ratios:

$$\frac{\Delta\sigma_{Ps}}{\sigma_{Ps}} = \frac{1}{\sigma_{Ps}} \int \left(\frac{d\sigma}{d\Omega}\right)_{Ps} d\Omega. \tag{2.3.19}$$

If we set the integral range to be that for the atoms at the center of the gas cell(5° cone range), we can approximately get this ratio from the work by Khan and Ghosh (1983) on the total and differential cross sections of the positronium formation in He shown in Table 2.2.4&2.2.5 and the Fig 2.2.7. From their result, we calculated the ratio to be ~1/410 for the positron energy of 28 eV. Since the corresponding positronium energy would be 19.1 eV, from the Fig. 2.3.3 we have f_{or} to be 19.8%. From the value of Ar pressure of 10^{-3} torr (n is proportional to pressure, and n is known for 780 torr) and l_d of 22 cm, and using the Eqs. (2.3.17)-(2.3.19), we can obtain the positronium beam intensity at the annihilation plate corresponding to the measured total cross section for Ps formation in Ar of 3.75 πa_o^2 at the positron energy of 28 eV(the corresponding positronium energy is 19.1 eV) is(Fornari and others 1983)

$$I_{Ps} \approx 9.3 \times 10^{-5} I_o, \tag{2.3.20}$$

which agrees rather well, within the experimental error, with the value of $\sim 10^{-4}$ we measured in our beam(see Fig. 2.3.6 and related text). Of course, the estimate we carried out above not only is based on many approximations, but also ignores a few factors such as various positronium scattering processes in the gas cell, the transverse energy of the positron beam, and positronium formation by the double collision. It is only intended as very approximate systematic comparison between our positronium beam and other experimental measurements. Some of the processes that are not taking into consideration are discussed elsewhere(Brown 1987). It is hoped that more detailed and accurate comparison can be made when more experimental or theoretical efforts on the positronium formation in Ar are reported.

§2.4 The Sample Selection And Preparation

To select the first sample surface for the positronium surface scattering experiments, several factors have been taken into the consideration. For the first experiment, it is desirable to choose the sample which would produce maximum effect that this experiment is trying to observe, in this case, the positronium reflection, therefore the inelastic scattering process or any other process which would cause the loss of the positronium energy or number of positronium atoms (the ionization of positronium, for example) should be eliminated during the positronium interaction with the sample as much as possible, for the energy loss of scattered positronium atoms would result in the reduction of the specular reflection of the positronium atoms from the surface and disappearance of any possible diffractions, and loss of positronium atoms would reduce the scattered positronium atoms that we can measure. The recent theoretical work (Ward and others 1987) have indicated that there is noticeable effect from the free electron-positronium scattering process on the energy of scattered positronium atoms. Because of the similarity between the mass of electrons and that of positronium atoms (a positronium atom has a mass twice of that of an electron), the energy transfer is highly probable during the electron-positronium elastic scattering. The cross sections calculated for this process in the low energy range are significant. Also indicated in the same theoretical effort is that the spin conversion effect, an ortho-positronium atom being converted into a para-positronium atom resulting in a quick decay, can not be ignored during the electron-positronium scattering process. The positronium atoms also can be ionized in the electron-positronium scattering, resulting in the loss of total number of positronium atoms (Peach 1989). The insulator single crystal seemed to be the ideal samples for the reason given above. The large band gap energy is desirable to reduce the excitation process. The single crystals with large lattice parameters would be convenient for the future diffraction measurements, because the larger the lattice parameter, the lower energy range the diffraction

features would be located (the diffraction features are associated with the reciprocal lattice of the crystal). A sample with a surface which can be cleaned and be kept clean easily in the high vacuum environment (but not necessarily ultra-high vacuum) for a reasonably long period of time is also required because of the vacuum environment in our experimental chamber and relative long duration of the measurement due to the available intensity of positronium beam. To evaluate fully the potential of the positronium surface scattering as a surface study probe, surfaces that are well studied and understood by other surface techniques are the more favorable choices among all the possible surfaces. The measurements from those surfaces, would be easily compared with the results from other techniques, and the advantages and the limitation of this probe can thus be recognized. The last three factors are also applied for the selection of the other samples.

After taking all the factors discussed above into the consideration, we chose the ionic insulator single crystal LiF(100) surface as our first sample. Besides being an ionic crystal in which all electrons are tightly bond to the ion cores and having a large band gap, it is also can be clean fairly easily and can be kept clean in the regular high vacuum environment. It is also a surface studied by various surface techniques including the surface diffraction techniques such as the low energy electron diffraction, low energy positron diffraction, and atom surface diffraction. The table 2.4.1 lists some important properties of LiF(100).

Table 2.4.1 Some properties of LiF crystal studied.

crystal structure:	NaCl structure
surface studied:	(100)
ionic distance (Li–F):	2.014Å
lattice parameter a:	4.02Å
band gap energy:	14.2 eV

The decision of using a metal surface for our second experiment was based on our desire to explore the feasibility of the metal surface study by the positronium scattering. For this purpose, a common metal surface which represents the typical metal surfaces is needed. The first metal surface for our experiment should also be the one without the surface reconstruction, as it may complicate the theoretical treatment and require better vacuum environment. The last three factors we discussed for the first sample selection also apply to this selection. It also desirable to have the the crystal with relative large lattice parameters as our second sample. The relative easiness of the sample preparation is also an essential factor here. Equally important is that the surface studied by the positronium scattering should be a well studied and understood surface by other techniques for the reason given above. The Cu(100) surface is the one we chose for our second experiment of the positronium surface scattering. The Table 2.4.2 lists the some structure properties of the cooper sample studied.

Table 2.4.2 Some properties of Cu crystal studied.

crytal structure:	fcc
surface studied:	(100)
Nearest-neighbor distance:	2.55Å
lattice parameter a:	3.61Å

The LiF crystal we used for our experiments is the high purity LiF crystal purchased from the Harshaw. A large surface area is needed because the beam size of our positronium beam is fairly large. The typical size of the sample for our experiment is one inch square with thickness of $1/8''$. Since we used the LiF(100) surface, this surface can be obtained by simply cleaving the crystal at the proper direction. For the surface, it is believed that a better surface condition would be obtained if the cleaving is carried out in situ at the high vacuum environment. The cleaving in situ,

however, does require a more complicated set up and some accumulated experiences for the operators. It has been employed in some other experiments with much smaller cross section samples. Because of the large cross section of our LiF sample, cleaving in situ would be much more difficult and complicated. The experiments on LiF(100) surfaces carried out by atoms scattering have shown the surfaces obtained by cleaving in the air were sufficient clean providing other precaution and cares were given to the surface after they were putting into the vacuum. The results by low energy positron diffraction (Mills and Crane 1985) for both air cleaved and vacuum cleaved surface showed that while there was a slight improvement in the experimental data, there was no significant improvement or new features in the data from the vacuum cleaved surface when it was compared with the data from the air cleaved surface. Even though the facility to cleave the LiF in situ in the vacuum to obtain a cleaner surface may be designed and implemented in the future, the crystal sample has been cleaved in the air just before installed onto the sample holder and put into the the chamber for this research project. The chamber evacuation is usually followed immediately after the cleaving and installation of sample crystals.

After the chamber is evacuated to the ultimate base pressure, the sample surface is cleaned by heating the sample surface to 200 to 300°C mainly to eliminate any water molecules absorbed by the LiF(100) surface. In the very early stage of the experiment, the measurement was carried out with the sample in room temperature. As will be discussed in Chapters 3&4, no specular reflection was observed from the surface at the room temperature. Only after the sample was heated to above 150°C, the specular reflection was observed. Since then, the sample has been kept around 160°C during most of the experiments except the one used to study the surface temperature effect on the positronium specular reflection from the surface.

The surface condition was not monitored actively during most of the measurement

on LiF(100) surface because the LEED facility was not installed then. After the LEED facility is available, a fairly sharp LEED patterns were observed for the LiF(100) surface at room temperature after the heating. The intensity of the LEED pattern was greatly reduced when the sample surface was heated up likely due the Debye-Waller effect, even though a pattern was still visible when the sample was heated to about 160°C. This difference between the positronium reflection measurements and LEED observation will be discussed in Chapter 4.

The preparation of Cu crystal surface is similar to a typical single crystal surface preparation procedure, though little more involved than that used for LiF(100) surface. The sample is cut by a electric spark cutting machine from a high purity single crystal rod of 1.25 in. diameter with axis in (110) direction so the sample surface is of an elliptical shape with a flat cut on side of long axis. The minimum diameter of the sample is more than one inch. After the spark cutting, the surface was chemically and mechanically polished by the material group in Applied Science Division at BNL. After the sample was installed and the chamber was evacuated to the ultimate base pressure, the sample surface was sputtered by the Ar ions of 500–1000 eV generated by the ion gun and a 1×10^{-5} torr (corrected for Ar) Ar environment in the experimental chamber. For the first time, several hours of sputtering were needed. The sputtering has been carried out with the ion beam having an angle of 30 to 60 degree with the normal of the surface to reduce the ion implantation effect and to cover a larger area of the surface. After ion sputtering, the sample was gradually heated to 600° to anneal out any surface damage caused by ion sputtering. The annealing normally took about a few minutes, after which the sample was gradually cooled down to the room temperature. This procedure would normally result in a very sharp LEED pattern when the sample is checked by the LEED facility.

The surface was also monitored by the Auger facility. A very small amount of im-

purity detected before the sputtering was disappeared after the procedure described above was carried out. Initially, a small amount of S was detected at the surface after the annealing and was suspected to be the small amount of S in bulk diffusing to surface as the result of heating the sample. There are two common approaches to eliminate it, one is to bake the sample in a hydrogen environment for two to three days, and the other approach is sputtering the surface while the sample is heated for a period of time thus allowing the S to diffuse to the surface and be removed by the sputtering. We took the second approach and had the sample sputtered while heated for a few cycles of several hours. No S has been observed by the Auger measurement after this one time treatment. To ensure the cleanness of the surface, sputtering and annealing cycle was carried out before every experiment running cycle and monitored by the LEED and Auger facility. The sputtering time was reduce to 20$\sim$30 minutes from several hours that were needed for the first treatment and the energy of bombarding ions was reduce to 500 eV for this routine procedure. The Auger measurements have been carried out before every experimental cycle after the sputtering and annealing procedure and no observable contamination was found. The Auger measurements have also carried out at ends of some experimental cycles to check that there is any surface contamination during or at end of the experimental cycles and no significant surface contamination was found despite relative high Ar pressure in the experimental chamber during the experimental cycles. Nevertheless, the sputtering-annealing procedure was carried out at the beginning of every experimental cycle to ensure that any possible small amount of contamination that could be accumulated on the surface after a period of time but could not be detected by the regular retarded Auger facility would be removed.

Chapter 3
THE EXPERIMENTAL MEASUREMENTS

The main goal of this research project is to explore the feasibility of developing positronium into a surface study probe through a series of experiments of the positronium surface scattering and surface reflection. It was hoped that some quantitative information on the positronium surface interaction and positronium surface scattering could be obtained through these experiments. The HFBR mono-energetic positronium described in the previous chapter was constructed by us to facilitate these experiments. In this chapter, the measurements carried out after the completion of the HFBR positronium beam will be presented. They include our measurements of the positronium reflection from a LiF(100) surface and our preliminary measurements of the positronium scattering from a Cu(100) surface. Taking advantage of our positronium detection set up in the experimental chamber and the high positron intensity available to us at the time, we also measured the positronium emission from these two surfaces when bombarded with low energy ($\leq$ 150 eV) positrons because we believed that these measurements would provide us some information on positronium surface interaction and on the energetic positronium production which is very important for future efforts on studies of the positronium surface interaction.

In the following section, a general description of our experiments will be given. The general approach that we took in our data processing which includes the background subtraction and proper normalization will be described. Then, the results of our measurements of the positronium reflection from a LiF(100) surface, our preliminary measurements of the positronium scattering from a Cu(100) surface, and our

measurements of the positronium emission from these two surfaces will be reported. A discussion of these results will be offered in the next chapter.

§3.1 The Experiments And Data Processing

The experiments carried out in this project so far are the measurements of the positronium reflection from a LiF(100) surface, the measurements of the positronium scattering from a Cu(100) surface, and the positronium emission from both surfaces. All those measurements were performed with the experimental set up described in Chapter 2. Fig. 3.1.1 is a reproduction of Fig. 2.2.13, which illustrates the experimental chamber we used to conduct the measurements. As shown in the figure, the position of the detector set up is defined by the angle ψ, the position of the sample is defined by the angle θ_i, the angle between the normal of the sample surface and the direction of the beam, and the reflection(scattering) angle is given by $\theta_r = \psi - \theta_i$. Two types of measurements were taken for all the experiments. One type of the measurements, similar to I-V curve measurements for other particle scattering and diffraction, was the measurements of the scattered positronium fraction as a function of the positronium energy, or, for the case of positronium emission measurements, the measurements of the emitted positronium fraction as a function of the positron incidence energy, with fixed scattering geometry(i.e. the ψ, θ_i, and θ_r were not changed during the measurements). For simplicity, we call this type of measurements "energy scan" runs. The other type of measurements, similar to the angular scan measurements in X-ray scattering, is the measurements of the same quantities as a function of the incidence angle θ_i and the scattering angle θ_r for a constant incidence energy. We call these measurements "angular scan" runs or "rocking curves." In the following sections, each type of measurements and its data processing will be described. Those effects that affect our data for each type of measurements will also be discussed.

3.1.1 The angular scan runs — In this type of measurements, the energy of the

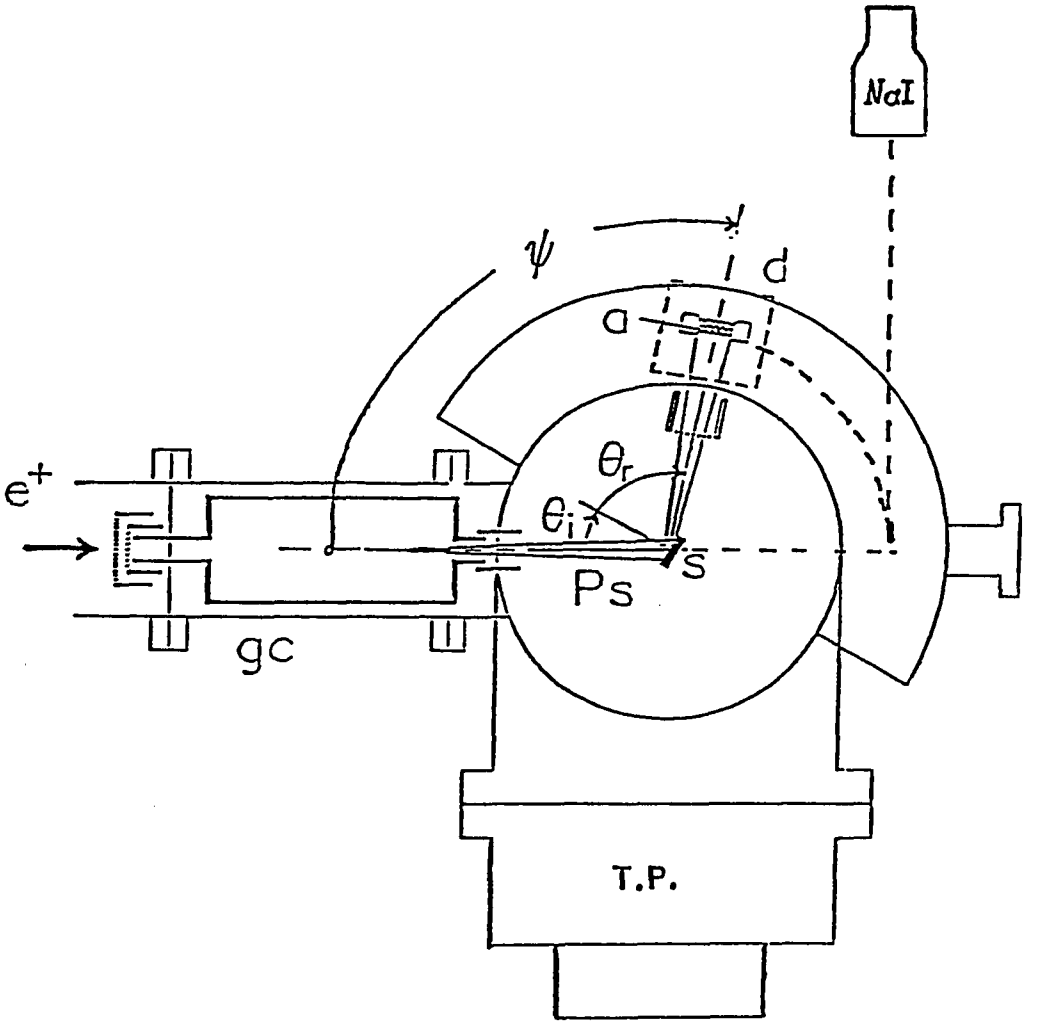

Figure 3.1.1 The top view of the gas cell and the experimental chamber (not to scale). The notations are: *gc* for the gas cell; *s* for the sample; *a* for the annihilation plate; *d* for the detector set up including the annihilation plate and two BGO scintillator detectors (see Fig. 2.2.12 for the geometry of the detector set up); *NaI* for the NaI scintillator detector; and *T.P.* for the turbo-molecular pump.

incident positronium for positronium scattering experiments or the positron incidence energy for positronium emission experiments was kept constant. In the positronium scattering experiments, the gas cell was biased at a fixed voltage, so the positrons in the gas cell had a fixed energy and the positronium atoms produced in the gas cell therefore also had a fixed energy. As discussed in the previous chapter, the baffle tube after the gas cell was employed in our experiments as a positron rejector for the positronium scattering experiments by biasing it at higher positive voltage (typically, 200 ~300 V) than the positron beam energy. In principle, both the detector set up and the sample can be rotated around the center of the experimental chamber. For the positronium surface scattering studies, it would even be desirable to measure the scattering fraction of positronium at various scattering angles with a fixed incidence angle. The practical experimental condition, however, made this type of measurements highly formidable. Yet the measurements with a fixed detector position (constant ψ) but various incident angles (θ_i) and scattering angles (θ_r) were much more manageable. The difficulty mainly rose from the heavy shielding of the detector against various types of background γ-rays. As discussed in previous chapter, the internal heavy metals were installed as part of the detector set up to reduce the background γ-rays generated by the annihilation taking place in the gas cell and experimental chamber during the experiments and the heavy lead shielding (up to four inches thick lead all around the BGO detectors) was also employed to reduce the background γ-rays, especially the high energy photons capable of triggering the coincidence counts of the detector set up, from the operating neutron reactor where this set up was located and from the cosmetic rays. The internal shielding reduced the angular resolution and the angular accuracy of the internal part of the detector set up and also made the automation of the detector's rotation difficult. The heavy external shielding made it almost impossible to change the positions of the BGO detectors frequently. Due to the guiding magnetic field, the energy window of the

detector electronics also had to be re-adjusted when the BGO detectors' position were changed. On the other hand, the sample rotation was controlled by a stepping motor which could be operated by our data acquisition computer. This made measurements with various incidence angles (θ_i) but fixed detector position(ψ) much more tractable. All our angular scan runs were carried out with varying incidence angle(θ_i) and a fixed detector position. The incidence angle usually was varied in a range centered around the specular reflection condition defined by $\theta_i = \theta_r = \psi/2$. The minimum angle step for the sample rotation is 1.8 degree and its accuracy was estimated at about $\pm 2°$. This was also the angular resolution and accuracy of the incidence angle θ_i. The accuracy of the detector's positioning ψ depended on its position. While it was less than $\pm 1°$ at the position facing the beam where $\psi = 180°$, it was about $\pm 5°$ at the other scattering angles. These variation was due to the lack of proper alignment facility in the experimental chamber and had been partially rectified at the later stage of the experiment, resulting in higher accuracy.

Various measurements were also added to the actual measurement procedure to facilitate the background subtraction from the experimental data in the data processing. There is an appreciable effect from the high energy background γ-rays, even with our constant effort to eliminate it. This background is mainly due to two types of the background: the surrounding background radiation independent of the positron beam, such as the radiation from the operating neutron reactor in which the experimental facility was located and cosmic rays, and the background radiation related to our positron and positronium beam such as annihilation taking place in the gas cell and the experimental chamber other than the vicinity of the annihilation plate and the small fraction of un-moderated or partially moderated high energy positrons. As discussed earlier, some of the effects were reduced, but not completely eliminated by our shielding. To subtract these background effects from our experimental measurements, we had at least two approaches to take. One of the approaches was to

take the same measurements but with the positron beam electrically turned off by the grid in front the gas cell as discussed in Chapter 2. In this process all the signals we measured were not from the scattering events that we tried to detect. By subtracting the counts from this "beam off" measurement, we would eliminate the effect from the surrounding background and the effect of high energy positrons, but not the effect of the annihilation taking place in the gas cell and the experimental chamber caused by the "beam on." Another approach was to take similar measurements with the positron beam on but with the sample rotated facing away from the detector set up so no scattering (or emission of positronium) could be detected, the measurement would contain the background effect from the surroundings and most of the background effect from the annihilation in the gas cell and experimental chamber (there would be a very small reduction from this effect for the turned away sample situation because of the attenuation through the sample for some of the annihilation and lack of annihilation on the flight path of scattered positronium between the sample and the detector), but not the effect by the high energy positron, if such effect was significant. Ideally, we would take the measurements for the beam on and beam off situation for the sample in the desirable position and then take similar measurement for the sample turned away from the detector. With all the measurements, we would first subtract the beam off counts from the ones for beam on, then subtract the resultant counts for negative sample angles (sample facing away from the detector) from those for positive sample angles. In the actual data taking, the computer which controls the data acquisition was programed to take the measurement for different sample angle θ_i with the beam on and the beam off (the computer also controls the HV power supply biasing the grid). The counting time for each point in the sweep usually was kept short so all data taken in one scan are under similar condition of the positron beam intensity (the source half life time is 12.8 hrs.), but the angular scan is usually repeated many times to accumulate sufficient number of counts. This procedure can

be illustrated by an example of the data processing carried out for one of our angular scan runs. From this procedure, we can also see that we can approximately reduce some of the steps mentioned above to increase the available beam time for the total measurements.

Shown by the Figs. 3.1.2&3.1.3 are the experimental total counts of a single BGO detector and of the coincidence by two BGO detectors described in Chapter 2 for one of our angular scan runs on a LiF(100) surface heated to 160°C. The positronium energy was 18.7 eV and the detector set up was positioned at $\psi = 120°$. The "•" in the figures represent the counts for the beam on condition, and the "o" represent the counts for the beam off condition. It is very clear that while the BGO have very high background counts, resulting a very small, yet recognizable count difference between counts for the sample turning towards the detector (positive sample angle θ_i) and those for the sample facing away from the detector (negative sample angle θ_i), the coincidence counts only reflect very small portion of the background signal and show significant count difference between counts for positive and negative sample angles. This was the very reason that the coincidence counts were used instead of the single detector counts in our final data processing for calculating the scattered positronium fraction even though later has higher total counts. Fig. 3.1.4 shows the resultant counts of our subtracting all the counts (for positive and negative sample angle) for the beam off condition from their corresponding counts for the beam on condition. Fig.3.1.5 shows the same result with the counts for negative angle folded to the positive angle, the counts for positive angles are represented by the "•" while those for negative angles are represented by "o." The dash lines are average counts value for the negative angles.

Since the counts for negative angles represent the background which should not depend on the sample positions, we consider the small variation in the counts for

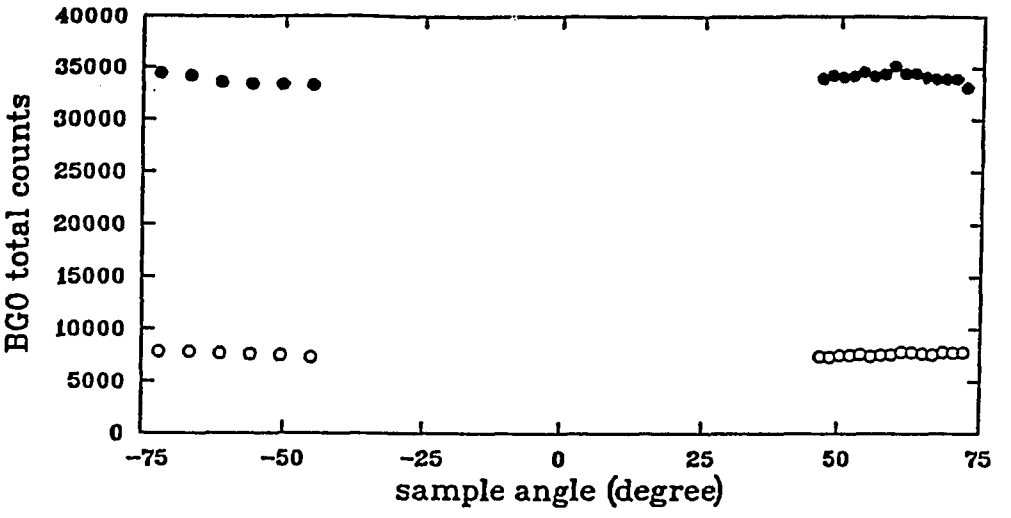

Figure 3.1.2 The single BGO total counts of a Ps angular scan from a LiF(100). Both the beam on counts "•" and beam off counts "o" are displayed in the figure. The positronium energy was 18.7 eV and $\psi = 120°$.

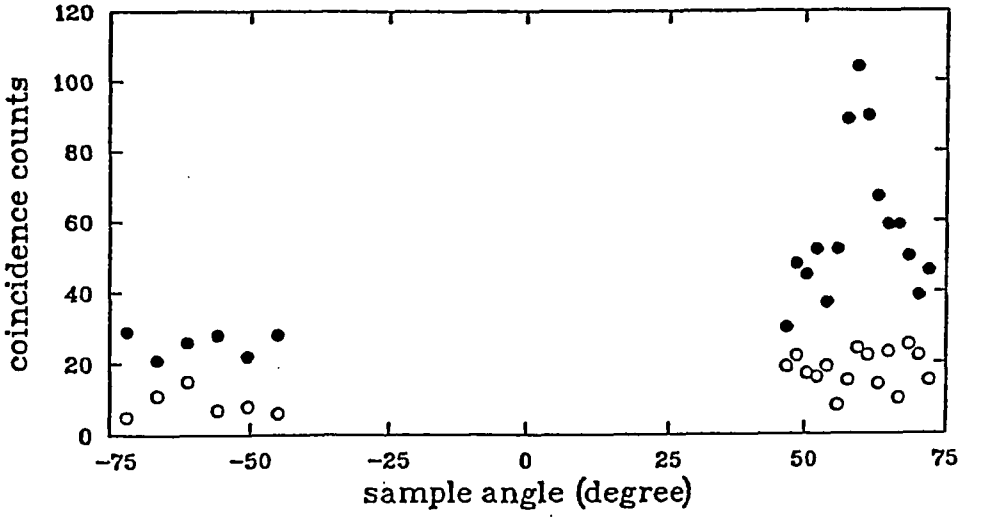

Figure 3.1.3 The coincidence counts for the same measurement of Fig. 3.1.2 with "• representing the beam on counts and "o" representing the beam off counts.

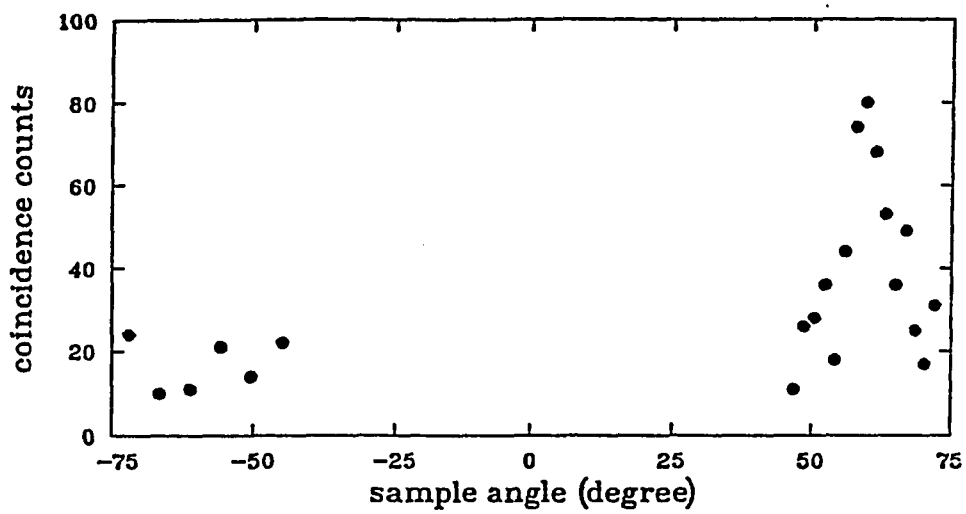

Figure 3.1.4 The resultant coincidence counts from the beam on counts minus the beam off counts for same measurement shown in Fig. 3.1.3.

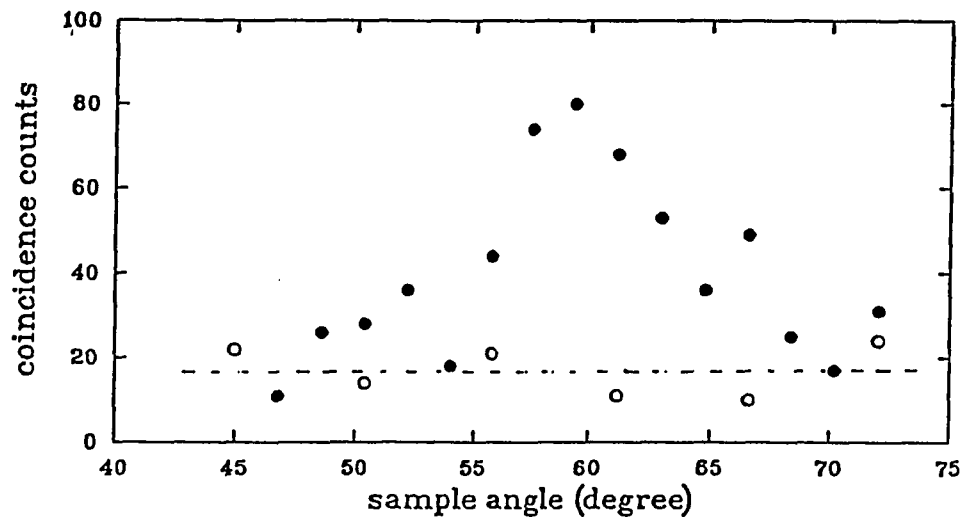

Figure 3.1.5 The same as Fig. 3.1.4 but with the resultant counts for negative sample angles (o) folded to the positive sample angles and displayed with the counts for positive sample angle (•). The dash line indicates the averaged count for the negative sample angles.

different negative sample angles was mainly due to random fluctuation. The averaged count value(see dash line in Fig. 3.1.5) for the negative sample angles was then subtracted from all the counts for different positive sample angles. The result is shown in Fig. 3.1.6.

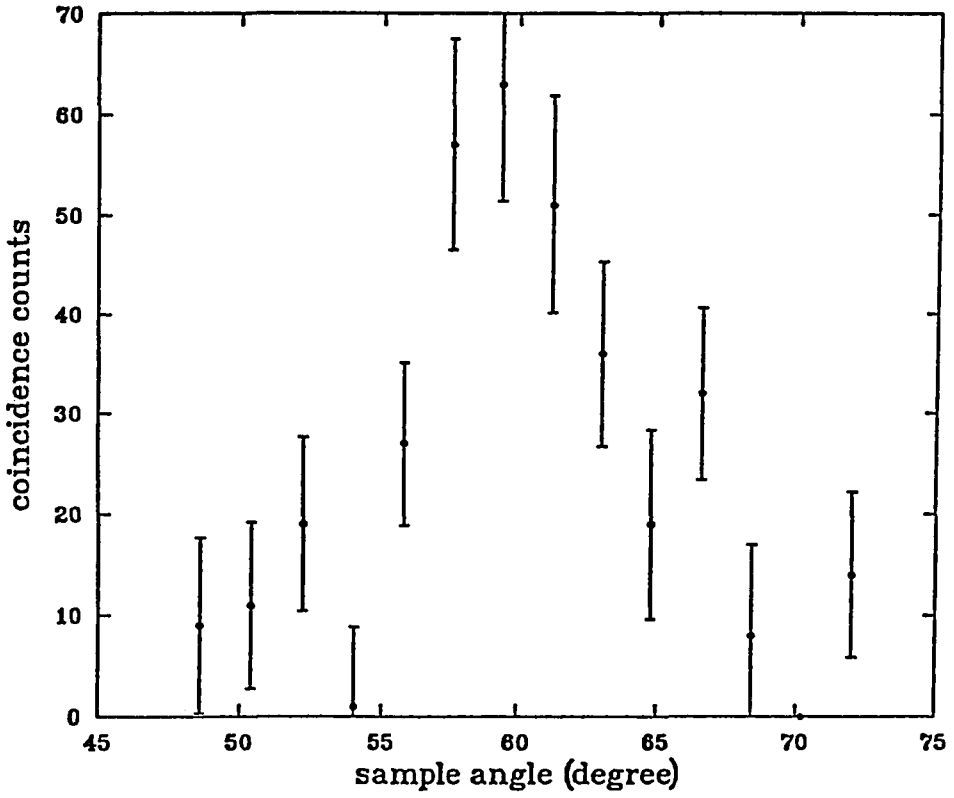

Figure 3.1.6 The net coincidence counts after subtracting the averaged count for the negative angles. The error bars are the combined statistical errors from the counts for both positive and negative sample angles.

The counts shown in Fig. 3.1.6 are the counts with most background subtracted. The error bars reflect the combination of statistic error in the counts for both negative angles and positive angles. To obtained the scattered fraction of positronium by the surface, these counts have to be proper normalized by the total number of positronium

striking the surface. Since the counts of positronium striking the surface can not be obtained simultaneously when measuring the positronium scattering, we use the positron intensity before or after the run as a reference to bridge the result of the positronium formation measurement carried out separately to this run. The result of the positronium scattering or reflection measurements can be scaled to the count rate of scattered or reflected positronium detected by the detector per positron. The result of the positronium formation run is also scaled to the coincidence count rate of formed positronium detected by the detector per positron at any given positronium energy. Since the flight paths (see §2.3 for detail) of positronium atoms from the exit of the gas cell to the detector without presence of the sample and from the exit of the gas cell to sample and then scattered to the detector are same, and the detector efficiency and reception solid angle are also kept the same, we can normalized the scaled scattered positronium count rate by the scaled positronium formation count rate. Special attention have to be given in both scaling of the detected positronium count rate (for both formation and scattering process) and normalization of the count rate to obtain the scattered fraction, because of the short life time of our positron source and fairly large size of our positronium beam. The available positron beam intensity decays with a half life time of 12.8 hrs., so the proper steps described in section 2.3.3 have to be taken when scaling the detected count rate of detected positronium with measured positron intensity at certain reference time in both of the positronium formation case and the positronium scattering case. Another important factor has to be taken into account is the interception of the positronium beam by the sample surface. Because of the fairly large size of our positronium beam, the surface could only intercept the entire beam if $|\theta_i| < \theta_B$ where the θ_B depends on the beam size of our positronium beam and the sample size. For the case where $|\theta_i| > \theta_B$, the fraction can be estimated by the shape of the sample and shape of the beam cross section. For the LiF crystal sample with a width of 7/8 inch and a height of 1 inch, and assuming the beam flux

is homogeneous with a diameter d_B smaller than 7/8 inch, the interception fraction is given by:

$$f_i = \left(\frac{2}{\pi}\right)\left[\left(\frac{\cos\theta_i}{\cos\theta_B}\right)\sqrt{1-\left(\frac{\cos\theta_i}{\cos\theta_B}\right)^2} + \arcsin\left(\frac{\cos\theta_i}{\cos\theta_B}\right)\right], \qquad (3.1.1)$$

where the θ_B is given by beam diameter d_B (in inches) as: $\theta_B = \arccos(8d_B/7)$. For our positronium beam, with one inch diameter annihilation plate, the beam at the sample is estimated to be 0.575″ (or 1.46cm) in diameter, resulting a θ_B of 48.9°. The Fig. 3.1.7 shows the interception fraction for the LiF sample. From above argument, it can be seen that the counts taken for the LiF sample positioned at θ_i that are greater than 48.9° have to be scaled to compensated the factor of missing the part of the positronium beam.

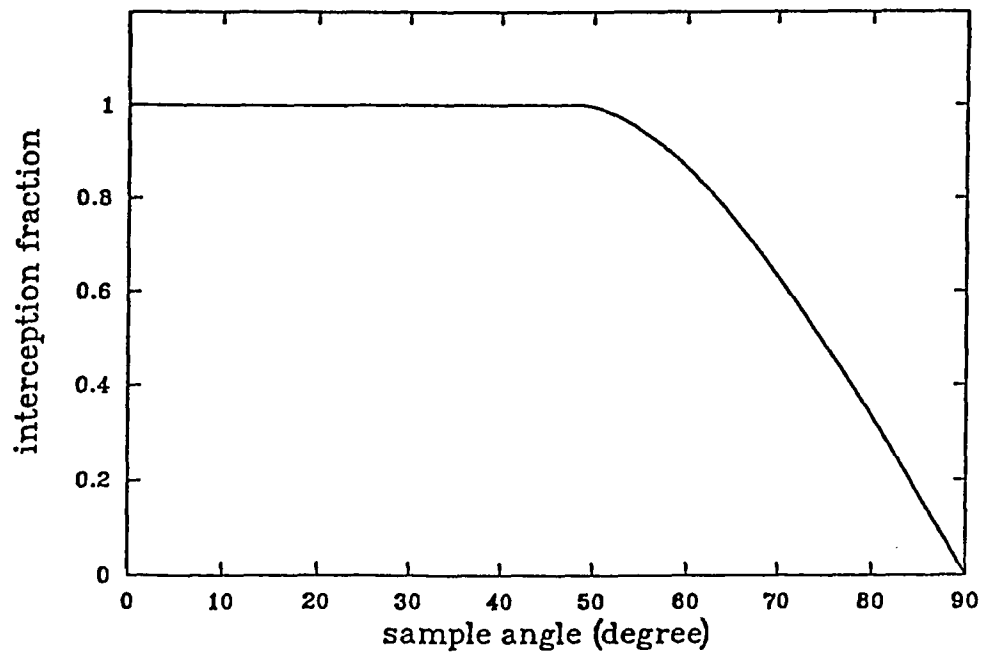

Figure 3.1.7 The interception fraction of the positronium beam by the LiF sample as a function of sample angle θ_i.

Fig. 3.1.8 shows the normalized scattered fraction of this angular scan with the

sample's missing of the positronium beam compensated. The error bars in the figures reflect the statistic errors of count rates for both negative and positive angle, but not the error in measuring the positronium formation.

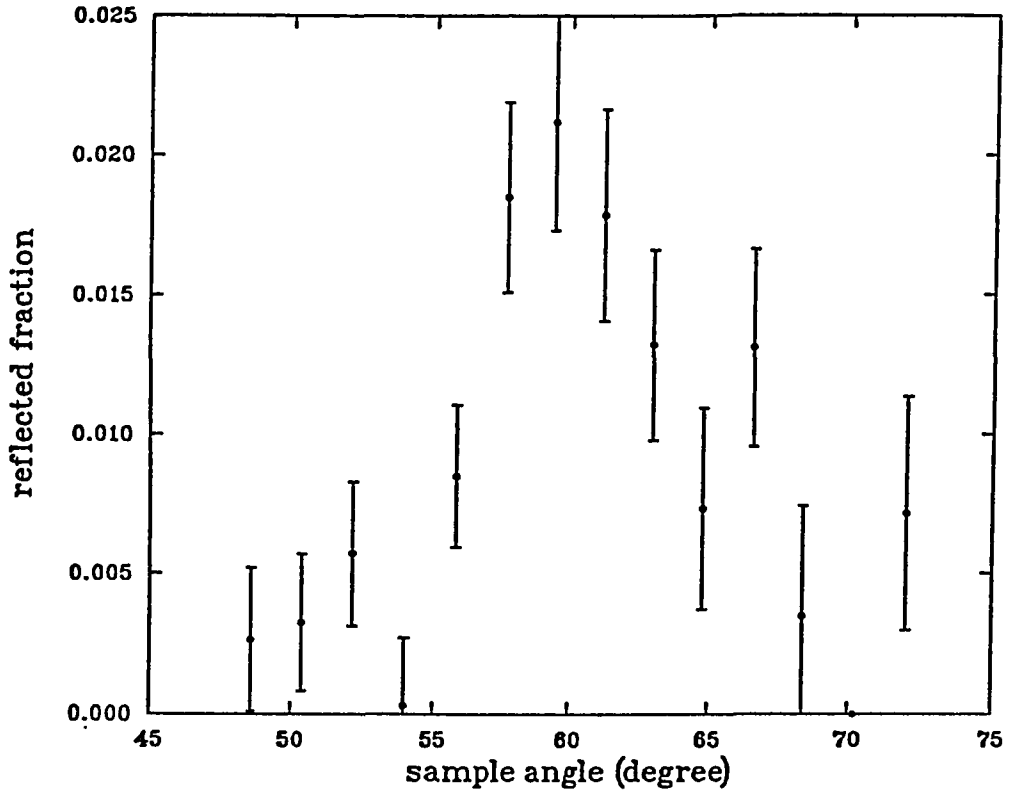

Figure 3.1.8 The reflected fraction of positronium as a function of the sample angle θ_i from a LiF(100) surface. The positronium energy was 18.7 eV and the detector was positioned at $\psi = 120°$.

In principle, all the angular scan measurements can be taken and processed with this approach. It is, however, much more desirable to reduce the data taking time spent on the collection of background information since our positron beam intensity decays fairly quickly. As can be seen from above example, three quarters of data

taking time were used to collect the information for background subtraction in this approach. It seemed that the contribution from the high energy positron was not significant comparing to other background related or not related to the positron or positronium beam. Since the only background effect can not be included in the counts for negative angles is that from the high energy positron, we can approximately eliminate the beam off counting which reflects the insignificant effect of the high energy positron. To assess this approximation approach, we compare the results of background subtracted counts with and without beam off subtraction. In Fig. 3.1.9, the "•" are the same counts as shown in Fig. 3.1.6 derived by subtracting averaged count for negative angles as well as the beam off counts; the "◇" represent the counts by simply subtracting the averaged beam on count for the negative angles from the beam on counts for the positive angles. It is clear that the two result are the same within the error bars. Therefore, we can reduce the background taking time by only taking the beam on count.

Since we assume that the variation in the counts for negative sample angles is mainly due to random fluctuation, we can further reduce the number of positions of negative sample angles in the angle scan measurements. Number of positions in these type of run was usually kept at the minimum needed to have an averaged count with a acceptable statistical error.

All the angular scan measurements which will be presented in the following sections for LiF(100) surface were taken similar to the one described above and were also treated similarly. Those which do not have beam off measurements will be mentioned. All the angular scan measurements carried out for Cu(100) surface are without taking beam off counts. Because the sample size of Cu(100) is much larger (about 1.5″ in minimum width) than that of LiF(100) surface and the shape of the Cu(100) surface is very irregular, the data for the Cu(100) surface are not compensated for the count

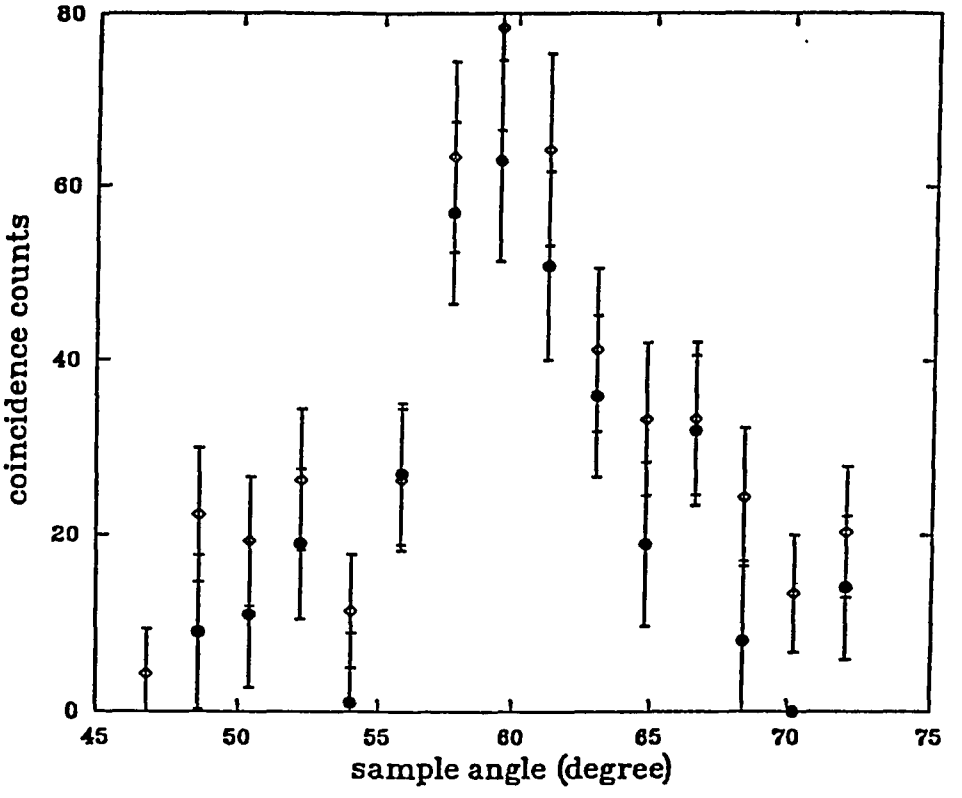

Figure 3.1.9 The comparison between two different approaches of subtracting background counts: "•" represent the results derived from subtracting the beam off coincidence counts from the corresponding beam on counts and then subtracting the averaged resultant count for the negative sample angles from those for positive angles; "◇" represent the results from simply subtracting the averaged beam on coincidence count for negative angles from those for the positive angles.

loss of partially missing the positronium beam.

The angular scan runs for positronium emission measurements were carried out in similar way and the data were processed similarly. The main difference in the data processing is that the data are normalized by the positron intensity not the

positronium beam intensity. For some experiments in which the positron intensity was measured by the NaI detector as described in Chapter 2, the calibrated ratio of the NaI count to coincidence count was used. The measured emitted positronium fractions which will be reported in the following section for both the LiF(100) and Cu(100) surfaces were not compensated for the possible count loss of partially missing the positron beam during the angular scan, instead, these effect will be discussed in Chapter 4. Because LiF is an ionic crystal and there is no conduction electron available for positronium formation, the positronium formation with positrons whose energies are just above the threshold energy E_{th} (see Chapter 4 for detailed definition of E_{th}) may be less favorable than for those higher energy positrons, so the background effect from the high energy positrons may not be negligible for the measurements on the LiF(100) surface, even though the number of the un-moderated high energy positrons is extremely low comparing to that of low energy positrons. We took the precaution by taking the beam off counts for the positronium emission measurements from LiF(100) surface. For Cu(100) surface which is a metal surface with relatively high density of conduction electrons, we expected the effect from the high energy positrons would be negligible especially considering the extremely low percentage of those high energy positrons (this speculation was confirmed by our measurements). In all the positronium emission measurements for the Cu(100) surface, the beam off counts were not taken. Only the counts for negative angles were taken and the averaged values were used as the background counts to be subtracted from the counts for positive sample angles. The additional information about the each individual positronium emission measurement will be given when the data are presented.

3.1.2 The energy scan runs — The energy scan runs were carried out similarly to the angular scan runs, but with fixed incidence angle at various positronium energies. Same as in the angular scan runs, the detector was kept at a fixed position (ψ) during the whole measurement. In the actual run, the measurements were taken as the energy

of positronium was varied by varying the bias voltage on the gas cell (for discussion on the control of formed positronium energy, see Chapter 2 for detail) with the sample positioned at the positive θ_i, usually in specular reflection condition $\theta_i = \psi/2$. Then the sample was rotated to the negative θ_i and the above measurement was repeated to obtain the background data. Similar to the angular run cases, the beam off counts were only taken for some measurements. The data were also processed similarly. The following example will illustrates the general procedure we used for the energy scan data which will be reported in the following section.

The Figs. 3.1.10&3.1.11 show the total counts as a function of the gas cell potential from the single BGO detector and from the coincidence counting of two BGO detectors for one of the Ps energy scan runs on a LiF(100) surface, in which the detector was position at $\psi = 100°$ and the sample angle was at $\theta_i = 50.4°$. In each case, (a) is the measurement taken with sample positioned with a positive θ_i, while (b) is the measurement taken with the sample positioned with the negative θ_i, and symbols used are "•" for beam on counts and "o" for beam off counts. Again, only the coincidence data were used for the final result because they had much higher signal to noise ratio and were less affected by the background.

Similar to the angular scan run we discussed before, the averaged beam off counts for the positive and negative angles were subtracted from the respective beam on counts. Then the net counts (those after the beam off subtraction) for the negative angle were subtracted from the net counts for the positive angle. After the background count subtraction, the final counts then were scaled to the reference time where the positron intensity is known (as discussed for angular scan above and for the positronium formation in Chapter 2). Then the positron intensity at the reference time was used as a bridge to normalize the reflected positronium detected by the detector. Using the relation between the gas cell potential and the formed positronium energy

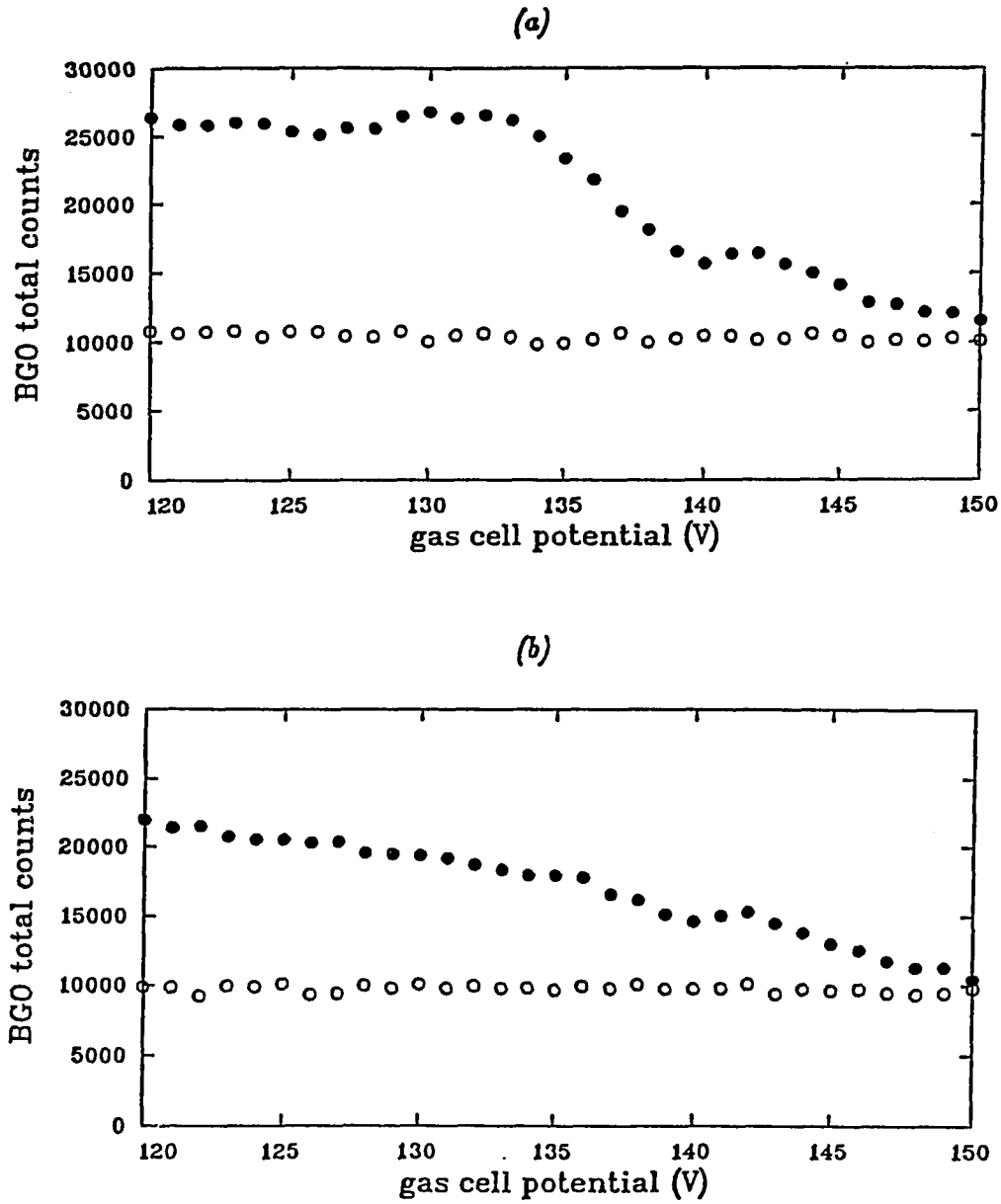

Figure 3.1.10 The single BGO total counts from one of the Ps energy scan runs on a LiF(100) surface. The detector was positioned at $\psi = 100°$ and the sample was rotated at the specular reflection position $\theta_i = 50.4°$. The "•" are the counts collected at the beam on and "o are the counts collected at the beam off. The same measurement was taken both at $\theta_i = 50.4°$ (a) and at $\theta_i = -50.4°$ (b).

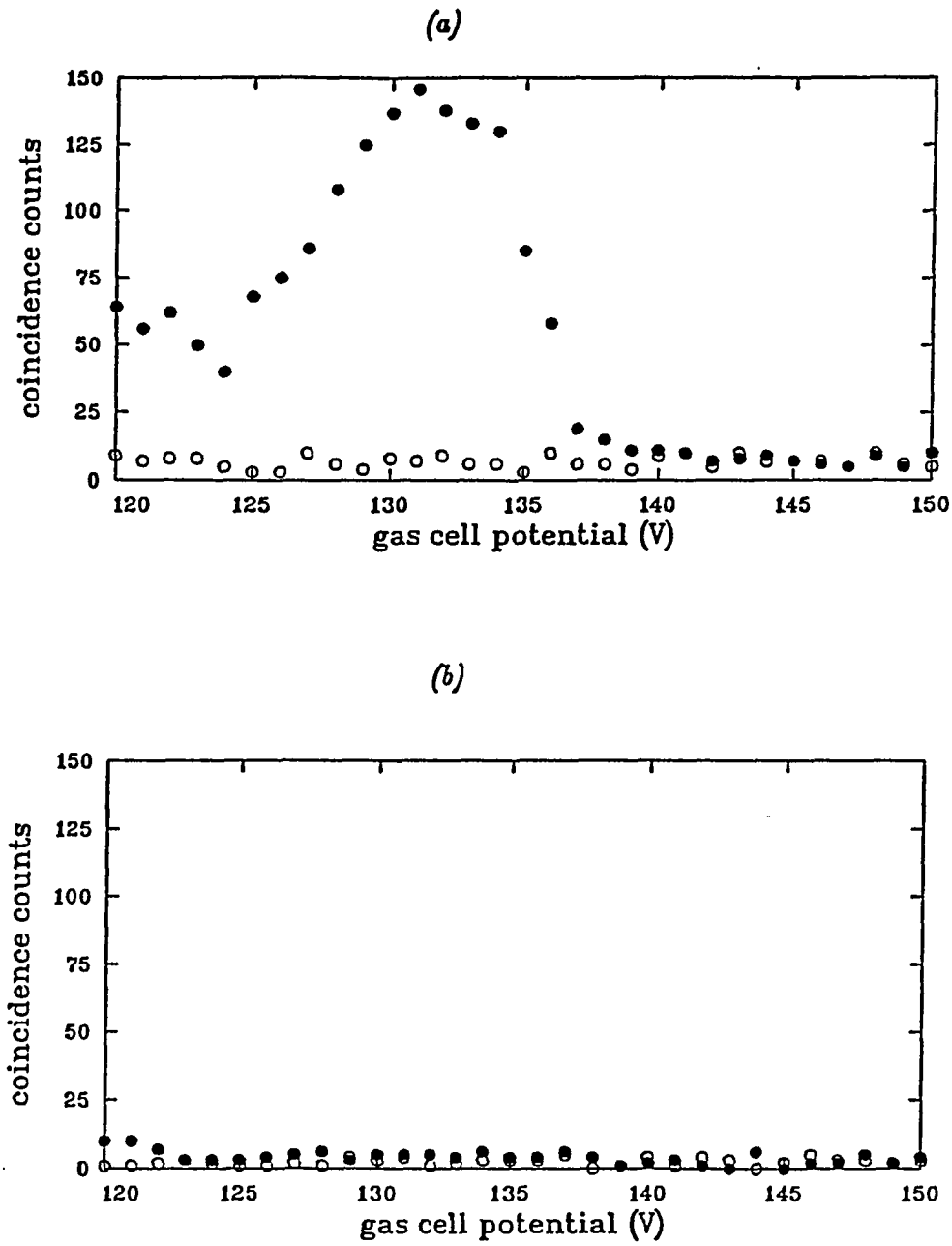

Figure 3.1.11 The coincidence for the same measurement of Fig. 3.1.10. The notations are the same as in the Fig. 3.1.10. The measurement taken for the positive sample angle is displayed at (a) and the measurement taken for the negative sample angle is displayed at (b).

(see Chapter 2), the results can be expressed as a function of the positronium energy. Fig. 3.1.12 shows the final normalized reflected fraction of positronium. The error bars reflect the statistical error from the counts for both the positive and negative angles.

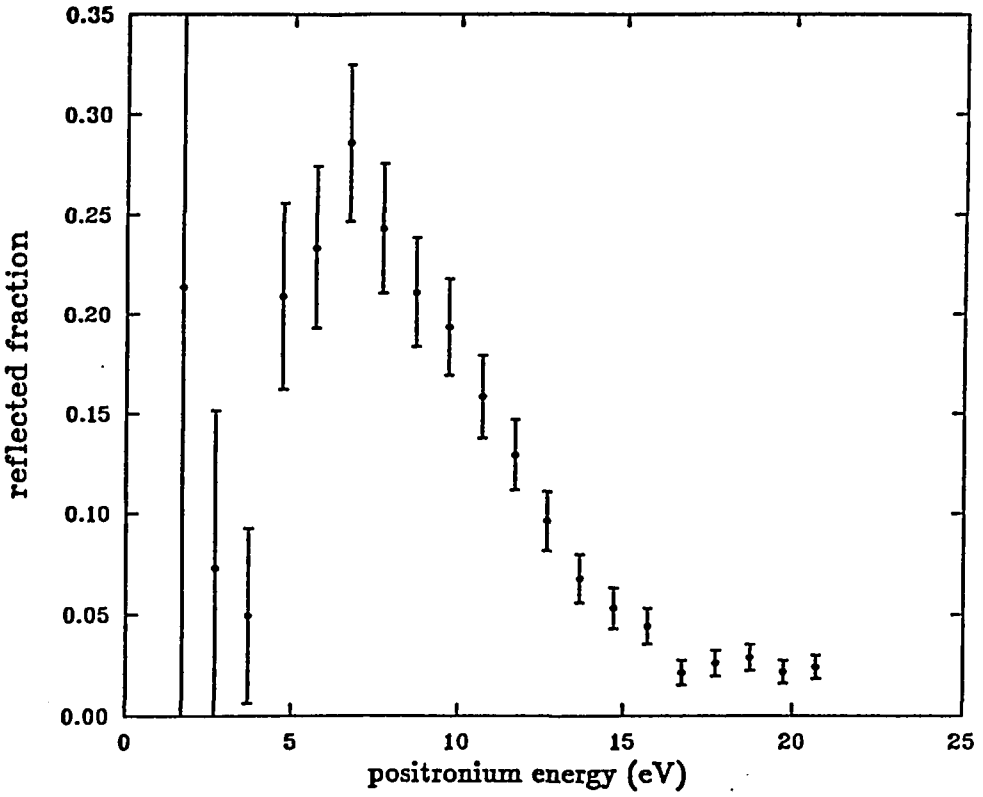

Figure 3.1.12 The reflected fraction of positronium as a function of the positronium energy. $\psi = 100°$ and $\theta_i = 50.4°$.

From the Fig. 3.1.11, it can be seen that the coincidence counts for background (including the coincidence counts for the negative sample angle at both beam on and beam off and for the positive sample angle at beam off) are approximately independent on the positronium energy. It also can be seen that the coincidence counts for the positive sample angle at beam on are about same as that for the beam off when

the gas potential is higher than the maximum positronium formation potential (as the positronium energy E_{Ps} is related to gas cell potential V_g and positron beam energy E_{beam} by $E_{Ps} = E_{beam} - eV_g - E_{th}$ where E_{th} is the positronium formation threshold energy, no positronium can be formed if V_g is greater than $[E_{beam}-E_{th}]/e$) and those also approximately represent the background coincidence count for the energy scan. These approximations can be utilized to cut down the time used for background data measurement, especially in the case where only limited beam time is available. For example, measurements for the beam off data can be eliminated to increase the measurement time for the beam on measurements resulting less statistical error, if only short beam time is available. Other approximations we used to deal with the short available Ps beam time to get reasonably accurate results also include using the averaged beam off coincidence counts for the positive angle as approximate background coincidence counts or using averaged beam on coincidence counts for the positive sample angle with gas cell potential higher than the maximum positronium formation potential as the background coincidence count, and then subtracting it from the beam on coincidence counts for different positive positronium energy points. These approximations, however, only apply to the coincidence counts but not the single detector counts because the additional background which is on the same order of the magnitude of the signal we try to detect would have to be considered.

The energy scan runs for positronium emission were carried out similarly. Again as discussed for angular scans, the results were normalized by the positron intensity rather than the positronium formation counts. And the calibrated count ratio of NaI count to coincidence count was used for the experiments in which the measurement of the positron intensity was carried out by the NaI detector. The measurements for positronium emission from a LiF surface were conducted by taking counts for sample at $\pm\theta_i$ with beam on and beam off for every energy point, while the measurements for positronium emission from a Cu surface were conducted by taking counts for $\pm\theta_i$

with only beam on for every energy point. The reason for this difference in procedure is the same as given in the discussion on angular scans.

3.1.3 Other measurements — Most of our measurements fell into one of the two types of measurements described above. Only a few measurements we took were slightly different. One of these exceptions was the measurements taken with fixed sample angle θ_i, detector ψ, and positronium energy, but some other conditions such as the sample temperature, beam on or off, and beam valve closed or open. This type measurements were carried out either to study some other factors on the positronium surface scattering or to estimate the scattering fraction in the short time or to obtain the background count information. Another type of exception to the regular angular or energy scan run was actually either similar to the angular scans but with the sample angle varied not around specular position or similar to the energy scan run but with θ_i very different from the $\psi/2$, the specular reflection condition. This kind of measurements was carried out in an attempt to observe the surface diffraction effect. Unfortunately, it was found that the effect is not strong enough to be detected by the current set up, either higher intensity beam or lower background environment is needed to carry on the search further. The future positronium beam in Building 480 at BNL seems to have both the desirable characteristics. It has been hoped more information can be obtained with this beam in the near future.

§3.2 The Positronium Reflection From A LiF(100) Surface

In this section, the experimental results from our positronium reflection from a LiF(100) surface will be reported. Those measurements included the positronium reflection for the detector positioned at $\psi = 100°$, $120°$, and $130°$, and the measurements on the reflection changes due to the changes of the sample temperatures. The results will be represented in terms of the reflected fraction unless otherwise specified (the only exception is the sample temperature study where only the scaled coinci-

dence counts are reported). The data processing procedure to obtain the reflection fractions are similar to the example given in the section 3.1. Some of the approximation approaches to reduce the background count collecting time, which are discussed in section 3.1 were used in some of these measurements.

All the measurements represented below will show clearly the positronium specular reflection from a LiF(100) surface. The measurements reported below will also show that this specular reflection increases with the sample temperature in the temperature region from room temperature to 200° C. At the room temperature the specular reflection was not observed.

3.2.1 The detector positioned at $\psi = 100 \pm 5°$ — The experimental measurements of positronium reflection fraction from a LiF(100) surface with the detector positioned at $\psi = 100 \pm 5°$ will be reported here. The Table 3.2.1 lists some important parameters for the angular scan runs for this detection geometry and Table 3.2.2 list the main parameters for the energy scan runs for the same detection geometry. The Fig. 3.2.1 shows the angular scan result for the sample heated at 345 ± 10°C and Fig. 3.2.2 shows the results of the angular runs for the sample heated at 160 ± 10°C. The Figs. 3.2.3 shows the positronium specular reflection fraction as a function of the positronium energy for the sample heated at 345 ± 10°C; the Fig. 3.2.4 shows the same measurement for the sample heated at 160 ± 10°C.

Table 3.2.1 Operating parameters for the angular scan runs.

positronium energy (eV)	sample temperature(°C)	Figure number
7.7	345±10	3.2.1
10.7	160±10	3.2.2 (a)
17.7	160±10	3.2.2 (b)
40.0	160±10	3.2.2 (c)

Table 3.2.2 Operating parameters for the energy scan runs.

sample angle θ_i	sample temperature(°C)	Figure number
50.4°	345±10	3.2.3
50.4°	160±10	3.2.4

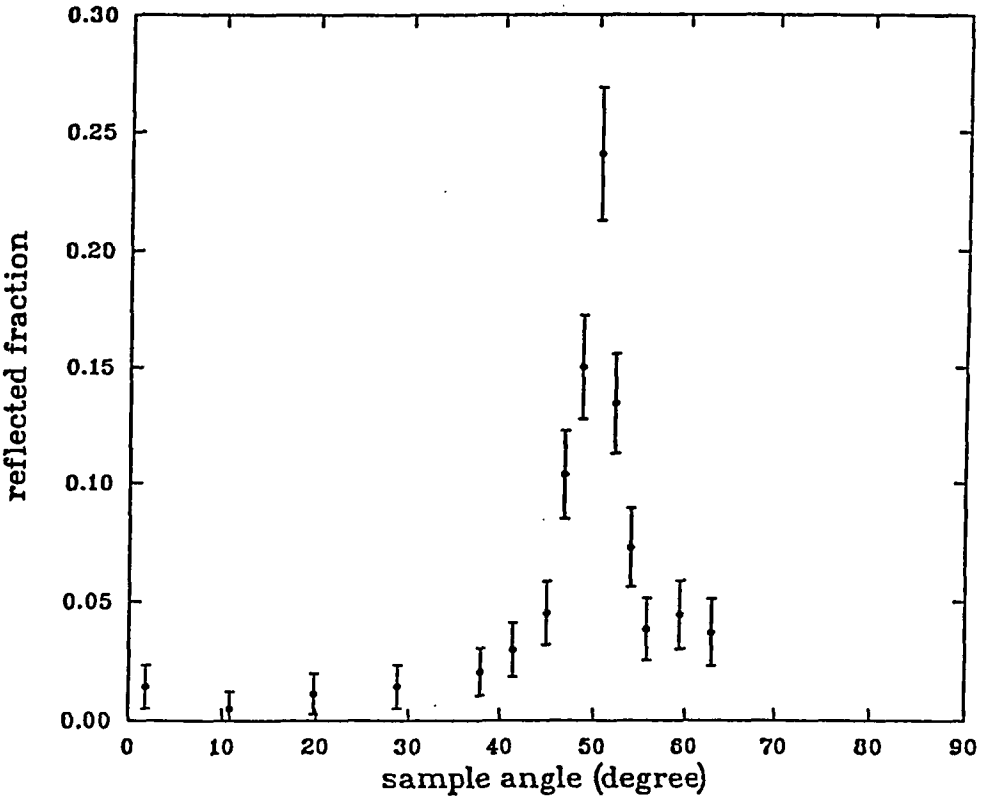

Figure 3.2.1 The reflected fraction of positronium as a function of the sample angle θ_i. The positronium energy is 7.7 eV, ψ = 100°, and T = 345°C.

For the angular scan runs, only the run of the positronium energy at 10.7 eV was taken with the beam off counts collected for both positive and negative angles and subtracted from the beam on counts before the counts for negative angle were averaged and subtracted from the positive counts as discussed in section 3.1.1. The runs with

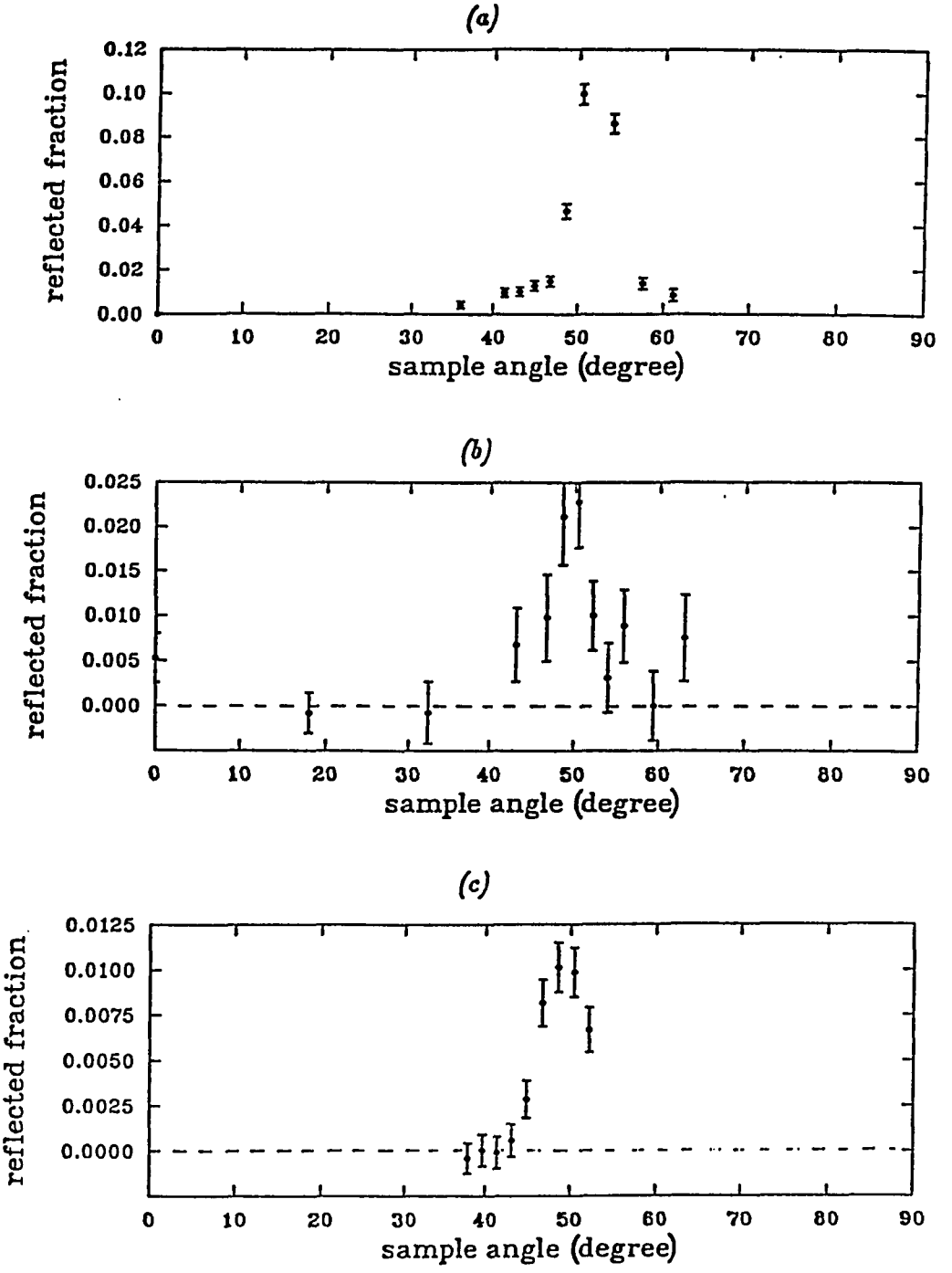

Figure 3.2.2 The reflected fractions of positronium as a function of the sample angle θ_i for different positronium energies: (a) $E_{P_s} = 10.7$ eV; (b) $E_{P_s} = 17.7$ eV; (c) $E_{P_s} = 40.0$ eV. $\psi = 100°$ and T = 160°C.

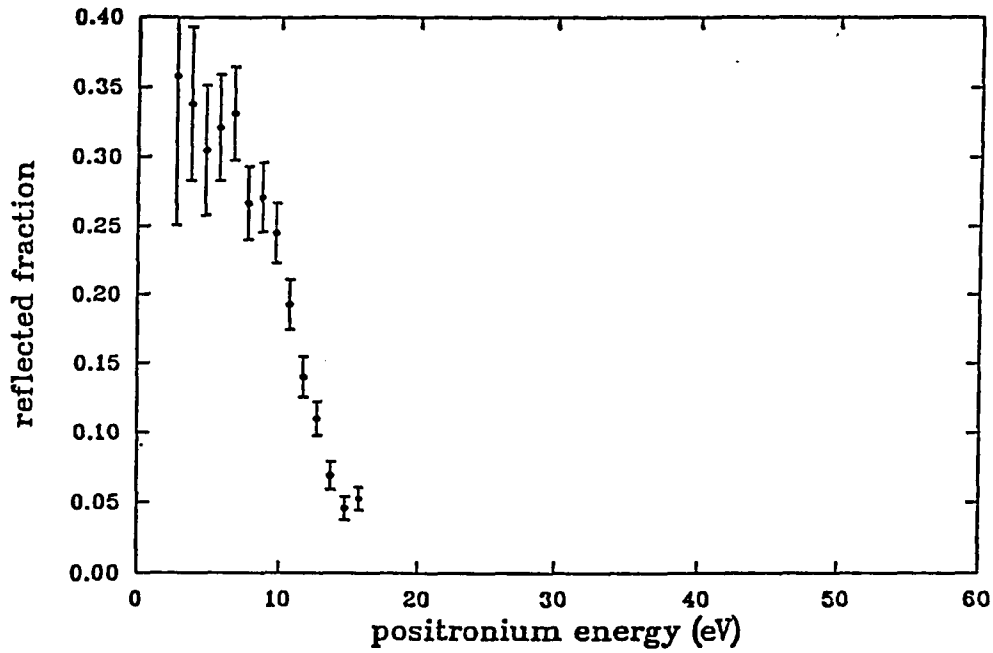

Figure 3.2.3 The reflected fraction of positronium as a function of the positronium energy for T = 345°C, $\psi = 100°$, and $\theta_i = 50.4°$.

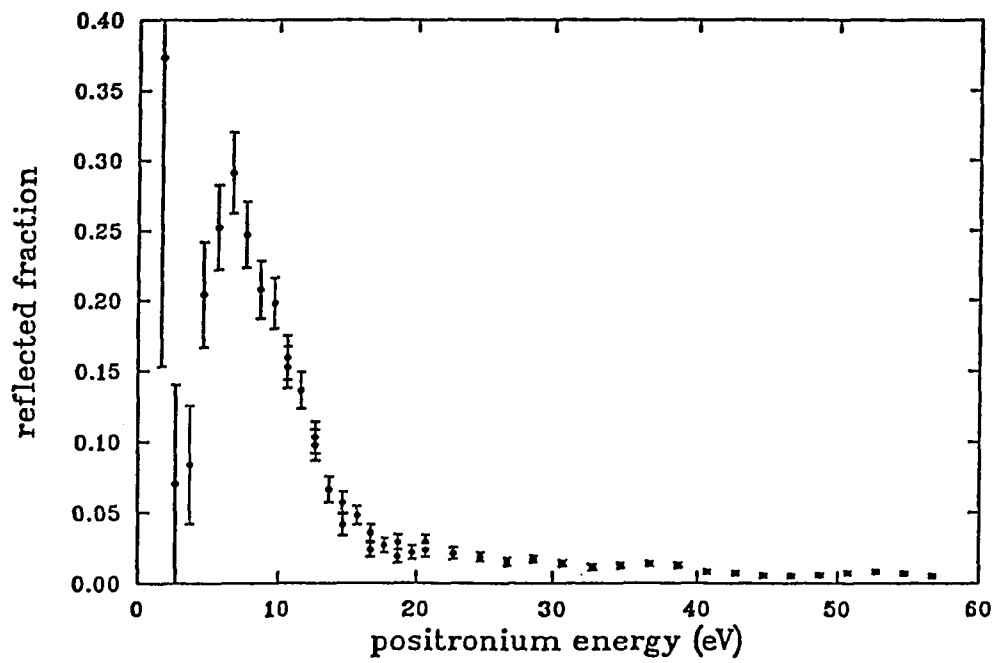

Figure 3.2.4 The reflected fraction of positronium as a function of the positronium energy for T = 160°C, $\psi = 100°$, and $\theta_i = 50.4°$.

the positronium energy at 17.7 eV and 7.7 eV were taken with the approximation approach without beam off counts collected, while an extrapolated background counts were used for the run of 40.0 eV.

The energy scan run result for the sample heated at 160°C is the combination of two runs. They were processed as shown in the example of section 3.1.2. The measurement for the sample heated at 345° was taken at both $\theta_i = \pm 50.4°$ but only counted with the beam on condition, a good approximation discussed in sections 3.1.1&3.1.2. From the figures shown in this sections, we can observe that the reflected fraction of positronium from a LiF(100) surface is higher when the sample is heated at higher temperature. This phenomenon will be discussed more in the later sections and in the next chapter.

3.2.2 The detector positioned at the $\psi = 120 \pm 5°$ — All the measurements taken for this detection geometry were carried out with the sample heated at 160 ± 10°C. The important parameters for those run are listed in the Tables 3.2.3&3.2.4. The Fig. 3.2.5 shows the result for the angular scans while the Fig. 3.2.6 shows the result for the energy scans. Both the measurements for the energy scans were taken, within the experimental uncertainty of the sample angle, at the sample position of the specular condition.

Table 3.2.3 Operating parameters for the angular scan runs.

positronium energy (eV)	sample temperature(°C)	Figure number
6.8	160±10	3.2.5 (a)
18.7	160±10	3.2.5 (b)

The data processing of angular scan measurement for positronium energy of 18.7 eV has been illustrated in section 3.1.1; the angular scan result for positronium energy of 6.8 eV was obtained similarly but without beam off counts. The

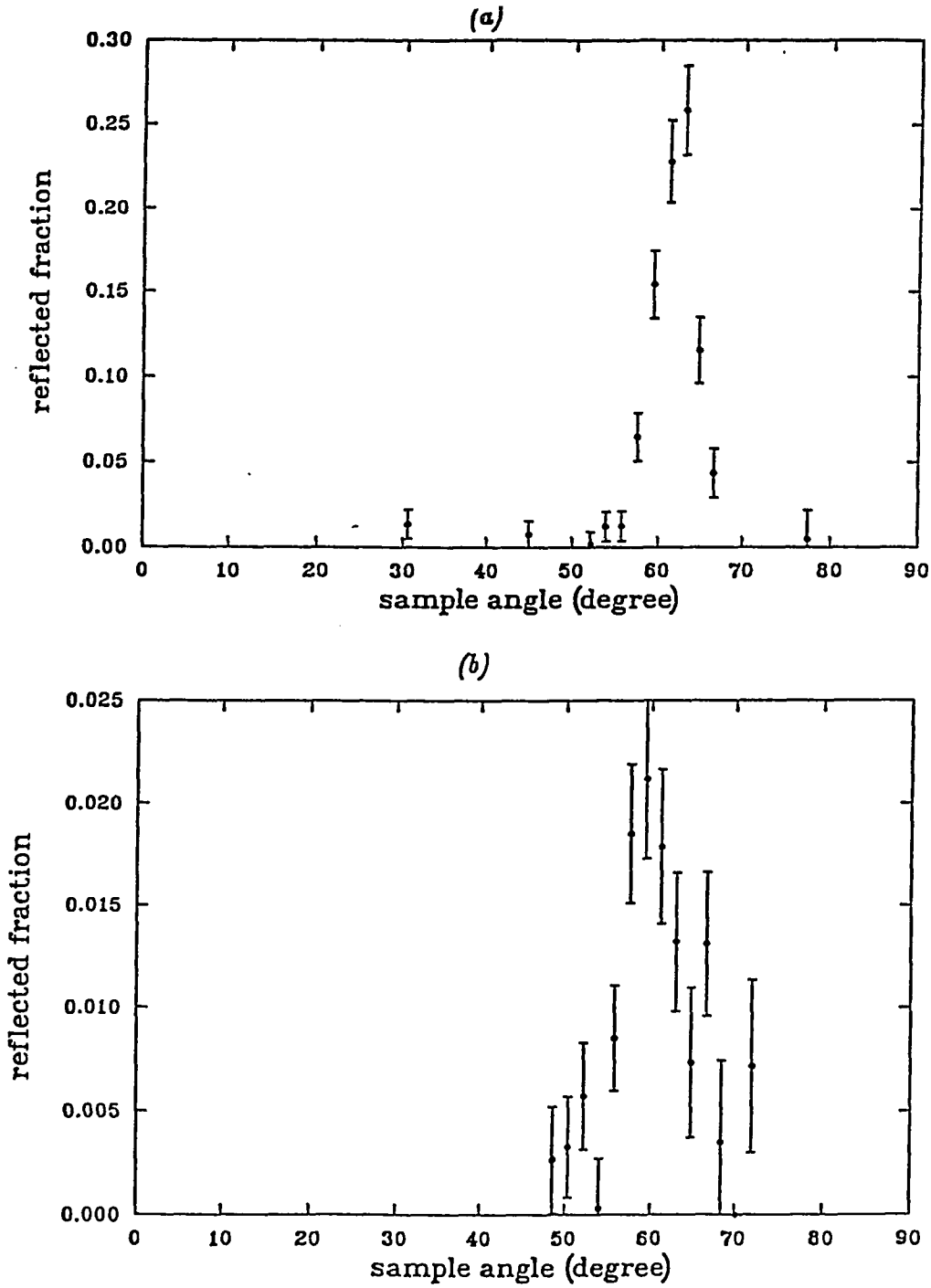

Figure 3.2.5 The reflected fractions of positronium as a function of the sample angle θ_i for different positronium energies: (a) $E_{P_s} = 6.8$ eV and (b) $E_{P_s} = 18.7$ eV at $\psi = 120°$.

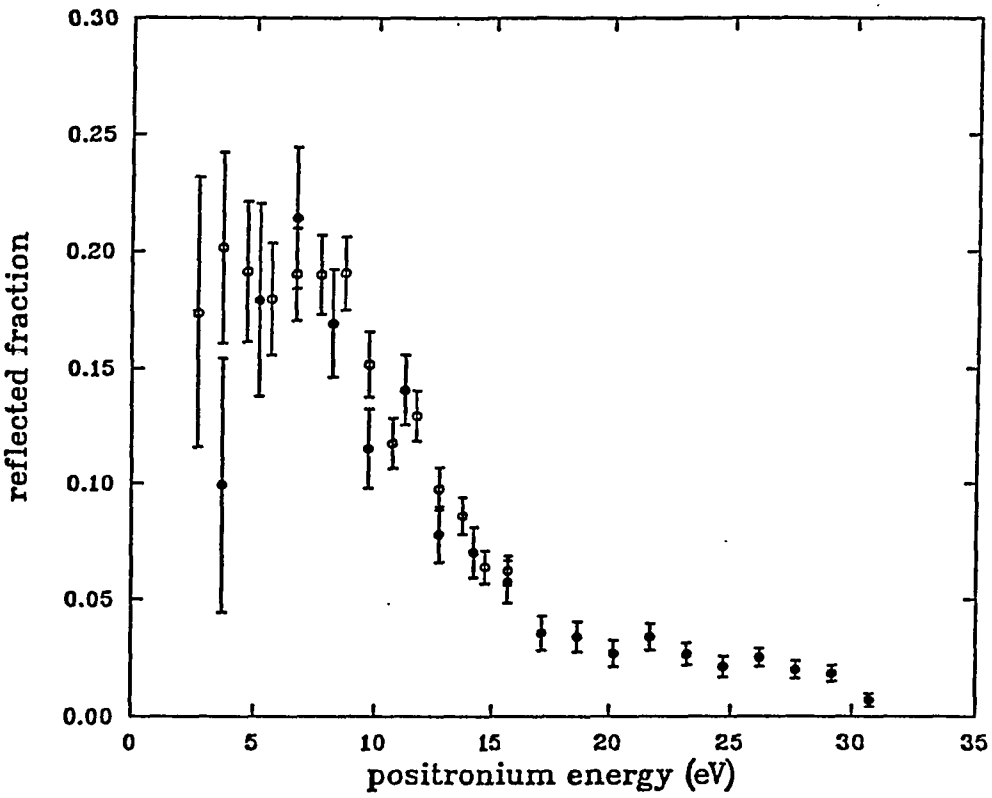

Figure 3.2.6 The reflected fractions of positronium as a function of the positronium energy for $\psi = 120°$, $\theta_i = 59.4°$ (•) and $\theta_i = 61.2°$ (○).

Table 3.2.4 Operating parameters for the energy scan runs.

sample angle θ_i	sample temperature(°C)	Figure number
59.4°	160±10	3.2.6(•)
61.2°	160±10	3.2.6(o)

energy scan runs results were obtained with similar procedures.

3.2.3 The detector positioned at $\psi = 130 \pm 5°$ — Only very limited measurements were taken in this geometry. Fig. 3.2.7 shows the angular scan result for the positronium energy of 25.7 eV and Fig. 3.2.8 shows the energy scan result for the sample angle of 64.8°. Both measurements were performed with the sample heated at 160 ± 10°C. Both the data are processed with similar procedure demonstrated in sections 3.1.1&3.1.2 and the other detection geometries.

3.2.4 The temperature dependence measurements — All the temperature dependence measurements presented here were carried out with the detector positioned at $\psi = 100 \pm 5°$ and positronium energy of 10.7 eV. The Fig. 3.2.9 shows the comparison of the observed reflected fractions of positronium as a function of the sample angle θ_i at two different temperatures. The data are processed as described before. The "o" represent the reflected fraction of positronium for the sample at room temperature; the "•" represent the reflected fraction of positronium for the sample heated to 200 ± 10°C. While the positronium specular reflection is clearly visible for the heated sample, no specular reflection can be observed for the sample at room temperature. To further illustrate the temperature dependence of this specular reflection, Fig. 3.2.10 shows the scaled coincidence counts at the different sample temperatures. They were all taken with the sample rotated at $\theta_i \sim \psi/2$, the specular reflection condition, for certain period time. The counts then were scaled according to the starting time of the measurements to compensated the decay of the beam intensity.

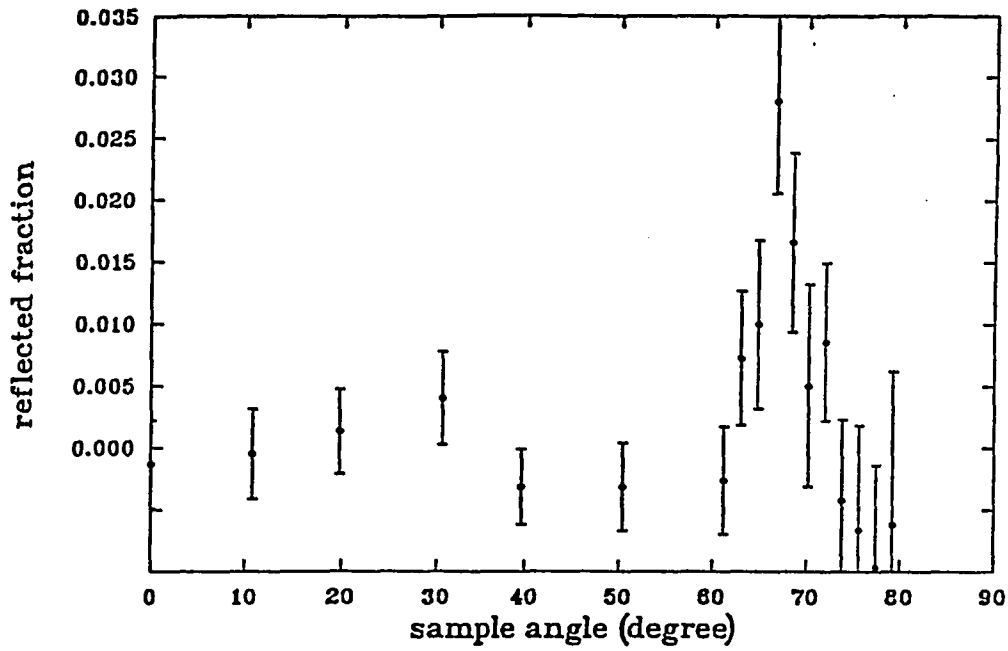

Figure 3.2.7 The reflected fraction of positronium as a function of the sample angle θ_i. $E_{P_s} = 25.7$ eV and $\psi = 130°$.

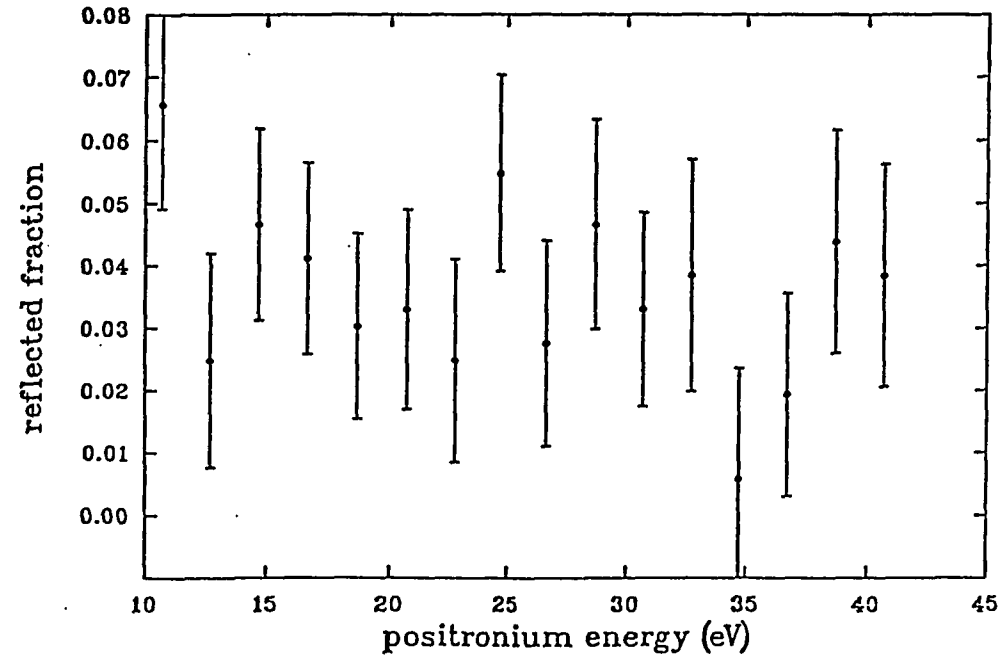

Figure 3.2.8 The reflected fraction of positronium as a functions of the positronium energy. $\psi = 130°$ and $\theta_i = 64.8°$.

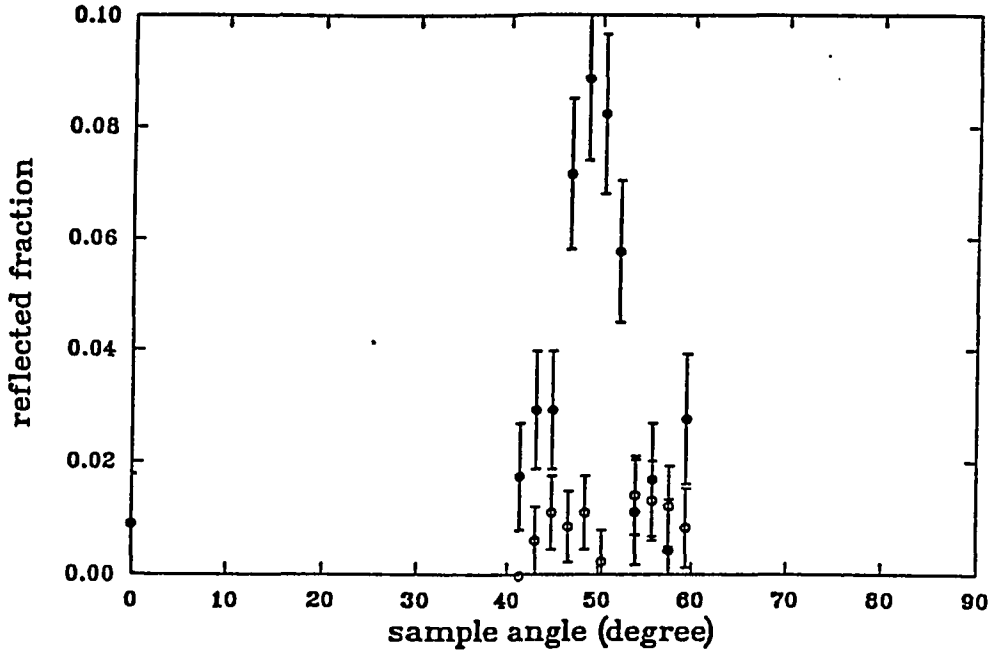

Figure 3.2.9 The reflected fractions of positronium as a function of the sample angle θ_i for different sample temperatures: T = 200°C (•), and T = 22°C (o). E_{P_s} = 10.7 eV.

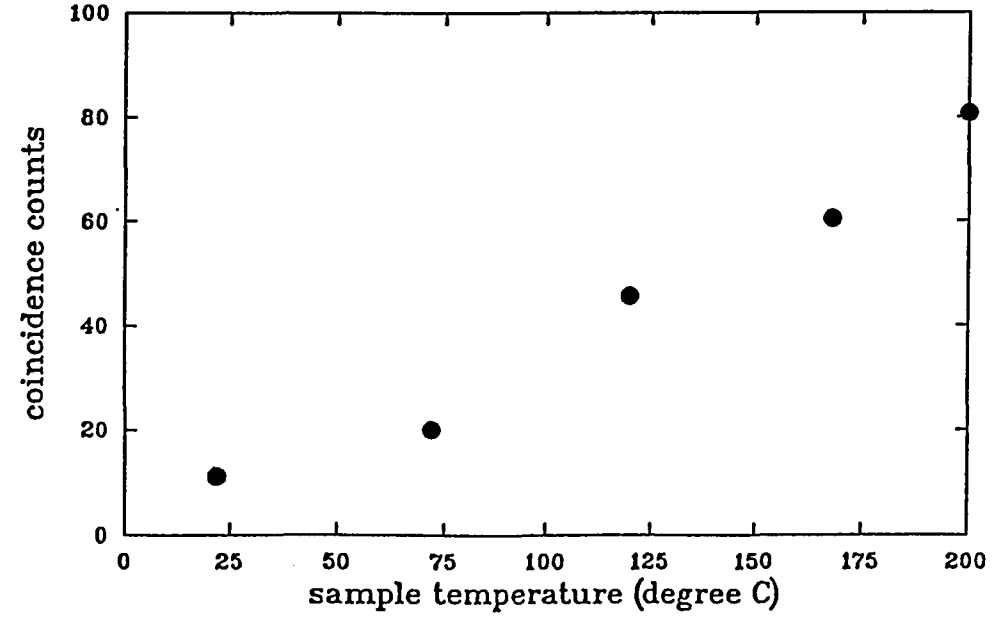

Figure 3.2.10 The coincidence counts of reflected positronium at $\psi = 100°$, $\theta_i = 50.4°$, and E_{P_s} = 10.7 eV for different sample temperatures.

A monotonic increase behavior was observed. A later measurement indicated that the increase saturated at the temperature above 300°C.

3.2.5 The surface diffraction — The efforts have been made to observe the two dimensional diffraction by the periodicity on the surface. Both energy scans in the range of 0 to 70 eV with the detector at $\psi = 100°$ and sample at $\theta_i = 72°$ or 19.8° and the angular scan in the range of 0 to 90° at the positronium energy of 50 eV with same detection geometry were performed. The results so far, however, are negative. Some discussion about its absence will be given in the next chapter.

§3.3 The Positronium Scattering From A Cu(100) Surface

All the measurements of positronium scattering from a copper surface were carried out similarly to those for LiF(100) surface. All the measurements, except one, were performed with a single crystal Cu(100) surface heated at 170 ± 10°C. The single crystal Cu(100) surface was prepared as described in section 2.4 before each measurement was taken. The only exception was the measurement carried out on a polycrystal oxygen free copper surface, which was taken at the time mainly to compare with the measurements for a LiF(100) surface. The surface, in this case, was not prepared and the measurement was performed with the surface at the room temperature. No specular reflection of positronium from this untreated "cold" copper surface was observed. The scattered fraction was found very low. The measurements on the single crystal Cu(100) surface after that were carried out with a well prepared and heated ($170 \pm 10°$) sample surface. Even though, no specular reflection was observed with our experimental set up, the scattered fraction of positronium from the well prepared surface was considerable higher than that measured from the untreated polycrystal copper surface at the room temperature. The measurements for the Cu(100) surface were performed with the detector set up positioned at $\psi = 100°$ and 130°. Those measurements will be reported in the following sections. Because of

the limited positronium beam time and the much lower scattered fraction of positronium from a Cu(100) surface than that from a LiF(100) surface, the measurements reported here have fairly large statistical error and are considered just as the preliminary results. It is hoped that measurements with larger counts accumulation will be carried out in the near future when the HFBR reactor starts up again.

3.3.1 The detector positioned at $\psi = 100 \pm 5°$ — The angular scan runs were carried out on a untreated polycrystal copper surface at the room temperature to make the comparison with the similar measurements on LiF(100) surface (see the result in 3.2.1) because this sample surface was the back surface of the sample heater-holder assembly which could be rotated into the beam at the approximate position of the LiF(100) surface and make it easy to compare its measurements with those on the LiF(100). Fig. 3.3.1 shows the result of the angular scan run on this untreated copper surface at the room temperature. The positronium beam energy is 10.7 eV. The background was subtracted by subtracting the averaged counts for the negative sample angles from those for the positive sample angle before the time scaling and the normalization to the beam intensity. The partly missing of the positronium beam at the larger sample angle was not compensated (as only the information on the order rather than actual value of the scattered fraction was needed).

It was hoped that the scattered fraction of positronium would increase and possibly the specular reflection would be observed if the copper surface used be a well prepared single crystal surface heated at above the 150°C. Table 3.3.1 lists the coincidence counts taken with the detector positioned at $\psi = 100°$, the sample angle $\theta_i = 50.4°$, the positronium beam energy at 10±0.5 eV. To observed the effect of various background, the coincidence counts for the conditions of the beam off by the biasing the grid with +300V (noted in Table 3.3.1 as "beam off") and the mechanical interruption of the beam by shutting off the beam valve (noted as valve closed

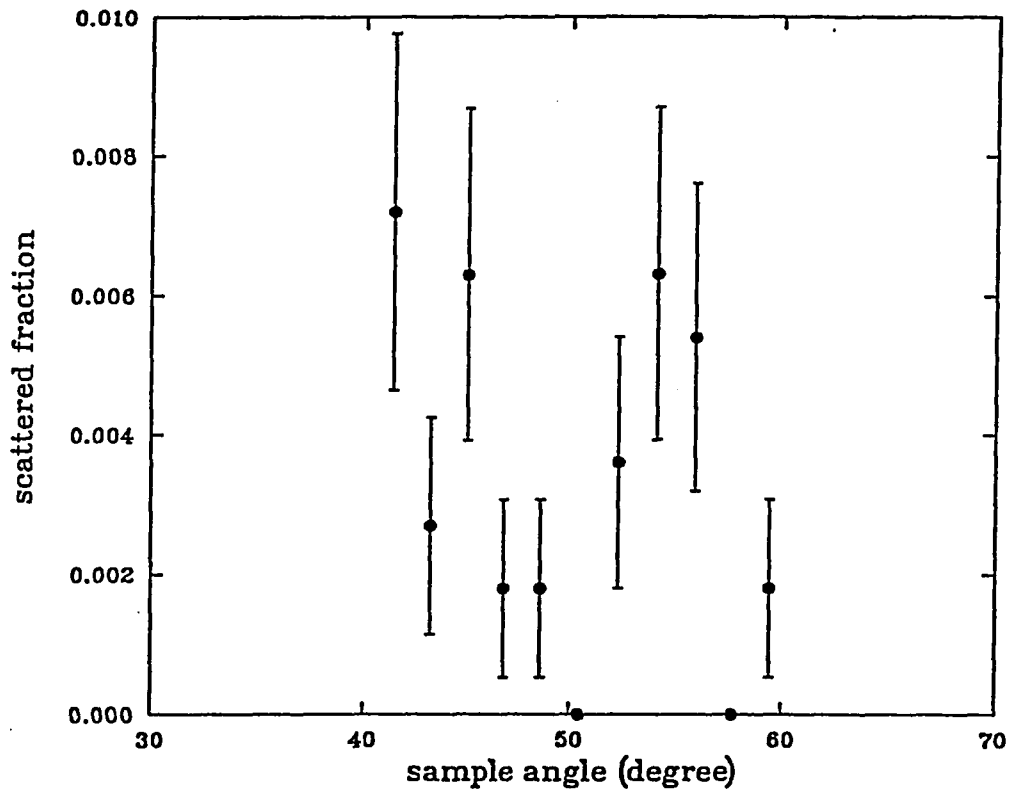

Figure 3.3.1 The reflected fraction of positronium from a polycrystal copper surface at room temperature. $\psi = 100°$ and $E_{P_z} =$ 10.7 eV. The error bars reflect the statistical error only.

in the table) were also measured. From the table, it can be seen that there was observable positronium scattering from the Cu(100) surface (after the subtraction of the background) which warrants the further study of the positronium scattering from the Cu(100) surface; it also can be seen that the effect of higher energy positrons was not significant (there was virtually no difference between the electrical beam off and mechanical beam off, the later will stops all the positrons while the high energy positron can pass the rejection grid.).

Fig. 3.3.2 shows the results of the angular scans on the Cu(100) surface at this detection geometry. Some of the important operating parameters are given in table

Table 3.3.1 The coincidence counts of the scattered positronium.

running condition	counting time	coincidence counts
"beam on"	8000 sec.	36
"beam off"	8000 sec.	16
valve closed	8000 sec.	15

3.3.2. The background was subtracted by using the averaged count for the negative angles for the run of the positronium energy at 10 eV. A extrapolated background count from the run at 10 eV and the run listed by the Table 3.3.1 was used to process the data for the run of the positronium energy at 50 eV. The error bars reflect the statistical error only. No specular reflection can be observed, but the scattered fraction is considerably larger than that measured for an untreated polycrystal surface at the room temperature.

Table 3.3.2 Operating parameters for the angular scan runs.

positronium energy (eV)	sample temperature(°C)	Figure number
10	170±10	3.3.2 (a)
50	170±10	3.3.2 (b)

Table 3.3.3 Operating parameters for the energy scan runs.

sample angle θ_i	sample temperature(°C)	Figure number
50.4°	170±10	3.3.3(•)
50.4°	170±10	3.3.3(o)

The results of the two energy scan runs are shown in Fig. 3.3.3 and some of the important parameters are given in Table 3.3.3. The averaged beam off counts was used as the background for both the higher energy range run (denoted by "o") and

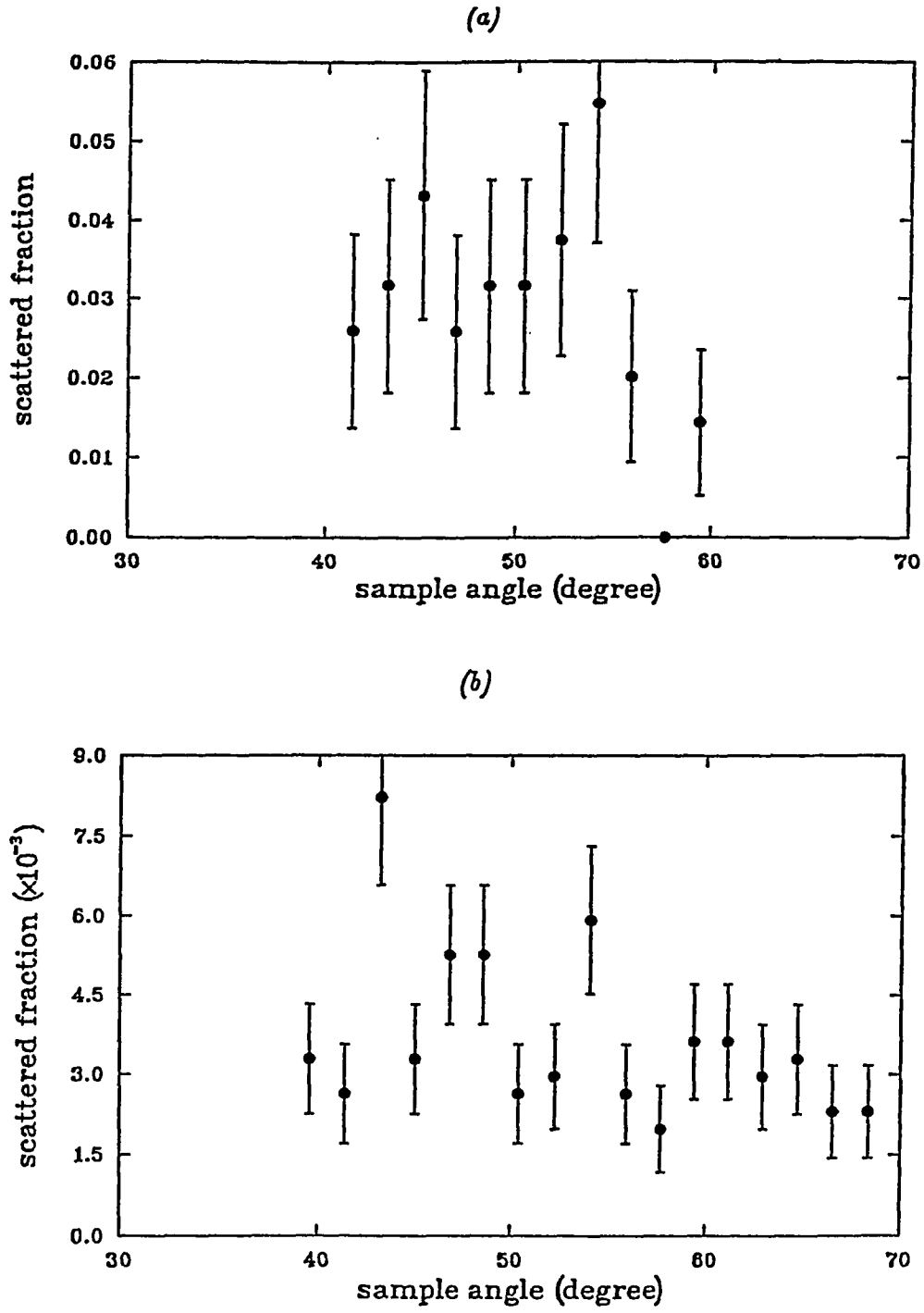

Figure 3.3.2 The scattered fraction of positronium as a function of the sample angle θ_i at two different positronium energies: (a) 10 eV and (b) 50 eV with detector positioned at $\psi = 100°$.

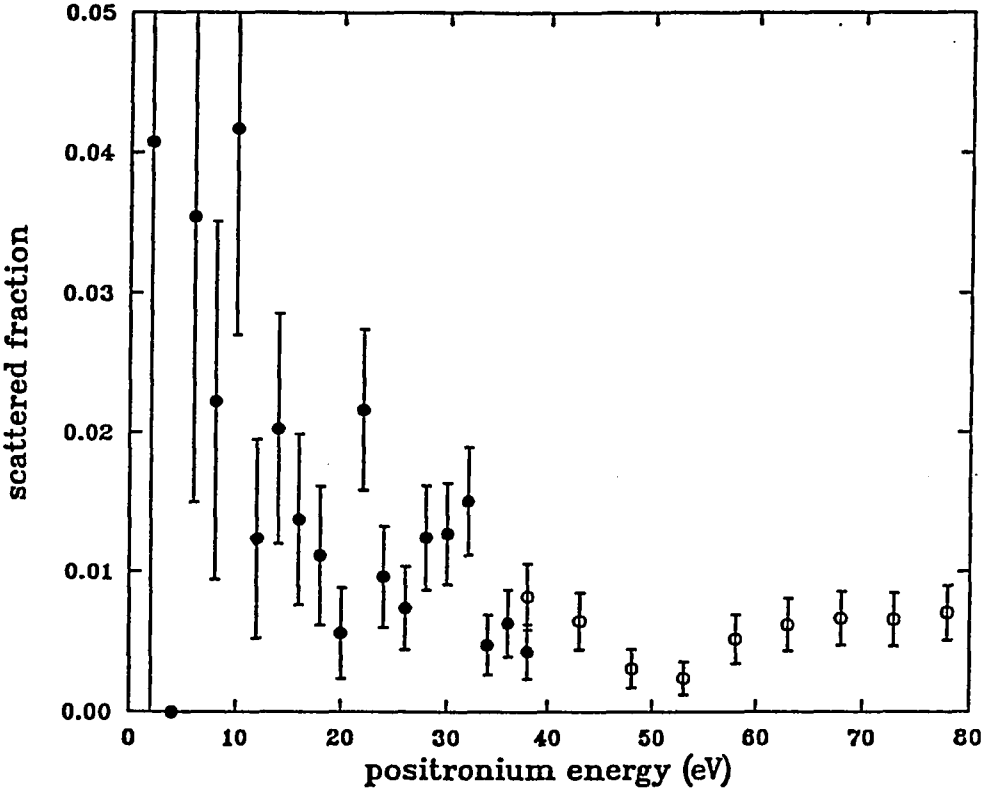

Figure 3.3.3 The scattered positronium fraction of positronium as a function of energy measured in two experiments ("•" and "o") with sample angle $\theta_i = 50.4°$ and detector positioned at $\psi = 100°$.

the lower energy range run (denoted by "•).

3.3.2 The detector positioned at $\psi = 130 \pm 5°$ — The measurements carried out for this detection geometry are shown in Figs. 3.3.4&3.3.5. All the measurements were performed with the sample heated to 170°C. The angular scan run result shown by Fig. 3.3.4 was done with positronium beam energy at about 51 eV. The background was subtracted by subtracted averaged count for the negative sample angles from those for the positive sample angles. The error bars reflect the statistical error only. The energy scan run result shown in Fig. 3.3.5 was measured with the sample

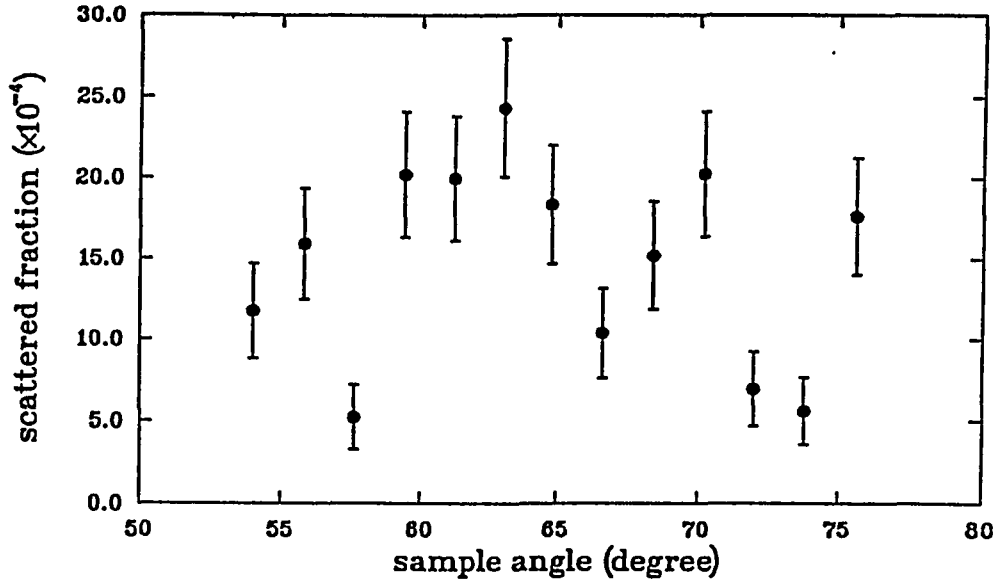

Figure 3.3.4 The scattered fraction of positronium as a function of the sample angle θ_i at the positronium energy of 51 eV with the detector positioned at $\psi = 130°$.

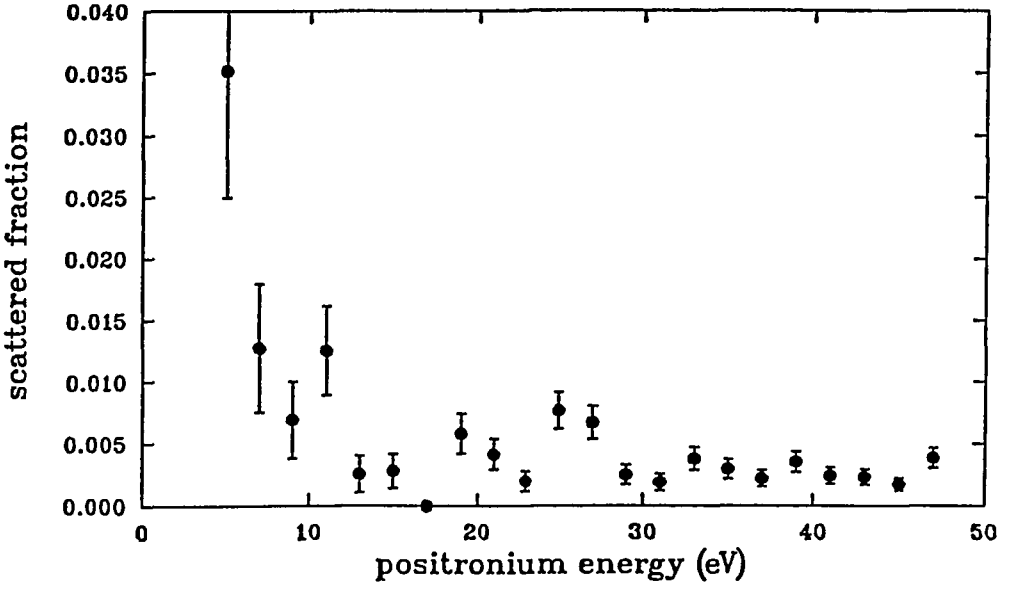

Figure 3.3.5 The scattered fraction of positronium as a function of the positronium energy measured at the sample angle $\theta_i = 64.8°$ and detector positioned at $\psi = 130°$.

positioned at $\theta_i = 64.8°$, the specular reflection angle for this detection geometry. The background count obtained by averaging the counts for the energy point below the positronium energy at zero (i.e. the gas cell potential above the maximum voltage for positronium formation, see section 3.1.2) was subtracted from the total counts before the time scaling and normalization by the positronium beam intensity.

§3.4 The Positronium Emission From LiF(100) And Cu(100) Surfaces

The positronium emission measurements were taken on the same set up we took the positronium scattering fraction measurements. The only difference in set up was the gas cell was grounded and the gas baffle tube after the gas cell was not used as positron rejector, instead, was electrically floated at the same voltage as the sample surface to help obtaining a better deceleration. It was this same voltage of the baffle tube and the sample that controlled the positron incident energy. The grid-tube assembly in front of the annihilation plate was still used as a positron rejector to prevent the positron travelling into the vicinity of the annihilation plate. The axial magnetic guiding field (about 80 gauss) would also prevent any low energy positrons travelling to the detector. The measurements were carried out similarly as in the positronium scattering case, with both angular scan and energy scan runs carried out for each surface.

3.4.1 The positronium emission from a LiF(100) surface — All the measurements of the positronium emission from a LiF(100) surface were taken with detector positioned at $\psi = 100°$ and sample heated to $170 \pm 10°$C. As discussed in section 3.1.3, the measurements reported here were all taken for both positive and negative angles at both the beam on and beam off conditions. The final results were produced by subtracted the beam off counts from their corresponding beam on counts for every data point, then the averaged value of the counts for negative angles after the beam off subtraction was subtracted from the corresponding counts for the positive sample

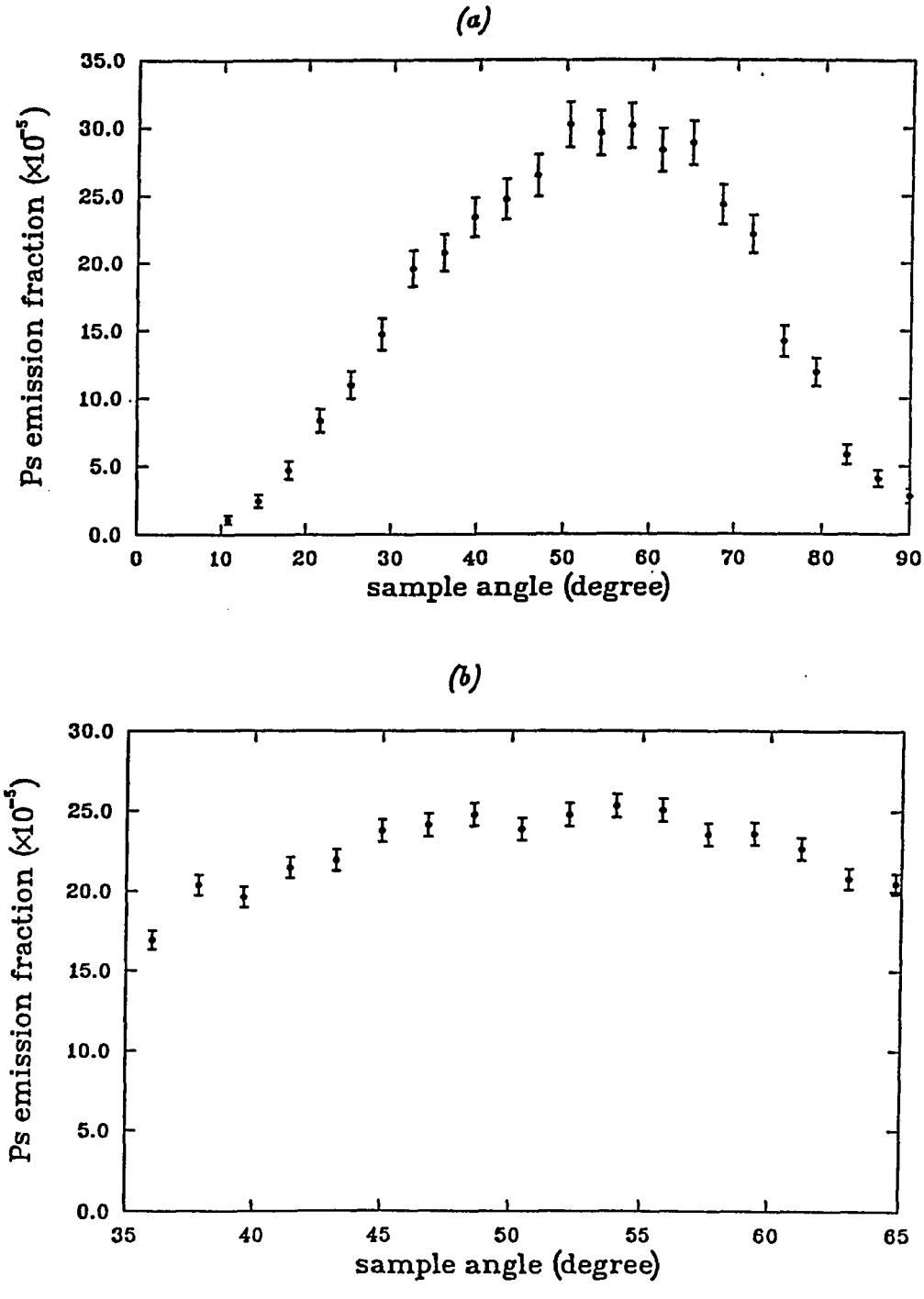

Figure 3.4.1 The positronium emission fractions as a function of the sample angle θ_i at the positron incidence energy of 150 eV measured at different angle ranges. The detector was positioned at $\psi = 100°$.

angles before the time scaling and normalization by the positron intensity.

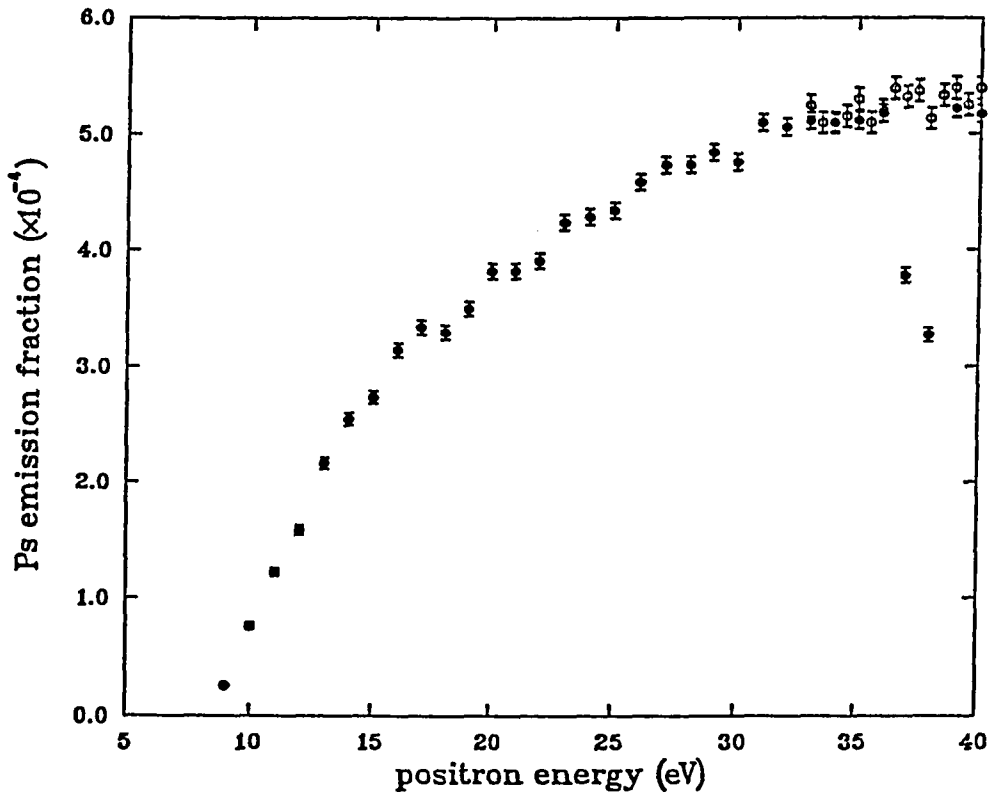

Figure 3.4.2 The positronium emission fraction as a function of the positron incidence energy measured at the sample angle θ_i = 50.4° and the detector positioned at ψ = 100°. Two measurements ("•" and "o"in the figure) were taken under the same condition.

The angular scan of the positronium emission was taken with the positron incidence energy at 150 eV, because the measurements was taken when the positron beam was set at 150 eV and the sample was internally grounded. The measurement shown in Fig. 3.4.1 (a) was taken for sample angles ranged from 0° to 90° with a 3.6° step, while the result show in Fig. 3.4.1 (b) was taken in a smaller sample angle

range with a smaller step of 1.8°.

Both two energy scan runs were taken with sample at $\theta_i = 50.4°$, about $\psi/2$, and the results are shown in the Fig. 3.4.2. The measurement for the larger energy range (denoted by "•") was taken first with an energy step of 1 eV, then second measurement (denoted by "o") was taken with a 0.5 eV energy step in the region where a large fluctuation was observed in the first measurement. The minimum positron incidence energy for the positronium emission from a LiF(100) to be observed with our experimental set up was 9 ± 1 eV.

3.4.2 The positronium emission from a Cu(100) surface — The positronium emission from a Cu(100) surface was measured with the detector positioned at $\psi = 100 \pm 5°$ and the sample heated to $170 \pm 10°$C. Both angular scan runs and energy scan runs were carried out on the surface sputtered by the Ar ions with and without annealing afterwards. In the all the experiments, the surface was prepared as described in section 2.1, sputtered by the Ar ions to clean the surface contamination then heated up to 600° to annealed out the surface damage by the ion bombardment. If no additional ion bombardment was employed on the surface, it will be denoted as annealed surface in the following description, while the "sputtered" will be used to denote the surface that was again bombarded with Ar ions at energy of 500 eV for approximately 15 minutes after the regular sample preparation to create some controlled surface damage.

Table 3.4.1 lists some of the important operation parameters for the angular scan runs. The results of these runs are shown in Fig. 3.4.3. Table 3.4.2 lists some of the important operation parameters for the energy scan runs. Their results are shown in Figs. 3.4.4&3.4.5. The data were analysed similarly but without beam off counts. As discussed in section 3.1.3, the background from the high energy positron is negligible in this case.

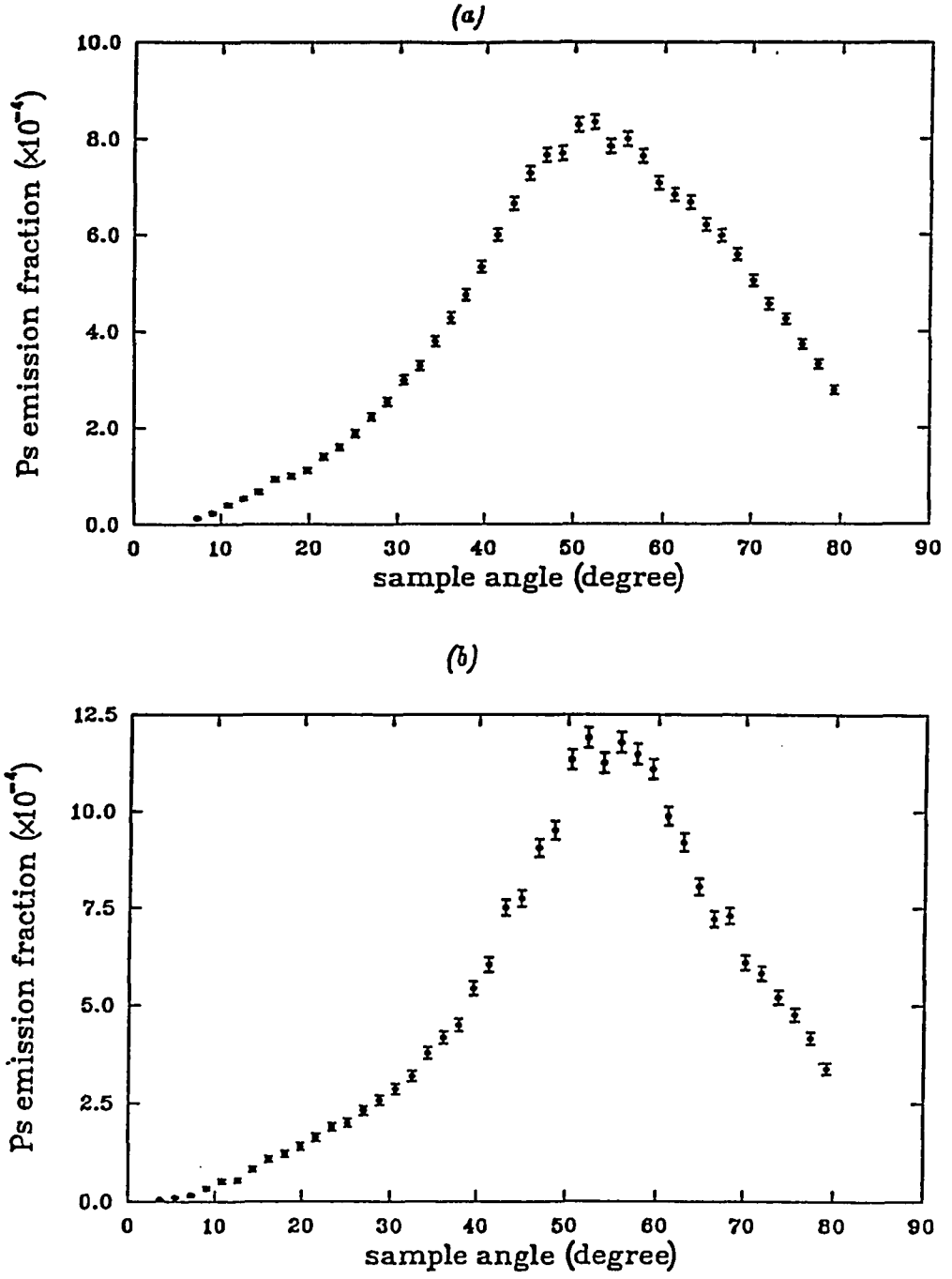

Figure 3.4.3 The positronium emission fraction as a function of the sample angle θ_i measured from (a) the annealed Cu(100) surface at the positron energy of 38 eV and (b) the sputtered Cu(100) surface at the positron energy of 30 eV. The detector was positioned at $\psi = 100°$.

Table 3.4.1 Operating parameters for the angular scan runs.

positron energy (eV)	surface condition	Figure number
38	annealed	3.4.3 (a)
30	sputtered	3.3.3 (b)

Table 3.4.2 Operating parameters for the energy scan runs.

sample angle θ_i	surface condition	Figure number
50.4°	annealed	3.4.4(•)
50.4°	annealed	3.4.4(o)
50.4°	annealed	3.4.5(a)
50.4°	sputtered	3.4.5(b)

It is can be seen that the positronium emission fraction is peaked at about 30 eV positron incidence energy and at $\theta_i = 54 \pm 3°$. The peak in its angular scan runs is much sharper than that for the LiF(100) surface. After the ion sputtering at the surface, the peak in the angular scan sweep seemed to become narrower. There are also some distinct features in the energy scan spectrum which can be seen both before and after the ion sputtering. These results will be discussed in the next chapter.

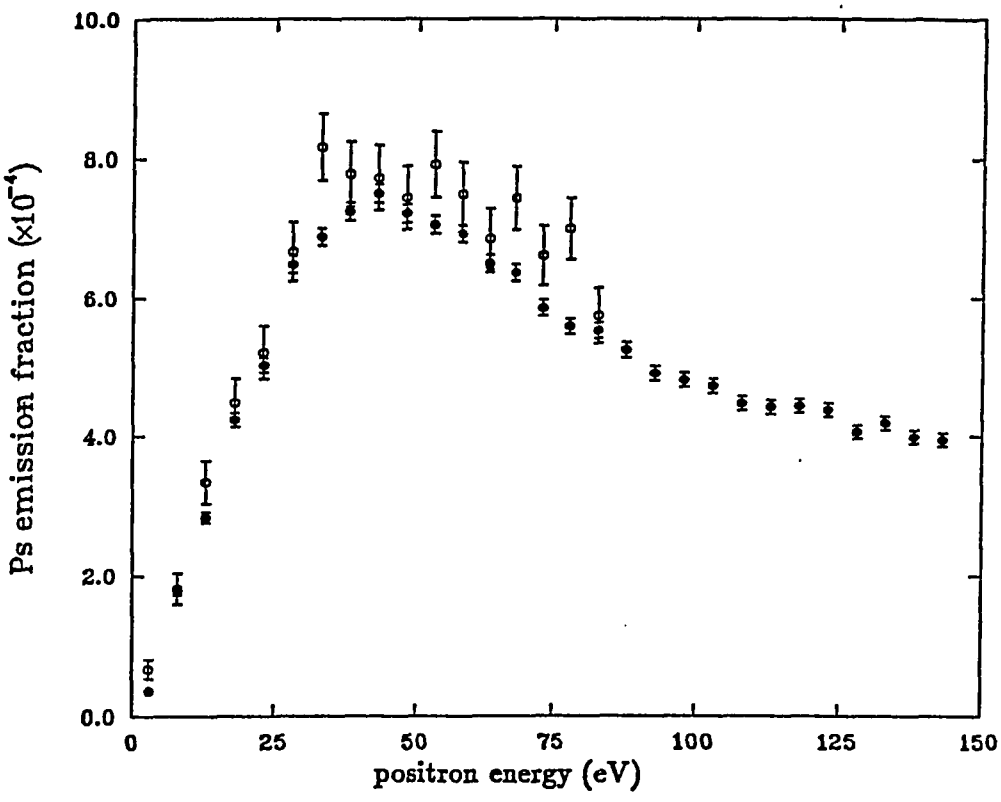

Figure 3.4.4 The positronium emission fractions as a function of the positron incidence energy from two measurements taken with the sample angle $\theta_i = 50.4°$ and the detector positioned at $\psi = 100°$.

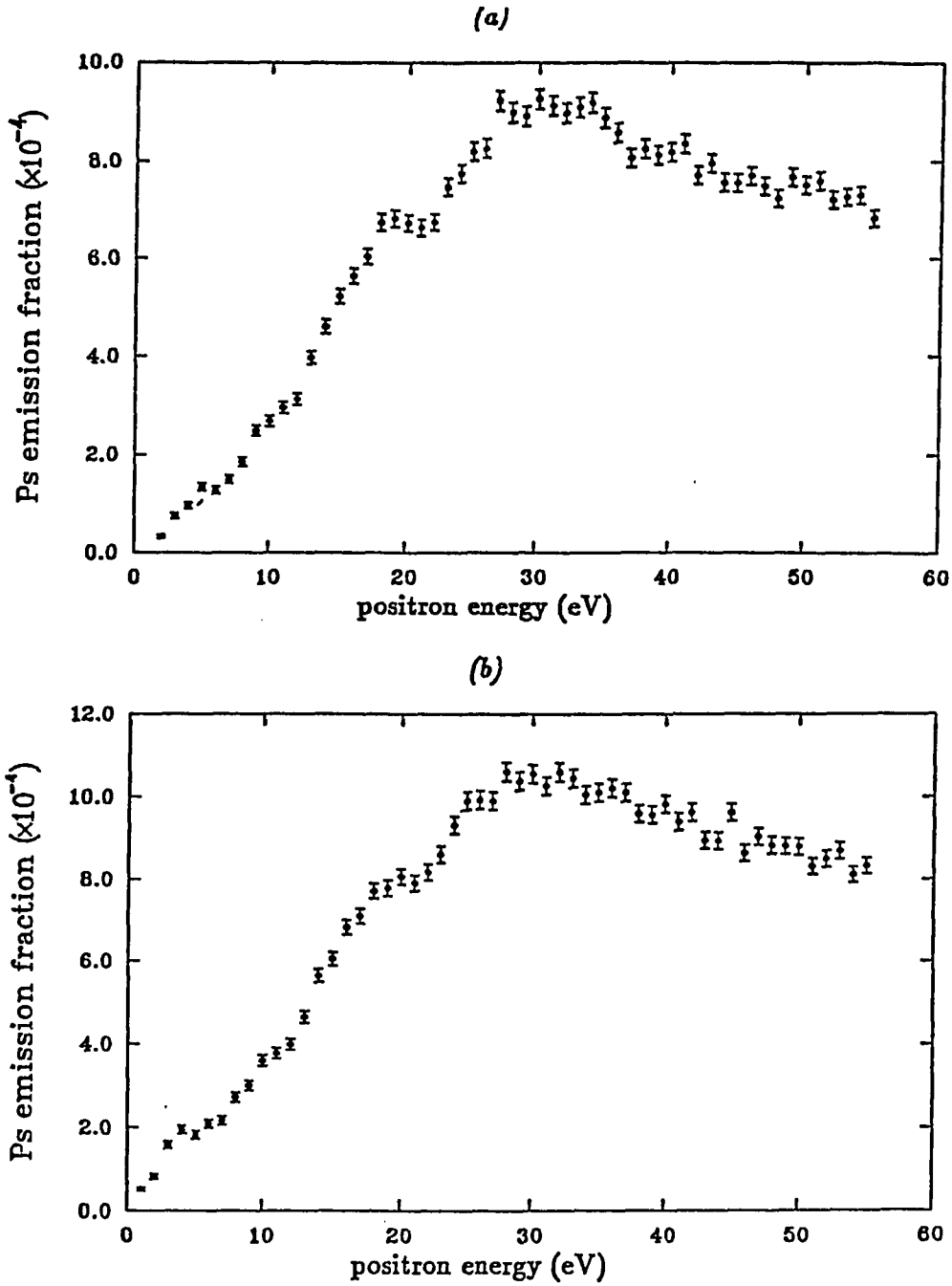

Figure 3.4.5 The comparison of the positronium emission fractions measured with (a) an annealed Cu(100) surface and (b) a sputtered Cu(100) surface at various energies with the sample angle $\theta_i = 50.4°$ and the detector positioned at $\psi = 100°$.

Chapter 4
DATA ANALYSIS AND DISCUSSION

The experimental results reported in the previous chapter are the first experimental information obtained on the positronium reflection and scattering from different solid state surfaces. With a correct interpretation, they can offer an important clue to the understanding of the positronium interaction with solid state surfaces and also indicate the full potential of positronium as a surface study probe. In this chapter, the effort to interpret our experimental results will be reported. It will include the discussion on the experimental results of the specular reflection of positronium from a LiF(100) surface, the positronium scattering from a Cu(100) surface, and the positronium emission from both surfaces bombarded with low energy ($\leq$ 150 eV) positrons. It is hoped that a better understanding of the positronium interaction with solid state surfaces will be achieved through the following discussion and the information generated in this treatment will benefit the future research in this area.

§4.1 The Positronium Specular Reflection From A LiF(100) Surface

Our experimental observation of the positronium specular reflection reported in the Chapter 3 have following interesting characteristics: (1) The reflection of positronium from a clean LiF(100) surface is strongly peaked at the specular direction. There was no significant amount of isotropic background. (2) The observed FWHM of this specular peak in our angular scan measurements is about 6° which is about the same as the estimated the angular divergence of our positronium beam. (3) The intensity of this specular reflection is energy dependent varying from about 30% at energies

below 7 eV to about 1% at the energies up to 50 eV. (4) The positronium specular reflection from the LiF surface is also sensitive to the temperature of the sample. The maximum specular reflection intensity was obtained with the sample heated to above 300°C, while no visible positronium specular reflection was observed when the sample was at room temperature. (5) The maximum intensity of the positronium specular reflection from the LiF surface also depends on the incident angle of positronium. It decreased when the incident angle θ_i (see Chapter 2&3 for the definition of θ_i) increased. Even though we could not measure the energy of the reflected positronium, from (1) and (2), it is clear that this specular reflection is the result of dominantly elastic scattering, because any inelastic scattering process in which positronium atoms lose appreciable amount of energy would either greatly broaden the angular scan peak and create an observable nearly isotropic background or, diminish the angular peak significantly. The other characteristics listed above are closely related to the interaction of positronium with the LiF surface.

As discussed in Chapter 1, only a very few theoretical efforts have directed at the energetic positronium interaction with surfaces, various atoms and ion cores. As a result, there is no available theoretical model which we can use to interpret our experimental result. A very simple one dimension potential step model with a complex potential was proposed (Weber and others 1988) as the first step to understand our observation. This model seemed to explain the energy dependence of the specular reflectivity qualitatively, but it can not explain all the experimental results and some of the conclusions drawn from the interpretation of the experimental data were highly debatable. In the following section, this simple model and its application in interpreting the experimental data will be illustrated. An overall discussion about the model including its implication, its limitation, and its difficulties will be given.

The difficulties the previous model was facing motivated us to look for a better

theoretical model which would include the effects on the positronium interacting with surfaces that have been ignored by the above simple model so it would be more suitable for the interpretation of our experimental observation. A theoretical model based on the combination of potential well, potential step, and first layer of the ion core scattering will be proposed along with the discussion of the underlying physics principle it based on. Its results in comparison with the experimental observation will be presented. The conclusions from this model will be discussed. The possible causes of the loss of detected positronium and its angle dependence as well as the temperature dependence of the specular reflection from LiF will also be discussed in the following sections.

4.1.1 The single step potential model — Because there was no any available theoretical model which would be applicable to the positronium reflection from a LiF surface at the time we obtained our experimental results, the simplest possible model was first considered (Weber and others 1988). Assuming that the wave function of positronium takes the form of a plane wave and the interaction of positronium with a LiF surface can be represented by an one dimensional step potential along the direction normal to the surface, the problem was reduced to solving the one dimensional Schrödinger equation:

$$i\hbar\frac{\partial}{\partial t}\psi(x,t) = \Big(-\frac{\hbar^2}{2m}\frac{\partial^2}{\partial x^2} + V(x)\Big)\psi(x,t). \tag{4.1.1}$$

With $\psi(x,t)$ written as $\psi(x)\exp(-iEt/\hbar)$, Eq. (4.1.1) is reduced to:

$$\Big(-\frac{\hbar^2}{2m}\frac{\partial^2}{\partial x^2} + V(x)\Big)\psi(x) = E\psi(x). \tag{4.1.2}$$

In this model, the potential takes the following form:

$$V(x) = \begin{cases} 0, & \text{if } x < 0; \\ V_s, & \text{if } x > 0, \end{cases} \tag{4.1.3}$$

where V_s is a constant potential. Assuming V_s is real, the wave function would just take the form of one dimensional plane wave

$$\psi(x) \propto \begin{cases} \exp(\pm ik_o x) & \text{for } x < 0; \\ \exp(\pm ik_{in} x) & \text{for } x > 0, \end{cases} \tag{4.1.4}$$

with wave vectors k_o and k_{in} for the cases of $x < 0$ and $x > 0$ respectively expressed as:

$$\begin{aligned} k_o^2 &= \frac{2m}{\hbar^2} E \\ k_{in}^2 &= \frac{2m}{\hbar^2}(E - V_s), \end{aligned} \tag{4.1.5}$$

if $E \geq V_s$. If $E \leq V_s$, the wave function would be the same form at the region $x < 0$ but become $\exp(\pm K_{in} x)$ for $x > 0$ with:

$$K_{in}^2 = \frac{2m}{\hbar^2}(V_s - E). \tag{4.1.5'}$$

The $E = E_{P_s} \cos^2 \theta_i$ is the energy of positronium projected at the normal direction and V_s is the interaction potential. In this simple model, the positronium reflection becomes plane wave reflection by this step potential. Assuming the incident wave takes the form of $\exp(ik_o x)$, then the wave function, for $E \geq V_s$, can be written as:

$$\psi = \begin{cases} \exp(ik_o x) + r \exp(-ik_o x), & \text{for } x < 0; \\ t \exp(ik_{in} x), & \text{for } x > 0, \end{cases} \tag{4.1.6}$$

From the continuity of ψ and $\partial\psi/\partial x$ at the boundary x=0, r can be solved as:

$$r = \frac{k_o - k_{in}}{k_o + k_{in}}. \tag{4.1.7}$$

The reflection coefficient R is given by:

$$R = |r|^2 = \frac{(k_o - k_{in})^2}{(k_o + k_{in})^2}. \tag{4.1.8}$$

Similarly, for $E < V_s$, the wave function can be written as:

$$\psi = \begin{cases} \exp(ik_o x) + r\exp(-ik_o x), & \text{for } x < 0; \\ t'\exp(-K_{in} x), & \text{for } x > 0, \end{cases} \tag{4.1.9}$$

and r can be solved similarly to be:

$$r = \frac{k_o - iK_{in}}{k_o + iK_{in}}. \tag{4.1.10}$$

From Eq. (4.1.10), it is obvious that R is unity for all the E that are smaller or equal to V_s.

To apply this model to the experimental result, another factor has to be taken into the consideration. That is the Ps specular reflection coefficient does not approach the unity at the lower energy limit in our observation. This is probably due to the positronium loss at the surface (see discussion in later section) and imperfection of the surface condition. To account for this fact, a factor R_o is added, and R is expressed as:

$$R = \begin{cases} R_o \dfrac{(k_o - k_{in})^2}{(k_o + k_{in})^2}, & \text{for } E > V_s; \\ R_o, & \text{for } E \leq V_s. \end{cases} \tag{4.1.11}$$

The V_s is corresponding to the inner potential of positronium in the LiF crystal, from the theoretical estimate of 3 eV binding energy of Ps inside the LiF (Dupasquier 1983) and the experimental observation of ~4 eV minimum energy of positronium emitted from a LiF(100) surface bombarded by the 0.1–4keV positrons (Tuomisaari and others 1989), the V_s is estimated to be 4 eV. Fig. 4.1.1 shows the comparison between the experimental results ("•") and the reflection coefficients (the solid line) predicted by Eq. (4.1.11) for the case of Ps incident angle $\theta_i = 50.4°$ with $R_o = 0.3$. The discrepancy is very visible for $E_{P_s} > V_s/\cos^2\theta_i$.

It is clear that there is more reflection or scattering than what can be accounted for by this simple real potential step. One of the factors was not accounted for in

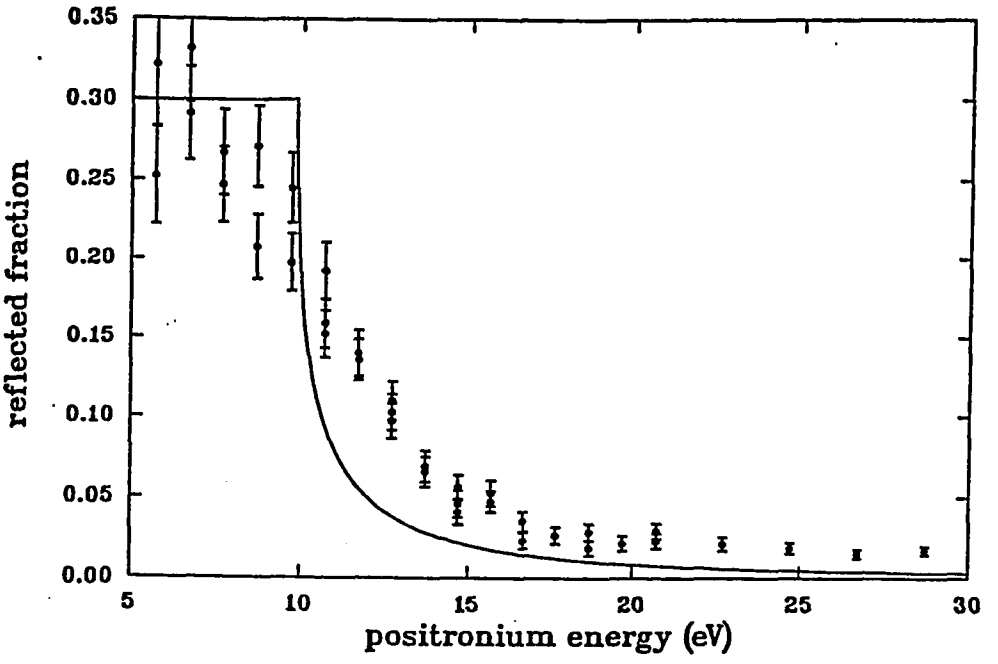

Figure 4.1.1 The comparison between the observed reflected fraction of positronium from a LiF(100) surface as a function of the Ps energy ("•") and that predicted by the Eq. (4.1.11) (solid line).

this model is the possibility of the positronium break up at the surface and in the bulk if positronium can penetrate into the bulk. An imaginary part of the potential which represents the loss of positronium was proposed (Weber and others 1988) as a possible factor which might contribute to the scattering as the unitarity prohibits the existence of inelastic scattering without the existence of the elastic scattering. A sharp reduction in the density probability would promote a large reflection of the incident wave.

If the V_s is a complex potential that can be expressed as:

$$V_s = V_r + iV_i, \tag{4.1.12}$$

then the wave function can be expressed similarly to Eq. (4.1.6) as:

$$\psi = \begin{cases} \exp(ik_o x) + r\exp(-ik_o x), & \text{for } x < 0; \\ t\exp(-K_{in}x + ik_{in}x), & \text{for } x > 0, \end{cases} \tag{4.1.13}$$

The wave vectors can be expressed similarly to Eq. (4.1.5) as:

$$\begin{aligned} k_o^2 &= \frac{2m}{\hbar^2}E, \\ k_{in}^2 - K_{in}^2 &= \frac{2m}{\hbar^2}(E - V_r), \\ 2k_{in}K_{in} &= -\frac{2m}{\hbar^2}V_i. \end{aligned} \tag{4.1.14}$$

When the V_i is positive, k_{in} and K_{in} have opposite signs, causing the amplitude of the wave decaying down along the propagation direction and representing the loss of positronium. When the V_i is negative, the amplitude increases along the propagation direction, representing the creation of positronium. For our case here, V_i always has to be positive. If the values of V_r and V_i are known, the values of k_{in} and K_{in} can be evaluated from Eq. (4.1.14) as:

$$\begin{aligned} k_{in}^2 &= \left(\frac{1}{2}\right)\left[\left(\frac{2m}{\hbar^2}\right)(E - V_r) + \sqrt{\left(\frac{2m}{\hbar^2}\right)^2 (E - V_r)^2 + \left(\frac{2m}{\hbar^2}V_i\right)^2}\right], \\ K_{in}^2 &= \left(\frac{1}{2}\right)\left[\left(\frac{2m}{\hbar^2}\right)(V_r - E) + \sqrt{\left(\frac{2m}{\hbar^2}\right)^2 (E - V_r)^2 + \left(\frac{2m}{\hbar^2}V_i\right)^2}\right]. \end{aligned} \tag{4.1.15}$$

Similarly, from the boundary condition at the $x = 0$, the reflection coefficient can be obtained as:

$$\begin{aligned} r &= \frac{k_o - k_{in} - iK_{in}}{k_o + k_{in} + iK_{in}}, \\ R = |r|^2 &= \frac{(k_o - k_{in})^2 + K_{in}^2}{(k_o + k_{in})^2 + K_{in}^2}. \end{aligned} \tag{4.1.16}$$

To understand how V_i affects the value of R, we consider the derivative of R with regard to V_i. Utilizing Eq. (4.1.16) and the following result of Eq. (4.1.15):

$$\frac{dk_{in}^2}{dV_i} = \frac{dK_{in}^2}{dV_i} > 0 \tag{4.1.17}$$

except it vanishes to zero at $V_i = 0$, we have that

$$\frac{dR}{dV_i} = 2k_o k_{in}^{-1} \left(\frac{dK_{in}^2}{dV_i}\right) \frac{3k_{in}^2 - k_o^2 - K_{in}^2}{[(k_o + k_{in})^2 + K_{in}^2]^2}. \tag{4.1.18}$$

Since both the factor in front of the expression and the denominator are positive, the sign of the derivative depends only on the numerator which also can be expressed as:

$$3k_{in}^2 - k_o^2 - K_{in}^2 = \sqrt{\left(\frac{2m}{\hbar^2}\right)^2 (E - V_r)^2 + \left(\frac{2m}{\hbar^2} V_i\right)^2} - \left(\frac{2m}{\hbar^2}\right)(2V_r - E). \tag{4.1.19}$$

From Eq. (4.1.19) it is clear that:

$$\begin{aligned} &\frac{dR}{dV_i} < 0 \quad \text{if } V_i^2 < V_r(3V_r - 2E); \\ &\frac{dR}{dV_i} = 0 \quad \text{if } V_i^2 = V_r(3V_r - 2E); \\ &\frac{dR}{dV_i} > 0 \quad \text{if } V_i^2 > V_r(3V_r - 2E). \end{aligned} \tag{4.1.20}$$

Eq. (4.1.20) indicates that for $V_r > 0$, when $E < (3/2)V_r$ the R decreases with the increase of V_i at small value of V_i then increases with the further increase of V_i; when $E \geq (3/2)V_r$, R always increases with the increase of V_i. When V_i approaches infinite, R always approaches unity.

Similarly to Eq. (4.1.11), a factor R_o is introduced when this model is used to fit the experimental data and Eq. (4.1.16) is expressed as

$$R = R_o \frac{(k_o - k_{in})^2 + K_{in}^2}{(k_o + k_{in})^2 + K_{in}^2}. \tag{4.1.21}$$

With Eqs. (4.1.14)&(4.1.21), we can expressed the wave vector inside the step as:

$$k_{in} = \left(\frac{1}{2}\right)\left[\rho\sqrt{\frac{2m}{\hbar^2}E} \pm \sqrt{\frac{2m}{\hbar^2}(E\rho^2 - 2V_r)}\right],$$
$$K_{in}^2 = \frac{2m}{\hbar^2}E\left[\frac{1}{2}\rho^2\left(1 \pm \sqrt{1 - \frac{2V_r}{E\rho^2}}\right) - 1 + \frac{V_r}{2E}\right], \tag{4.1.22}$$

where $\rho = (R_o + R)/(R_o - R)$. The two solutions are valid at different energy regions and merge at the point where $E\rho^2 = 2V_r$. For our experimental data, the applicable solution is the one with the plus sign. With Eq. (4.1.22), we can also calculate the corresponding mean free path

$$\lambda = (1/2K_{in}\cos\theta_i). \tag{4.1.23}$$

Fig. 4.1.2 (Weber and others 1988) shows the values of the mean free path calculated from the experimental values of R for $\theta_i = 50.4°$, $V_r = 4$ eV, and $R_o = 0.29$. The solid line in the figure is a two parameter linear fit to this result in energy region above the 15 eV. Fig. 4.1.3 (Weber and others 1988) shows both the reflected fraction calculated with this linear fit λ (solid line) and the experimental results ("•" and "o"). The reflected fraction predicted with only the real part of V_s is also included (dash line) in the figure.

This simple one dimensional potential step model seems to explain the experimental results. The existence of the imaginary potential is also qualitatively in agreement with our expectation that some of the incident positronium would be ionized at the surface and the incident positronium atoms can not penetrate very deeply into the bulk. The calculated mean free path, about 0.75 Å (< positronium diameter) above 20eV and approaching to zero when $E = E\cos^2\theta_i$ near the V_r, however, seems to be too short to be consistent with the recent positronium emission experimental result reported by other researchers (Tuomisaari and others 1989) and our measurements

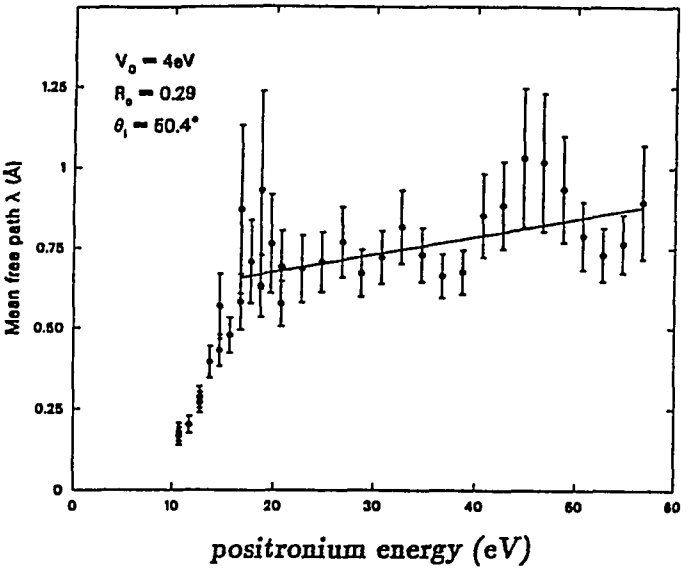

Figure 4.1.2 The positronium mean free path calculated from the experimental results with Eq. (4.1.22) and Eq. (4.1.23). The solid line is a least-square linear fit (Weber and others 1988).

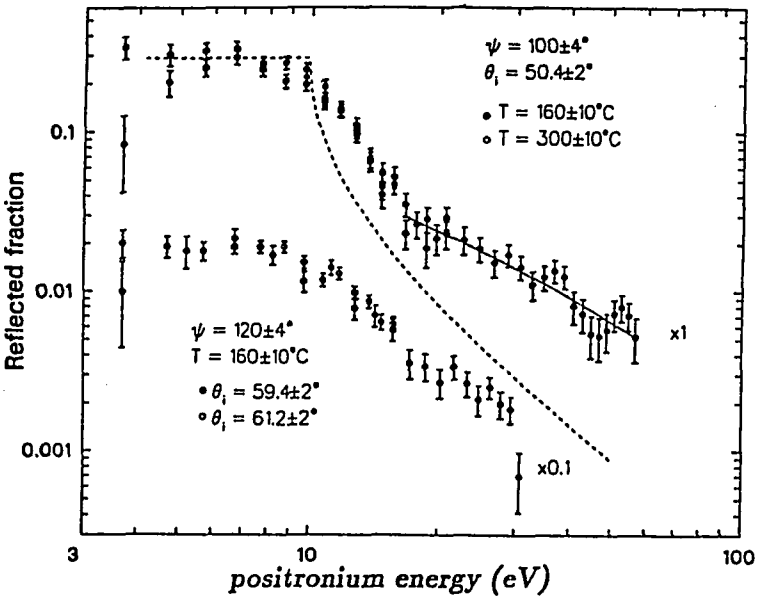

Figure 4.1.3 The comparison of the Ps reflected fractions measured by the experiments and calculated (solid line) by the values of linearly fitted λ from Fig. 4.1.2 (Weber and others 1988).

represented in Chapter 3 (also see discussion in later section). In both measurements, the results indicated strongly that, at least, a significant portion of positronium emitted was from the positronium formed in the bulk in the vicinity of the positron implant depth and diffused back to the surface. An appreciable amount of positronium was still emitted with the positron incident energy as high as 2keV which can penetrate at least a few hundred Å into the bulk (Tuomisaari and others 1989). These results were not in agreement with the extremely short mean free path predicted by this model. If the large absorption of positronium only takes place at the surface, then the step potential model which assume a uniform complex potential through out the bulk is not a proper representation of the interaction.

Another difficulty this simple model faces is the sudden change in slope in the calculated mean free path near 15 eV. The suggestion that a possible broad Bragg peak may explain this slope change is inconsistent with the model itself, because the first Bragg peak is expected to be at above 20 eV with assumption of $V_r = 4$ eV and the extremely short mean free path (~0.75 Å) makes even a very broad Bragg peak impossible to exist.

This model also can not predict the results at other incident angles. Since K_{in} calculated from the experimental results for $\theta_i = 50.4°$ only depends on the value of $E = E_{P_s} \cos^2 \theta_i$ and the value of K_{in} is independent of θ_i in this model, the experimental results for other θ_i should be predicted correctly from Eq. (4.1.16) with a proper adjustment of R_o to account for differences in the surface loss of Ps for different θ_i. In fact, the predicted reflection probabilities R_{θ_i} for other θ_i should satisfy the relation $R_{\theta_i}(E_{P_s}) = f_1 R_{50.4°}(f_2 E_{P_s})$ where f_1 is a constant factor to account for the difference in R_o and $f_2 = \cos^2 \theta_i / \cos^2 50.4°$ is a constant factor to account for the difference in projection angles. In a log-log scale plot such as Fig. 4.1.3, these two factors represent a constant shift in both x and y directions without changing

the shape of the curve. We, therefore, can compare the results for two different θ_i in Fig. 4.1.3 without further computation, if we shift the plot for the $\theta_i \approx 60°$ so that the point of $E_{P_s} = 16$ eV $(=V_r/\cos^2 60°)$ matches the point of $E_{P_s} = 9.84$ eV $(= V_r/\cos^2 50.4°)$ in the plot for $\theta_i = 50.4°$. From Fig. 4.1.3, it is clear that this simple shift can not match the two plots as the one for $\theta_i \approx 60°$ drops slower than the other in the region of $E_{P_s} > V_r/\cos^2\theta_i$.

There are several important factors that were completely ignored by this step potential model. They include the long range interaction between the ion cores in the solid and the incoming positronium atoms and the scattering process by the top layer ion cores. Because the separation between the two charges of a positronium atom is twice that of a hydrogen atom and the binding energy is, however, only one half the value for a hydrogen atom, a positronium atom is highly polarizable, which would result in a long range attractive force between a positronium atom and the ion cores in the solid. Since LiF is an ionic insulator, the first layer of ion cores is expected to be much more exposed in comparison with a metal surface where a large amount of conduction electrons is present at the surface. Therefore, there should be a noticeable effect from the positronium scattering off the first layer of ion cores.

Since the only experimental basis for the conclusion of the extremely short mean free path (< 0.75Å) and large imaginary potential (~23eV at 50 eV of positronium energy) is the discrepancy between the prediction of a real step potential and the experimental result, it can be argued that the other factors such as those mentioned above should be take into consideration before a large amount of the imaginary potential is introduced. In the next sections, a theoretical model which includes the other effects will be proposed, described, and discussed. With this model, the experimental results can be fairly closely predicted without introducing a large imaginary potential.

4.1.2 The reflection from a well-step potential — One of the important contributing factors that was ignored in the one dimensional step potential model discussed above is the long range interaction between incoming positronium atoms and the ion cores in the crystal. Since the positronium atoms are highly polarizable, this interaction is mainly the attractive van der Waals interaction for positronium some distance away from the surface. Only when positronium approaches to surface very closely and the wave function of electrons in a positronium atom begin to overlap with the wave function of the electrons in the ion cores, does the interaction become strongly repulsive. There have been a considerable number of research efforts, theoretically and experimentally, carried out to study the gas-surface interaction (see Hoinkes 1980 for a review) in gas atom-surface scattering and diffraction studies. Even though the parameters and the detailed shapes vary from one type of gas atoms to another, the atom-surface potentials for gas atoms interacting with various surface are found to be almost universally attractive and approximately proportional to the inverse powers of the distance. This attractive potential does not approach to negative infinity when atoms approach the surface, but is cut off by the repulsive interaction. A similar interaction was proposed for positronium at metal surfaces (Platzman and Tzoar 1985, 1986). Fig. 4.1.4 reproduced from (Platzman and Tzoar 1986) shows the effective potential for positronium interacting with a surface. Even though this potential was proposed mainly for the understanding of the surface trapped positrons at metal surfaces, it is reasonable to assume that this concept is applicable even to ionic insulator surfaces, but with a steeper repulsive edge due the highly localized charge density (in comparison with metal surfaces where the electron density has larger "smearing" effect). This assumption is consistent with the gas atom-surface studies in which relatively strong selective absorption effects have been observed on a large number of ionic crystal surfaces including LiF(100) surface (Hoinkes 1980, Meyers and Frankl 1975, Derry and others 1978). While the well depth may vary from one surface to

another, the width should be on the order of the diameter of positronium atoms ~1Å. Similar to the gas atom-surface interaction, it can be argued that this potential well is almost constant parallel to the surface because it is caused by the positronium atom interacting with a fairly large number of ion cores in the crystal (Hoinkes 1980). Therefore, it can be treated as an one dimensional problem.

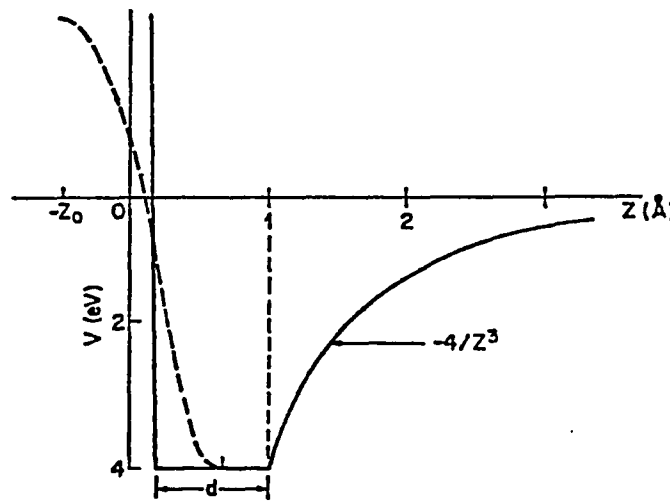

Figure 4.1.4 The effective potential for Ps interacting with a surface. The solid line is the parametrized model of the more accurate form of potential represented by the dash line (Platzman and Tzoar 1986).

Applying this concept to the case of the positronium specular reflection from a LiF surface, we hope that it would reflect the actual positronium interaction with the surface more accurately. As a first attempt, we replace the attractive potential well shown in Fig. 4.1.4 by a square well with two variable parameters, the well's depth V_w and width d, to simplify the computation. (If necessary, calculations with a more accurate potential can be carried out in the future.) The potential at the surface

along the normal direction then can be written as:

$$V(x) = \begin{cases} 0, & \text{if } x < -d; \\ -V_w, & \text{if } -d < x < 0; \\ V_s, & \text{if } x > 0. \end{cases} \tag{4.1.24}$$

Both V_w and V_s are positive and real. Using a plane wave function to represent the incident positronium atom, the wave function then can be expressed as:

$$\psi(x) = \begin{cases} \exp(ik_o x) + r\exp(-ik_o x), & \text{if } x < -d, \\ A\exp(ik_w x) + B\exp(-ik_w x), & \text{if } -d < x < 0, \\ C\exp(ik_{in} x), & \text{if } x > 0, \end{cases} \tag{4.1.25}$$

where the the wave vectors for each regions are given by:

$$\begin{aligned} k_o^2 &= \left(\frac{2m}{\hbar^2}\right) E, \\ k_w^2 &= \left(\frac{2m}{\hbar^2}\right)(E + V_w), \\ k_{in}^2 &= \left(\frac{2m}{\hbar^2}\right)(E - V_s), \end{aligned} \tag{4.1.26}$$

where $E = E_{P_s}\cos^2\theta_i > V_s$. Again, similar to the step potential case, the value of r, A, B,C can be solved from the continuity condition of ψ and $\partial\psi/\partial\psi$ at $x = -d$ and $x = 0$. They are give by:

$$\begin{aligned} A &= \frac{2k_o(k_w + k_{in})\exp(-ik_o d)}{(k_o + k_w)(k_w + k_{in})\exp(-ik_w d) + (k_o - k_w)(k_w - k_{in})\exp(ik_w d)}, \\ B &= \frac{2k_o(k_w - k_{in})\exp(-ik_o d)}{(k_o + k_w)(k_w + k_{in})\exp(-ik_w d) + (k_o - k_w)(k_w - k_{in})\exp(ik_w d)}, \\ C &= A + B, \end{aligned} \tag{4.1.27}$$

and

$$r\exp(i2k_o d) = \left[(k_o^2 - k_w^2)(k_w^2 + k_{in}^2) + (k_o^2 + k_w^2)(k_w^2 - k_{in}^2)\cos 2k_w d \right.$$
$$\left. + i2k_o k_w (k_w^2 - k_{in}^2)\sin 2k_w d\right]$$
$$\Big/ \left[(k_o^2 + k_w^2)(k_w^2 + k_{in}^2) + 4k_o k_w^2 k_{in} + (k_o^2 - k_w^2)(k_w^2 - k_{in}^2)\cos 2k_w d\right]. \tag{4.1.28}$$

From Eq. (4.1.28), we can calculate the reflection coefficient R as:

$$\begin{aligned} R =& |r|^2 = |r\exp(i2k_o d)|^2 \\ =& \Big\{ \left[(k_o^2 - k_w^2)(k_w^2 + k_{in}^2) + (k_o^2 + k_w^2)(k_w^2 - k_{in}^2)\cos 2k_w d\right]^2 \\ & + 4k_o^2 k_w^2 (k_w^2 - k_{in}^2)^2 \sin^2 2k_w d \Big\} \\ & \Big/ \left[(k_o^2 + k_w^2)(k_w^2 + k_{in}^2) + 4k_o k_w^2 k_{in} + (k_o^2 - k_w^2)(k_w^2 - k_{in}^2)\cos 2k_w d\right]^2 . \end{aligned} \tag{4.1.29}$$

From Eq. (4.1.29), we can see that R becomes one when $E = V_s$ and it reduce to Eq. (4.1.8) when $V_w = 0$ or $d = 0$. Since d should be on the order of the positronium diameter, we take it as 1 Å. V_w should be on the same order as the one proposed for a Al surface, 4 eV. Again, similar to Eq. (4.1.11), we have to add a factor R_o to account for for the reflection fraction being less than unity at very low energy region. Fig. 4.1.5 shows the results of Eq. (4.1.29) for $V_w = 4$ eV (—), 3 eV (- - -), 2 eV (···), 1.5 eV (— - —), and 1 eV (—·—) respectively with $\theta_i = 50.4°$, $V_s = 4$ eV, $d = 1$ Å, and $R_o = 0.3$. This result match the experimental results, in general, much better than the result of a real potential step shown in Fig. 4.1.1, but the reflected fractions predicted are still lower than the experimental results. Eq. (4.1.29) is not applicable to the case where $E < V_s$.

To extend the result of Eq. (4.1.29) to the region of $E < V_r$ and to include the effect of some positronium loss in the bulk, we generalize the formulation further to include complex potential $V_s = V_r + iV_i$ and a complex wave vector $k_{in} + iK_{in}$ in the

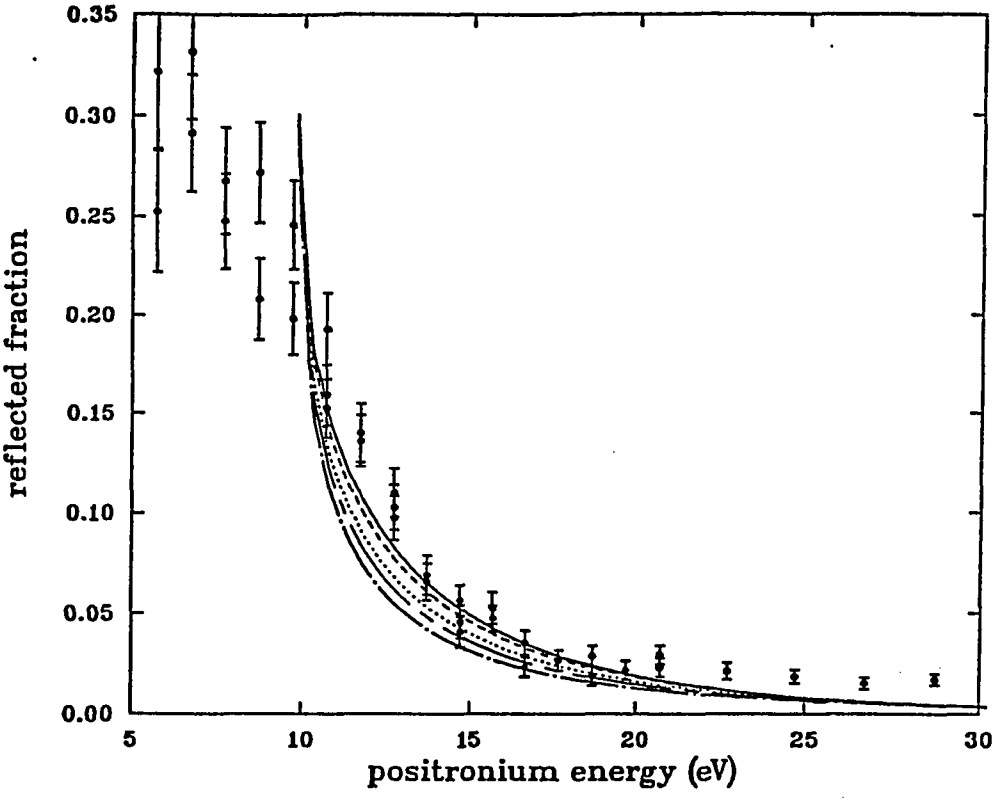

Figure 4.1.5 The calculated reflected fraction as a function of positronium energy by Eq. (4.1.28) for V_w = 4 eV(—), 3 eV(- - -), 2 eV(···), 1.5 eV(— - —), and 1 eV(—·—) respectively with $\theta_i = 50.4°$, V_s = 4 eV, d = 1 Å, and $R_o = 0.3$. The experimental results ("•") shown in Fig. 4.1.1 are also plotted for the comparison.

$x > 0$ region similar to the Eqs. (4.1.12)&(4.1.13). The k_{in} and K_{in} related to E and V_s by Eqs. (4.1.14)&(4.1.15) and while the wave function take the same form as given in Eq. (4.1.25) for $x < 0$ (outside the crystal), the wave function for $x > 0$ becomes:

$$\psi(x) = C\exp(-K_{in}x + ik_{in}x), \quad \text{for } x > 0. \tag{4.1.30}$$

The continuity at the boundaries yields the similar expression for A, B, C, and r

as in Eqs. (4.1.27)&(4.1.28) except replacing the k_{in} by $k_{in} + iK_{in}$. For reflection coefficient, it is given by:

$$\begin{aligned} r\exp(i2k_o d) = &\left[(k_o^2 - k_w^2)(k_w^2 + k_{in}^2 + K_{in}^2) + (k_o^2 + k_w^2)(k_w^2 - k_{in}^2 - K_{in}^2)\cos 2k_w d\right. \\ &\left. +2k_w K_{in}(k_o^2 + k_w^2)\sin 2k_w d\right] \\ &+ i\left[2k_o k_w(k_w^2 - k_{in}^2 - K_{in}^2)\sin 2k_w d - 4k_o k_w^2 K_{in}\cos 2k_w d\right] \\ &\Big/ \left[(k_o^2 + k_w^2)(k_w^2 + k_{in}^2 + K_{in}^2) + 4k_o k_w^2 k_{in}\right. \\ &\left. + (k_o^2 - k_w^2)(k_w^2 - k_{in}^2 - K_{in}^2)\cos 2k_w d + 2k_w K_{in}(k_o^2 - k_w^2)\sin 2k_w d\right], \end{aligned} \tag{4.1.31}$$

and

$$\begin{aligned} R = &|r|^2 = |r\exp(i2k_o d)|^2 \\ = &\Big\{\left[(k_o^2 - k_w^2)(k_w^2 + k_{in}^2 + K_{in}^2) + (k_o^2 + k_w^2)(k_w^2 - k_{in}^2 - K_{in}^2)\cos 2k_w d\right. \\ &\left. +2k_w K_{in}(k_o^2 + k_w^2)\sin 2k_w d\right]^2 \\ &+ 4k_o^2 k_w^2\left[(k_w^2 - k_{in}^2 - K_{in}^2)\sin 2k_w d - 2k_w K_{in}\cos 2k_w d\right]^2\Big\} \\ &\Big/ \left[(k_o^2 + k_w^2)(k_w^2 + k_{in}^2 + K_{in}^2) + 4k_o k_w^2 k_{in}\right. \\ &\left. + (k_o^2 - k_w^2)(k_w^2 - k_{in}^2 - K_{in}^2)\cos 2k_w d + 2k_w K_{in}(k_o^2 - k_w^2)\sin 2k_w d\right]^2. \end{aligned} \tag{4.1.32}$$

When $E < V_r$ and $V_i = 0$, it can be shown from Eq. (4.1.32) that R becomes unity or R_o if such a factor is introduced (similar to the cases before) to account for the non-unity reflection coefficient at the very low energy region, resulting in a flat at the energy region of $E < V_r$ (or $E_{P_z} < V_r/\cos^2\theta_i$). This does not agree with the experimental result. The discrepancy is likely due the finite probability of the ionization of positronium atoms in the solid especially when their kinetic energy exceeds the binding energy of positronium. To account for this effect, a small value

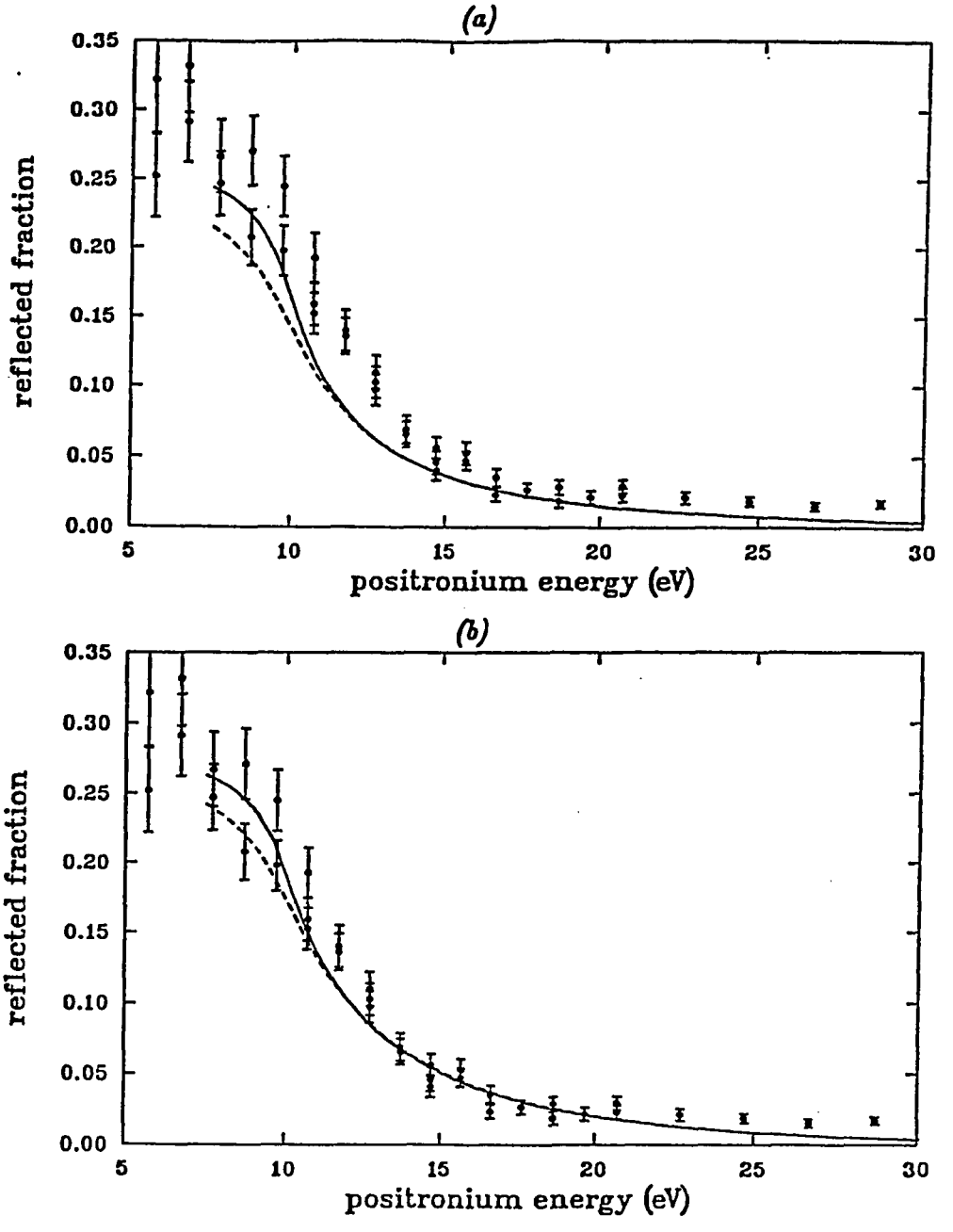

Figure 4.1.6 The calculated reflected fraction of positronium as a function of positronium energy for two different well depths: (a) 1.5 eV and (b) 4 eV and for two different values of imaginary potential: 0.3 eV (—) and 0.5 eV (---). $V_r = 4$ eV, $d = 1$ Å, $\theta_i = 50.4°$, and $R_o = 0.3$ for all calculated values. The corresponding experimental data ("•") are also shown for a comparison.

of the imaginary potential can introduced. In Fig. 4.1.6, the calculated reflected fractions are compared with the experimental results. The calculations included a factor R_0 of 0.3, the same factor used in the previous calculation, and were performed for two different well depths: (a) 1.5 eV and (b) 4 eV and for two different values of the imaginary potential in the crystal: 0.3 eV(—) and 0.5 eV(---). The other parameters are the same as the previous calculations. This addition of the imaginary potential of a small magnitude makes the calculated reflected fraction to reflect the general energy dependence of the experimental results much more closely than the previous calculation. Even though neither of the curve fit the experimental data exactly, the curves with smaller value, 0.3 eV, of imaginary potential seem to make a better match.

The introduction of the attractive potential well in addition to the potential step can predict the experimental results significantly more closely than the simple real potential step could, yet without introducing a very large imaginary potential. There is, however, still some visible difference between the calculated values of the reflected fractions and those measured by the experiments; the calculated values are smaller, in general, than those from the experiments. This difference is likely, as it was discussed in the previous section, due to the fact that our calculation did not reflect the scattering effect by the top layer ion cores of the crystal. In the next section, the effect of the top layer ion core scattering will be assessed. The attempt will be made to take this effect into our calculation.

4.1.3 The positronium scattering by ion cores — Both Li^+ and F^- ion cores have closed shell electronic structure but with one extra charge. It is, therefore, expected that the long range interaction between a positronium atom and an ion core would dominantly be the interaction between the positronium atom and this extra charge. Only when the positronium atom approaches the ion core fairly closely, within a

distance on the order of the ion core radius, the strong repulsive interaction due the wave functions overlapping of the electrons in the ion core and in the positronium would start to take a significant effect. The interaction between a charge and a positronium atom at a large distance is the attractive interaction between the charge and the induced dipole of the positronium atom by the electric field generated by this charge at the location of the positronium atom. For incident positronium atoms that do not have sufficient energy to penetrate the ion cores deeply, the scattering is mainly influenced by the attractive interaction. The repulsive interaction will, however, contribute to the scattering even in the low positronium energy range by cutting this attractive interaction off at the close distance. For positronium atoms with large kinetic energy which enables them to penetrate, at least, partially the ion core, additional effects from the repulsive interaction also have to be considered.

At the present time, the only available information on positronium atom or ion core scattering were those early theoretical efforts to estimate the positronium-helium (Fraser 1961b, Fraser and Kraidy 1966) and positronium-hydrogen scattering (Fraser 1961a, Hara and Fraser 1975, Drachman and Houston 1976) mainly at the positronium energy range below the positronium binding energy of 6.8 eV; there is no information on positronium ion core scattering available to us. Since our main interests are the positronium scattering in the positronium energy range of 5–50 eV, the results from the calculations mentioned above are off the range. The difference between ion cores and He or H atoms also make difficult to apply those results to our system directly even in the lower energy range. Those calculations of total scattering cross section, especially the ones for positronium-helium (which has a closed shell electron structure resembling that of a Li^+ ion core but without extra charge) scattering (with the result of $\sim 11\ \pi a_o^2$ at the positronium energy of 6.8 eV, see Fraser and Kraidy 1966), do strongly suggest, however, that the scattering effect from the ion cores should be too significant to be ignored.

To carried out our estimate of the positronium ion core scattering, several approximations have to be made. In the following calculation, only the long range attractive potential from the induced dipole term of a positronium is considered except that a factor of $[1 - \exp(-r^2/2r_o^2)]$ is also included to account for the vanishing of the attractive potential at very near distance due the short range repulsive interaction. To calculate the attractive potential between a charge and a positronium atom, the case of a positronium atom in a constant electric field is considered. Using the second order stationary perturbation theory, the energy of positronium in a electrical field E can be expressed as (Merzbacher 1970):

$$E_n = E_n^{(0)} + < n|e\mathbf{E}\cdot\mathbf{r}|n > + e^2 \sum_{k\neq n} \frac{< n|\mathbf{E}\cdot\mathbf{r}|k >< k|\mathbf{E}\cdot\mathbf{r}|n >}{E_n^{(0)} - E_k^{(0)}}. \qquad (4.1.33)$$

The $E_n^{(0)}$ is the energy level of a positronium atom in the vacuum. The second term vanishes for the ground state of positronium because the even parity of the S state. The third term is the second order term $E_n^{(2)}$ can be further reduce to:

$$E_n^{(2)} = e^2|\mathbf{E}|^2 \sum_{k\neq n} \frac{|z_{nk}|^2}{E_n^{(0)} - E_k^{(0)}}, \qquad (4.1.34)$$

where $z_{nk} = < n|z|k >$. Fortunately, this term has been evaluated before for the ground state of a hydrogen atom to be (Merzbacher 1970):

$$E_0^{(2)}(H) = -\frac{9}{4} a_o^3 |\mathbf{E}|^2, \qquad (4.1.35)$$

where a_o is the bohr radius. As discussed in Chapter 2, the positronium wave function is approximately same as that of a hydrogen with r scale by a factor of 2 (replacing a_o by $2a_o$ in the wave function of H) and energy level is half of that of hydrogen. For positronium, we can simply replace the a_o by $2a_o$ in Eq. (4.1.35) to get the corresponding energy correction for positronium ground state as:

$$E_0^{(2)}(Ps) = -18 a_o^3 |\mathbf{E}|^2. \qquad (4.1.36)$$

For a point charge, $\mathbf{E} = q/r^2$ and $q = \pm e$ for Li^+ and F^- respectively. If we consider this energy correction term is the scattering potential and add the term discussed above to account for the vanishing of the attractive potential at very small distance due to the short range repulsive interaction, we have:

$$V(\mathbf{r}) = V(r) = -\left[1 - \exp\left(-\frac{r^2}{2r_o^2}\right)\right] \frac{18a_o^3e^2}{r^4}, \tag{4.1.37}$$

where r_o is the parameter characterizing the cut off distance of the attractive potential and should be on the order of the ion core radius. Using the first order Born approximation (Merzbacher 1970):

$$\begin{aligned} f_{\mathbf{k}}(\mathbf{k}') &\approx -\frac{m}{2\pi\hbar^2}\int \exp(-i\mathbf{k}'\cdot\mathbf{r}')V(\mathbf{r}')\exp(i\mathbf{k}\cdot\mathbf{r}')d\tau' \\ &= -\frac{2m}{\hbar^2}\int_0^\infty \frac{\sin|\mathbf{k}-\mathbf{k}'|r'}{|\mathbf{k}-\mathbf{k}'|r'}V(r')r'^2dr', \end{aligned} \tag{4.1.38}$$

when $V(\mathbf{r}) = V(r)$, where $m = 2m_e$ is the mass of positronium (which is twice of that of an electron). If we put $V(r)$ of Eq. (4.1.37) into Eq. (4.1.38), we have:

$$\begin{aligned} f_{\mathbf{k}}(\mathbf{k}') &\approx \frac{36m\,e^2a_o^3}{\hbar^2}\int_0^\infty \frac{\sin|\mathbf{k}-\mathbf{k}'|r'}{|\mathbf{k}-\mathbf{k}'|r'^3}\left[1-\exp\left(-\frac{r'^2}{2r_o^2}\right)\right]dr', \\ &= 72a_o^2|\mathbf{k}-\mathbf{k}'|\int_0^\infty \frac{\sin z}{z^3}\left[1-\exp(-\alpha z^2)\right]dz, \end{aligned} \tag{4.1.39}$$

where $\alpha^{-1} = 2r_o^2|\mathbf{k}-\mathbf{k}'|^2$, $m = 2m_e$, and $a_o = \hbar^2/e^2m_e$ were used in the second step. Noticing that:

$$\begin{aligned} \int_0^\infty \frac{\sin z}{z^3}\left[1-\exp(-\alpha z^2)\right]dz &= \left(\frac{1}{2}\right)\int_{-\infty}^\infty \frac{\sin z}{z^3}\left[1-\exp(-\alpha z^2)\right]dz \\ &= \left(\frac{1}{2i}\right)\int_{-\infty}^\infty \frac{\exp(iz)}{z^3}\left[1-\exp(-\alpha z^2)\right]dz \\ &= \frac{\alpha\pi}{2}, \end{aligned} \tag{4.1.40}$$

where the residue theorem was used in the last step of derivation, and

$$|\mathbf{k} - \mathbf{k}'| = 2k \sin(\theta/2), \tag{4.1.41}$$

we have:

$$f(\theta) = \frac{9a_o^2\pi}{r_o^2 k \sin(\theta/2)} \tag{4.1.42}$$

and

$$\sigma(\theta) = |f(\theta)|^2 = \frac{81\pi^2 a_o^4}{r_o^4 k^2 \sin^2(\theta/2)}. \tag{4.1.43}$$

Here the θ is the scattering angle, the angle between $\mathbf{k}$ and $\mathbf{k}'$, and should not be confused with the θ_i used before and later.

With the result of Eq. (4.1.43), the effect of the top layer ion core scattering to the specular reflection can be estimated. Even though the ion cores are closely packed in the crystal, the comparisons made between the theoretical calculation and experimental results in the low energy electron diffraction (LEED) and low energy positron diffraction (LEPD) have proved that the taking the sum of all the scattering waves (including the multi-scattered waves) from each individual ion core with its proper phase factor added is a good approximation in predicting the experimental results (Pendry 1974, Horsky and others 1989a). We can also adapt this approach in our estimation. The relatively short mean free path and weak binding of positronium make the multi-scattering effect of positronium very insignificant so we can apply the kinematic approach in our estimation. That is simply to add all the scattered waves from all the top layer ion cores. Since all the scattered waves from the ion cores of the top layer in specular direction are in phase, forming the specular reflection peak, we can simply add the amplitudes of scattered waves from those ion cores within the coherence length l_c and add the intensity of scattered waves from those outside the coherence length. In two dimension case, all the amplitudes of the scattered waves

by those within the coherence area S_c (instead of the coherence length) will be added. Even though the Li^+ and F^- ions have opposite charges, the interaction between the those ions and positronium atoms is all attractive interaction as shown earlier. The cut off parameters are expected to be different from two different types of ion cores because of the different ion core sizes, but we can approximately use an "averaged" value for all the ion cores for our estimation. If the coherence area is not infinitely large, the specular reflection peak would have certain width corresponding to a solid angle $\Delta\Omega$. The total specular reflected fraction from the top layer ion cores then can be written as:

$$R_{ion} = S_c n_s^2 \sigma(\theta) \Delta\Omega, \tag{4.1.44}$$

where n_s is the number of ion cores per area. Since the magnitude of the angular width $\Delta\Omega$ of the specular peak is inverse proportional to the coherence area, it is can be shown* that:

$$\Delta\Omega = \frac{4\pi^2}{k^2 S_c} \tag{4.1.45}$$

under the condition that S_c is large enough so that $\Delta\Omega$ does not exceeds the actual detecting solid angle. The coherence length in each direction can be estimated by the following relation from Pendry (1974):

$$l_c = \frac{2\pi k^{-1}}{\left[2\sin^2\alpha\overline{\Delta\theta^2} + \cos^2\alpha\overline{(\Delta E/E)^2}\right]^{1/2}}, \tag{4.1.46}$$

where α is the angle between l_c and k, $\overline{\Delta\theta^2}$ is the mean square angular spread of the incident beam, and $\overline{(\Delta E)^2}$ is the mean square spread in energy. Using the parameters of our beam, we can estimate the coherence area in our experiments, which was indeed large enough (on the order of $2.5 \times 10^3\ k^{-2}$) to satisfy the condition for Eq. (4.1.45).

* See similar argument in Kittel 1976, p. 69.

Therefore, the specular reflected fraction by the top layer ion cores can be expressed as:

$$R_{ion} = \frac{4\pi^2}{k^2} n_s^2 \sigma(\theta). \tag{4.1.47}$$

It is easy to see that the scattering angle θ related to the specular incident angle θ_i by:

$$\theta = \pi - 2\theta_i. \tag{4.1.48}$$

Using Eqs. (4.1.43), (4.1.47)&(4.1.48), we can estimate the specularly reflected fraction contributed by the top layer ion cores. Fig. 4.1.7 shows the calculated top layer ion core contribution using above result for $\theta_i = 50.4°$ (—) and $\theta_i = 60°$ (---). A value of 3 Å (three times of the averaged ion core radii of Li^+ and F^-) was used for the parameter r_0. Fig. 4.1.8 shows the comparison of this result (—) for $\theta_i = 50.4°$ to the measured reflected fraction of positronium ("•"). The calculated ion core contribution deviates noticeably from the experimentally measured total reflected fraction at the energy range near $V_r/\cos^2\theta_i$ ($\sim$ 10 eV) and also has a higher value than the experimental result in the higher energy range. This can be explained by the fact that the effect of the surface potential, which is expected to be significant at the energy range near $V_r/\cos^2\theta_i$, was not included in the above comparison and the effect of the positronium loss at the surface was not included either. It is expected that predicted value should agree with experimental fairly well if all the effects are taken into the consideration.

4.1.4 The estimation of the total reflected fraction — In the previous sections, the effects of surface potential and ion core scattering have been estimated separately. To compare with the experimental results, both effects should be considered. The imperfection and the surface loss of positronium should be taken into the consideration as well, but these two factors are very difficult to estimated exactly. For our first attempt, a constant factor R_0 is used to account approximately these surface related

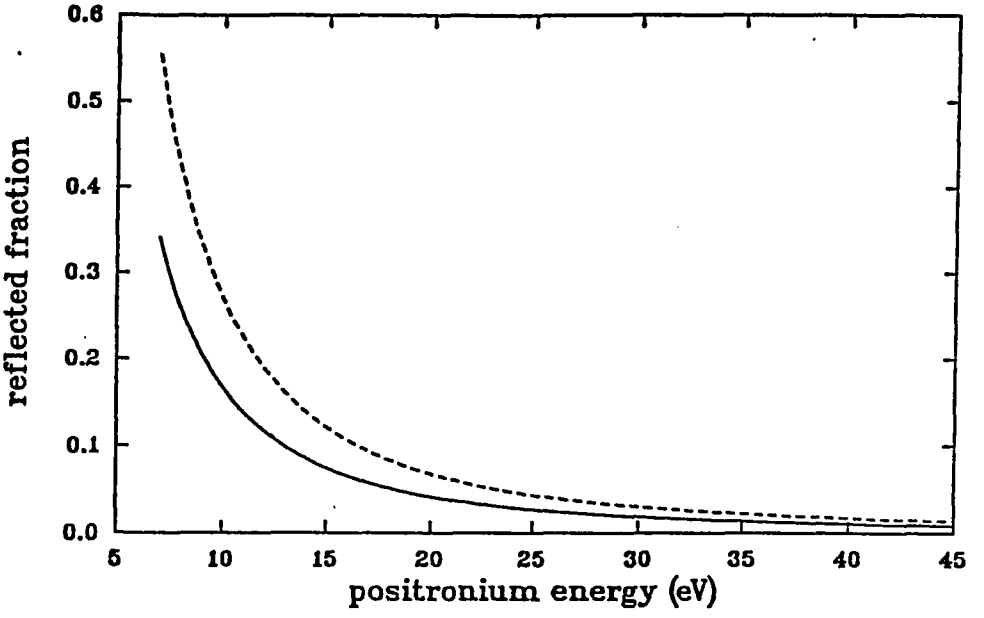

Figure 4.1.7 The calculated reflected fraction of positronium by the top layer of LiF(100) surface for $\theta_i = 50.4°$ (—) and $\theta_i = 60°$ (---). $r_0 = 3$Å is used in this calculation.

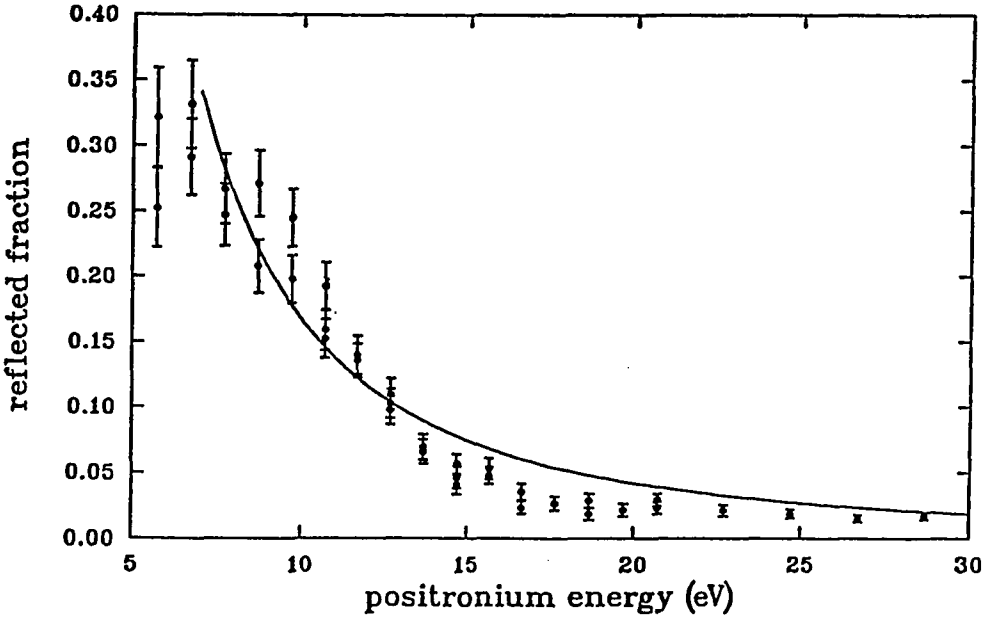

Figure 4.1.8 The comparison between the calculated result (—) shown in Fig. 4.1.7 and the experimentally measured total reflected fraction ("•") from LiF(100) surface at $\theta_i = 50.4°$.

effects. It is also assumed for the simplicity that it is independent of positronium energy and applies to the reflection by surface potential and top layer ion cores equally. With this assumption, the estimated reflected fraction can be expressed as*:

$$R_{total} = R_o \left(R_p + R_{ion} \right), \tag{4.1.49}$$

where R_p given by Eq. (4.1.32) is the reflection coefficient of the surface (well-step) potential and R_{ion} given by Eq. (4.1.47) is the contribution from the top layer ion cores. Fig. 4.1.9 (a) shows the comparison of the predicted values (—) by Eq. (4.1.49) with the experimental results ("•") for the positronium specular reflection from a LiF(100) surface at $\theta_i = 50.4°$. The calculation was carried out with $V_w = 1.5$ eV, $d = 1$ Å, $V_r = 4$ eV, $V_i = 0.3$ eV, $r_o = 3$ Å, and $R_o = 0.3$. Fig. 4.1.9 (b) shows the similar comparison for the specular reflection at $\theta_i = 60°$ with the exactly same set of parameters except that R_o used in this case is 0.1. The calculated values match the experimental results fairly well especially for $\theta_i = 50.4°$. In the calculation for the above comparison, the parameters used were not chosen to give a optimum point by point match, instead the emphasis was to reflect the general energy dependence consistently for both incident angles with minimum number of variables and without changing the parameters that suppose to be independent of the incident angle θ_i.

It should be pointed out this model is still a rather crude approximation, even though the efforts have been made to include most of the significant effects into it. Some of the assumptions used for the model are still over simplified and some of them may be only valid within certain ranges. The imaginary potential in the crystal, for example, may not be a constant for all the energies. The factor R_o used here may also vary with the energy of positronium because the reduction of specular reflection by imperfection of the surface, contamination of the surface, and ionization of positronium at the surface, all of which R_o represents, may depend on

* This is approximate estimation. The possible coherence interference between these two processes has to be taken into consideration in more accurate calculations in the future

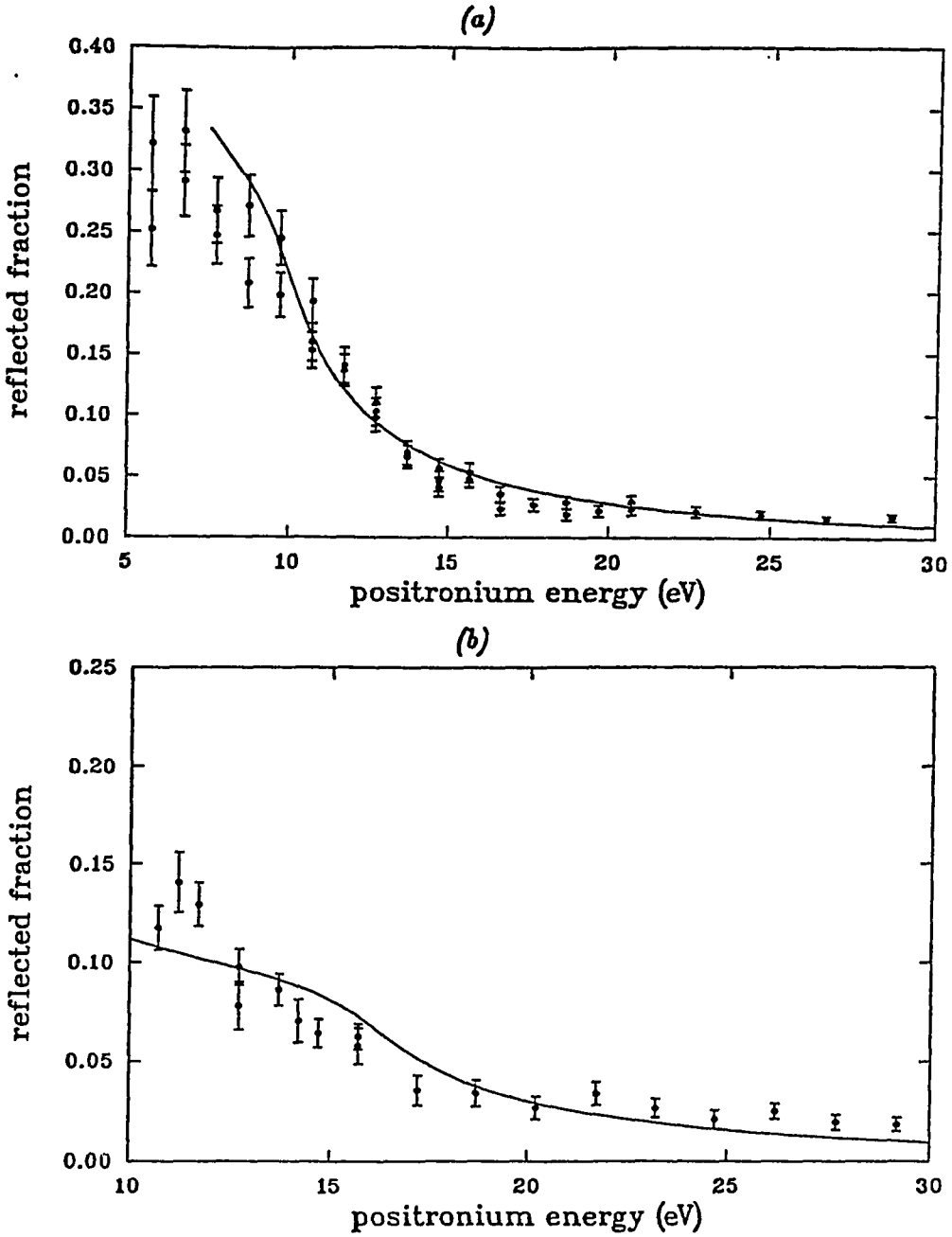

Figure 4.1.9 The estimated reflected fractions (—) by Eq. (4.1.49) for the Ps specular reflection from a LiF(100) surface at (a) $\theta_i = 50.4°$ and (b) $\theta_i = 60°$ with $V_w = 1.5$ eV, $d = 1$ Å, $V_r = 4$ eV, $V_i = 0.3$ eV and $r_o = 3$ Å. The factor R_o is taken to be 0.3 and 0.1 for (a) and (b) respectively. The experimental results ("•") are also shown for a comparison.

the positronium energy. It may also be over simplified to assume the same factor R_o for both the effect of surface potential reflection and top layer ion core scattering. It is not clear that how close a approximation it is to replace a rather complicated shaped potential well by a simple square well. The semi-classical estimate of the positronium-ion core scattering cross section, which is carried out without considering the other interaction channels when they energetically allowed, such as excitation and ionization (break up) of positronium, may affect the accuracy of the final prediction. The effect of the repulsive interaction may possibly be underestimated in this calculation too. With all these unknown factors present, it is not very surprising that there are some small difference between the calculated reflected fractions and those measured in the experiments. This model in general, however, does reflect the energy dependence of experimentally measured reflected fraction fairly closely.

It is expected that the positronium loss in the crystal at just above the threshold energy of Ps break up would be rather complicated and would not be represented well by a constant imaginary potential. This could explain the small difference between the experimentally measured results and predicted value in the energy range of just above the threshold energy for Ps break up (~6.8 eV) to $V_r/\cos^2\theta_i$. At higher energy range, the reduction effect (R_o) on ion cores scattering is also expected to be reduced considerably when the positronium energy increases. At even higher energy range, the effect from the second layer of ion cores may also have to be considered. All these factors may contribute to a slightly underestimated reflected fraction at the higher energy range for this model.

More experimental data are needed to further explore the validity of this model. More sophisticated approach may be adopted in the future to improve the accuracy of the model prediction. From the comparison and discussion in this and previous sections, it is, however, fairly clear that this model, by far, represents the available

experimental results most closely.

This model, if verified by future experiments, has several interesting implications. One of them is the possibility of the surface resonance experiment with a high resolution positronium beam. If there is a potential well at the surface, there should be at least one bound state existing. The observation of selective absorption in the specular reflection would be then possible with a high resolution positronium beam and a proper geometry arrangement. Similar observation has been made on LiF and other surfaces with a helium atoms beam (Meyers and Frankl 1975, Derry and others 1978, Hoinkes 1980). Another implication of this model is that there is significant positronium scattering effect from the top layer ion cores even at relatively high energy range, therefore, the future positronium surface diffraction experiments are very feasible and may be carried out in not so far future.

4.1.5 The intensity of the Ps reflection and its temperature dependence — The maximum intensity of the Ps specular reflection was observed to be far less than unity at even very low energy range and also seemed to be dependent of the positronium incident angle θ_i. Its variation at the different sample temperature was also observed. In this section, a discussion focusing on the possible cause and its implications will be given.

As shown in Chapter 3 and the previous section in this chapter, the reflected fraction does not approach to unity when the positronium energy is below minimum energy to penetrate the barrier potential and even at energies below the positronium break up threshold energy of 6.8 eV. A factor R_0 has to be used in all our modeling of the Ps reflection and this factor seemed to vary as the positronium incident angle changes. Several factors could possibly contribute to this loss. One of them is the imperfection of the surface condition. At low energy, a large portion of the Ps specular reflection is due to the surface potential. The local defects or dislocation of the ion

cores on the surface would make the surface potential deviated from its flatness or regularity, therefore, would cause the deviation from the specular reflection. The main contribution to the part of the specular reflection not related to the surface potential is the interference of all the wave functions of positronium scattered by the ion cores at the surface. Even though, all the scattered waves by ion cores on the surface in the specular direction would have the same phase shift, the deviation of the ion cores from their periodicity within the surface plane would broaden the specular peak thus decrease the peak intensity, and the deviation of the ion cores from their periodicity position in the direction normal to the surface would result in the the waves scattered by those ion cores out of the phase with rest of the scattered waves, thus reduce the specular reflection intensity.

Another possible cause of the reduction of the specular reflectivity is the contamination of the surface by additional foreign atoms or molecules. It can be a manifold effect. First, the physical presence of additional atoms or molecules on the surface can modify both the shape and intensity of the surface potential thus affect the specular reflectivity, the additional scattering by its presence can also reduce the coherence of the ion core scattering at the surface. The additional atoms or molecules may also form certain bounds with the ion cores on the surface, thus change the structure on the microscopic scale or induce the dislocation of the ion cores. This will then have a similar effect as the imperfection of the surface does, which we discussed earlier. The additional atoms or molecules may also provide additional inelastic scattering or absorption channels for the positronium, this could greatly reduce the positronium specular reflection. Because LiF is a highly hygroscopic crystal, the surface absorption of water can be a very important effect. In the helium surface diffraction experiments (Meyers and Frankl 1975), it was found that the LiF(100) surface that was cleaved in situ in an ultra high vacuum environment provided a higher specular reflection intensity of helium than those surface cleaved in the air then heated in the vacuum.

It was also found that those surface that was cleaved in situ and had high specular reflectivity would also suffer an intensity decrease with the time even in the low 10^{-9} torr range and had to be re-cleaved within two to three days to maintain the high reflectivity. Furthermore, it was found that the intensity of helium atom specular reflection dropped rapidly when water vapor was introduced as a test of the effect of the possible water layer on the crystal surface. Another observation made in helium surface diffraction and reflectivity studies was that long time heating of the crystal at 250° C resulted in a poorly cleaved surface and thus reduced the specular reflection considerably. Since the positronium specular reflection, especially in the lower energy range, is very similar to the helium specular reflection from a LiF(100) surface, some effects can be speculated. One of the speculation one can make is that the contamination, either the surface absorption of water or some other surface contamination, can be partially removed from the surface when the sample surface is heated, yet some of the surface contamination effects may be irreversible or can not be removed entirely. The similar effect caused by the impurity(especially water) accumulation on the surface for a period of time can take place on the in situ cleaved surfaces. If so, it would explain why the surface had to be cleaved again after two to three days to maintain the high intensity of helium specular reflection. Since our sample was cleaved in the air, this could be a part of the reason for low specular reflectivity. It is possible that the surface structure can be affected by the long term heating. If it is true, it would explain the observation in the helium scattering experiment. It would then contribute to the reduction of the Ps specular reflection intensity because our sample had always been heated when the measurements were taken.

Our observation of the temperature dependence of the Ps specular reflection, which was reported in Chapter 3, strongly suggested that the presence of some surface contamination, possibly water overlayer on the surface. Since our experiments usually require relatively long period time to obtain necessary data, some more ad-

ditional contamination can be accumulated to affect the specular reflectivity if the sample is not heated. This observation also suggested that the significant portion of surface contamination can be removed by the heating as we observed a considerable improvement when the sample temperature was gradually increased. Even though the temperature dependence measurement was only taken for the case that the sample was being gradually heated and the circumstance prevent us from testing the similar measurement with the sample being gradually cooled down, failure to observe any Ps specular reflection without heating the sample in the early stage of this research project even after the sample was heat-treated seems to suggest that similar behavior would be observed when sample is cooling down have we had opportunity to do so. The effect of the heating to the surface structure, however, could not be evaluated effectively from our observation. The increase of the specular reflection intensity observed when sample was heated could not completely rule out the possibility of the minor surface damage by heating that might take place because the increase of the intensity due to the elimination of surface contamination might overshadow the heating effect on the surface structure. It is hoped that such test can be performed on the vacuum cleaved LiF(100) surface in an ultra high vacuum environment so that Ps specular reflection may be observed at the room temperature with the intensity comparable to the one we measured when sample is heated. Then the heating effect on the surface would be easier to observed as the effect of removal of the surface contamination would be minimum.

The effect of the lattice vibration in our positronium specular reflection measurement is estimated to be very small and can not be the dominant reduction factor. This is can be easily seen from the evaluation of the Debye-Waller factor $\exp(-2w)$. This factor for atoms in the bulk of a simple crystal with only one atom per unit cell

can be express as (Pendry 1974):

$$\begin{aligned} I &= I_0 \exp(-2w) \\ &= I_0 \exp\left(-\frac{3|\mathbf{k}-\mathbf{k}'|^2 T}{M k_B \Theta_D^2}\right), \end{aligned} \tag{4.1.50}$$

where the M is the mass of the atom in the crystal, Θ_D is the Debye temperature, and k_B is the Boltzmann constant. The expression for the crystal with more than one atom per unit cell would be more complicated but similar in their temperature dependence. For the specular reflection, we know that:

$$\begin{aligned} \mathbf{k}'_{\parallel} &= \mathbf{k}_{\parallel}, \\ \mathbf{k}'_{\perp} &= -\mathbf{k}_{\perp}. \end{aligned} \tag{4.1.51}$$

The Eq. (4.1.50) then can be written as:

$$I = I_0 exp\left[-24\left(\frac{m_{P_s}}{M}\right)\left(\frac{E\cos^2\theta_i}{k_B\Theta_D}\right)\left(\frac{T}{\Theta_D}\right)\right], \tag{4.1.52}$$

where E is the positronium incidence energy and m_{P_s} is the mass of the positronium. Even though this formulation is for the crystal with one atom per cell, we can use it to estimate roughly the Debye-Waller effect in LiF crystal from it. LiF crystal has a relative high Debye temperature of 730 K (Ashcroft and Mermin 1976). If we take the mass of Li as the mass of atom in the crystal, we can approximately estimate the limit of the reduction factor (the reduction is expected to be less than this estimate as F has much larger mass which, according Eq. (4.1.52), would result in a smaller effect.). For positronium of 10 eV with $\theta_i = 50.4°$, the Debye-Waller effect would reduce the intensity to 81.4% of the original intensity when sample is heated at 350°C. The positronium energy with less incident energy would have a much smaller reduction effect. It is clear that the Debye-Waller effect can not be the dominant contributing factor to the reduction of the Ps specular reflection at the low energy range.

The surface condition of LiF(100) surface was also monitored by the LEED in the later stage of our experiment. It was noted that a fairly sharp LEED pattern was observed with the sample at the room temperature both before and after the sample was heated. This difference between the LEED observation and positronium measurements could be explained by the different energy ranges of the electron beam and the positronium beam. While most of our LEED observation was carried out at energy range of 30 eV to 120 eV, the positronium specular reflection had been observed at energy range below 30 eV. The difference between the LEED observation and positronium specular reflection measurements also suggested the high sensitivity of the positronium specular reflection to the surface condition. It also reinforces the argument given in the Chapter 1 that the positronium reflection and scattering from a surface would have similar high surface sensitivity as that of conventional atom surface scattering and diffraction.

There are also some possible causes for the reduction of Ps specular reflection intensity that would have effects only on the positronium measurements, yet could be the most dominant effects. Two examples of such possible causes are the positronium loss at the surface and possible contamination of our positronium beam by the positronium atoms formed in the excited states. It is known that the electric field at the surface of a crystal can be quite large, typically about $\sim$10 eV/Å, in the direction normal to the surface. Since it is comparable to the electric field in a positronium atom, which binds the positron and the electron together, the probability of the ionization of the positronium atoms in this field should be quite large*. This effect would have a bigger effect on the positronium atoms with lower velocity along the direction normal to the surface because it would take them longer time to pass the

* The ionisation probability per unit time for the case of hydrogen in an electric field, whose magnitude is much smaller than one in atomic unit, is given by Landau and Lifshits (1977). A similar result can be obtained for positronium with a proper scaling. This result is not directly applicable to this case where magnitude of the electric field is a fraction of one in atomic unit, but does suggest the ionisation probability could be a fraction of unity in this field.

field region than those of higher energies. It also would make the positronium atoms with larger θ_i to suffer more loss than those with smaller θ_i at the same positronium energy because the time that the positronium atoms take to pass the field region is inverse proportional to $\cos\theta_i$. This would explain the lower R_o for $\theta_i = 60°$ than that for $\theta_i = 50°$.

If a positronium atom travels with a velocity parallel to the surface thus normal to the electric field, it would also experience the motional magnetic field, which, if large enough, could cause the mixing of the $m = 0$ states of ortho-positronium and para-positronium. The mixing state would cause the transition of some ortho-positronium atoms to para-positronium atoms, a loss of the observable positronium because of the quick decay of para-positronium. The motional magnetic field $\mathbf{B}_m$ related to the electric field $\mathbf{E}$ experienced by incident positronium can be expressed as:

$$\begin{aligned} \mathbf{B}_m &= -\gamma \frac{\mathbf{v}}{c} \times \mathbf{E}, \\ |\mathbf{B}_m| &= \frac{\gamma v}{c} |\mathbf{E}| \sin\theta_i \end{aligned} \tag{4.1.53}$$

where $\gamma = 1/\sqrt{1-(v/c)^2}$ and c is the speed of light in the vacuum. At the first glance, it seems that this would be a very significant effect, because the $\mathbf{B}_m$ is about 1.136×10^4 gauss for the positronium atoms of 10 eV with incidence angle of 50°. However, because the narrow region where the field is effective, the transition probability is very small except when positronium atoms travel parallel to the surface in the field region. The width of this field region is only on the order of 1Å, the time needed for a positronium atom with energy greater than 1 eV to pass the field region would be less than 10^{-15} second, so we can estimate this effect without concerning the positronium decay. This also makes $\Delta E_1 t/\hbar$ to be much smaller than one (ΔE_1 is the fine structure energy splitting between the ortho- and para-positronium, see also the discussion in section 2.2.1). The transition probability then can be approximately

expressed as (Dirac 1958):

$$P = \left(\frac{g_e \mu_o l}{c\hbar}\right)^2 |\mathbf{E}|^2 \tan^2 \theta_i, \tag{4.1.54}$$

where g_e is the gyromagnetic ratio for electrons, μ_o is the Bohr magneton, and l is the width of the field region. It does not depend on the positronium energy. The term is negligible for the case where $l = 1$Å. It is not likely to be the significant effect for the loss of positronium at the surface. It could, however, play a role in the loss of positronium in the bulk of some crystals where a large electric field extends to a large region.

The possible contamination of the positronium beam by the positronium in 2S triplet states also could cause our measured reflected fraction lower than it should be. Since the positronium in 2S states can be ionized during the surface scattering much more likely than positronium in the ground state due to its larger size and smaller binding energy than those of positronium in the ground state, the reflected probability would be much smaller for the positronium atoms in the excited state. Yet their presence in the positronium beam would not reduce the measured the beam intensity which we used as the normalization factor to calculate the reflected fraction. Therefore, the presence of the positronium atoms in the excited state would reduced measured reflected fraction. It has been argued that the contamination of the positronium beam by the positronium atoms in the long life excited state is negligible because the high probability of break up and the large collision cross section with the gas atoms of those positronium atoms in the excited states would greatly reduce the percentage of the positronium atoms in the excited states in the positronium beam exiting the gas cell despite of their nonvanishing formation cross section. This argument, though is likely to be true, has never been tested in the experiments. It would be interesting to perform some quenching experiments to see if there is a significant portion of the positronium atoms in the long life excited state.

4.1.6 The possible positronium diffraction — The goal of this project was mainly to explore the feasibility of the low energy positronium diffraction (LEPSD). As the first step, our effort was centered on estimating the Ps-ion core scattering effect through measuring the reflected or scattered positronium atoms from surfaces. Encouraged by the relative large Ps specular reflection from a LiF(100) surface, we also attempted to detect diffraction peaks in our experiment with the same surface. The result is inconclusive.

The diffraction of positronium by a surface can be from either the interference scattering by the ion cores at the different lattice points on the same layer, or the interference scattering between the different layers of ion cores. A specular reflection can be the result of surface potential, or the constructive interference scattering of the ion cores within the same layer because the phase factors are the same for all waves scattered in the direction of a specular reflection ($\Delta \mathbf{k}_{\|} = 0$) by the ion cores within the same layer, or the combination of both. If the specular reflection is, at least, partially from the ion core scattering, it, then, may be possible to observe the specular reflection intensity peaked at the certain energies due to the constructive interference of the positronium atom scattered by different layers of ion cores (commonly called "Bragg peaks"), if both the mean free path of the positronium atoms in the sample and the coherence length of the positronium beam are large enough. For specular reflection measured from a LiF(100), the energies at which the reflected intensity is peaked can be expressed as (Kittel 1976 and Pendry 1974):

$$E_n = \frac{\frac{\hbar^2}{2m_{ps}}\left(\frac{n\pi}{d}\right)^2 + V_r}{\cos^2\theta_i} = \frac{4.652\, n^2\, eV + V_r}{\cos^2\theta_i} \tag{4.1.55}$$

where $d = 2.01\text{Å}$ is the nearest ionic distance of LiF and V_r is the real part of the

potential in the crystal defined similarly as in sections 4.1.1 and 4.1.2. In above calculation, the Li^+–F^- distance d is used as the lattice constant and the lattice is assumed to be a simple one atom per unit cell cube (the Li^+ and F^- ions are treated as same ion cores). The same result would be obtained, if we consider separately the diffraction effects from Li^+ and F^-, each of which are positioned in the fcc structure with a cubic lattice constant of $2d$, because the property of the structure factor of a fcc structure (Kittel 1976). Table 4.1.1 lists the first two calculated Ps Bragg peak energies for a LiF(100) surface with $V_r = 0$ and 4 eV at different incidence angle θ_i.

Table 4.1.1 The first two two calculated Bragg peak energies.

incidence	$V_r = 0$		$V_r = 4$ eV	
angle θ_i	E_1 (eV)	E_2 (eV)	E_1 (eV)	E_2 (eV)
50.4°	11.45	45.80	21.29	55.64
60.0°	18.61	74.43	34.60	90.43
70.0°	26.05	104.19	48.44	126.58

Only the Ps specular reflection measurement taken for $\theta_i = 50.4°$ has data points in the range covering the peak positions. The measurements taken for other θ_i all had energy range too limited to detect any Bragg peaks. The data for $\theta_i = 50.4°$ shown on Fig. 4.1.10 shows that the reflected fraction appears to have local maxima at the energies near the calculated Bragg peak energies for $V_r = 4$ eV, but these local maxima are very broad and are of small magnitudes. The intensity of these peaks is just above the lower limit of our measurement. Even though the relatively short coherence length of our positronium beam and the expected relatively short mean free path of positronium in the LiF crystal could explain the broadness of the Bragg diffraction peaks, more experimental data taken with higher beam intensity at a lower background environment are need to prove its presence conclusively. More measurements also needed to understand the maximum around 37 eV which has

similar characteristic as those near the Bragg diffraction energies yet can not be explained by the Bragg diffraction.

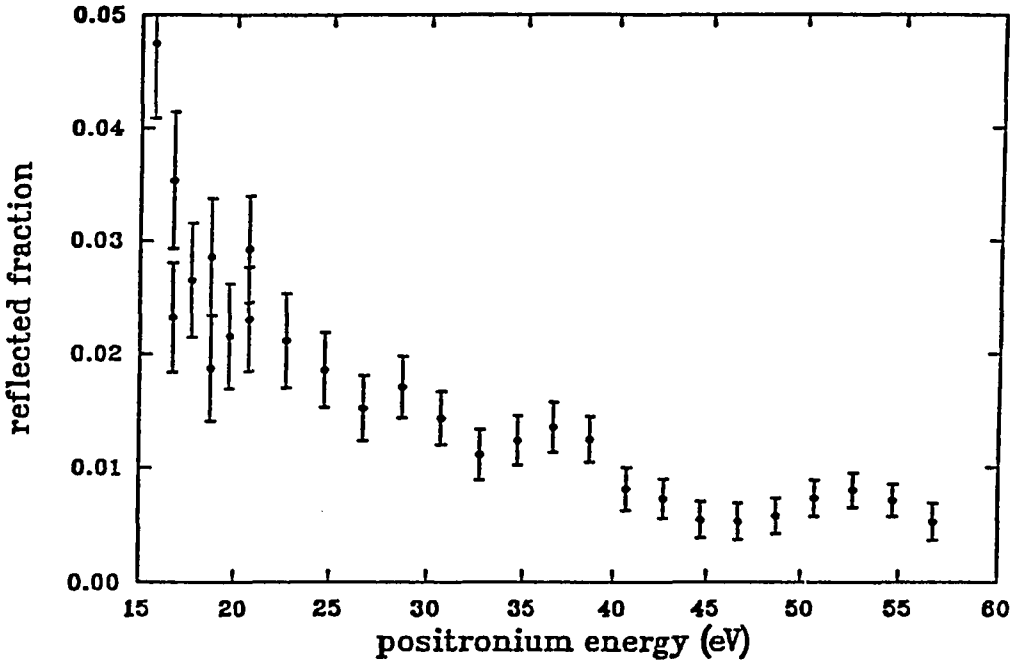

Figure 4.1.10 The reflected fraction of positronium from a LiF(100) as a function of the positronium energy taken at $\psi = 100°$ and $\theta_i = 50.4°$.

We also attempt to detect the diffraction structure by the constructive interference of the positronium atoms scattered by the ion cores on the top layer. The condition for such diffraction can be written as(Pendry 1974):

$$\Delta \mathbf{k}_{\parallel} = \mathbf{G}, \tag{4.1.56}$$

where

$$\mathbf{G} = m\left(\frac{\pi}{d}, 0\right) + n\left(0, \frac{\pi}{d}\right) \tag{4.1.57}$$

and m and n have to be both even or odd due to the structure factor. Because the design of our experimental set up, the detector angle ψ has to be at least 100°, and

incident beam, the normal of the surface, and the detected beam all have to be in the same plane. This makes the Eq. (4.1.56) to be:

$$\mathbf{k}'_{\parallel} = \mathbf{k}_{\parallel} + 2l\left(\frac{\pi}{d}, 0\right), \tag{4.1.58}$$

where l is any positive number. This experimental set up also makes such a measurement in our positronium beam energy range to be only taken with either a near glancing incidence and a detection near normal direction or a near normal incidence and a near glancing detection. Such geometry, plus relatively high energy (which resulted in a larger penetration depth of incident positronium and thus a higher positronium loss in the bulk) required by the diffraction, seems to make counts of detected positronium lower than the lower limit of our measurement, thus no information can be extracted from our experimental data. It is hoped that more measurements will be taken either with a positronium beam of higher intensity or will be taken in a very low background environment, or with a different detection geometry in not so far future.

§4.2 The Positronium Scattering From A Cu(100) Surface

To explore the feasibility of the low energy positronium beam as a new probe for metal surface studies, we performed the positronium scattering measurements on a single crystal Cu(100) surface. The main goal of this effort was to obtain some qualitative information on the positronium-ion core and the positronium-electron scattering at metal surfaces, thus to facilitate the future application of the low energy positronium atom beam to metal surface studies.

The results of the measurements were presented in Chapter 3. No high reflectivity of positronium like the one obtained from a LiF(100) surface at the lower positronium energy range was observed. The measurements of the angular scan runs did not show conclusively that there was specular reflection. The positronium scattering from the surface, however, was observed with noticeable intensity in a large energy

range up to about 80 eV. The positronium emission measurements we conducted with positrons of similar energy (more of which will be discussed in the next sections) clearly showed that the majority of those positronium atoms we detected can not be from the positronium formation by those positrons that were originally part of the incident positronium atoms and were liberated as the result of the positronium atoms' breaking up in the metal surface or near surface region, because of the efficiency of positronium emission from the same surface with the incident positrons of similar energy was much smaller than the scattered fraction we measured.

There is no available information on the positronium scattering by the ion cores. The ion cores in metals are much more complicated than those close shell ion cores such as Li^+ and F^- in ionic crystal which we discussed in previous sections and the positronium scattering cross sections by those ion cores are much more difficult to estimate. Therefore, we centered our effort on the understanding of the difference between the result from the positronium scattering measurements on a Cu(100) surface and the positronium specular reflection measurements on a LiF(100) surface instead of on the prediction of the experimental measurements with some simplified models as we did early for a LiF surface, and on the estimation of the scattering effect.

One of the main difference between an ionic single crystal like LiF and a single crystal metals is the conduction electron density. In an ionic crystal, the electrons are tightly bound to the ion cores to form the close shells and few conduction electrons exist without external excitation. In a metal crystal, the conduction electron density is fairly large on the order of 10^{23} cm^{-3}. Furthermore, for metals with a large population of *d* electrons, the effective electron density is even larger (resulting in a smaller r_s) due to the contribution from the *d* electrons (Isaacson 1975). This high electron density make the existence of positronium atoms in metals impossible, because the electron density is on the same order as that in a positronium atom and the positron

thus can not distinguish the electron that originally bound to it from those in the environment. This high electron density would also heavily influence the interaction of positronium with metal surfaces.

It is known that the electron density of a metal would not vanish at surface abruptly, instead, they would decrease approximately as an exponential decay with a decay factor typically on the order of 1 $Å^{-1}$ (Smith and others 1989). This extended electron density "outside" of metal surfaces would play an important role in the positronium interaction with metal surfaces. Several processes can take place when ortho-positronium atoms approaches the surface: (a) the binding energy of positronium will decrease as the positronium atoms get closer to the surface and eventually vanish if the positronium atoms penetrate into the surface because of the presence of the high electron density (also called "screen effect," and can also be understood as the increase of the dielectric constant to infinity). (b) the positronium-electron interaction will take place. It includes positronium-electron elastic scattering, positronium ionization during the positronium electron scattering, the positronium conversion, i.e. the ortho-positronium being converted to para-positronium as the result of the electron spin exchange between the electron in the positronium atom and the electrons nearby (also called "spin flip") during the positronium electron interaction, and the positronium atoms decay by "pick up" annihilation, i.e. the positron in the positronium atom annihilates with another electron in the environment instead of the one bound to it. (c) Some positronium atoms will be ionized in the strong electric field near the surface as discussed in the last section. (d) Those of a very few positronium atoms survive all above process would be able approaches the top layer ion cores fairly closely before most of them are dissociated by the screen effect in the bulk of the metal, or annihilated by the pick up annihilation or the conversion process in the bulk. A small fraction of those few positronium able to approach the top layer ion cores, however, is expected to be scattered by the ion cores towards the vacuum. (e)

The vanishing of positronium binding energy in the bulk of metals can be effectively expressed as a gradually increasing potential with a maximum value of the binding energy of positronium in the vacuum. This potential would reflect the incident positronium atoms.

Among the processes described above, a majority of them would cause either the loss of positronium energy or the loss of positronium atoms. The positronium electron interaction is a good example. The effect of the positron-electron scattering in the energy range below the inelastic scattering threshold (<5.1 eV) has been theoretically studied (Ward and others 1987). A fairly large total elastic scattering cross section was found in the study, about 200 πa_o^2 at 0.05 eV and 44 πa_o^2 at 4.1 eV. Because of the similarity between the electron mass and mass of positronium ($m_{P_s} \approx 2m_e$), large kinetic energy transfer during the electron-positronium scattering is possible. The same calculation found equally large momentum transfer cross section in the center of mass frame, about 220 πa_o^2 at 0.05 eV and 39 πa_o^2 at 4.1 eV. This process is thus a process of large energy loss on a metal surface where the electron density is relatively high. The positronium conversion cross section was also calculated in the same study and found to be significant, at least in the low energy range, about 12 πa_o^2 at 0.05 eV and 5.5 πa_o^2 at 4.1 eV. The conversion of ortho-positronium to para-positronium would result in the positronium's decaying through two photon decay and thus a much short life time for the positronium atoms, representing a loss of positronium atoms. The positronium ionization during the positronium-electron scattering has also been estimated (Peach 1989). The cross section was reported to increase gradually starting from the threshold energy of 6.8 eV to the maximum value of about 5.6 πa_o^2 at energy of 21.5 eV and to decrease very slowly at higher energies. This is another process which contributes to the loss of positronium atoms. The pick up annihilation process is also believed to be significant due the high electron density, a further reduction of incident positronium atoms. All of these loss processes

related to the positronium-electron scattering are much more significant at a copper surface than at the a LiF surface. The ionization of positronium atoms by the large electric field at the surface is also a very significant effect, which contributes to the loss of incident positronium. These loss processes would qualitatively explain why so few positronium were detected to be elastically scattered back to the vacuum by the copper surface. Only a very few positronium atoms would be able to survive all these loss processes to approach the top layer ion cores to be scattered back to the vacuum.

The heavy loss of positronium energy or positronium atoms can all be considered as the inelastic scattering of positronium atoms with a very large inelastic scattering cross section. This, however, would naturally raise a question that why the large inelastic scattering did not cause a significant elastic scattering that usually accompanies the large inelastic scattering as the result of the continuity requirement of wave function; furthermore, why the real part of potential (process (e)) in the copper did not produce a large reflection at the lower energy range as the one we observed from a LiF(100) surface at the lower energy range. The complexity of the surface electronic structure and lack of the exact and detailed information on positronium interaction with electrons and ion cores at a large energy range make it impossible to estimate the positronium reflection from metal surface. The arguments can be made, however, to explain qualitatively the difference in Ps reflectivity between a Cu(100) surface and a LiF(100) surface and to answer the above questions. The key factor to the low reflectivity is the high loss probability and gradual fall off of the surface potential. Since the real of part of the surface potential are mainly comes from the screen effect of the high electron density in the bulk, the extension of the electron density beyond the surface and its gradual fall off would result in the similar behavior of the real part of the surface potential. Similarly, because the majority of the inelastic scattering processes (including both the positronium loss process and positronium energy loss process) is the direct result of the electron density, it is expected that it would follow

the spatial change of the electron density at the surface. Thus we can approximately consider the change of the total surface potential to be similar to that of the electron density at the surface. It then would result in a low positronium reflectivity by the surface potential. This can be illustrated by expanding the treatment of Landau and Lifshitz (1977) of the reflection from a potential:

$$V(x) = \frac{V_0}{1 + \exp(-\alpha x)}, \tag{4.2.1}$$

where $x > 0$ represents the space outside the surface, $x < 0$ represents the space in the bulk, and V_0 is a constant complex potential expanded from the constant real potential of Landau and Lifshitz (1977) as:

$$V_0 = V_r + iV_i. \tag{4.2.2}$$

If we define wave vector k_0, $k = k_r + iK_i$ as:

$$\begin{aligned} k_0^2 &= \frac{2m}{\hbar^2}E \\ k^2 &= \frac{2m}{\hbar^2}(E - V_0), \end{aligned} \tag{4.2.3}$$

where m is the mass of positronium and $E = E_{Ps}\cos^2\theta_i$. From Eq. (4.2.3) we can express k_r and K_i in terms of E, V_r, and V_i as:

$$\begin{aligned} k_r^2 - K_i^2 &= \frac{2m}{\hbar^2}(E - V_r), \\ 2k_r K_i &= -\frac{2m}{\hbar^2}V_i, \end{aligned} \tag{4.2.4}$$

and solve it to be:

$$\begin{aligned} k_r^2 &= \left(\frac{1}{2}\right)\left[\left(\frac{2m}{\hbar^2}\right)(E - V_r) + \sqrt{\left(\frac{2m}{\hbar^2}\right)^2(E - V_r)^2 + \left(\frac{2m}{\hbar^2}V_i\right)^2}\right], \\ K_i^2 &= \left(\frac{1}{2}\right)\left[\left(\frac{2m}{\hbar^2}\right)(V_r - E) + \sqrt{\left(\frac{2m}{\hbar^2}\right)^2(E - V_r)^2 + \left(\frac{2m}{\hbar^2}V_i\right)^2}\right]. \end{aligned} \tag{4.2.5}$$

The one dimensional Schrödinger equation

$$\left(-\frac{\hbar^2}{2m}\frac{\partial^2}{\partial x^2}+V(x)\right)\psi(x)=E\psi(x). \tag{4.2.6}$$

can be solved by following the treatment of Landau and Lifshitz (1977). If we define a new variable as:

$$\xi=-\exp(-\alpha x), \tag{4.2.7}$$

and express wave function as:

$$\psi=\xi^{-ik/\alpha}\omega(\xi), \tag{4.2.8}$$

then the Schrödinger equation becomes:

$$\xi(1-\xi)\omega''+\left(1-\frac{i2k}{\alpha}\right)(1-\xi)\omega'+\left(\frac{k^2-k_o^2}{\alpha^2}\right)\omega=0, \tag{4.2.9}$$

which has the solution of the form of a hypergeometric function:

$$\omega=a\,F(i[k_o-k]/\alpha,-i[k_o+k]/\alpha,1-i2k/\alpha,\xi), \tag{4.2.10}$$

where a is a normalization constant. This solution has the asymptotic form as:

$$\psi\approx\begin{cases}a(-1)^{-ik/\alpha}[C_1\exp(ik_ox)+C_2\exp(-ik_ox)], & \text{when } x\to-\infty\ (\xi\to-\infty),\\ a\exp(ikx) & \text{when } x\to\ \infty\ (\xi\to 0),\end{cases} \tag{4.2.11}$$

where C_1 and C_2 are given in terms of complex variable Gamma function as:

$$\begin{aligned}C_1&=\frac{\Gamma(-i2k_o/\alpha)\,\Gamma(1-i2k/\alpha)}{\Gamma(-i(k_o+k)/\alpha)\,\Gamma(1-i(k_o+k)/\alpha)},\\ C_2&=\frac{\Gamma(i2k_o/\alpha)\,\Gamma(1-i2k/\alpha)}{\Gamma(i(k_o-k)/\alpha)\,\Gamma(1+i(k_o-k)/\alpha)}.\end{aligned} \tag{4.2.12}$$

If we put $k = k_r + iK_i$ into Eq. (4.2.12) we have:

$$C_1 = \frac{\Gamma(-i2k_o/\alpha)\,\Gamma((1+2K_i/\alpha) - i2k_r/\alpha)}{\Gamma(K_i/\alpha - i(k_o+k_r)/\alpha)\,\Gamma((1+K_i/\alpha) - i(k_o+k_r)/\alpha)},$$
$$C_2 = \frac{\Gamma(i2k_o/\alpha)\,\Gamma((1+2K_i/\alpha) - i2k_r/\alpha)}{\Gamma(K_r/\alpha + i(k_o-k_r)/\alpha)\,\Gamma((1+K_i/\alpha) + i(k_o-k_r)/\alpha)}. \tag{4.2.13}$$

From the asymptotic form of wave function at $x \to \infty$, we can calculate the reflection coefficient R to be:

$$R = \frac{|C_2|^2}{|C_1|^2}. \tag{4.2.14}$$

Using the properties of gamma functions of complex variable, we can further simplify the expression for R. For $V_i = 0$, if $E > V_r$ then $K_i = 0$, the R reduce to the expression given by Landau and Lifshitz (1977):

$$R = \left(\frac{\sinh[\pi(k_o - k_r)/\alpha]}{\sinh[\pi(k_o + k_r)/\alpha]}\right)^2; \tag{4.2.15}$$

if $E \leq V_r$, $k_r = 0$, then $R = 1$ because $\Gamma(z^*) = \Gamma^*(z)$. If V_i is not zero, then we can expressed R as:

$$R = \frac{K_i^2 + (k_o - k_r)^2}{K_i^2 + (k_o + k_r)^2} \frac{\left|\Gamma(1 + K_i/\alpha - i(k_o+k_r)/\alpha)\right|^4}{\left|\Gamma(1 + K_i/\alpha + i(k_o-k_r)/\alpha)\right|^4}. \tag{4.2.16}$$

We can use this result to illustrate the effect of the gradually decreasing surface potential.

Fig. 4.2.1 shows the reflection coefficients calculated from Eq. (4.2.16). The real part of the potential V_r was taken to be 6.8 eV, the positronium binding energy in the vacuum, as the binding energy in the metal was assume to be zero. The imaginary potential V_i was taken to be 10 eV. The solid line is the result if we assume the

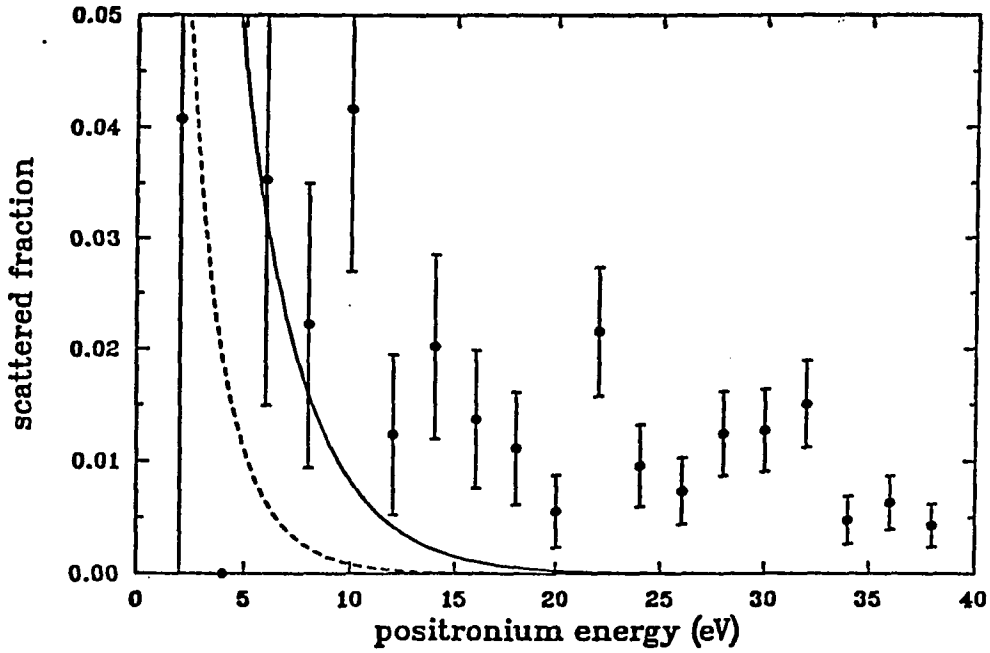

Figure 4.2.1 The reflection coefficients calculated from Eq. (4.2.16) with $V_r = 6.8$ eV and $V_i = 10$ eV. The solid line is the result for $\alpha = 1.5$ Å^{-1} and the dash line line is the result for $\alpha = 1$ Å^{-1}. The experimental result ("•") is also included as a reference.

decay factor $\alpha = 1.5$ Å^{-1} and the dash line is the result of $\alpha = 1.0$ Å^{-1}. Since α reflects how much the electron density is being extended to the vacuum at the metal surface, i.e. a large value of α represents a quick cut off of the electron density outside of the surface while a small value of α represents a slower decay of the electron density beyond the surface, we can see clearly from Fig. 4.2.1 that slower the electron density decays, smaller reflection it would result in. The experimental result was also included as a reference. The above calculation of the reflection by this relatively simple surface potential is intended only for illustration of the effect of the extended electron density and qualitative understanding of the reflection by the metal surface, it did not include the effect of positronium scattering by the top layer ion cores. Since

this effect is very difficult to estimate theoretically, we can not effectively estimate the total reflection from a metal surface theoretically. Therefore, no attempt has been made to use this model to predict our experimental results or to fit the result by changing the parameters. The parameters used in above calculation were either chosen to be consistent with the result of other research finding or selected just as a typical values for our illustration. The value of 6.8 eV for the real part of surface potential was chosen because of the difference in Ps binding energy; the value of 1.0 and 1.5 $Å^{-1}$ were used because they were on the same order of the result of some other theoretical treatment of Cu(100) surface(Smith and others 1989); the 10 eV was used for imaginary potential because the inelastic loss was expected to be rather large in the metal surface and a relative large value would be appropriate.

Even though we can not make accurate prediction. We can gain some insight from our experimental result with the help of above illustration. It is fairly clear from above illustration that we can reasonably assume that the majority of the detected positronium atoms were from the positronium atoms scattered by the top layer ion cores instead of by an effective surface potential, thus the intensity we measured reflected the magnitude of the positronium scattering from the top layer ion cores. This would be a very encouraging information for the future positronium diffraction experiments, because the scattered fraction we measured was on the order of a few percent to a few thousandths in a relative large energy range, suggesting strongly that the future positronium diffraction experiments are feasible. This assessment is consistent with our analysis for the positronium specular reflection from a LiF(100) surface presented in previous section. In the Ps specular reflection measurements we found that the reflection intensity was on the same order in the higher energy range where the effect of the surface potential became vanishing small, indicating similar Ps scattering magnitude by ion cores. Since the long range interaction of positronium with ion cores is expected to be weaker than the strong Coulomb interaction

experienced by the electrons and the short range interaction of positronium with ion cores (mainly due to the wave function overlap of the electrons in positronium atoms and those in the ion cores) is expected to be on the same order of that experienced by electrons, the scattering magnitude of positronium by the ion cores, therefore, is expected to be about the same or less than that of electrons. Our measurements seemed to be consistent with the early LEED study on a clean Cu(100) surface (Andersson 1969) in which a (00) beam (specular reflection) intensity of a few percent (at the low energy end of the measurement range) to a few thousandths (at large energy) was reported.

The lack of a strong specular reflection might be contributed by the "smearing effect" of the electrons at the surface. As discussed early, only a very few of incident positronium atoms would be able to approach the top layer ion cores closely to be scattered by them due to the heavy loss during the positronium-electron interaction at the surface. A fraction of those being scattered would be scattered towards the direction of vacuum. The intensity of scattered positronium by the ion cores at the surface is expected to be peaked at the specular direction due to the constructive interference of the scattered positronium. Since the scattered positronium atoms may suffer similar loss that all the positronium atoms experience during the incidence, the coherence of the top layer ion core scattering may be reduced and the interference peak may be smeared by this interaction, thus resulting in a very broaden peaks that we could not clearly identify with the positronium beam intensity available at the time. It is hoped that more measurements with higher intensity of positronium beam in a low background environment in the future may identify it more conclusively.

It was also found in the experiment that the measured scattered fraction of positronium in the specular direction at $\theta_i = 64.8°$ is noticeably less than that at $\theta_i = 50.4°$. More measurements are needed to understand this observation. It can

only be speculate at the present time that this may be due to the positronium ionization by the strong electric field at the surface region whose effect is stronger for those positronium with larger θ_i. Another possibility is the loss of interception of the positronium beam because of the relative large cross section of our positronium beam. Because a large surface area sample with a complicated shape was used, the factor of the positronium interception was not taken into the consideration. The large surface area may result in an imperfection of the sample surface preparation especially at the outer section of the sample surface and only a fraction of the surface area would effectively contribute to the positronium scattering. This would reduce scattered fraction at large θ_i. More experiments measurements, however, are needed to verify these two speculations.

Another interesting observation reported in Chapter 3 is the much lower scattered fraction of positronium which we measured from an un-treated polycrystal copper surface at room temperature. It is nearly one order lower than the one we measured from a treated (see Chapter 2 for the procedure) single crystal (100) surface at the same positronium incidence energy. The lower scattered fraction of positronium could be caused by the impurity at the surface, defects on the surface, or the lack of constructive interference of positronium scattering by the top layer ion cores due to the nature of polycrystal. Since our data are limited at the present time, we can not determine which one or which combination of above factors contribute most to the difference in measured scattered fraction of positronium from two different copper surfaces, but we do can conclude that the positronium scattering from a metal surface is quite sensitive to the surface condition, thus may be a potential surface study tool for characterizing the surface condition of the metal surfaces. More experimental tests are needed for a complete understanding of this effect and for future applications to the surface studies.

§4.3 The Positronium Emission From Surfaces

The positronium emission measurements reported in Chapter 3 not only helped us to understand our positronium reflection and scattering experimental results, but also provided us some new insights into the positron interaction and positronium formation mechanism in bulks and at surfaces of solid state. These will be discussed in this section.

4.3.1 The positronium emission from a LiF(100) surface — Being one of ionic crystals, LiF does not have the high conduction electron density as metal crystals do. The positronium formation in LiF, therefore, is mainly either by the positrons' capturing electrons liberated during the incident positron energy loss process ("spur" model) or the direct capture of valence electrons by positrons ("Ore" model). The threshold positron incidence energy E_{th} for the positronium formation by the Ore process can be expressed as:

$$E_{th} = E_g - E_B, \tag{4.3.1}$$

where E_g is band gap energy of LiF which is about 14.2 eV and the E_B is the binding energy of positronium. For those positrons whose energies are above the E_{th} but below the band gap energy, the only large energy loss process is the positronium formation. Therefore, it is expected that positronium formation through direct capture of valence electrons would be maximum at this region ("Ore gap"). If the positron incident energy below the threshold energy given above, the only energy loss channel is the phonon emission. Thus the positrons with energy below E_{th} would be able to maintain energetic (having energy higher than thermal energy) for a fairly long period of time and no positronium can be formed unless there are conduction electrons available from other excitation process. For positrons with incidence energy larger than the band gap energy would quickly lose their energy through excitation of electron-hole pairs until their energy below the E_g. Those whose residual energy fall into the "Ore gap" would

have finite probability to form positronium. If positron incidence energy is much higher than the band gap energy, relatively large population of electron-hole pairs can be created by the incident positrons. Those liberated electrons can be captured by the positrons diffusing back to the surface to formed positronium. The positronium atoms formed through this ("spur") process would have larger positronium energy than that of those positronium atoms formed in "Ore gap." Because the binding energy of positronium in crystal is smaller than that in vacuum, there is a narrow transition region at the surface positronium binding energy changes between two limits. Thus the "Ore gap" is expected wider near surface than that in the bulk. This wider region makes possible for those energetic positrons whose energies are below the E_{th} in the bulk to form positronium near the surface. Because of larger diffusion length of those energetic positrons (due to their non-thermal energy), they can, as suggested by Lynn and Neilson (1987) contribute significantly to the positronium formation through this process. The energy of positronium formed by these non-thermal positrons (with energy below the E_{th} in bulk) near surface through Ore process would be lower than that of positronium formed in bulk through "Ore" process or "spur" process.

While the total positronium emission from a surface bombarded by positrons is clearly contributed by all the process discussed above (if energetic allowed). The proportion of each contribution is less clear. The recent study of the positronium emission from alkali halides (Tuomisaari and others 1989) suggested that the dominant positronium formation process is through direct valence electron captures ("Ore" process) for almost all alkali halide crystals they studied with the exception of LiF, from which emitted positronium energy spectra seemed to contain the components both from "Ore" process and "spur" process. This study also suggested, with their experimental observation that the energy distribution of emitted positronium became narrower when the positron incidence energy was increased, that a significant portion of the positronium emitted from alkali halide surfaces is formed in the bulk through

direct valence electrons captures then diffuse to the surface. They also estimated the angular distribution of emitted positronium by measuring the emission at the several detection angles and conclude that the angular distribution of emitted positronium is strongly peaked at the direction normal to the surface with the exception of LiF which seemed to be near isotropic (following $\cos\theta$ distribution).

Our measurements taken at the time when above information was not available seem to be consistent with their report. Fig. 4.3.1 shows the comparison between our experimental result ("•") for positron incidence energy of 150 eV and calculated intensity(—) of positronium emission using the assumption that the positronium was emitted near isotropically proportional to $\cos\theta$ (θ is the emission angle) with the change of interception of the positron beam at the different incident angle θ_i taking into consideration (similar to the discussion on the interception of the positronium beam given in section 3.1, the interception of the positron beam also follows similar relation of Eq. (3.1.1) with different θ_B). The calculated intensity is normalized to the maximum value of the experimental results. The calculated values seemed to fit the experimental values except in very smaller sample angle range. This deviation may come from that the emission is not perfect isotropic. The near isotropic emission seems to suggest a large portion of the positronium detected at this positron energy is formed by the positrons with non-thermal energy near the surface, because the ones formed through bulk "Ore" process would be emitted with energy about the same as positronium work function and with an angular distribution strongly peaked at the direction normal to the surface. The small deviation also suggested that there was probably also a small portion of the emitted positronium was formed in the bulk with "Ore" process and diffused to the surface.

In our experimental measurement of Ps emission as a function of positron energy, we failed to observed the drop of the positronium emission fraction expected when the

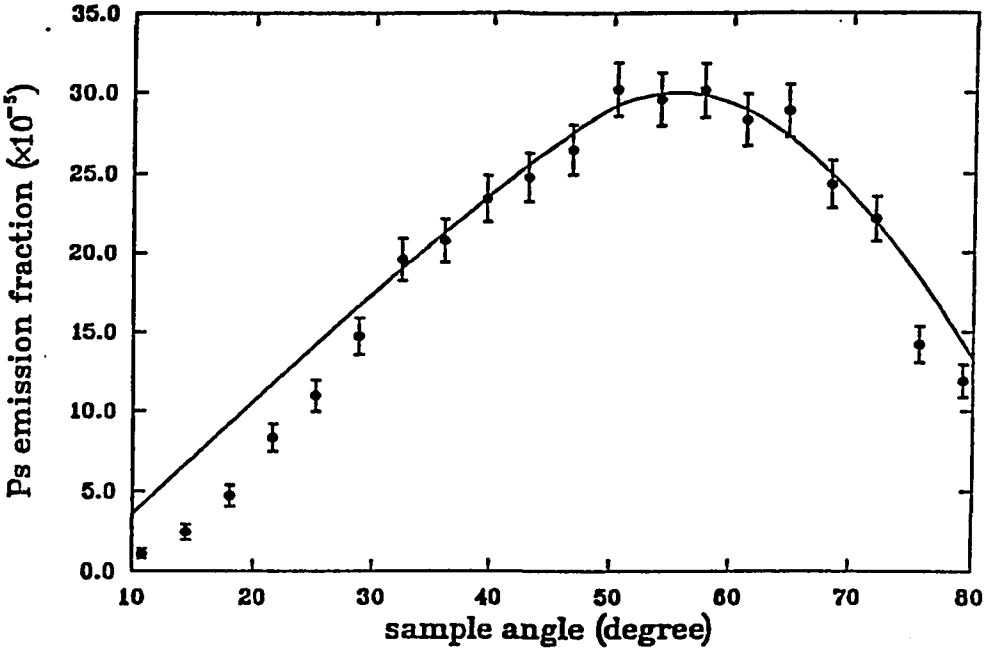

Figure 4.3.1 The angular dependence of the positronium emission from a LiF(100) surface with the positron incidence energy of 150 eV. The calculated values (in solid line) assuming Ps emitted proportional to $\cos\theta$ (θ is the emission angle) are compared with the experimental values ("•"). The calculated values are normalized to the peak value of experimental results.

positron energy became greater than the band gap energy, opening another energy loss channel, instead, the positronium emission fraction increased as the positron incidence energy increased within our measurements range. We were not able to extend our measurement of the positron energy dependence of the positronium emission to a larger energy range due to the external non-physics constraint. The emitted fraction of positronium was measured with our detector about 15 cm away and the decay on flight path was not compensated because we were unable to determine the positronium energy due to the lack of the necessary instrumental set up. The emitted fraction would appear higher for those positronium with higher energy because they suffered

less loss on the flight path. It is not clear if this would contribute to our failure to observed the drop of emitted Ps intensity at the energy around band gap energy. We did observe the positronium formation threshold effect, i.e. we did not observe any emitted positronium atoms until the positron incidence energy reached about 9 eV. This threshold value was between the threshold energy of 11.2 eV calculated with the theoretically predicted binding energy of 3 eV in LiF and the threshold energy of 7.4 eV calculated with the Ps binding energy of 6.8 eV in vacuum. It could be an indication that the positronium emitted at the very low energy range was formed at the near surface region. More experiments are desirable for further understanding the positronium formation process. It is hoped that more measurements in a larger energy range may be performed in the future if the condition permits.

4.3.2 The positronium emission from a Cu(100) surface — The original motivation of our measurements of the positronium emission from a Cu(100) surface was to see quantitatively the effect of the positronium emission from a copper surface and thus to estimate the possible contribution of the positronium formation by the positrons that were ionized from the incident positronium atoms at a Cu(100) surface to the scattered fraction of positronium we measured in our observation of the positronium scattering by a Cu(100) surface. Our measurements which were reported in Chapter 3 not only provided us this information but also provided some additional information on the characteristics of the positronium formation with low energy positrons' incidence, which may be helpful to the future construction of high efficiency mono-energetic positronium beam in a relatively large energy range and other applications of the positronium formation by low energy positrons' incidence to surface studies.

The positronium emission fraction we measured is on the order of one thousandth or less. This fraction also includes the factor of decay on the flight path from the

sample surface to the detector which is about 15 cm. The survival fraction would be from 8% for positronium of 1 eV to 63% for positronium of 30 eV. Since we could not measure the energy of the emitted positronium we detected due to the lack of proper instrumentation, we did not attempt to compensate for the positronium decay on the flight path in the presentation of our measurements in Chapter 3. The above survival fraction together with the emission fraction we measured in the positron energy range of zero to 30 eV, however, can help us to estimate the limit of possible contribution of the positronium formation at the Cu(100) by positrons liberated from incident positronium atoms due to the positronium break up. We can easily conclude from our measurements that the contribution of the positronium formation by the positrons from the break up of the incident positronium can not be the dominant contribution to the scattered fraction of positronium we measured, which is on the order of a few thousandths to a few percent. Therefore, we concluded in the previous section that the scattered fraction of positronium we measured must be from the scattering of positronium by the Cu(100) surface, most likely by the top layer ion cores at the Cu(100) surface.

Our initial measurement designed to the give the information discussed above also showed some interesting feature that motivate us to pursue a little further. The measurement of the positron energy dependence of the positronium emission over a relative large energy range (See Fig. 3.4.4) showed that the emission fraction we measured reached its maximum at about 30 eV for our experimental geometry and decreased to its half maximum at the positron incidence energy of 150 eV. This was a strong indication that the positronium atoms emitted were not formed by the positrons that were thermalized in the copper and diffused to the surface (as we discussed in the section 2.2.2), because it was known that the energy dependence of the positronium emission by those thermalized positrons diffusing back to the surface follow a different pattern. If f_o is the branching ratio for emitted Ps, i.e. the relative

fraction of those positrons at the surface that form the positronium, the positronium emission from the thermalized positrons diffusing back to the surface can be express as (Mills 1979, Schultz and Lynn 1988):

$$f = \frac{f_0}{1 + E/E_0}, \tag{4.3.2}$$

and E_0 is on the order of a few keV. It is, therefore, very unlikely that the emitted positronium atoms we detected were dominantly formed by the thermal positrons. This conclusion was consistent with the earlier time of flight measurement of the positronium emission from a Cu(100) surface (Howell and others 1986), in which the positronium energy spectra were taken for positrons with incidence energies of 50, 150, 250 eV, and up to 2000 eV. A higher energy component was observed in the emitted positronium energy spectra, most prominently at 50 eV positron incidence energy, the lowest positron incidence energy in that experiment.

To obtain some qualitative information on the contribution to the measured positronium emission by both the thermal positrons and non-thermal positrons, we were searching for a way to eliminate, or at least reduce, the contribution from one type formation so the respective contributions could be estimate by analyzing the difference in total positronium emissions we measured. We adapted the approach of introducing surface defects by Ar ion bombardment. The earlier time of flight measurement of the positronium (Howell and others 1986) reported a sharp reduction of the positronium emission from a Cu(100) surface by the thermal positrons after the surface treated with an ion bombardment. Even though no detailed information was given in that report, we expected at the time that the ion bombardment would introduce some surface defects that would partially trap the thermal positrons and those very low energy non-thermal positrons, while have little effect on those elastically or nearly elastically back-scattered positrons. A fairly detailed observation on the effect of Ar ion bombardment on a Al(110) surface to the positronium emission

by the thermal positrons diffusing back to the surface was reported (Vehanen and others 1985). In this study, a significant reduction of the positronium formation by the thermal positrons was found even with the bombardment of relatively low energy Ar ion of 400 eV. We believed that the ion bombardment would have similar effect on a Cu(100) surface. The comparison was made by measuring the positronium emission from a cleaned Cu(100) surface (see section 2.4 for the cleaning procedure) with or without additional bombardment of 500 eV Ar ions with similar intensity as in the Al surface study. The results of these measurements were reported in Chapter 3 Figs. 3.4.3&3.4.5.

As discussed before, our experimental set up limited the frequent changes of the detector position, so we measured the emission fraction as a function of the sample angle θ_i with fixed detector position ψ (emission angle would vary with θ_i as $\psi - \theta_i$). Though it is not the direct angular distribution of the positronium emission, what we measured reflected the general angular distribution of the positronium emission, especially the angular spread width. The measurement taken on the annealed (no additional ion bombardment) Cu(100) surface (Fig 3.4.3(a)) showed a narrower angular spread than the measurements we took from a LiF(100) surface (Fig 3.4.1(a)) where we believed that the emission was nearly isotropic. The measurement taken after the ion bombardment seemed to have even narrower angular spread. If we compare the measurements from the annealed Cu(100) surface (Fig. 3.4.3(a)) and from the LiF(100) surface (Fig 3.4.1(a)), we may suggest there were two components: one similarly shaped as the measurement from the LiF(100) surface that was nearly isotropic, and the other that was peaked at the certain sample angle with fairly narrow angular spread, but the evidence was rather ambiguous. The measurement taken from the Cu(100) surface after the additional ion bombardment, however, seemed to support this hypothesis more strongly as the feature of two component became more evident than the measurement from the annealed Cu(100) surface. It seemed more

accurate to say that the isotropic component was reduced in its relative intensity to the other narrower component resulting in a ostensibly smaller FWHM value. Since the positronium formed by the thermal positrons or the very low energy non-thermal (also called "epithermal") positrons is expected to be emitted with rather large angular spread, while the positronium formed by the positrons elastically back-scattered by the crystal is expected to be emitted with a narrower angular spread related to the Fermi energy level, the above comparison seemed to confirm our original speculation that the dominant contribution to the positronium emission we detected was not from the positronium formation by thermal positrons. The observation that the intensity of the main peak in our angular scan measurement was not reduced by the ion bombardment, but the relative intensity of the isotropic component seemed to be reduced by the ion bombardment, (a result, likely, of reduction of the positronium emission by the thermal and epithermal positrons due the surface defect trapping induced by the ion bombardment) was consistent with this speculation as well. The measurements of energy dependence of the emitted positronium taken with and without additional ion bombardment at the sample angle θ_i close to the peak position also seemed to confirm this speculation, as the main feature of the energy curve at lower energy range was not changed after the ion bombardment.

If we assume the positronium atoms we measured were those formed on the surface mainly by those positrons that were elastically back-scattered by the crystal, we can estimate the peak position of the emission angle for given incidence angle by conservation of the energy and the total momentum parallel to the surface. The positronium energy E_{P_s} can be written as:

$$E_{P_s} = E_+ + E_B - \phi_-, \tag{4.3.3}$$

where E_+ is the incident positron energy, E_B is the binding energy of positronium, and ϕ_- is the electron work function for Cu(100) surface (about 4.59 eV for Cu(100)

surface). If we assume the positronium are formed by the positrons that are elastically back-scattered by the crystal, then the emitted positronium momentum parallel to the surface $\mathbf{P}_{\|}$ would be:

$$\mathbf{P}_{\|} = \mathbf{p}_{\|} + \hbar\mathbf{k}_{\|}, \tag{4.3.4}$$

where the $\mathbf{p}_{\|}$ is the incident positron momentum parallel to the surface and the $\mathbf{k}_{\|}$ is the electron wave vector parallel to the surface. If we assume the emission angle to be θ_r (to be consistent with the definition we made for the Ps reflection measurement, see section 2.2.3) and define the direction of the $\mathbf{p}_{\|}$ as the y axis direction then

$$\theta_r = \arcsin\left[\frac{\sqrt{2m_eE_+}\sin\theta_i + \hbar k_y}{\sqrt{4m_e}\sqrt{E_+ + (E_B - \phi_-)}}\right], \tag{4.3.5}$$

where m_e is the mass of an electron. If we assume that the probability of the positronium formation is the same for all the electrons on the Fermi level, then the emission angles should be be peaked at:

$$\theta_r^{peak} = \arcsin\left[\sin\theta_i\sqrt{\frac{E_+}{2E_+ + 2(E_B - \phi_-)}}\right], \tag{4.3.6}$$

with the maximum and minimum emission angle $\theta_r^{\pm}$ for $\pm k_f$ (where $k_f = \sqrt{2m_eE_f/\hbar^2}$ is the Fermi wave vector):

$$\theta_r^{\pm} = \arcsin\left[\frac{\sqrt{E_+}\sin\theta_i \pm \sqrt{E_f}}{\sqrt{2}\sqrt{E_+ + (E_B - \phi_-)}}\right]. \tag{4.3.7}$$

where E_f is the Fermi energy of copper (about 7 eV). We can calculate the values of expected emission angle θ_r for our experimental result using the value of θ_i at the maximum emission fraction. Table 4.3.1 lists both calculated and experimental values for θ_r for our two angular scan runs.

Table 4.3.1 The comparison of the θ_r calculated by Eq. (4.3.6) to those measured in the experiments.

Exp.	positron	calculated			Exp.
θ_i	energy(eV)	θ_r^+	θ_r^{peak}	θ_r^-	θ_r^{peak}
52.2°	38.0	57.0°	32.9°	14.4°	$48 \pm 5°$
54.0°	30.0	61.9°	33.5°	12.9°	$47 \pm 5°$

It is clear that our measured maximum emission angles were larger (the emission was more parallel to the surface) than calculated the peak emission angles, though they were still well below the value of θ_r^+. The similar result was reported by the earlier positronium emission measurements from a Al(100) and a Cu(100) surfaces with positrons of near glancing angle incidence (Gidley and others 1987). The maximum emission angle was reported to be 10~15° larger than calculated. It was argued then that this emission angle shift could be due to the unequal probability of positronium formation for electrons with initial momentum in different directions, strongly favoring those whose momentum parallel or closely parallel to $p_{||}$ of incident positrons. However, we can not compare the positron energy dependence measurement with this earlier study because such measurement was not reported. Very recently, Ishii and Shindo (1990) reported their success in predicting the angular distribution of earlier experimental measurements including the emission angle shift (of Gidley and others) assuming a mostly elastic process.

It should be pointed that the contribution to the total positronium emission by the epithermal positrons is expected to be significant. Our experimental set up, however, is more sensitive to those positronium formed by the elastically or nearly elastically back-scattered positrons because they would have higher energies and thus suffer less decay loss on the flight path between the sample surface and our detector (about 15 cm apart). The broad component in our angular scan measurement was believed to be largely contributed by the positronium formed by the epithermal positrons.

The measurements of positron incidence energy dependence of positronium emission from a cleaned Cu(100) surface with and without the ion bombardment both had its broad maxima at 28~32 eV positron incidence energy. It is not clear at the present time whether the maxima are due to the positron energy dependence of the positronium formation cross section as observed for the positronium formation in gases or due to the effect of the Bragg diffraction as the first Bragg peak is expected to be at 28.4 eV, which closely coincides with the positron energy of the maximum emission. More measurements of the positron energy dependence of the positronium emission fraction with different incident angles are needed to analyse it further. Another prominent feature which appeared on both the positron energy dependence curves is the distinct deviation from the smooth increase at the positron energy of ~18 eV. It closely resembles the common feature at threshold of an energy loss process observed in various experiments. The reported experimental plasmon energy of 19.1 eV for copper (Isaacson 1975) strongly suggested that we were observing the plasmon energy loss effect. The further measurements with different incident angles of positrons are needed to confirm it because the plasmon energy loss should be independent of the positron incident angles.

The indication of our measurement that a large portion of the emitted positronium from a Cu(100) surface were formed by the positrons that were elastically backscattered by the crystal strongly suggests that this type of the positronium emission could be used in the future energetic positronium production. It may be possible to construct a variable-energy positronium beam with relative high efficiency by this positronium production process. The positronium emission process has been used for the surface studies. Almost all the measurements were carried out with positrons of incident energy of 100 eV or more. The dominant contribution to the total positronium emission then would be the one by the thermal or epithermal positrons. The positronium atoms emitted through this process generally have fairly low energy on

the order of positronium work function of a few eV. For those experiments rely on the measurements of ortho-positronium atoms emitted, the low positronium energy would result in a heavy decay loss in the flight path and thus small signal to noise ratio. Our observation suggests that measurements should be performed at the lower positron incidence energy to obtain the maximum energetic positronium emission for each experimental geometry (the value is expected to depend on the experimental geometry). One of the possible application would be the surface magnetism studies. The first application of the positronium emission on the surface magnetism was reported (Gidley and others 1982) with positron incidence energy of 300–1500 eV. The research effort, however, was not continued partially due to the low level of detected signals (Gidley 1989). Our measurement would provide an alternative approach which not only would increase the detection signals of the emitted ortho-positronium atoms at the a distance from the surface, but also make the measurements extremely surface sensitive because of a lower incidence energy of the probe. This is also may be applied to study the overlayer of magnetic materials on a non-magnetic substrate which has fairly high reflectivity of low energy positrons, such as Fe on a Ag or Cu substrate or Ni on a W substrate. The plasmon energy loss observation by the positron experiments has not been reported. Our measurement, if verified in future experimental observations, could be the first positron measurement of plasmon energy loss. It is hoped that more measurement with different sample will be carried in the not too far future.

Chapter 5
SUMMARY

Utilizing the HFBR high intensity mono-energetic positron beam at Brookhaven National Laboratory (BNL), a mono-energetic positronium beam was successfully constructed, and has been used to conduct various positronium surface interaction experiments. Our efforts have been described and discussed in the previous chapters. A summary of our effort and an outlook for the future work will be given in this chapter.

§5.1 Summary Of The Present Work

The high intensity mono-energetic positron beam at BNL had been constructed to facilitate various experiments of the positron and positronium interaction with solid state surfaces. This beam uses the highly radioactive isotope Cu^{64} produced by irradiating Cu^{63} in the HFBR as the positron source. The radioactive copper is fabricated into a single crystal film with a (111) surface by the epitaxial growth on a single crystal W(110) substrate, and thus used in most of times, as a self-moderated low energy positron source. In a few occasions, a W(100) foil was used as a transmission moderator with the radioactive copper used only as a fast positron source when self-moderation process failed to deliver high enough intensity of moderated positrons. The mono-energetic positrons, after being filtered by $\mathbf{E} \times \mathbf{B}$ filter to eliminate the un-moderated high energy positrons, are magnetically guided out of the shielding block house to the experimental set up. This positron beam has been providing the mono-energetic low energy positrons of intensity $3 \times 10^6 \sim 1 \times 10^8$ e^+/sec. for sev-

eral experiments of positron and positronium interaction with solid state surfaces including the research project described in this thesis.

A mono-energetic positronium beam was constructed in the High Flux Beam Reactor at BNL to take the advantage of the high intensity positron beam. The positronium atoms were produced by the positrons' charge-exchange collisions with Ar atoms. The mono-energetic positrons produced by the high intensity positron beam were magnetically guided into a gas cell filled with Ar atoms of 1×10^{-3} torr. A fraction of those positrons would formed positronium during the positron Ar atom collisions. The positronium formation was believed to be peaked strongly in the forward direction. Those positronium formed within the 2.5° half angle cone in forward direction were collimated and guided to the experimental chamber. The gas cell was differentially pumped to keep the experimental chamber and the positron beam source chamber in a much lower(a few orders of magnitude lower) pressure. The gas cell was also electrically floated to control the positron energy in the gas cell, and thus the energy of formed positronium. The additional gas baffle tubes and grids were used to eliminate the residual positrons from entering the experimental chamber or the detector. This positronium production set up has provided up to 2000 mono-energetic positronium atoms per second to our positronium surface reflection and scattering measurements.

The positronium reflection and scattering experiments have been carried out on two different surfaces: an ionic crystal LiF(100) surface and a Cu(100) surface. The positronium emissions from these two surfaces after the low energy ($\leq$150 eV) positron's incidence were also measured. Those measurements with a proper analysis and correct interpretation provides a deeper understanding of the positronium interaction with surfaces and very helpful information for the development of the new surface probe: the positronium surface scattering.

In our measurements of the positronium reflection from a LiF(100) surface, we observed a strong positronium specular reflection from the surface, up to about 30% at energies below 7 eV and 1~3% at energy of 50 eV. The angular width of this speculalerly reflected peak was observed to be about the same of the angle divergence of the incident positronium beam, and isotropic background was very low. We thus concluded that the positronium reflection we detected from a LiF(100) surface is dominantly elastic reflection. A strong temperature dependence of the specular reflection was observed. The specular reflectivity also found to depend on the incident angle of positronium.

Different theoretical models have been considered for understanding of our experimental observation. Among them, the model that considers both the reflection from the surface potential and scattering from the top layer ion cores seems to predict our experimental observation most closely and is consistent with other experimental observations. In this model, the surface potential consists of a well potential before the surface representing the long range attractive interaction of positronium with the ion cores in th solid due to the polarization of the positronium and a step potential in the bulk representing the averaged screening effect of the ion cores that results in the less binding energy of the positronium in crystal, and the scattering effect from the top layer ion cores is approximately estimated by considering the interaction of induced dipole of a positronium atom with each ion core at the top layer. The calculation based on this model suggested that while the strong positronium specular reflection we measured at lower energy range was due to both the surface potential reflection and top layer ion core scattering, the reflection of non-vanishing intensity at large energy was mainly due to the top layer ion core scattering.

Our experimental measurements and the analysis with above model strongly support our expectation that there is significant scattering effect by the ion cores at the

top layer of the LiF(100) surface, and thus the low energy positronium surface diffraction is feasible. Our very prelimanary search of the diffraction peaks did not yield any conclusive evidence of the diffraction possibly due to our limited beam intensity and limitation of our detection geometry.

We did not observed that the reflectivity approached to unity at very low energy range. The possible cause could be the imperfection of the surface, the surface contamination, the loss of the positronium at the surface due to the large electric field at the surface region, and the possible contamination of our mono-energetic positronium beam by the positronium atoms formed in the long life excited states. We also observed a strong temperature dependence of the specular reflectivity. This was believed to be due to the surface contamination by additional atoms or molecules, very likely water molecules. These observation also confirmed our expectation that positronium reflection and scattering by a surface is very sensitive the surface condition.

The positronium scattering measurements have also been carried out on both a un-treated polycrystal surface and a cleaned Cu(100) surface. No strong specular reflection similar to the one measured from a LiF(100) surface was observed. The positronium scattering of relative high intensity (on the order of $10^{-3} \sim 10^{-2}$) from a cleaned Cu(100) surface over a relative large energy range (up to 80 eV) was observed. The positronium scattering from the un-treated polycrystal copper surface was also observed but with the intensity of almost one order of magnitude lower than that from the cleaned Cu(100) surface. The scattering intensity also depended on the positronium incident angle, similar to the observation of Ps specular reflection by a LiF(100) surface.

Our analysis showed that the lack of strong specular reflection from Cu(100) surface was probably due to the large inelastic scattering by the large conduction electron density which extended from surface to the vacuum with an exponential decay factor

on the order of 1Å. The inelastic scattering process could include the positronium-electron elastic scattering in which there is high probability of the positronium energy loss, the positronium ionization due to the positronium-electron collision, the ortho-positronium conversion (to para-positronium) by electron spin exchange between the electrons in positronium atoms and conduction electrons, the pick up annihilation by conduction electrons, and the positronium ionization by the large electric field at the surface region. The beam intensity at the time also limited sensitivity to the low intensity specular reflection. Our analysis also showed that the observed scattering could not dominantly be due to the surface potential that represents this inelastic scattering and the changing of the positronium binding energy by the screening effect of conduction electrons. The positronium emission measurements taken from the same surface with similar energy eliminated the possibility that the positronium atoms we detected in the scattering measurement could be mainly due to the positronium formation by the positrons liberated from the incident positronium atoms. Therefore, we concluded that the scattered fraction of positronium we measured was mainly due to the positronium scattering by the top layer ion cores of the surface.

The relative high intensity of the positronium scattering we measured indicated that there was significant positronium-ion core scattering taking place at the surface, which would make the future surface positronium diffraction feasible. The difference in the scattering intensities from un-treated polycrystal copper surface and a cleaned Cu(100) surface also offered a further confirmation that the positronium surface scattering is very sensitive to the surface condition.

The scattered fraction positronium from a Cu(100) surface at large energy was on the same order of magnitude as the specular reflected fraction of positronium from the LiF(100) surface at the similar energy range, $10^{-3} \sim 10^{-2}$. This is not surprising since the effects were expected to be from the positronium ion core scattering at this

energy range for both cases. It, however, does strongly suggested the positronium ion core scattering would be strong enough to produced detectable diffraction effects, and thus further exploration efforts on positronium surface diffraction is fully warranted.

The positronium emission measurements we took on the two surfaces, on which the positronium reflection and scattering measurements were taken, proved that they not only were very helpful to us in understanding our positronium surface reflection and scattering measurements, but also provided some new information on the energetic positronium production and the surface study by the positronium formation measurements.

Our measurements showed that no emitted positronium from the LiF(100) surface was detected directly by our detector at 15 cm away from the surface until the incident positron energy reached 9±1 eV. As the incident positron energy increased, the number of emitted positronium atoms we detected also slowly increased and plateaued at the about 35$\sim$ 40 eV, the upper limit of our measurement. The angular measurement we took at the incident positron energy of 150 eV, however, did show a noticeable reduction of detected positronium emission from that detected at the positron incidence energy of 40 eV. Our angular measurement also showed that most of the emitted positronium atoms we detected at the incident positron energy of 150 eV were emitted nearly isotropically, closely proportional to the cosine of the emission angle with a small anisotropic component, indicating a large portion of the emission of positronium at that energy range might be contributed by the Ps formation near surface by epithermal positrons of relative high energy and a small portion of it possibly by the "Ore" process in the bulk.

The positronium emission from a Cu(100) surface bombarded by the low energy positrons was measured, at first, to help us estimate the effect of the positronium emission by the positrons liberated from the incident positronium atoms to our

positronium scattering measurements. Its result clearly showed that the positronium atoms we detected in the scattering measurements could not dominantly come from this process and thus must from the direct scattering of the incident positronium atoms by the surface.

The positronium emission measurements we took from a cleaned Cu(100) surface with and without the surface damage by the Ar ion bombardment clearly showed that a large portion of emitted positronium atoms were by the surface electron capture of the elastically or nearly elastically back-scattered positrons, and thus the corresponding emitted positronium were of relative large energy. Our measurements also showed that intensity of emitted positronium atoms we detected in our geometry was peaked at about 30 eV, roughly coincided with the first positron Bragg diffraction energy. We also observed a very noticeable fluctuation feature in our positron energy dependence measurement of the Ps emission, which closely resembles a common energy loss or absorption feature. This feature was observed to be at ~18 eV. Since the plasmon energy of copper is 19.1 eV and there is no other known process would result in such a fluctuation, we considered that this observed fluctuation was very likely due to the excitation of plasmon that resulted in an energy loss of some incident positrons and a reduction of positronium emission. If so, this would be the first plasmon energy loss in metals observed with positrons. More measurements with different incidence angles, different surfaces are very desirable to further verify our speculation.

The effort reported in this thesis has provided some new information on the positronium interaction with surfaces. It has confirmed the early expectation that the positronium surface scattering would be a very surface sensitive probe and strongly suggested that further research effort on the development of the positronium surface scattering is not only fully warranted but also would provide some new insight into the fundamental properties of the positronium interaction. The results of our effort

also indicated that future efforts should be made in several areas.

§5.2 Suggested Future Efforts

With the current experimental set up, several measurements would be helpful for understanding of the positronium surface scattering and the assessment of the full potential of this technique as a surface probe. The positronium surface scattering measurements should be performed with a single crystal semi-conductor surface. Its result would be useful to test our current theoretical understanding of the interaction process because of the unique properties of the semiconductors. More importantly, it would also indicate the effectiveness of the positronium surface scattering for the studies of semi-conductor surfaces. The similar measurements should be taken with a optically smooth glass surface. Being a surface of an amorphous insulator, glass surface provide an ideal disordered surface structure with very low conduction electron density. This measurements would verify our speculation that the specular reflection depends on the ordering of the surface. It would also provide the first direct information on the positronium interaction with the amorphous surface. The same measurements may be performed on the single crystal of quartz (SiO_2) surface. It would provide a very interesting comparison between the measurements on a highly ordered and a highly disordered surfaces with similar compounds. The earlier work (Sferlazzo and others 1985) also showed evidence of the positronium formation and diffusion in the bulk of quartz. As the recent work (Tuomisaari and other 1989) on positronium emission measurements reported that positronium emission spectra of a LiF(100) surface were quite different from the spectra of all other alkali halides surfaces which were similar to each others, some new insight may be gained by measuring the positronium specular reflection from other alkali halide surfaces, a high purity NaF(100) surface for example.

Another interesting surface for the positronium surface scattering measurements

is the single crystal MgO surface. It is not only a well studied surface by various techniques, but also widely used substrates for various epitaxial growth of metal foils ranged $1 \sim 10^4$Å. If a single crystal MgO surface possesses similar high specular reflectivity of positronium, then it would be very interesting to measure the change in reflectivity as the metal overlayer or layers are deposited onto this substrate. Our observation has indicated clearly the high surface sensitivity of this type of measurements.

More positronium emission measurements from a Cu(100) surface and other metal with different incident angles, possibly with different coating of the metals of smaller Fermi energy, would provide some valuable information on the energetic positronium production with metal surfaces and the design of future positronium beams. It would also determine conclusively whether the fluctuation feature we observed was the plasmon loss feature, more importantly, whether this would be a new approach to measure the plasmon energy loss by positrons. The surface magnetism and magnetic overlayer studies with positronium emission by low energy (preferably, at the maximum Ps emission energy which usually below 100 eV pending on the detection geometry) positron incidence should also be actively pursued.

Though a number of interesting experiments such as one described about can be carried out with our existing experimental set up, it would be desirable, at some point, to modified our experimental chamber to make it more suitable for the surface diffraction experiments. The modified experimental set up should allow the detector to be positioned at very small detector angle ψ (ψ has to be greater than 95° at the present set up) or out of the plane define by the incidence beam and the normal of the sample surface. This additional capability would allow the surface diffraction measurements to be taken in the relative low positronium energy range without large incidence angle θ_i or large scattering angle θ_r (as our measurements showed that the

positronium scattering with either large energy, or large incident angle θ_i, or scattering angle θ_r might result in a very small scattered fraction.) and would allow researcher to detect the diffraction features more easily and conclusively.

At present, the construction of the high intensity positron beam at Building 480 of Brookhaven National Laboratory is at its finishing stage. The source chamber of this newly constructed beam was designed to utilize the newly discovered solidified Neon moderator (Mills and Gullikson 1986, Khatri and others 1990). The first stage testing with a capsulated Na^{22} source of about 100 mCi has yielded a moderated positron beam intensity of more than 3×10^6 e^+/sec. It is expected this beam will be able to deliver a high intensity moderated positrons of 10^9 e^+/sec. when the irradiated copper isotope is used as the source. The future positronium surface scattering experiments are expected be conducted with this beam as the moderated positron source. Not only this beam will deliver a much higher intensity slow positrons, it is also located in an environment of relatively low radiation background, These would greatly enhance the detection sensitivity of the positronium surface scattering experiments and may enable researcher to identify the diffraction effects that could not identify in our measurements due to the limit of the detection sensitivity.

Another effort currently under the way is the construction of a pulsed positronium beam at Brookhaven National Laboratory. It is designed either to use a Na^{22} source (for initial testing) or to be used in conjunction with the newly constructed high intensity positron described above. Different from the positronium beam we used for our experimental effort, this beam will enable the researchers to analyze the energy distribution of the scattered positronium by the time of flight technique. Therefore, the elastic and inelastic scattering effects can be separated and detailed Ps energy loss information at the surface can be obtained to help researchers to achieve a deeper understanding of the positronium surface interaction. Since this beam can also deliver

pulsed positrons, it also can be used to continue our measurements of the energetic positronium production at the metal surfaces. The energy spectra of the emitted positronium from metal surfaces will become obtainable with this beam.

The energy analysis capability of the newly constructed beam will also make the use of the carbon foil for positronium production practical (see section 2.2.2). The use of the carbon foil instead of the gas cell would, in turn, provide an ultra high vacuum environment highly desirable for the surface study experiments. It would be possible to measure the positronium scattering by a surfaces with a controlled amount of adsorbate on the surface.

A great number of interesting experiments can be performed if a highly collimated positronium beam available. Among them, the positronium surface resonance effect, which would give a insight into the positronium surface interaction potential, may be observed with a highly collimated Ps beam. Similar effects has been observed in the scattering and diffraction by electrons (McRae 1979), positrons (Horsky and others 1989), and gas atoms (Hoinkes 1980). Because of the strong effect of conduction electron density on the low energy positronium surface scattering, the highly collimated positronium beam may also be use to study the structure and charge density of very thin semi-conductor foils of a few Å by measuring the scattered positronium and the transmitted positronium, if there exist one or several channels in the thin foil along which the electron density is low enough to permit the passage of positronium atoms. The positron beam of very high intensity would make the collimation affordable (as the collimation usually results in a reduction of the beam intensity). The newly constructed high intensity positron beam with the newly constructed positronium beam may provide researcher such an opportunity to carry out above experiments.

The positronium surface scattering is still a rather under-developed area. The effort reported in this thesis was a systematical attempt to explore this new territory.

It is our hope and belief that the positronium surface scattering will be fully utilized in the future surface studies and the information we obtained in our effort will encourage and benefit the future effort in this field.

REFERENCES

Andersen, J. U., W. M. Augustyniak, and E. Uggerhoj, 1971, Phys. Rev. **B 3**, 705.

Anderson, Carl D., 1932, Science **76**, 238; Phys. Rev. **41**, 405.

Anderson, Carl D., 1933, Phys. Rev. **43**, 491.

Andersson, Stig, 1969, Surface Science **18**, 325.

Ashcroft, Neil W., and N. David Mermin, 1976, *Solid State Physics*, Philadelphia: Saunders College.

Beling, C. D., and M. Charlton, 1987, Contemp. Phys. **28**, 241.

Beling, C. D., R. I. Simpson, M. Charlton, F. M. Jacobsen, T. C. Griffith, P. Moriarty, and S Fung, 1987, Appl. Phys. **A 42**, 111.

Beling, D. D., R. I. Simpson, M. G. Stewart, Y. Y. Wang, S. Fung, J. C. H. Wai, and T. N. Sun, 1987, Phys. Status Solidi **102**, 537.

Berko, Stephan, and Hugh N. Pendleton, 1980, Ann. Rev. Nucl. Part. Sci. **30**, 543.

Berko, S., 1983, 1983, in *Positron Solid-State Physics*, Proceeding of the International School of Physics Enrico Fermi, Course LXXXIII, 1981, edited W. Brandt and A. Dupasquier, Amsterdam, New York, and Oxford: North-Holland Publishing Company, p. 64.

Bhatia, A. K. and Richard J. Drachman, 1985, Phys. Rev. **A 32**, 3745.

Brandes, G. R., K. F. Canter, and A. P. Mills, Jr., 1988, Phys. Rev. Lett. **61**, 492.

Brandt, Werner, and Robert Paulin, 1977, Phys. Rev. **B 15**, 2511.

Britton, D. T., P. A. Huttunen, J. Mäkinen, E. Soininen, and A. Vehanen, 1989, Phys. Rev. Lett. **62**, 2413.

Brown, B. L., 1985, in *Positron Annihilation*, edited by P. C. Jain, R. M. Singru and K. P. Gopinathan, Singapore: World Scientific Publishing Co., p. 328.

Brown, B. L., 1986, *POSITRON [ELECTRON]-GAS SCATTERING*, edited by Walter E. Kauppila, Talbert S. Stein, and Jogindra M. Wadehra, Singapore: World Scientific, p 212.

Brown, B. L., 1987, Ph.D. dissertation (Brandeis University), available from University Microfilms Inc., Ann Arbor, Mich., USA.

Brusa, R. S., Grisenti, S. Oss, A. Zecca, and A. Dupasquier, 1985, Rev. Sci. Instrum. bf 56, 1531.

Canter, Karl F., 1984, *Positron Scattering in Gases*, edited by John W. Humberston and M. R. C. McDowelll, New York and London: Plenum Press, p 219.

Canter, K. F., P. G. Coleman, T. C. Griffith, and G. R. Heyland, 1972, J. Phys. **B 5**, L167.

Canter, K. F., A. P. Mills, Jr., and S. Berko, 1975, Phys. Rev. Lett. **34**, 177.

Canter, K. F., and A. P. Mills, Jr., 1982, Can. J. Phys. **60**, 551.

Canter, K. F., G. R. Brandes, T. N. Horsky, P. H. Lippel, and A. P. Mills, Jr., 1987, in *Atomic Physics with Positrons*, edited by J. W. Humberston and E. A. G. Armour, New York: Plenum, p. 153.

Chang, Tianbao, Tang Hsiaowei, and Li Yaoqing, 1985, in *Positron Annihilation*, edited by P. C. Jain, R. M. Singru and K. P. Gopinathan, Singapore: World Scientific Publishing Co., p. 212.

Charlton, M., 1985, Rep. Prog. Phys. **48**, 737.

Charlton, M., and G. Laricchia, 1990, J. Phys. **B**: At. Mol. Opt. Phys. **23**, 1045.

Chen, D. M., 1987, Ph.D. dissertation (City University of New York), available from University Microfilms Inc., Ann Arbor, Mich., USA.

Chen, D. M., S. Berko, K. F. Canter, K. G. Lynn, A. P. Mills, Jr., L. O. Roellig, P. Sferlazzo, M. Weinert, and R. N. West, 1987, Phys. Rev. Lett. **58**, 921.

Chen, D. M., S. Berko, K. F. Canter, K. G. Lynn, A. P. Mills, Jr., L. O. Roellig, P. Sferlazzo, M. Weinert, and R. N. West, 1989, Phys. Rev. **B 39**, 3966.

Cherry, W., 1958, Ph.D. dissertation (Princeton University), available from University Microfilms Inc., Ann Arbor, Mich., USA.

Chu, Steven, and Allen P. Mills, Jr., 1984, Phys. Rev. Lett. **48**, 1333.

Chu, Steven, Allen P. Mills, Jr., and John L. Hall, 1984, Phys. Rev. Lett. **52**, 1689.

Cook, D. R., T. N. Horsky, and P. G. Coleman, 1984, Appl. Phys. **A 34**, 237.

Costello, D. G., D. E. Groce, J. W. McGowan and D. F. Herring, 1972, Phys. Rev. **B 5**, 1433.

Dale, J. M., L. D. Hulett, and S. Pendyala, 1980, Surf. Interface anal. **2**, 199.

DeBenedetti, S., C. E. Cowan, and W. R. Ronneker, 1949, Phys. Rev. **76**, 440.

DeBenedetti, S., 1967, in *Positron Annihilation*, Proceeding of the 1st. International Conference on Positron Annihilation, Detroit, 1965, edited by A. T. Stewart and L. O. Roellig, New York/London: Academic Press, p. 3.

Derry, G., D. Wesner, S. V. Krishnaswamy and D. R. Frankl, 1978, Surface Science **74**, 245.

Deutsch, M., 1951, Phys. Rev. **82**, 455.

Deutsch, M., 1951, Phys. Rev. **83**, 866.

Deutsch, Martin, and Everett Dulit 1951, Phys. Rev. **84**, 601.

Diana, L. M., S. C. Sharma, L. S, Fornari, P. G. Coleman, P. K. Pendleton, D. L. Brooks, and B. E. Seay, 1985, in *Positron Annihilation*, edited by P. C. Jain, R. M. Singru and K. P. Gopinathan, Singapore: World Scientific Publishing Co., p. 431.

Diana, P. G. Coleman, D. L. brooks, P. K. Pendleton, D. M. Norman B. E. Seay, and L. M., S. C. Sharma, 1986, *POSITRON [ELECTRON]-GAS SCATTERING*, edited by Walter E. Kauppila, Talbert S. Stein, and Jogindra M. Wadehra, Singapore: World Scientific, p 297.

Dirac, P. A. M., 1930, Proc. Cambridge Philos. Soc. **26**, 361.

Dirac, P. A. M., 1958, in *The Principles of Quantum Mechanics*, London: Oxford University Press.

Dorikens, M., L. Dorikens-Vanpraet, D. Segers, and I. Lemahieu, 1987, Appl. Phys. **A 43**, 257.

Drachman, Richard J., and S. K. Houston, 1976, Phys. Rev. **A 14**, 894.

DuMond, J. W. M., D. A. Lind, and B. B. Watson, 1949, Phys. Rev. **75**, 1226.

Dunning, F. B., 1989, *"Atomic Physics in Surface Studies: An Overview,"* in the proceeding of XV International Conference on the Physics of Electronic and Atomic Collisions, at New York City, New York, 1989.

Dupasquier, A, 1983, in *Positron Solid-State Physics*, Proceeding of the International School of Physics Enrico Fermi, Course LXXXIII, 1981, edited W. Brandt and A. Dupasquier, Amsterdam, New York, and Oxford: North-Holland Publishing Company, p. 510.

Dupasquier, A., and A. Zecca, 1985, Riv. Nuovo Cimento **8**, 3.

Engleman, R., Jr, R. A. Keller, C. M. Miller, Nicholas S. Nogar, and J. A. Paisner, 1987, Nucl. Instrum. Methods **B26** 448.

Feidenhans'l, R., 1989, Surface Science Reports **10**, 105.

Fornari, L. S., L. M. Diana, and P. G. Coleman, 1983, Phys. Rev. Lett. **51**, 2276.

Fraser, P. A., 1961, Proc. Phys. Soc. **78**, 329.

Fraser, P. A., 1961, Proc. Phys. Soc. **79**, 721.

Fraser, P. A., and M Kraidy, 1966, Proc. Phys. Soc. **89**, 533.

Frieze, W. E., D. W. Gidley, and K. G. Lynn, 1985, Phys. Rev. **B 31**, 5628.

Fromme, Dieter, George Kruse, Wilhelm Raith, and Günther Sinapius, 1986, Phys. Rev. Lett. **57**, 3031.

Gidley, D. W., A. R. Köymen, and T. Weston Capehart, 1982, Phys. Rev. Lett. **49**, 1779.

Gidley, D. W., R. Mayer, W. E. Frieze, and K. G. Lynn, 1987, Phys. Rev. Lett. **58**, 595.

Graff, G., R. Ley, A. Osipowicz, and G. werth, 1984, Appl. Phys. **A 33**, 59.

Gramsch, E., J. Throwe, and K. G. Lynn, 1987, Appl. Phys. Lett. **51**, 1862.

Griffith, T. G., 1984, in *Positron Scattering in Gases*, edited by John W. Humberston and M. R. C. McDowell, New York and London: Plenum Press, p. 53.

Groce, D. E., D. G. Costello, D. F. Herring, and J. W. McGowan 1968, Bull. Am. Phys. Soc., **13**, 1397.

Gullikson, E. M., and A. P. Mills, Jr., 1986, Phys. Rev. Lett. bf 57, 376.

Hara, S. and P. A. Fraser, 1975, J. Phys. **B 8**, L472.

"*HFBR Handbook*" edited S. Shapiro, D. C. Rorer, and H. Kuper, 1983, Upton New York: Brookhaven National Laboratory Informal Report.

Hoinkes, H., 1980, Rev. Mod. Phys. **52**, 933.

Horsky, T. N., G. R. Brandes, K. F. Canter, C. B. Duke, S. F. Horng, A. Kahn, D. L. Lessor, A. P. Mills, A. Paton, K. Stevens, and K. Stiles, 1989a, Phys. Rev. Lett. **62**, 1876.

Horsky, T. N., G. R. Brandes, K. F. Canter, P. H. Lippel, and A. P. Mills, Jr., 1989b, Phys. Rev. **B 40**, 7898.

House, James Van, and Arthur Rich, 1988, Phys. Rev. Lett. **61**, 488.

Howell, R. H., R. A. Alvarez, and M. Stanek, 1982, Appl. Phys. Lett., **40**, 751.

Howell, R. H., P. Meyer, I. J. Rosenberg, and M. J. Fluss, 1985, Phys. Rev. Lett. **54**, 1698.

Howell, R. H., I. J. Rosenberg, and M. J. Fluss, 1986, Phys. Rev. **B 34**, 3069.

Howell, R. H., I. J. Rosenberg, P. Meyer, and M. J. Fluss, 1987a, Phys. Rev. **B 35**, 4555.

Howell, R. H., I. J. Rosenberg, M. J. Fluss, R. E. Goldberg, and R. B. Laughlin, 1987b, Phys. Rev. **B 35**, 5303.

Issacson, Diane, 1975, Internal Report, Radiation and Solid State Laboratory, New York University.

Ishii, Akira, 1988, Private Communication.

Ishii, Akira, and Shigeru Shindo, 1990, to be published in Surface Science.

Khan, Pritikana, and A. S. Ghosh, 1983, Phys. Rev. **A 28**, 2181.

Khan, Pritikana, P. S. Mazumdar, and A. S. Ghosh, 1985, Phys. Rev. **A 31**, 1405.

Khatri, R., M. Charlton, P. Sferlazzo, K. G. Lynn, A. P. Mills, Jr., and L. O. Roellig, 1990, to be published in Appl. Phys. Lett..

Kittel, Charles, 1976, *Introduction to Solid State Physics*, 5th ed., New York, London, Sydney, and Toronto: John Wiley & Sons, Inc..

Landau, L. D., and E. M. Lifshitz, 1977, *QUANTUM MECHANICS (Non-relativistic Theory)*, Oxford, New York, Toronto, Sydney, Paris, and Frankfurt: Pergamon Press.

Lederer, C. Michael, Jack M. Hollander, and Isadore Perlamn, 1967, *Table of Isotopes*, New York, London, and Sydney: John Wiley&Sons, Inc., p 98.

Lewis, M. L., and V. W. Hughes, Phys. Rev. **A 8**, 625.

Lynn, K. G., and B. T. A. McKee, 1979, Appl. Phys. **19**, 247.

Lynn, K. G., and D. N. Lowy, and I. K. Mackenzie, 1980, J. Phys. **C 13**, 919.

Lynn, K. G., 1983, in *Positron Solid-State Physics*, Proceeding of the International School of Physics Enrico Fermi, Course LXXXIII, 1981, edited W. Brandt and A. Dupasquier, Amsterdam, New York, and Oxford: North-Holland Publishing Company, p. 609.

Lynn, K. G., B. Nielsen, and J. H. Quateman, 1985a, Appl. Phys. Lett. **47**, 239.

Lynn, K. G., A. P. Mills, Jr., R. N. West, S. Berko, K. F. Canter, L. O. Roellig, 1985b, Phys. Rev. Lett. **54** 1702.

Lynn, K. G. and Bent Nielsen, 1987, Phys. Rev. Lett. **58**, 81.

Lynn, K. G., M. Weber, L. O. Roellig, A. P. Mills., Jr., and A. R. Moodenbaugh, 1987, in *Atomic Physics with Positrons*, edited by J. W. Humberston and E. .A. G. Armour, New York and London: Plenum Press, p. 161.

Lynn, K. G., E. Gramsch, S. G. Usmar, And P. Sferlazzo, 1989, Appl. Phys. Lett. **55**, 87.

Madanski, Leon, and Franco Rasetti, 1950, Phys. Rev. **79**, 397.

Mandal, Puspajit, Sunanda Guha, and N. C. Sil, 1979, J. Phys. **B**: Atom. Molec. Phys., **12**, 2913.

Mayer R., Chun-Si Zhang, K. G. Lynn, W. E. Frieze, F. Jona, and P. M. Marcus, 1987, Phys. Rev. **B 35**, 3102.

McCoyd, G. C., 1965, Ph.D. dissertation (St. Johns University), available from University Microfilms Inc., Ann Arbor, Mich., USA.

McRae, E. G., 1979 Rev. Mod. Phys. **51**, 541.

McTague, J. P., M. Nielsen, and L. Passell, 1979, in *Chemistry and Physics of Solid Surface* **II**, edited by Ralf Vanselow, Florida: CRC Press, Inc., p. 439.

Melezhik, V. S., and F. R. Vukajlović, 1988, Phys. Rev. **A 38**, 6426.

Merzbacher, Eugen, 1970, *Quantum Mechanics*, 2nd ed., New York, London, Sydney, and Toronto: John Wiley & Sons, Inc..

Meyers, Jeffrey A., and D. R. Frankl, 1975 Surface Science **51**, 61.

Mills, A. P., Jr., S. Berko, and K. F. Canter, 1975, Phys. Rev. Lett. **34**, 1541.

Mills, A. P., Jr., 1979, Appl. Phys. Lett. **35**, 427.

Mills, A. P., Jr., 1980a, Appl. Phys. Lett. **37**, 667.

Mills, A. P., Jr., 1980b, Appl. Phys. **23**, 189.

Mills, Allen P., Jr., and P. M. Platzman, 1980, Solid State Comm. **35**, 321.

Mills, A. P., Jr., 1981, Phys. Rev. Letter **46**, 717.

Mills, Allen Paine, Jr., 1983, Phys. Rev. Lett. **50**, 671.

Mills, A. P., Jr., 1983, in *Positron Solid-State Physics*, Proceeding of the International School of Physics Enrico Fermi, Course LXXXIII, 1981, edited W. Brandt and A. Dupasquier, Amsterdam, New York, and Oxford: North-Holland Publishing Company, p. 432.

Mills, A. P., Jr., Loren Pfeiffer, and P. M. Platzman, 1983, Phys. Rev. Lett. **51**, 1085.

Mills, A. P., Jr., and William S. Crane, 1985a, Phys. Rev. **A 31**, 593.

Mills, A. P., Jr., and W. S. Crane, 1985b, Phys. Rev. **B 31**, 3988.

Mills, A. P., Jr., and E. M. Gullikson, 1986, Appl. Phys. Lett. bf 49, 1121.

Mills, A. P., Jr., E. D. Shaw, R. J. Chichester, and D. M. Zuckerman, 1989, Rev. Sci. Intrum. **60**, 825.

Mohorovičić, S., 1934, Astron. Nachr. **253**, 94.

Ore, A., and J. L. Powell, 1949, Phys. Rev. **75**, 1696.

Peach, G., 1989, in *Positron Annihilation*: Proceeding of the 8th International Conference on Positron Annihilation, at Gent, 1988, edited by L. Dorikens-Vanpraet, M. Dorikens, and D. Segers, Singapore, New Jersey, and Hong Kong: World Scientific Publishing, p. 423.

Pendry, J. B., 1974, *Low Energy Electron Diffraction*, The Theory and its Application to Determination of Surface Structure, London and New York: Academic Press.

Pierenne, J., 1946, Arch. Sci. Phys. Nat. **28**, 233.

Platzman, P. M. and N. Tzoar, 1985, in *Positron Annihilation*, edited by P. C. Jain, R. M. Singru and K. P. Gopinathan, Singapore: World Scientific Publishing Co., p. 941.

Platzman, P. M. and N. Tzoar, 1986, Phys. Rev. **B 33**, 5900.

Rich, Arthur, 1981, Rev. Mod. Phys. **53**, 127.

Robinson, I. K., 1990, in *Handbook on Synchrotron Radiation* **III**, edited by D. E. Moncton and G. S. Brown, Amsterdam: North-Holland Publishing.

Roellig, L. O., M. Weber, S. Berko, B. L. Brown, K. F. Canter, K. G. Lynn, A. P. Mills, Jr., S. Tang, and A. Viescas, 1987, in 1987, in *Atomic Physics with Positrons*, edited by J. W. Humberston and E. A. G. Armour, New York: Plenum, p. 233.

Roellig, L. O., 1988, in *Intense Positron Beams*, edited by E H. Ottewitte and W. Kells, Singapore, New Jersey, and Hong Kong: World Scientific, p 16.

Rosenberg, I. J., A. H. Weiss, and K. F. Canter, 1980, Phys. Rev. Lett. **44**, 1139.

Stroscio, Michael A, 1975, Phys. Reports **22**, 215.

Saam, B., M.Skalsey, and J. Van House, 1989, Phys. Rev. **C 40**, R1563.

Schultz, Peter J., L. R. Logan, T. E. Jackman, and J. A. Davies, 1988, Phys. Rev. **B 38**, 6369.

Schultz, Peter. J., and K. G. Lynn, 1988, Rev. Mod. Phys. **60**, 701.

Sferlazzo, P., S. Berko, and K. F. Canter, 1985, Phys. Rev. **B 32**, 6067.

Sferlazzo, P., S. Berko, and K. F. Canter, 1987, Phys. Rev. **B 35**, 5315.

Sferlazzo, S., S. Berko, K. G. Lynn, A. P. Mills, Jr., L. O. Roellig, A. J. Viescas, and R. N. West, 1988, Phys. Rev. Lett. **60**, 538.

Smith, N. V., C. T. Chen, and M. Weinert, 1989, Phys, Rev. **B 40**, 7565.

Stein, T. S., and W. E. Kauppila, 1982, Adv. At. Mol. Phys. **18**, 53.

Stewart, A. T. and L. O. Roellig, 1967, *Positron Annihilation*, Proceeding of the 1st international Conference on Positron Annihilation, Detroit, 1965, New York and London: Academic Press.

Surko, C. M., M. Leventhal, and A. Passner, 1989. Phys. Rev. Lett. **62**, 901.

Tuomisaari, M., R. H. Howell, and T. McMullen, 1989, Phys. Rev. **B 40**, 2060.

Vehanen, A., K. G. Lynn, Peter J. Schultz, and M. Eldrup, 1983, Appl. Phys. **A 32** 163.

Vehanen, A., J. Mäkinen, P. Hautojärvi, H. Huomm, J. Lahtinen, R. M. Nieminen, and S. Valkealahti, 1985, Phys. Rev. **B 32**, 7561.

Wallace, Philip R., 1960, *Solid State Physics* **10**, New York and London: Academic Press, p. 1.

Ward, S. J., J. W. Humberston, and M. R. C. McDowell, 1985, J. Phys. **B**: At. Mol. Phys. **18**, L525.

Ward, S. J., J. W. Humberston, and M. R. C. McDowell, 1987, J. Phys. **B**: At. Mol. Phys. **20**, 127.

Weber, M. H., S. Tang, S. Berko, B. L. Brown, K. F. Canter, K. G. Lynn, A. P. Mills, Jr., L. O. Roellig, and A. J. Viescas, 1988, Phys. Rev. Lett. **61**, 2542.

Weber, Marc H., 1988, Ph.D. dissertation (City University of New York), available from University Microfilms Inc., Ann Arbor, Mich., USA.

Weiss, Alex H., I. J. Rosenberg, K. F. Canter, C. B. Duke, and A. Paton, 1983, Phys. Rev. **B 27**, 867.

Weiss, A., R. Mayer, M. Jibaly, C. Lei, D. Mehl, and K. G. Lynn, 1988, Phys. Rev. Lett. **61**, 2245.

Wheeler, J. A., 1946, Ann. N.Y. Acad. Sci. **48**, 219.

Westbrook, C. I., D. W. Gidley, R. S. Conti, and A. Rich, 1987, Phys Rev. Lett. **58**, 1328.

Wolfenstein, L. and D. G. Ravenhall, 1952, Phys. Rev. **88**, 279.

Wu, Yiao-ye, Peter Dull, and K. G. Lynn, 1990, to be published in Appl. Phys. Lett..

Yang, C., 1950, Phys. Rev. **77**, 242.

Zafar, N., J. Chevallier, F. M. Jacobsen, M. Charlton, and G. Larrechia, 1988, Appl. Phys. **A 47**, 409.